Comparison Between CEF and HT-TGIC of Polyolefins Made by Ziegler-Natta and Metallocene Catalysts

by

Abdulaziz Alghyamah

A thesis
presented to the University of Waterloo
in fulfillment of the
thesis requirement for the degree of
Doctor of Philosophy
in
Chemical Engineering

Waterloo, Ontario, Canada, 2012

© Abdulaziz Alghyamah 2012

AUTHOR'S DECLARATION

I hereby declare that I am the sole author of this thesis. This is a true copy of the thesis, including any required final revisions, as accepted by my examiners.

I understand that my thesis may be made electronically available to the public.

ABSTRACT

Polyolefins are the most important commodity polymers today. Their end use properties polymers depend primarily on their molecular weight (MWD) and chemical composition (CCD) distributions. Several characterization techniques are used to analyze the microstructures of the polyolefins. High-temperature gel permeation chromatography (GPC) is the most widely used technique for MWD determination. Temperature rising elution fractionation (TREF) and crystallization analysis fractionation (CRYSTAF) are routinely used for CCD measurement. There have been significant improvements over the last few years on CCD characterization techniques for polyolefins with the introduction of crystallization elution fractionation (CEF) and high-temperature thermal gradient interaction chromatography (HT-TGIC). The main objective of this thesis was to conduct systematic studies on HT-TGIC and CEF to provide a better understanding on the separation mechanism of these new techniques and to find out operational conditions that enhance the resolution of the measured CCDs.

The effects of cooling rate, adsorption/desorption temperature range, heating rate and sample size on HT-TGIC fractionation were investigated using polyethylene and ethylene/1-octene copolymers made with metallocene catalyst. It was found out that HT-TGIC was relatively insensitive to the cooling rate within the range investigated in this study. However, the obtained profiles depended strongly on the heating rate applied during the desorption cycle. Chromatograms measured under faster heating rates were broader and had lower resolutions, supposedly due to co-desorption effects. Analysis of polyolefin blends by HT-TGIC showed that sample volume was a very important parameter affecting peak separation of the blend components; reducing the volume of the injected sample can be used to minimize the degree of co-adsorption and co-desorption effects.

The effect of solvent type on HT-TGIC analysis was investigated using o-dichlorobenzene (ODCB), 1,2,4-trichlorobenzene (TCB), and chloronaphthalene (CN). Polyolefin blends were analyzed using these solvents and the best resolution was obtained when ODCB was used as the mobile phase. The profiles obtained using TCB and CN were similar and both were strongly affected by the co-adsorption and co-desorption phenomena.

HT-TGIC profiles of ethylene homopolymers and ethylene/1-octene copolymers were also compared with the equivalent CEF profiles. Interestingly, it was found out that the differences between the profiles measured by these techniques decreased as the comonomer content increased, with CEF systematically measuring sharper profiles for samples with low 1-olefin comonomer content.

A new method was also developed to quantify the degree of co-crystallization of polyolefin blends analyzed by CEF and was used to quantify operating conditions that influenced co-crystallization. The results showed that co-crystallization can be minimized using slower cooling rates, but heating rates play a less important role.

A detailed study on the effect of CEF operating conditions on CCD resolution was also conducted using industrial LLDPE resins that have broad MWDs and CCDs. Cooling rate and solvent flow rate during the cooling cycle significantly affect the degree of co-crystallization of CEF profiles. However, varying the heating rate does not have a marked impact on these separations. The CEF profiles of these resins were compared with the equivalent HT-TGIC profiles, showing that CEF provided better peak separation than HT-TGIC.

Finally, a new mathematical model was developed to simultaneously deconvolute the MWD and CCD of polyolefins made with multiple site-type catalysts such as Ziegler-Natta catalysts. The model was applied to several industrial linear low-density polyethylene (LLDPE) resins to estimate the minimum number of active site types, the number average molecular weight, the average comonomer mole fraction, and the mass fraction of soluble and non-soluble polymer made on each site type.

ACKNOWLEDGEMENTS

I would like to thank my supervisor Professor Joao Soares for his support, encouragement, and valuable advice throughout the entire work of this thesis.

I am thankful to my supervisory committee members: Professor Harald Pasch, Professor Jean Duhamel, Professor Leonardo Simon, and Professor Zhongwei Chen.

I also want to thank my father Abdullah Alghyamah, my mother Sarah Alroashed, my wife Mai Almuzaini for their support, prayers, encouragement, and motivation. This achievement would never have been done without the invaluable help from them.

Finally, I would like to take this opportunity to acknowledge the financial support from King Saud University.

DEDICATION

To

My Father, Abdullah Alghyamah

My Mother, Sarah Alroashed

My Wife, Mai Almuzaini

TABLE OF CONTENTS

LIST OF FIGURES

LIST OF TABLES

LIST OF ACRONYMS

CCD	chemical Composition Distribution
CEF	crystallization Elution Fractionation
CN	chloronaphtalene
^{13}C NMR	carbon-13 nuclear magnetic resonance spectroscopy
CRYSTAF	crystallization analysis fractionation
DSC	differential scanning calorimetry
GPC	gel permeation chromatography
HDPE	high density polyethylene
HPLC	high performance liquid chromatography
HT-TGIC	high temperature thermal gradient interaction chromatography
IR	infrared
IV	intrinsic viscosity
LCB	long chain branches
LLDPE	linear low density polyethylene
MWD	molecular weight distribution
ODCB	o-dichlorobenzene
PDI	polydispersity index
SCB	short chain branches
TCB	1,2,4-trichlorobenzene
TREF	temperature rising elution fractionation

Chapter 1

INTRODUCTION

Polyethylene (PE) is one of the major worldwide commodity polymers. Conventionally, polyethylene resins are classified into three types according to their densities: low density polyethylene (LDPE), linear low density polyethylene (LLDPE), and high density polyethylene (HDPE). According to Chem-systems, the world production capacity of PEs in 2005 was approximately 65 million tons with a 6% growth rate.[1] With this growing demand, PE itself becomes technically more sophisticated and more application-specific. The required improvements in PE properties have become possible by the utilization of the latest findings in polymer science and engineering.

Figure 1.1 summarizes some characteristics of the three classes of polyethylenes. Each PE type has a characteristic molecular structure, production process, density range, and applications. LDPE is a homopolymer of ethylene that is produced by free radical high-pressure polymerization processes. As illustrated in Figure 1, LDPE has a highly branched structure with long chain branches (LCB) due to transfer to polymer reactions, and short chain branches (SCB) due to back-biting reactions. The density of LDPE can vary from 0.91 to 0.93 g/cm^3. HDPE has linear chain structure with no or very few short chain branches and up to 80% of the polymer can be in the crystalline phase, resulting in a high density polymer (density in the range of 0.94 to 0.965 g/cm^3).[2,3]

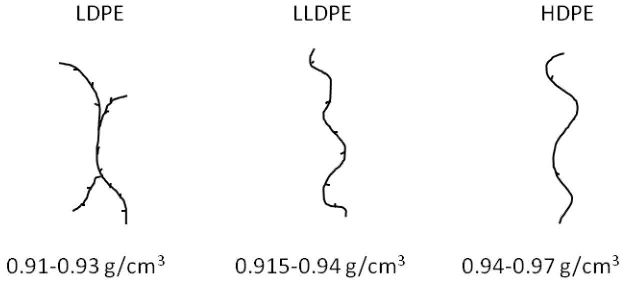

Figure 1.1 Microstructures of polyethylene types.

The third class of polyethylenes, known as LLDPE, is a copolymer produced by the copolymerization of ethylene with α-olefin such as 1-butene, 1-hexene, and 1-octene. These copolymers have densities similar to the LDPEs, but they possess linear molecular structures with SCBs distributed along the backbone of the polyethylene chains without any long chain branches like those of LDPE. In LDPE, SCBs are made by comonomer incorporation, contrarily to the back-biting mechanism prevalent in the production of LDPE.

Polyethylene has a very simple and regular structure that allows the chains to pack tightly into the crystalline state. However, the presence of branches disrupts the ordered arrangement of the macromolecular chains. A high level of SCBs and, to a lesser extent LCBs, means a large amount of crystal defects that decrease polymer crystallinity, density and melting temperature. In general, LCBs (typically 100 or more carbon atom long) affect solution viscosity and melt rheology, while SCBs affect the thermal, physical and mechanical properties of polyethylenes. The amount of SCBs increases by increasing the amount of α-olefin used in the copolymerization process. HDPE has less than 1% of α-olefin incorporated into the polymer backbone, while LLDPE has a comonomer content in the range of 2 to 8 mol%. By incorporating more than 8 mol% of comonomer, very low density polyethylene (VLDPE) and ultra low density polyethylene (ULDPE) can be produced as new families of LLDPE that have densities between that of LLDPE (0.915 g/cm^3) and ethylene/propylene rubber (0.86 g/cm^3). The applications of LLDPEs depend on their properties that, in turn, can be determined by their characteristic molecular structures. It is the variation of molecular weight (MW) average, molecular weight distribution (MWD), average comonomer content, and chemical composition distribution (CCD) or short chain branching distribution (SCBD) that provide the various properties of LLDPE to meet the requirements of specific applications.

1.1 MOTIVATION AND RESEARCH OBJECTIVES

Heterogeneous Ziegler-Natta catalysts make polymer with broad MWD and CCD, while metallocene catalysts make polymers with more uniform distributions. Because of this behaviour, Ziegler-Natta catalysts are considered to have two or more distinct site types, while metallocenes are classified as single-site catalysts. The MWD is usually measured by high-temperature gel permeation chromatography (GPC) and the CCD by either temperature rising elution fractionation (TREF) or crystallization analysis fractionation (CRYSTAF). The characterization of the comonomer fraction distribution has been improved significantly over the last few years with the introduction of crystallization elution fractionation (CEF) and high temperature thermal gradient interaction chromatography (HT-TGIC), which are the main subjects of this thesis. The effect of operational conditions on the obtained profiles will be discussed for both CEF and HT-TGIC in order to find out the set of conditions that enhances the resolution of the measured CCDs.

A mathematical model is needed to quantify the information provided by these analytical techniques and to relate it to the presence of multiple site types on Ziegler-Natta catalysts. Another main objective of this thesis was to develop a mathematical model to deconvolute the MWD and CCD of ethylene/α-olefin copolymers simultaneously, considering the room temperature soluble fraction commonly present in LLDPE.

1.2 THESIS CONTENT

A brief review of relevant information reported in the open literature regarding Ziegler-Natta and metallocene catalysts and polymerization mechanism is given in Chapter 2. Polyolefin characterization techniques are also reviewed in this chapter. Chapter 3 summarizes our results on the mathematical modeling of MWD and CCD using Stockmayer’s bivariate distribution. Chapter 4 describes the experimental details of the characterization techniques used in this thesis. Chapter 5 describes the effect of operating conditions on HT-TGIC. In Chapter 6, HT-TGIC profiles using three different solvents were compared. The study presented in this chapter shows that solvent type plays a major role in determining the significance of co-adsorption and co-desorption effects on HT-TGIC profiles. Finally, Chapter 7 discusses the effect of operating conditions on CEF analysis of ethylene/1-octene copolymers made with metallocene and Ziegler-Natta catalysts. Chapter 8 summarizes the conclusions for the entire work.

Chapter 2

LITERATURE REVIEW

2.1 ZIEGLER-NATTA AND METALLOCENE CATALYSTS

Ziegler-Natta catalysts are composed of a derivative of transition metals from the Periodic Table groups 4 to 8 (known as the catalyst) and an organometallic compound (known as the cocatalyst).[4,5] The typical transition metal compounds in Ziegler-Natta catalysts are $TiCl_4$, $TiCl_3$, VCl_4, and $VOCl_3$. The organometallic cocatalysts are mostly aluminum compounds such as trimethyl aluminum ($Al(CH_3)_3$) and triethyl aluminum ($Al(C_2H_5)_3$). The cocatalyst (AlR_3) in a Ziegler-Natta catalyst system acts as an alkylating and reducing agent. Ziegler-Natta catalysts are generally heterogeneous (insoluble in the reaction medium), although Ziegler-Natta vanadium catalysts are homogeneous.

In the 1940s, Ziegler and co-workers synthesized aluminum alkyls and combined them with transition metal salts to make catalysts for ethylene polymerization. The product was HDPE and the procedure was transferred into an industrial process within a few months.[6,7] Polyolefin manufacturers such as DuPont, Union Carbide and The Dow Chemical Company were able, in the late 1950s to the late 1960s, to copolymerize ethylene with α-olefin to produce LLDPE.[1] The catalyst described by Ziegler, $TiCl_3$, suffered from low activities. A step for removing catalyst residues (de-ashing) from the polyethylene was needed to achieve marketable products. The discovery of $MgCl_2$-supported $TiCl_4$ catalysts led to more than 100 times higher activities than those of $TiCl_3$ catalysts.[8,9] This catalyst system became the most common type of Ziegler-Natta catalyst not only because of its high activity but also because of its ability to produce polymer particles with excellent morphology. Figure 2.1 shows a representative chemical structure of a $MgCl_2$-supported $TiCl_4$ catalyst.

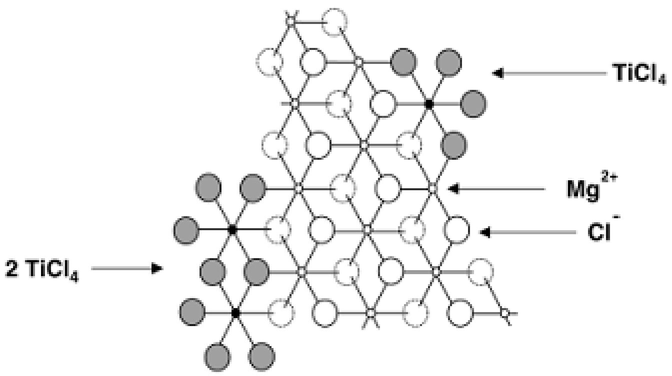

Figure 2.1 An example of a heterogeneous Ziegler-Natta catalyst.

Metallocene catalysts, on the other hand, are organometallic compounds composed of a transition metal (typically Ti, Zr, HF) bonded to one or more cyclopentadienyl rings (Cp) via π-bonds (Figure 2.2). Examples of metallocene catalysts are shown in Figure 2.3. Metallocene catalysts are generally activated by a cocatalyst that acts as alkylating and ionizing agent and forms metallocenium alkyl cations. Methylaluminoxane (MAO) is mostly used as a cocatalyst and is produced by the controlled hydrolysis of trimethylaluminum.[10] MAO is more effective as cocatalyst than other aluminoxanes such as ethylaluminoxane and isobutylaluminoxane.[11] In general, a large MAO to catalyst ratio is necessary to reach high polymerization activities (1000:1-50,000:1) in homogeneous systems.[12] Polymer properties such as MWD and density are affected by this ratio.[13,14,15,16] The nature and the number of cyclopentadienyl rings, the constituents of the bridge, if present, the cocatalyst type, and the nature of transition metal are important factors that regulate the catalytic behavior of metallocene catalysts towards the polymerization of olefins. These factors influence regio- and steroselectivity, hydrogen response, and catalyst activity, as well as comonomer incorporation capability and molecular weight of the product.[17,18,19,20]

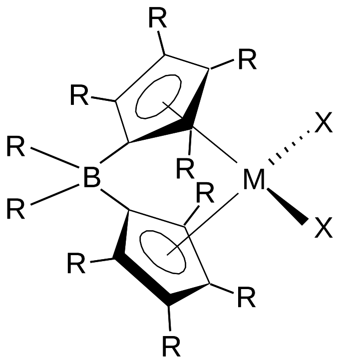

Figure 2.2 Generalized structure of a metallocene catalyst. M: transition metal; X: hydrocarbyl, alkylidene, halogen radicals; R: hydrogen, hydrocarbyl radicals; B – bridging group.

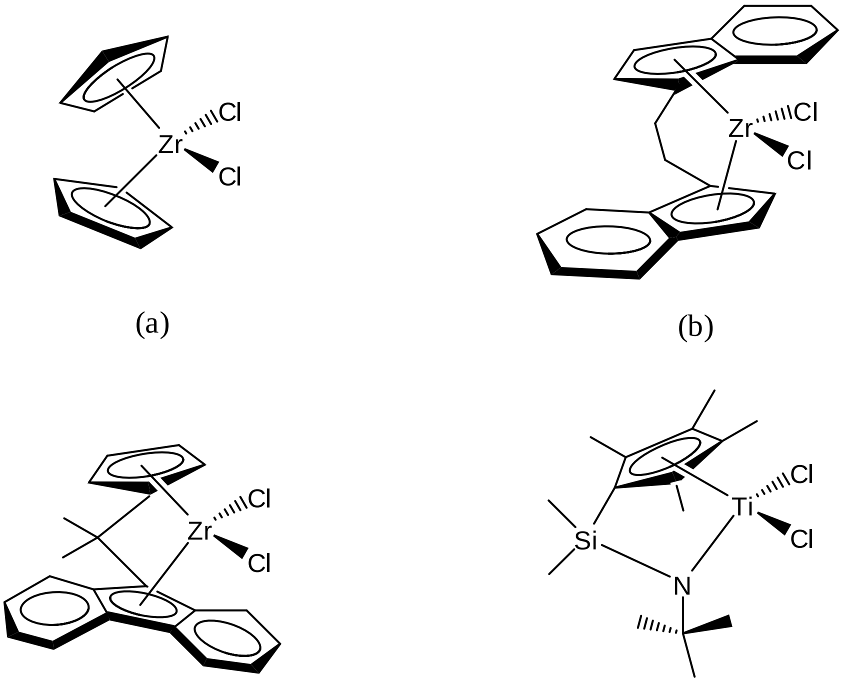

(a)
(b)
(c)
(d)

Figure 2.3 Some examples of metallocene catalysts: (a) Cp_2ZrCl_2; (b) rac-$Et(Ind)_2ZrCl_2$; (c) iPr(Flu)(Cp)$ZrCl_2$; (d) Constrained geometry catalyst (CGC).

Although it has a great influence on the metallocene activity, the exact role of the aluminoxane is not fully understood. In addition to acting as an alkylation agent and an impurity scavenger, aluminoxanes are involved in the formation of active sites, as shown schematically in Figure 2.4, and in the prevention of their deactivation by bimolecular processes. Eilertsen *et al*. studied the activation of metallocenes by MAO (Cp_2ZrCl_2 and Cp_2ZrMe_2, Cp= cyclopentadienyl, Me= methyl) using in situ IR spectroscopy.[22] They proposed a mechanism to explain the need for a required large MAO excess involves the formation of cages of dimmers or oligomers of MAO. Those cages tend to spread out the charge of the anion and facilitate the formation of the active site.

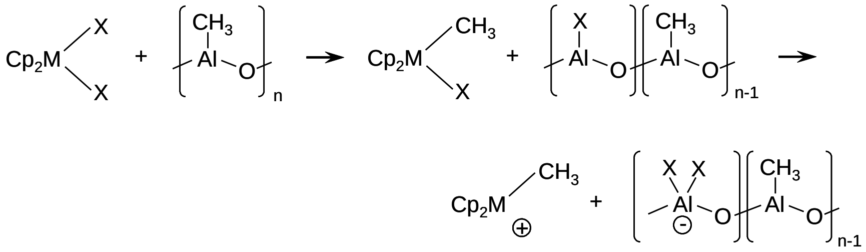

Figure 2.4 Activation of a metallocene catalyst using MAO cocatalyst.[21]

For the production of commercial LLDPE, the catalyst plays an important role in defining the molecular structures of the different grades of LLDPEs. Therefore, Ziegler-Natta LLDPE and metallocene LLDPE are commonly used to classify LLDPEs according to their parent catalysts. Heterogeneous Ziegler-Natta catalysts produce LLDPE with broad MWD and CCD, since the catalyst has more than one active site type, and each one produces PE chains with different average comonomer content and molecular weight.[23,24,25,26,27] Contrarily, metallocene catalysts make LLDPE with a much more uniform microstructure than Ziegler-Natta LLDPE because they are generally accepted to have only a single site type.

Kaminsky and co-workers studied the copolymerization of ethylene with 1-butene using Cp_2ZrCl_2/MAO and found that the product had a melting point that was lower than that of a similar copolymer (having the same average comonomer content) made with Ziegler-Natta catalyst.[28] These results support the assumption that Cp_2ZrCl_2 produces polymer with uniform comonomer distribution. The microstructural differences between Ziegler-Natta LLDPE and metallocene LLDPE are illustrated schematically in Figure 2.5, by showing the MWD and the average comonomer incorporation in the copolymer as a function of molecular weight.

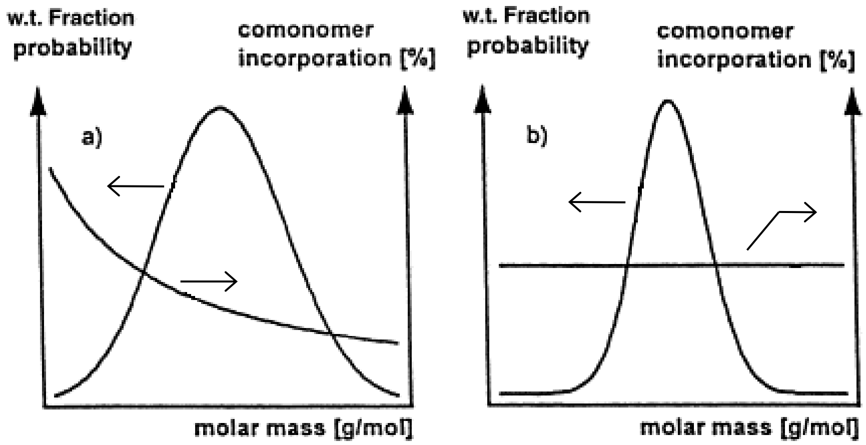

Figure 2.5 Schematic MWDs and α-olefin incorporation as function of MW for polyethylene made with Ziegler-Natta (a) and metallocene (b) catalysts.

The development of single-site catalyst technology paved the way to tailor the molecular structure of polyolefin products according to customer's demands by varying the catalyst structures and process conditions. Dow's constrained geometry catalyst (CGC) (Figure 2.3.d), a metallocene catalyst with a single cyclopentadienyl ring, is an example of a single-site type catalyst that is commercially used for tailor-making polymers. The catalyst shows high incorporation of α-olefins and high catalyst activity. CGC also forms LCBs during ethylene/α-olefin copolymerization. Therefore, the resulting copolymers have both excellent physical properties and melt processability as compared to LDPE and other metallocene LLDPE.[29]

The well-controlled microstructures of polymer made with metallocene catalysts can also be used to help develop polymerization models, since models created for single-site type catalysts can be extended to represent the more complex structures of polymers made with multiple-site type catalysts.[30,31]

2.2 POLYMERIZATION MECHANISM

Ziegler-Natta olefin polymerization is one of the most important catalytic processes in the commodity polymer industry. Since its discovery, this class of catalytic reactions aroused the interest of many research groups and discussion started on how the catalyst could transform ethylene into polyethylene. The mechanism of polymerization consists of three main steps: formation of active sites, propagation reactions, and chain transfer reactions. The polymerization mechanism and kinetics with Ziegler-Natta catalysts have been described in details in the literature.[24,25,31]

2.2.1 FORMATION OF ACTIVE SITES

The first step in the polymerization process is the reaction between catalyst and cocatalyst to form active sites. This reaction is shown in Figure 2.6. The cocatalyst (AlR_3) extracts two halogen atoms from, and transfers an alkyl group to, the transition metal. This step leads to the formation of a cationic active site and a cocatalyst product ($AlR_2X_2^-$) as a non-coordinating anion that is required to stabilize the catalyst.

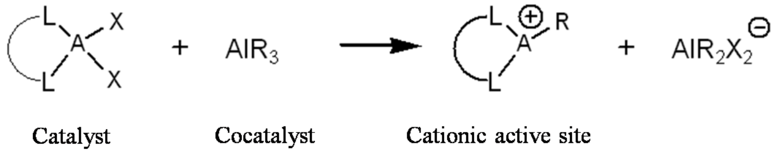

Figure 2.6 Formation of active site by reaction with cocatalyst, A: transition metal center, L: ligands, X: halogen atom, R: alkyl group.

2.2.2 PROPAGATION REACTIONS

After the formation of the active sites, ethylene may coordinate and insert onto the metal center, forming a living polymer chain. Different mechanisms have been proposed to explain this step; however, Cossee-Arlman's mechanism is one of the most accredited models for polymerization with coordination catalysts.[32,33,34] In this model, an incoming ethylene monomer coordinates to a vacant Ti site via its carbon double bond. It is assumed that the transition metal is under-coordinated, a 5-fold titanium site, in which one of the bonds is a titanium-carbon bond (Ti-C). This bond can belong to a methyl group, resulting from the alkylation reaction of the catalyst by the cocatalyst, or to a CH_2 unit of the already formed polymeric chain. In the next step, a transition state is formed in which the Ti-C and the carbon-carbon double bond of the incoming ethylene form a four-member ring structure as shown in Figure 2.7. This is followed by a final step in which the complete insertion of the monomer occurs between the carbon-metal bond. Once the insertion has been completed, the system comes to the initial catalytic state, i.e. a new free coordination site is generated at the vacant position of the former alkyl ligand. Then, a new cycle begins toward a new insertion that lengthens the growing polymeric chain by another monomer unit. Since the monomer is inserted between the carbon-metal bond, the kinetics of polymerization and the polymer microstructure are greatly affected by the electronic and steric environment surrounding the transition metal active site.

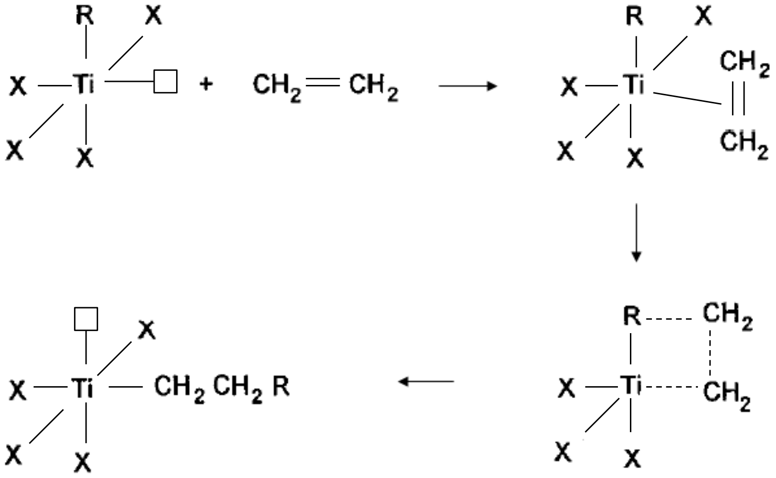

Figure 2.7 Coordination and insertion of ethylene into the active site of a transition metal catalyst according to the Cossee-Arlman's mechanism.

Both Kaminsky[11] and Corradini[35] have adapted the Cossee-Arlman mechanism to metallocene catalysts. There are two ways for ethylene to approach a metallocene catalyst such as Cp_2ZrR^+: a frontside or a backside attack. It has been reported by Lohrenz *et al.* that the frontside attack has a lower activation energy barrier than the backside orientation;

therefore, from a kinetic point of view, the frontside coordination is more favorable. [36] This suggests that two ethylene molecules may approach the metallocene catalyst from both sides, but only one will be inserted. That is why most of the theoretical work in the literature describing the ethylene polymerization with metallocenes system assumes a reaction order of one for the monomer concentration.

Ystenes[37,38] proposed an alternative mechanism for polymerization with coordination catalysts, known as the trigger mechanism (Figure 2.8). It considers the participation of two monomers during the insertion step. It is assumed that the active sites are never free; instead, they are always occupied by a coordinated monomer. The coordinated monomer is inserted into the growing chain if and only if another monomer is ready to replace it. Some researchers have reported reaction orders greater than one (1.0 to 2.0) with respect to monomer concentration, which agree with the trigger mechanism.[39,40]

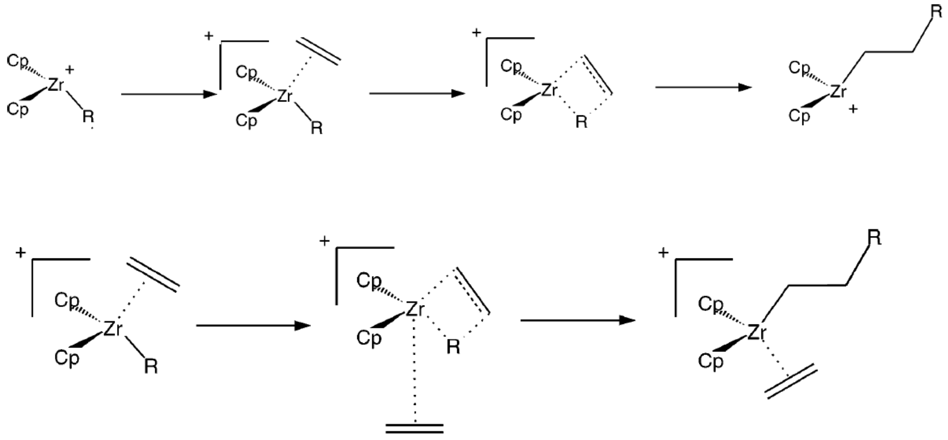

Figure 2.8 Cosse-Arlman's mechanism (top) and trigger mechanism (bottom) for a metallocene catalyst.

2.2.3 CHAIN TRANSFER REACTIONS

During propagation reactions, the length of the polymer chain increases by the repeated insertions of monomers into the carbon-metal bond until a chain transfer reaction takes place, resulting in a dead polymer chain and freeing up the active site to make another polymer chain. β-Hydride and β-methyl elimination (for the case of propylene) reactions lead to the formation of dead chains with vinyl groups. In the presence of certain catalysts (such as Dow's CGC), these vinyl-terminated dead polymer chains (also called macromonomers) can participate in further coordination steps which form long chain branches (LCB). The degree of LCB formation reactions depends on the nature of the catalyst. The ratio of chain propagation to β-hydride elimination is around 10^4:1 at 80 °C for ethylene polymerization using $TiCl_4/Al(C_2H_5)_3$.[41] Chain transfer can also proceed by transfer to hydrogen, monomer, or cocatalyst (Figure 2.9). The most important chain transfer reaction for industrial olefin polymerization processes is chain transfer to hydrogen.[42] Hydrogen can compete with ethylene monomers for the active sites and coordinate to the metal center forming a dihydrido complex. This complex facilitates the elimination of a saturated dead polymer chain and the formation of a new vacant site that can be used for further monomer insertions.[17,43] Han *et al.*[44], Kaminsky[45], and D'Agnillo *et al.*[46] showed that only traces of hydrogen are required to reduce the molecular weight of polymer produced by a zirconocene catalyst. Thorshang *et al.* studied the termination mechanism during ethylene polymerization with a metallocene catalyst (Cp_2ZrCl_2/MAO).[47] According to their results, transfer to monomer is suggested to dominate in this system. The same conclusion was supported by others.[36,46]

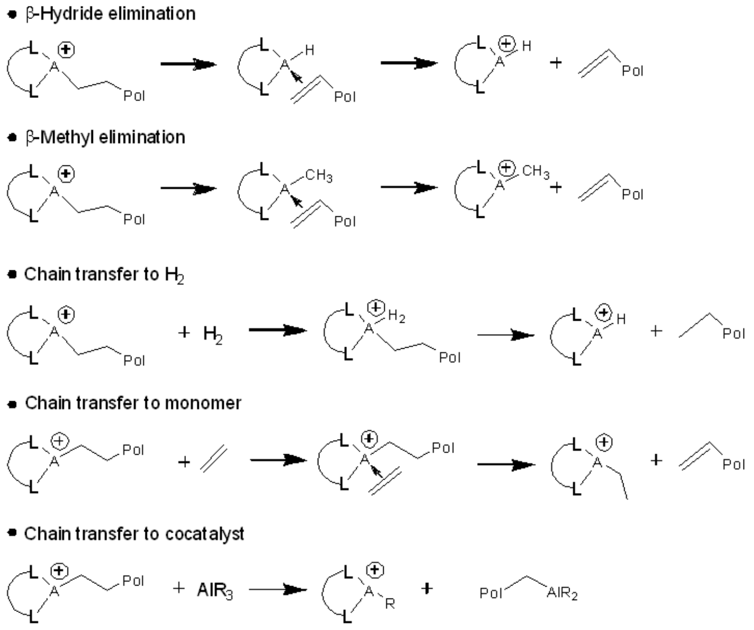

Figure 2.9 Chain transfer reactions, A: transition metal center, L: ligands, X: halogen atom, R: alkyl group.[31]

2.2.4 COPOLYMERIZATION WITH α-OLEFINS

The discussion in the previous sections describes the homopolymerization of ethylene with Ziegler-Natta and metallocene catalysts; it can be easily extended to the copolymerization of ethylene and 1-alkenes. Copolymerization is a very important process in the LLDPE industry. Although copolymerization of ethylene with α-olefins using Ziegler-Natta catalysts still dominates the LLDPE industry,[48,49] extensive studies have been directed to copolymerization using metallocene catalysts.[49,50,51,52] During copolymerization reactions with a given catalyst/cocatalyst system, the type of coordinating monomer and the type of the last monomer inserted into the growing chain affect the values of the propagation and chain transfer rate constants.[31]

The addition of α-olefins to the polymerization medium decreases the polyethylene molecular weight and crystallinity. Generally, it also increases the overall polymerization rate.[53,54,55,56] This is in contrast with standard copolymerization theory that predicts a decrease in polymerization rate because of the lower reactivity of α-olefins as compared with ethylene. The magnitude of the comonomer rate increase depends on the catalyst system and the type of comonomer employed.[57] Several causes, both chemical and physical, have been proposed to explain the comonomer effect. Using the trigger mechanism, it has been proposed that α-olefins coordinate at the active site and trigger the insertion of ethylene and, therefore, increase the propagation rate constant (k_p).[37,38] Kissin and coworkers[54,58,59] proposed an alternative hypothesis in which the presence of Ti-C_2H_5 bonds (formed after transfer to ethylene, or after transfer to hydrogen followed by the first ethylene insertion) in the active centers strongly decrease their reactivity because of the stabilization effect by an agostic interaction between the hydrogen of the methyl group and the titanium atom. However, the insertion of a higher α-olefin in the Ti-polymer bond prevents the formation of such dormant centers. Physical factors, on the other hand, may include pure diffusion phenomena, in which the diffusion of ethylene and/or aluminum alkyl is slow for catalyst particles surrounded by high density polyethylene produced in the absence of the α-olefin comonomer. However, the rate of monomer and cocatalyst diffusion is higher when copolymer of low crystallinity is formed around active sites.[53,60,61]

It has been reported that ethylene polymerization with a $TiCl_4/MgCl_2$ catalyst was accelerated by 1-hexene and the rate increase depended upon the Mg/Ti ratio. The greatest increase was found at a Mg/Ti ratio of 0.42; however, no comonomer rate increase was observed above a Mg/Ti ratio of 2.5.[62] Chen *et al.* studied the copolymerization of ethylene with 1-hexene using $TiCl_4/AlCl_3/MgCl_2$ and observed a significant increase (about 2-3 times) in copolymerization rate as compared with that of ethylene homopolymerization at the same conditions.[63] According to their results, when $AlEt_3$ was replaced by $Al(i\text{-}Bu)_3$, the comonomer incorporation was significantly increased. Other studies showed a rate increase of ethylene polymerization in the presence of propylene [64], 1-octene [65], and 4-methyl-pentene-1[65]. The rate enhancement of ethylene polymerization in the presence of α-olefin is a general trend for heterogeneous Ziegler-Natta catalysts.

Kinetic studies of ethylene copolymerization using a Cp_2ZrCl_2/MAO catalyst were carried out in the presence of propylene and 1-hexene. The magnitudes of the activity increase due to these comonomers were 1.5 and 2, respectively.[56] However, with metallocene catalysts the effect of the comonomer is not always positive. The work of Chien and Nozaki showed that 1-hexene reduces the polymerization rate of ethylene with a zirconocene catalyst (Cp_2ZrCl_2/MAO).[66] This result has been supported by the recent study of Awudza and Tait.[67] They studied homogeneous and silica-supported Cp_2ZrCl_2/MAO catalyst for the copolymerization of ethylene with 1-butene, 1-hexene, 4-methylpentene-1, and 1-octene. The results for the homogeneous catalyst at 70 °C indicated that there was a negative comonomer effect, while at 50 °C the comonomer increased the polymerization rate. The results for the supported catalyst showed a positive effect at both 50 and 70 °C. Active center studies showed that there was a reduction in active center concentration during copolymerization with the homogeneous catalyst at 70 °C, which may be used to explain the observed rate depression at this temperature.

2.3 CHARACTERIZATION TECHNIQUES OF POLYOLEFINS

Owing to the different nature of Ziegler-Natta and metallocene catalysts, a variety of LLDPEs with distinct microstructures are produced worldwide. The end-use properties of

LLDPEs depend not only on their average molecular weight and chemical composition, but also on their MWD and CCD or SCBD. Therefore, it comes as no surprise that the characterization of LLDPE in terms of MWD and CCD is of great interest in both industry and academia.

High-temperature gel permeation chromatography (GPC) has long been used to measure the MWD of polymers. Temperature rising elution fractionation (TREF) and crystallization analysis fractionation (CRYSTAF), which fractionate semicrystalline polymers according to their crystallizabilities from dilute solution, have been widely employed to measure the CCD of LLDPE. For the measurement of average short chain branching (or average copolymer composition), techniques such as Fourier-transform infrared spectroscopy (FTIR) and nuclear magnetic resonance (NMR) are available. Thermal fractionation by differential scanning calorimetry (DSC) may also be used as an alternative technique for polymer compositional characterization, although its quantitative interpretation can be quite difficult. The thermal segregation process, which occurs during isothermal and dynamic crystallization from the melt, can be used to characterize LLDPE chains according to their crystal sizes or methylene sequence distribution. Although DSC is solvent free and faster than TREF, the results are difficult to translate into the corresponding CCDs due to strong cocrystallization effects in the polymer melt.

Perhaps one of the most important applications of TREF is its use to study the multiple site nature of Ziegler-Natta catalysts. Usami *et al*, [68] in a landmark paper, compared the CCDs of four LLDPE samples made by different processes, as shown in Figure 2.10, with that of a LDPE sample. The four LLDPEs have broader and bimodal TREF profiles that can be related to the presence of at least two distinct types of active sites on the heterogeneous Ziegler-Natta catalyst used to produce them. Contrarily, LDPE has narrower and unimodal CCD, as expected from the free radical polymerization mechanism used to make it. Similar results were also obtained by other authors.[69,70]

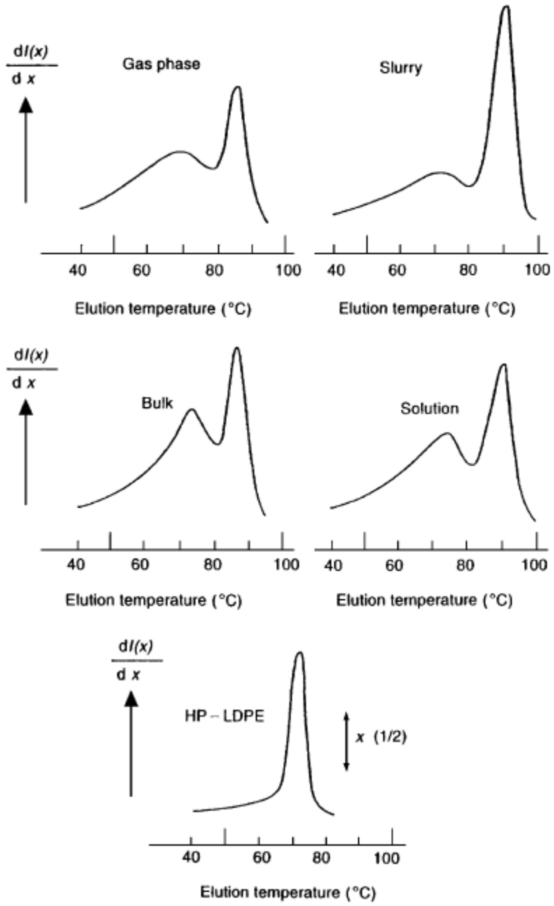

Figure 2.10 Comparison of TREF profiles of four LLDPEs, made by heterogeneous Ziegler-Natta catalysts at different conditions and of a LDPE made with high-pressure free radical polymerization.[68]

2.3.1 High-temperature GPC

High-temperature GPC, also known as high-temperature size exclusion chromatography (SEC), is the most common method for the determination of MWDs of polymers. Properties such as tensile strength tend to increase as MWD narrows, and properties such as elongation and yield strength tend to increase as MWD broadens. Therefore, the determination of MWD of polymers is essential to their understanding.

High-temperature GPC is a liquid chromatographic technique in which the polymer molecules are fractionated according to their hydrodynamic volume. In GPC analysis, a dilute polymer solution is injected into a solvent stream, which then flows through a series of columns packed with material of narrow particle size distribution and controlled pore sizes, such as cross-linked styrene-divinyl benzene gels. The smaller molecules are able to pass through most of the pores and, therefore, have a relatively long flow path through the column. The larger ones are excluded from all but the largest pores and hence elute first. As the polymer molecules elute from the column, they are detected by a concentration detector, such as a refractive index (RI) or, more recently, a single-frequency infrared detector, to produce an elution volume curve. In order to obtain a MWD, the column must be calibrated with a series of narrow standards of known molecular weight averages of the same type of the polymer being analyzed, resulting in a calibration curve relating log MW to retention volume. An alternative, and more commonly found approach, is to use the universal calibration method, in which a relationship between the hydrodynamic volume of the polymer standards (typically narrow MWD polystyrene) and the retention volume is used to accurately calibrate the GPC column. There is a linear and nearly universal relationship between log (IV•MW), as a direct measure of hydrodynamic volume, and the retention volume. Such a calibration curve is shown in Figure 2.11, where IV is the intrinsic viscosity. The relation between IV and MW is described by the Mark-Houwink equation or measured using an on-line differential viscometer.

Using GPC coupled with a viscometer, MWD and intrinsic viscosity distributions as function of MW were reported for polymer standards and commercial polymers.[71,72] Alternatively, the simultaneous measurement of light scattering intensity and polymer concentration allows for the direct determination of the weight average molecular weight of the eluted fraction, without the need of a calibration curve.[73] When a two-angle or a multi-angle light scattering detector is connected to a GPC, the radius of gyration (R_g) of the polymer coils in the detector cell as a function of their molecular weights can be obtained.[74]

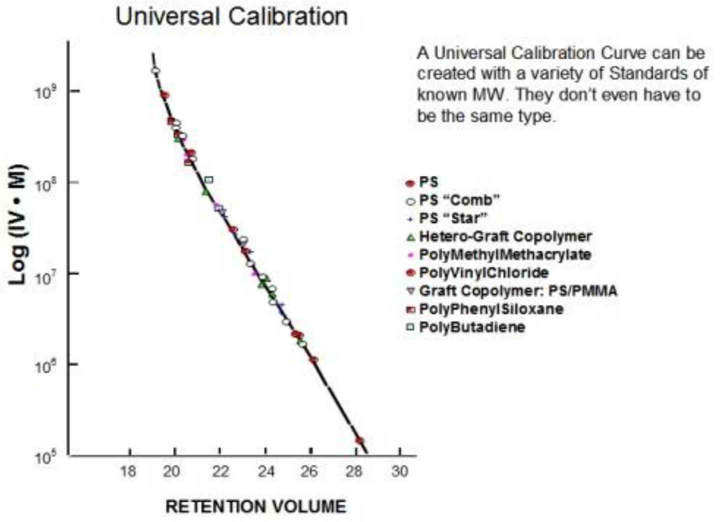

Figure 2.11 Universal calibration curve.

LLDPEs made with heterogeneous Ziegler-Natta catalysts have a complex relation between MWD and average comonomer content. When GPC is coupled to an FTIR detector, information on the average chemical composition of the chromatographic fractions can be measured,[75,76] as depicted in Figure 2.12.

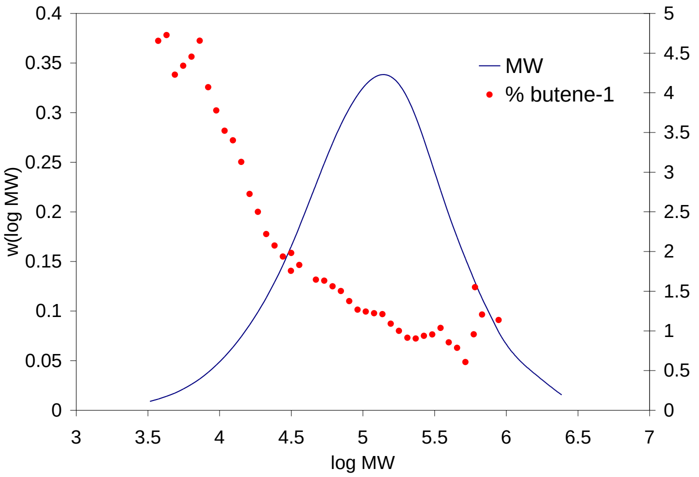

Figure 2.12 MWD and average comonomer content as a function of MW for a Ziegler-Natta LLDPE measured by GPC/IR instrument.[75]

This profile is in sharp contrast with that of a single-site metallocene LLDPE, where the average comonomer content in the copolymer does not depend on its molecular weight (Figure 2.5.b).[31,75]

2.3.2 TREF, CRYSTAF, and CEF

TREF and CRYSTAF are analytical techniques that fractionate semi-crystalline polymers based on differences in crystallizability of the macromolecules. In TREF analysis, the sample is first dissolved in a proper solvent, usually trichlorobenzene (TCB), at high temperature. Then, the solution is introduced into the TREF column which contains an inert support such as glass beads, silica gel or steel shots. This is followed by a crystallization step in which the temperature is slowly decreased down to room temperature, typically at 2 ^{o}C/h for enhanced resolution. Since polymer chains with higher comonomer fraction have a low crystallization temperature,[77] the polymer fractionation occurs as the temperature in the TREF column is reduced. The fractions precipitate from the solution and coat the support (ideally) in layers of different crystallinity.[78] The most easily crystallizable fraction, which has the lowest comonomer content, precipitates first and forms the innermost layer on the support. Contrarily, the fraction with the least crystallinity, which has the highest comonomer content, precipitates last and deposits on the outermost layer of the support (Figure 2.13). In the next fractionation step, the precipitated polymer is eluted with solvent at increasing temperatures. The solvent first removes the least crystalline fractions, followed by the more crystalline fractions. These fractions are collected in preparative TREF (P-TREF) mode or their concentrations are measured using an online temperature-insensitive IR detector in analytical TREF (A-TREF). P-TREF is used to fractionate polymer into fractions of larger sizes that can be characterized off line by ^{13}C NMR, FTIR, DSC, GPC, or any other analytical technique of interest. A-TREF requires a very small polymer sample (typically a few milligrams) and is only used to generate the CCD of the polymer.

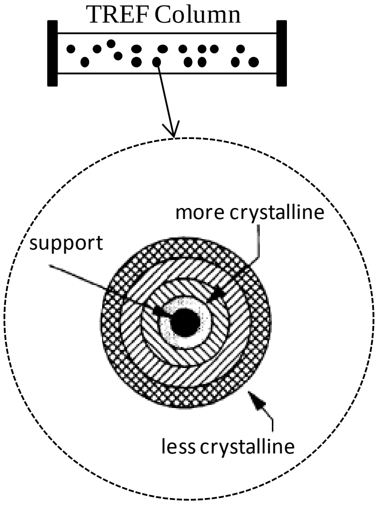

Figure 2.13 Polymer layers of different crystallinities coating the TREF support, exaggerated for illustration purposes.[79]

As mentioned above, fractionation in TREF is achieved by two temperature cycles: crystallization and elution. Monrabal [80,81] developed CRYSTAF as a faster alternative to TREF, since only the crystallization step is needed. In CRYSTAF, the polymer solution at high temperature is injected into a crystallization vessel that does not contain any support. The temperature is reduced at a slow, constant cooling rate. During crystallization, the polymer solution concentration is continuously monitored using an IR mass detector to obtain the cumulative curve of polymer solution concentration versus crystallization temperature. The first derivative of this integral curve gives the CRYSTAF derivative profile as a function of crystallization temperature. This curve is similar in shape to an A-TREF profile; however, CRYSTAF curves are shifted to lower temperatures, since TREF profiles are measured during polymer dissolution, while CRYSTAF curves are determined during polymer crystallization.

Recently, Monrabal *et al.*[82] developed a new fractionation technique, known as crystallization elution fractionation (CEF). Similar to TREF and CRYSTAF, CEF fractionates semicrystalline polymers according to their crystallizability. It also requires two temperature cycles like TREF (Figure 2.14). However, in CEF fractionation a small solvent flow is pumped through the column during the crystallization step. When the crystallization temperature of a fraction is reached, it is separated and deposited on the support while the other fractions are still soluble in the solvent and moving along the column until their crystallization temperatures are reached. Thus, CEF minimizes cocrystallization effects by segregating crystallites of different crystallizabilies within the column. Consequently, the analysis time is dramatically decreased without compromising the CEF resolution.

CEF is one of the polyolefin characterization techniques that will be studied in details in this thesis. More information about the CEF will be provided in the following chapters.

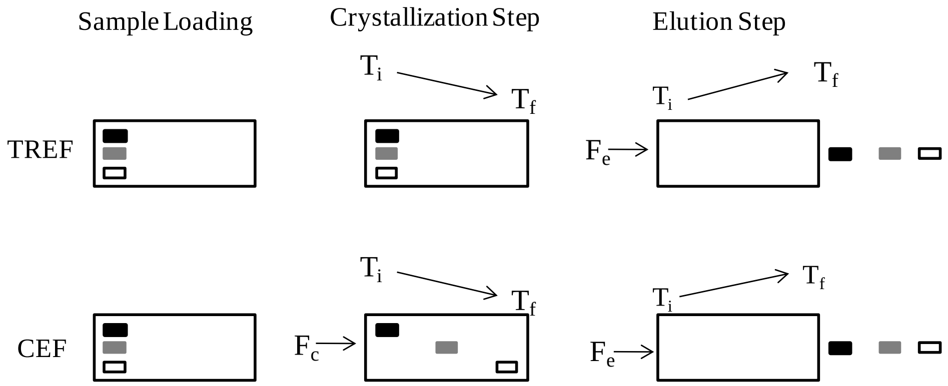

Figure 2.14 Separation diagram of three components by crystallizability. Top: TREF, and bottom: CEF.[82]

2.3.2.1 CALIBRATION CURVE

Both TREF and CRYSTAF can be calibrated to obtain CCDs from their elution or crystallization curves. Comonomer content and molecular weight are the main structural factors affecting the crystallizability of polymer molecules. Pennings[83] demonstrated that during crystallization of linear polyethylene from dilute solution, some molecules with similar molecular weight tend to cocrystallize. However, Wild *et al*.[84] generated a calibration curve relating TREF elution temperatures to short chain branching content which indicates that the molecular weight may not affect TREF peak positions strongly. They studied a series of narrow MWD linear polyethylene samples and showed that the elution temperature, and hence the polymer crystallinity, was independent of molecular weight for polymers with MW higher than 10,000. The study of Nieto *et al*.[85] illustrates that

CRYSTAF peak temperature is practically independent of molecular weight for samples with number-average molecular weights higher than 5,000. Figure 2.15 shows the relationship between chain length and CRYSTAF peak temperature. Therefore, TREF and CRYSTAF profiles are relatively insensitive to the molecular weights of most industrial LLDPE resins, since they usually have high molecular weights.

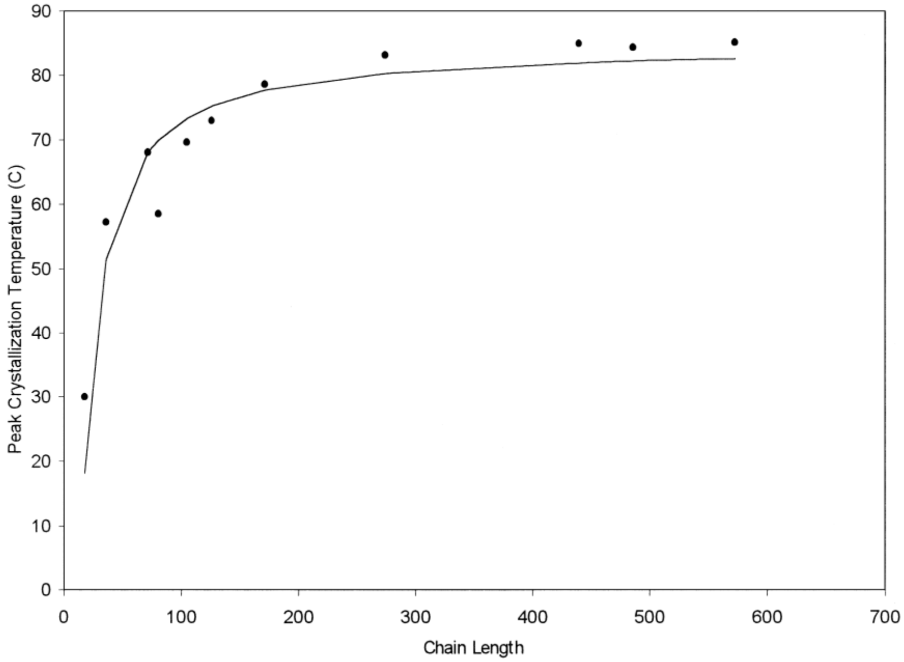

Figure 2.15 Effect of chain length on CRYSTAF peak temperature. [85]

In general, the relationship between comonomer content and elution or crystallization temperatures is linear, but not universal. As the comonomer content increases, the elution or crystallization temperature decreases.

Preparative TREF can be used to fractionate LLDPE samples made with heterogeneous Ziegler-Natta catalysts. The resulting narrow CCD fractions can be analyzed by ^{13}C NMR or FTIR spectroscopy to determine their average comonomer contents as a function of their elution temperatures and create a calibration curve. da Silva Filho *et al*. used this approach to calibrate TREF for ethylene/1-butene and ethylene/1-octene copolymers, as shown in Figure 2.16.[86] The two curves indicate that the calibration curve of ethylene/1-octene copolymers is shifted to lower temperatures with respect to that of ethylene/1-butene copolymers because the longer branches formed by 1-octene are more effective in disrupting the crystal regular packing than the shorter ones resulting from 1-butene.[87] Sarzotti *et al.* used ethylene/1-hexene metallocene copolymers with narrow, unimodal CCDs, covering a wide range of comonomer contents, to obtain a calibration curve for CRYSTAF.[88] These CRYSTAF profiles, illustrated in Figure 2.17, clearly show that the CCD of LLDPE tends to broaden as the comonomer content increases, as theoretically expected. The same trend has been reported in the presence of different α-olefins.[89]

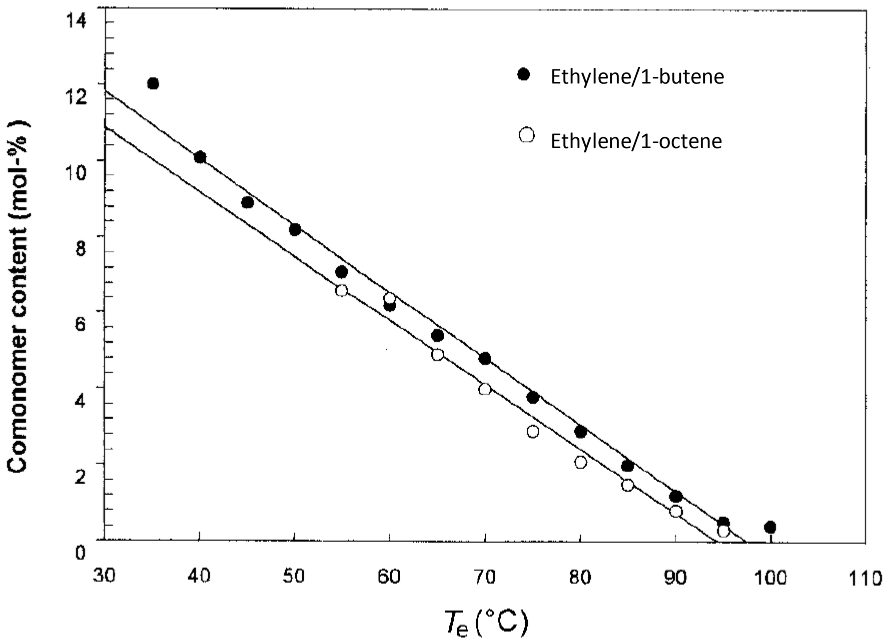

Figure 2.16 TREF calibration curves for ethylene/1-butene and ethylene/1-octene copolymers.[86]

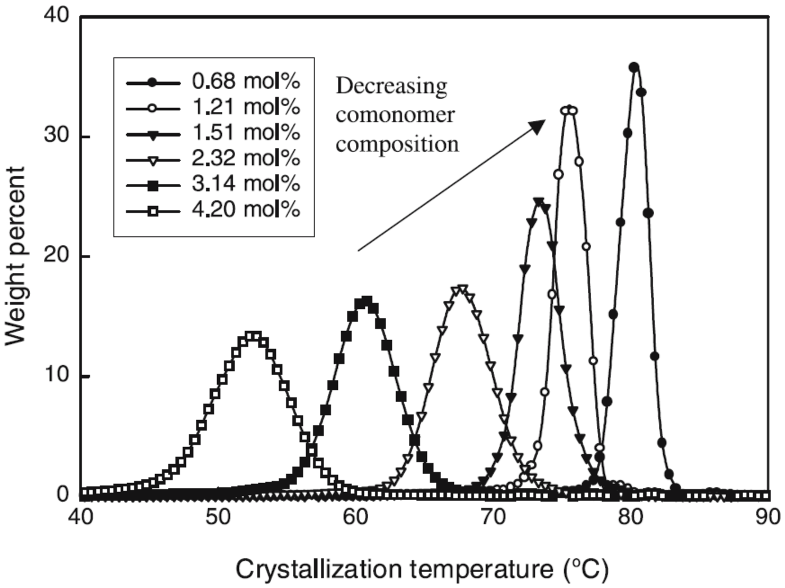

Figure 2.17 Effect of comonomer content on CRYSTAF profiles.[88]

2.3.2.2 EFFECT OF OPERATION CONDITIONS

The operation conditions of TREF and CRYSTAF affect the profiles generated by these instruments. As mentioned above, the crystallization step is of great importance for both techniques. The cooling rate is a key parameter, since it ensures that polymer molecules precipitate orderly according to their crystallizabilities, minimizing cocrystallization effects. The effect of cooling rate on TREF profiles is shown in Figure 2.18.[90] The CCDs shift to higher temperatures for slower cooling rates. The same trend is observed for CRYSTAF profiles; however, CRYSTAF peak temperatures are even more strongly affected by the cooling rate than TREF peak temperatures. Anantawarskul *et al*. found an empirical linear relationship between CRYSTAF peak temperature and the natural logarithm of the cooling rate.[90] They also studied the effect of heating rate during the elution step of TREF and observed that the profiles are shifted to higher temperatures at higher heating rates. Moreover, increasing the heating rate tend to broaden the TREF profiles since the solvent at higher heating rates will elute polymer over a wider range of crystallinities. From these observations, it was suggested that using a constant ratio of cooling rate: heating rate: solvent flow rate of 1:1:1 was required to have similar TREF profiles at different operation conditions (Figure 2.19). Aust *et al*. also studied the effect of operation conditions on the separation quality of TREF. Their results indicated that increasing cooling rate or heating rate had a negative effect on TREF efficiency. Moreover, they found that increasing the start temperature for crystallization had a strong positive effect on the quality of separation.[91] The authors concluded that using the optimized run parameters led to a significant increase in TREF resolution for ethylene/propylene copolymers.

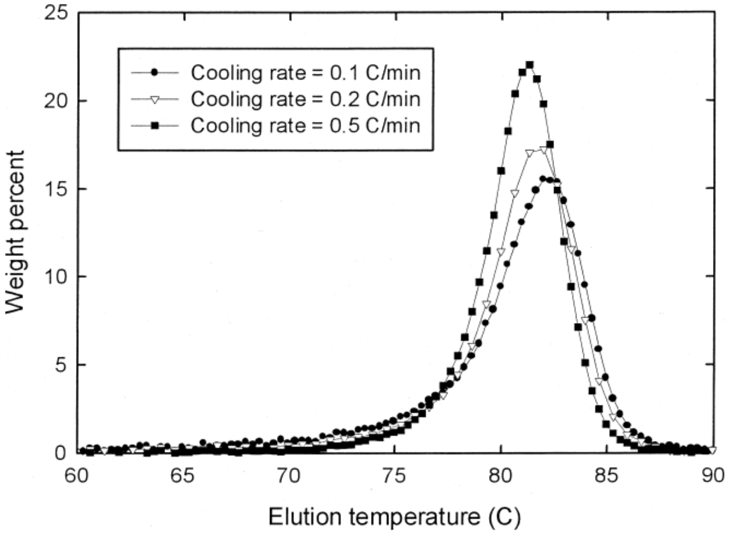

Figure 2.18 Effect of cooling rate on TREF profiles.[90]

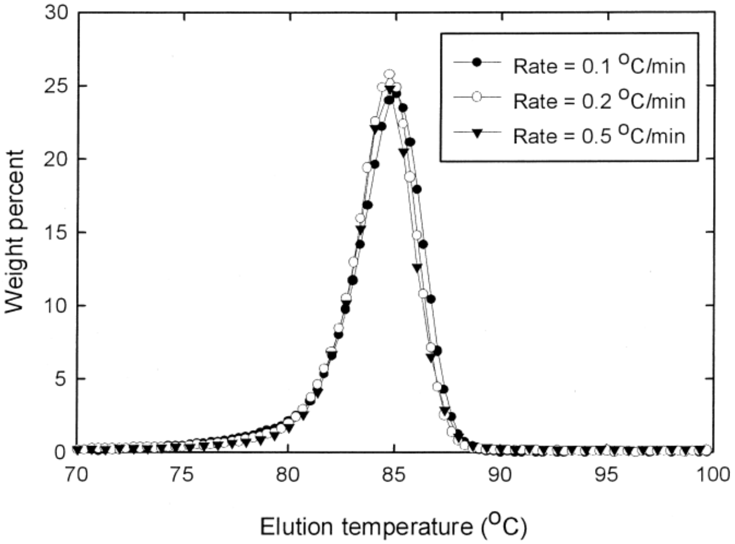

Figure 2.19 Comparison between TREF profiles of the same sample when the ratio of cooling rate: heating rate: solvent flow rate is 1:1:1.[90]

2.3.2.3 EFFECT OF CO-CRYSTALLIZATION

Co-crystallization is a phenomenon in which polymer chains of different compositions tend to crystallize together. Co-crystallization results in broadening of TREF and CRYSTAF peaks and tends to merge several peaks together when they are sufficiently close. The microstructural properties of the polymer and the operating conditions of TREF and CRYSTAF play a major role in determining the effect of co-crystallization. Wild *et al*.[84] investigated the effect of co-crystallization by studying the TREF profile of a blend of three polyethylene samples: one HDPE and two LLDPEs with different short chain branching frequencies (6.2 and 19.1 methyls per 1,000 carbon atoms). The comparison between the TREF curve of the blend and the curve resulting from the summation of TREF profiles of each polyethylene in the blend is shown in Figure 2.20. The good agreement between the two curves indicates that co-crystallization can be neglected in this case, since the samples have significantly different crystallizabilities. The same conclusion was found by Kelusky *et al*. [92] for a poly(ethylene vinyl acetate) and LLDPE blend.

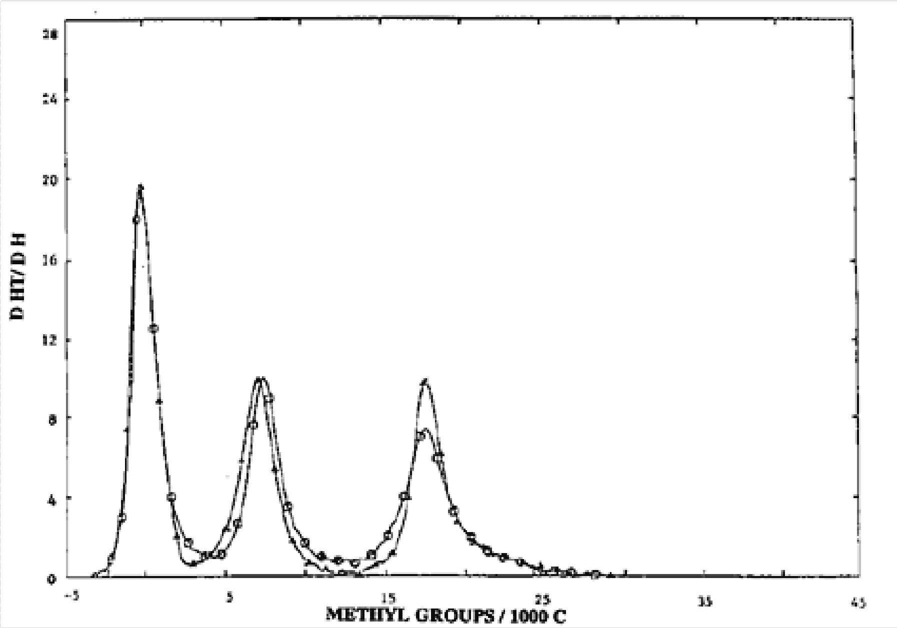

Figure 2.20 Cocrystallization effect for polyethylene samples: HDPE (left-hand peak), LLDPE having 6.2 (middle peak) and LLDPE with 19.1 (right-hand peak) methyls per 1000 carbon atom. Circles indicate TREF profile of an equimolar blend and triangles represent TREF profiles of individual blend components.[84]

On the other hand, Anantawaraskul *et al.*[90,93] observed a great influence of co-crystallization on CCDs measured by TREF and CRYSTAF for blends of ethylene/1-hexene copolymers with same number-average molecular weights and different comonomer contents. Their results (Figure 2.21) indicate that there is a strong co-crystallization effect at the highest cooling rate of 0.2 °C/min. The two peaks with low comonomer content (0.68 and 1.51 1-hexene mol %) are merged together. However, when the cooling rate is reduced to 0.05 °C/min, a trimodal TREF profile is clearly obtained, with each peak location corresponding to that of the parent sample. Similarly, a strong relationship between the cooling rate and co-crystallization was observed for CRYSTAF analysis. They reported that co-crystallization is less severe in TREF than in CRYSTAF and concluded that it is recommended to use TREF at low cooling rates to minimize the effect of co-crystallization when blends of similar crystallizabilities are analyzed.

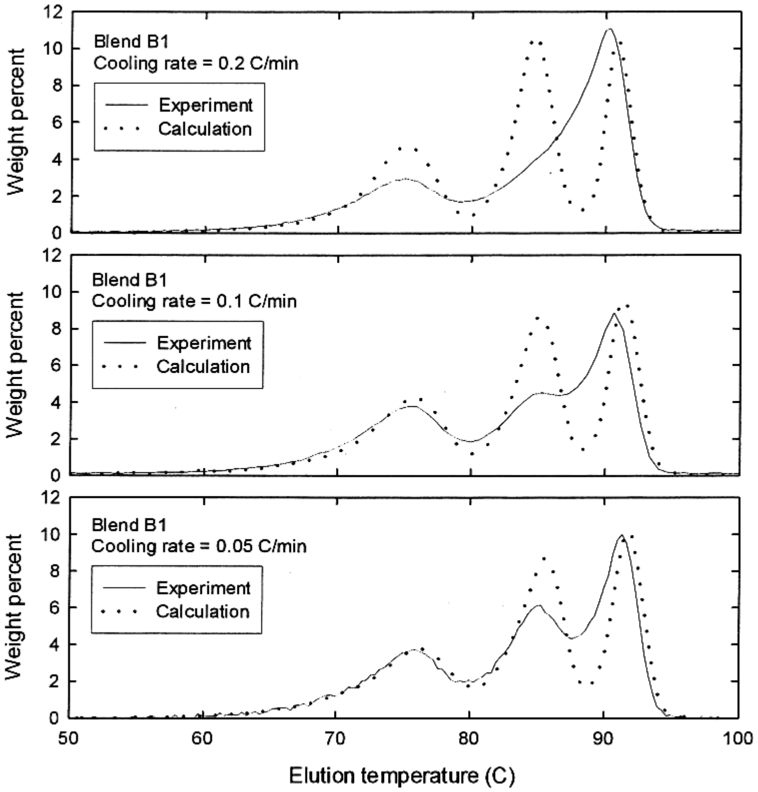

Figure 2.21 Effect of cooling rate on cocrystallization. Points indicate the TREF profiles of the individual blend components (LLDPE samples having the same molecular weight averages and different comonomer contents: 0.68, 1.51, and 3.14 mol%) and lines indicate the TREF profiles of the blends.[90]

Factors that affect co-crystallization may include the type of packing material inside the TREF column. It has been reported[94] that co-crystallization can be reduced by using a packing of glass beads instead of polymeric di-vinyl benzene (DVB) even at the fast TREF analyses at the rate of three to four hours per sample. Figure 2.22 shows that co-crystallization is much worse in the presence of DVB than with glass beads. The authors also reported that the type of the packing material affects co-crystallization more than the cooling rate. Therefore, it seems that co-crystallization can be minimized by the proper selection of TREF operation conditions and packing material for the TREF column.

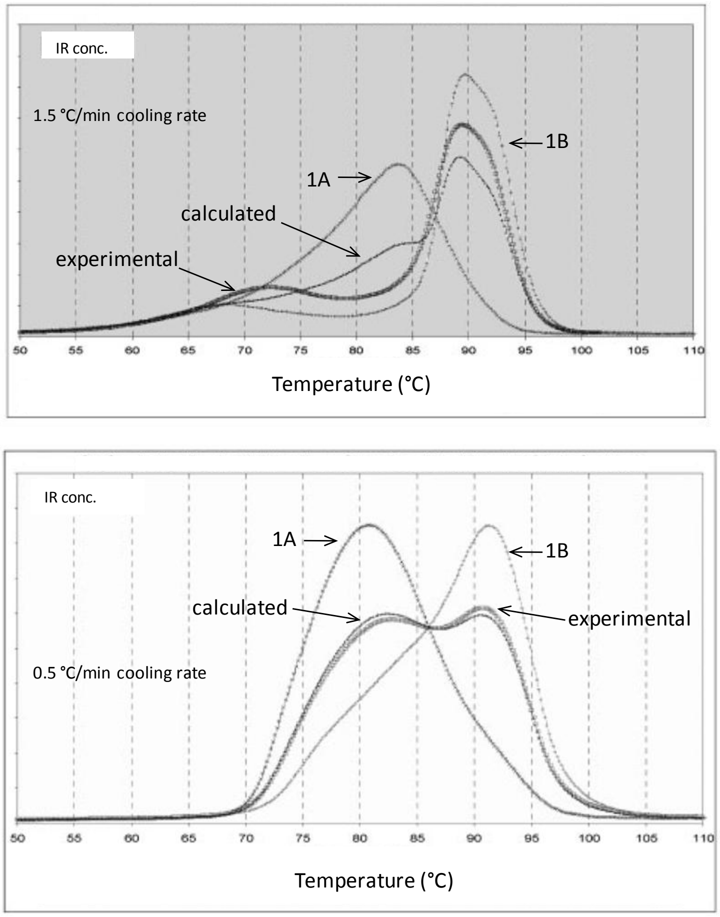

Figure 2.22 Comparison of cocrystallization effect in TREF with different packing materials: DVB (top) and glass bead (bottom). TREF profiles of individual samples (two polyethylene samples 1A and 1B), TREF profile of the blend, and calculated TREF profile are shown in each case.[94]

2.3.3 CROSS-FRACTIONATION (TREF-GPC)

Adding an IR detector to high-temperature GPC gives the average comonomer content across the MWD. Similarly, the measurement of molecular weight averages along the CCD is achieved by coupling TREF or CRYSTAF to a molar mass sensitive detector, such as a light scattering detector or a viscometer. However, the complete bivariate distribution of molecular weight and chemical composition can only be measured by cross-fractionation techniques which give more information about the microstructure of polyolefins. The most common cross-fractionation technique is TREF-GPC. Earlier cross-fractionation studies conducted by Wild *et al*.[84] were very time-consuming procedures using preparative TREF fractionation followed by off-line GPC analysis of the fractions. Nowadays, automated TREF-GPC cross-fractionation instruments are available commercially, making this technique much easier to run on a regular basis. The fractions eluted from the TREF columns are injected into GPC columns to measure their MWDs using the same instrumental set up.[94,95] An example of TREF-GPC results for a metallocene polyethylene blend is shown Figure 2.23. Polymer detection in the cross fractionation unit (Polymer Char, Valencia, Spain) can be obtained using an IR4 infrared detector. This detector has high sensitivity in polyolefins application and provides excellent long-term baseline stability. Recently, Polymer Char developed a new detector model, IR5, that has excellent sensitivity and baseline stability in both concentration and composition (branch content) signals.[96] The IR5 detector can be used to measure very low number of branches in HDPE resins.

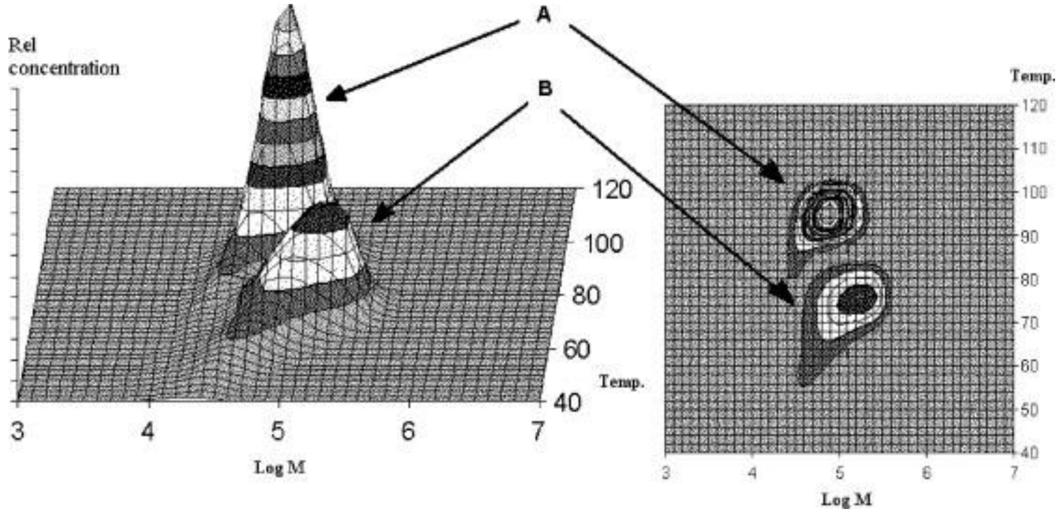

Figure 2.23 TREF-GPC cross fractionation results of a metallocene polyethylene blend: 3D-surface plot (left) and 2D countour plot (right); A and B are polyethylene components with 0.957 and 0.921 g/cm^3 density, respectively.[95]

Mirabella and Ford used TREF-GPC along with X-ray diffraction, ^{13}C NMR, and DSC to study the microstructure of Ziegler-Natta LLDPE.[70] They observed that short chain branching frequency decreased with increasing molecular weight in commercial LLDPE resins. The same results were found by several other research groups, indicating that this is a general trend for the microstructures of LLDPE resins made with heterogeneous Ziegler-Natta catalysts.

Studies done by several researches have focused on the cross-fractionation of LLDPEs made with different catalyst systems. Balbontin *et al.* [97] used TREF-GPC fractionation to study the microstructure of LLDPE resins made with heterogeneous Ziegler-Natta and homogenous zirconocene catalysts. Their results showed that the MWDs and CCDs of LLDPEs were greatly affected by catalyst type and process conditions. Homogenous catalysts make polymer with narrow CCD and constant average ethylene sequence length for all TREF fractions. Moreover, the narrow MWD of the polymer suggests that the homogenous zirconocene catalyst has only a single active site type. On the other hand, Ziegler-Natta LLDPEs have broad MWD and CCD, as shown by the cross fraction profile (Figure 2.24), which could be explained by the presence of multiple active site types on the catalyst. The same results were obtained by Usami *et al.*,[68] Cheng and Kakugo,[98] Soares and Hamielec,[99] and Migozzi and Nascetti.[100] Therefore, from GPC and TREF fractionation, the MWDs and CCDs of commercial LLDPE reflect the nature of the employed catalysts: broad distributions for Ziegler-Natta LLDPEs and narrow ones for metallocene LLDPEs.

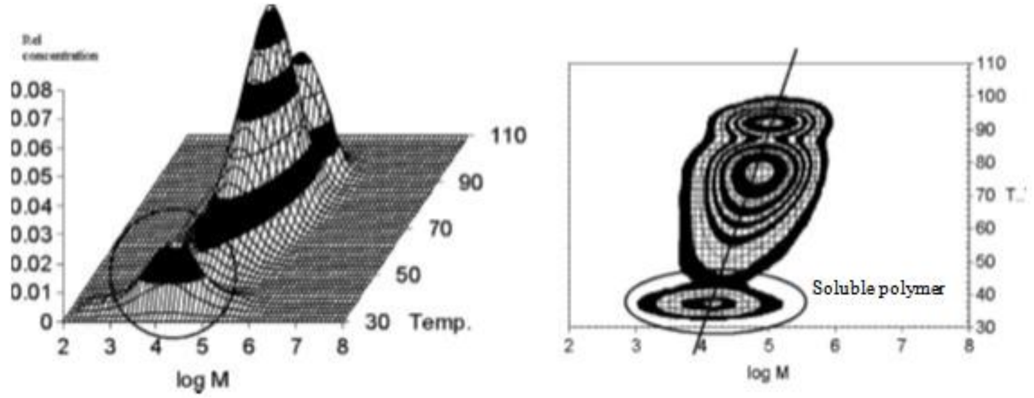

Figure 2.24 TREF-GPC cross fractionation results of a LLDPE: 3D-surface plot (left) and 2D countour plot (right). The solid line in the contour plot indicates the direct relation between the elution temperature and the molar mass.[95]

2.3.4 HT-HPLC Based on Precipitation-Redissolution

High-performance liquid chromatography (HPLC) is an important fractionation technique that separates complex polymers according to their chemical composition. Before 2003, the use of the HPLC was limited to ambient or slightly elevated temperature (up to 80 °C).[101,102] In 2003, Macko *et al*.[103,104] reported for the first time that HPLC could be used in a precipitation-redissolution mechanism to separate isotactic polypropylene (i-PP) from linear polyethylene using ethylene glycol monobutylether (EGMBE) as eluent. The HPLC column used in this research was packed with silica gel chemically modified with oligo(dimethylsiloxane).[105,106] The covalent bond between oligo(dimethylsiloxane) layer and silica gel is stable up to 350 °C – 380 °C. Therefore, it can be used for the characterization of polyolefins at high temperature such as 140 °C and 160 °C. The separation of isotactic polypropylene (i-PP) from polyethylene in this system is based on the fact that EGMBE is a good solvent for PP but a non-solvent for PE.[107] The main difficulty with this method is that the PE recovery decreases as the molecular weight increases. In addition, this method has poor resolution and is limited by the poor solubility of polyolefins.

To overcome these limitations, Heinz and Pasch[108] have used a gradient of the TCB (good solvent for both PE and PP). In this method, the polymer sample is dissolved in 1-decanol and injected to the HPLC column packed with modified silica gel. The mobile phase is then started with 100% EGMBE for 2 min. During this short period of time, the PP will be separated from the blend since EGMBE is a good solvent for PP, while PE precipitates on the column packing (EGMBE is a nonsolvent for PE). Then the volume fraction of TCB is increased linearly (within 3 min) to 100% and kept constant for about 3 min. The column outlet is connected to an evaporative light scattering detector (ELSD, model PL-ELS 100, Polymer Laboratories). The chromatogram of a PP-PE blend by this method is shown in Figure 2.25.

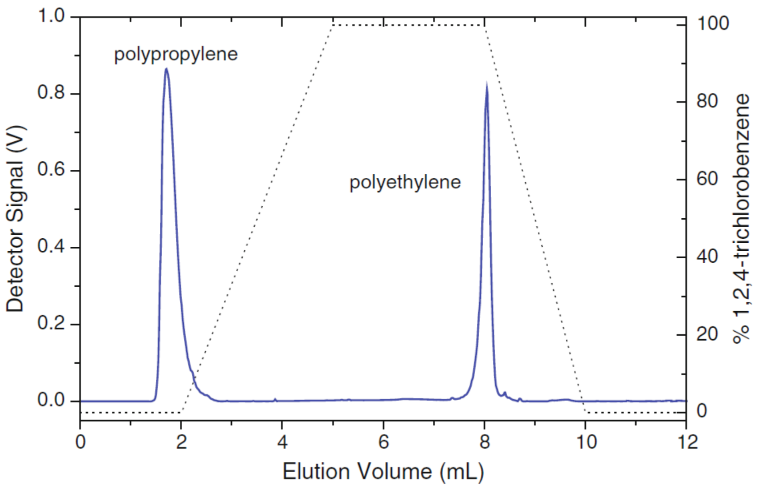

Figure 2.25 High-temperature gradient HPLC separation of a PE-PP blend. Column: modified silica gel, mobile phase: EGMBE-TCB, temperature: 140°C, detector: ELSD. The dotted line is the solvent gradient profile.[108]

Ethylene/propylene copolymers were analyzed by the same method (EGMBE/ TCB/ modified silica gel).[109] An example of the obtained results is shown in Figure 2.26. The EP copolymer sample was fractionated into PP homopolymer, propylene-rich fraction, and ethylene-rich fraction. This result was confirmed by coupling the HPLC system to an FTIR spectrometer via an LC transform interface. In this method the HPLC column outlet is sprayed at high temperature onto a rotating germanium disc to evaporate the solvent and deposit the polymer as a solid layer on the disc. The polymer is then analyzed off line with an FTIR spectrometer. [109] The same method was used to fractionate ZN-LLDPE resins containing butene or hexene as comonomer. The results indicate that the commercial LLDPE samples can be separated into two main fractions, as shown in Figure 2.27. For the first fraction (2.5 – 4.0 ml), the separation is controlled by the average molecular weight of the sample. This fraction represents the polymer chains with high comonomer content and low molecular weight averages. However, within the second fraction (7.5 – 8.5 ml), the fractionation is predominantly controlled by the short chain branching content, the length of short chain branches, and the intermolecular distribution of comonomer.[110]

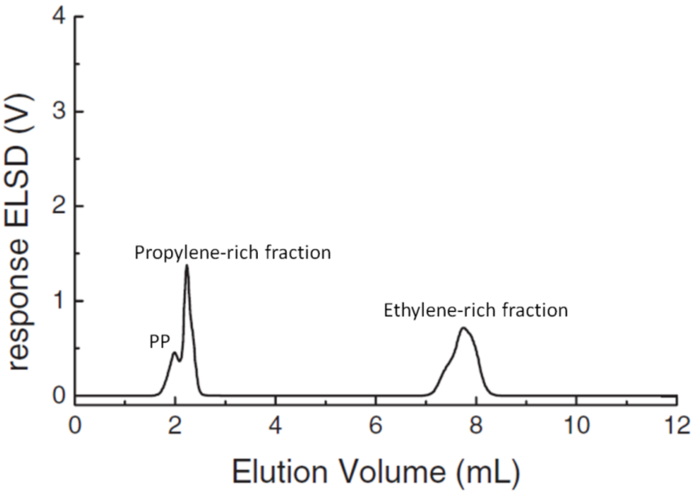

Figure 2.26 High-temperature gradient HPLC separation of an ethylene/propylene copolymer blend. Column: modified silica gel, mobile phase: EGMBE-TCB, temperature: 140°C, detector: ELSD.[109]

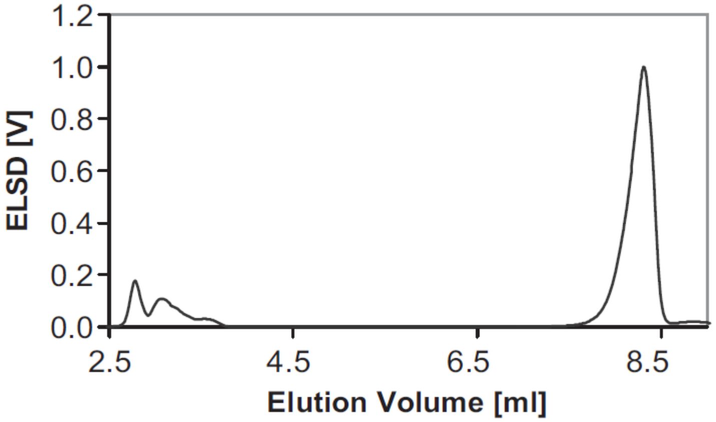

Figure 2.27 High-temperature gradient HPLC separation of an ethylene/butene LLDPE resin. Column: modified silica gel, mobile phase: EGMBE-TCB, temperature: 160°C, detector: ELSD.[110]

2.3.5 HT-HPLC Based on Adsorption-Desorption

The adsorption of PE on a chromatographic column packed with zeolites was first studied by Macko *et al*.[104] It has been reported that full or partial adsorption of PE and i-PP on the column packings was observed.[104,111] However, the recovery of the retained polymer from zeolites could not be obtained.

Macko and Pasch have used hypercarb® porous graphitic carbon (PGC) material instead of zeolites to achieve a selective separation of polyolefins. It has been shown that linear PE can be adsorbed on hypercarb® (PGC) from 1-decanol at 160°C.[112-114] In this chromatographic system, a solvent gradient starting from 100% 1-decanol and ending with 100% TCB is required to remove the retained polymer from PGC columns. The same method can be used to separate isotactic polypropylene (i-PP), atactic polypropylene (a-PP), and syndiotactic (s-PP) from each other.[114]

Ethylene/1-alkene and propene/1-alkene copolymers were fractionated by this adsorption HPLC technique.[115,116] The chromatograms of ethylene/1-hexene copolymers are shown in Figure 2.28. The elution volume of ethylene/1-hexene copolymers depends linearly on 1-hexene content. A calibration curve based on this linear dependence can be used to estimate the chemical composition of the sample from its position on the chromatogram, as illustrated in Figure 2.29. The incorporation of comonomer units into the polyethylene chains (or syndiotactic PP chains) disrupts the adsorption of these chains on the PGC column. Therefore, as the comonomer content increases, the elution volume of the polymer fraction decreases. Since isotactic PP chains and its blocks are not adsorbed on the PGC column, the addition of the adsorbing 1-alkene units increases the elution volume.

It has been reported that the molar mass and long chain branching of the polymer chains do not affect the adsorption of EP copolymers on PGC columns.[117] Molar masses greater than 15-20 kg/mol do not affect the elution volumes of linear PE[118] and ethylene/propylene, ethylene/butene, ethylene/octene copolymers.[119]

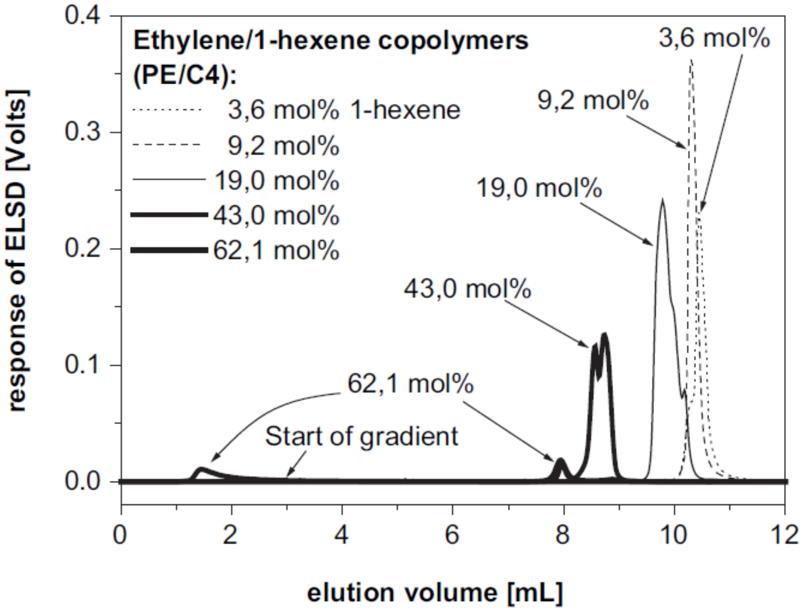

Figure 2.28 Chromatograms of ethylene/1-hexene copolymers. Column: Hypercarb®, Solvent gradient: from 100% 1-decanol to 100% TCB in 10 min, Temperature: 160 °C.[115]

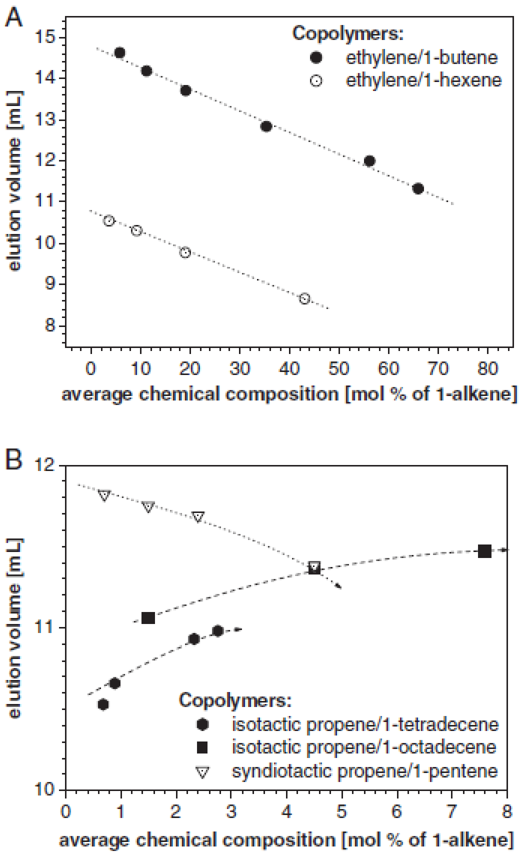

Figure 2.29 Relationship between elution volume and average comonomer content: (A) ethylene/1-alkene and (B) propene/1-alkene. Column: Hypercarb®, Solvent gradient: from 100% 1-decanol to 100% TCB in 10 min, Temperature: 160°C.[115]

Unlike crystallinity-based techniques, adsorption-based HPLC can be used to fractionate ethylene/1-alkene copolymers with high comonomer content in the range of (0-100%). The range of fractionation depends on the solvent type and the used temperature. It has been reported that (1-decanol/ TCB/ Hypercarb®) adsorption HPLC system can be used to fractionate ethylene/1-octene copolymers in the range of 0-60 % octene content at 175 °C,[120] and in the range of 0-100 % at 140 °C.[121]

The effect of carbon material type on the elution behavior of linear PE and PP with different tacticity was studied by Chitta *et al.*[122] They tested three different carbon column packings: porous graphite (hypercarb®), porous zirconium oxide covered with carbon (Zirchrom-CARB), and activated carbon (TA95). The results indicate that selective adsorption and therefore selective separation can be obtained with different sorbent/solvent systems. PP samples can be separated according to their tacticity using the 1-decanol/ TCB/ Hypercarb® system. Such separation cannot be achieved with 2-ethyl-1-hexanol/ TCB/ Zirchrom-CARB system.

Two-dimensional liquid chromatography (2D-LC) is an excellent tool for the investigation of polyolefins microstructure. For the first time, Ginsburg *et al.*[120,123] and Roy *et al.*[124] have hyphenated interactive HPLC with HT-GPC. Recently, Polymer Char (Valencia, Spain) developed and commercialized the HT-2D-LC system used by Ginsburg *et al.* (Figure 2.30). A blend of i-PP, a-PP, s-PP, and PE was fractionated by this system and the results are shown in Figure 2.31.

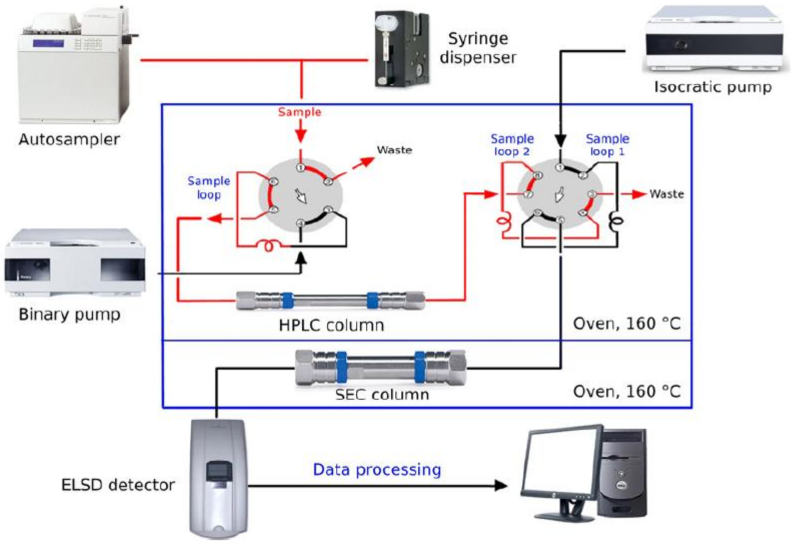

Figure 2.30 The experimental setup of HT-2D-LC.[120]

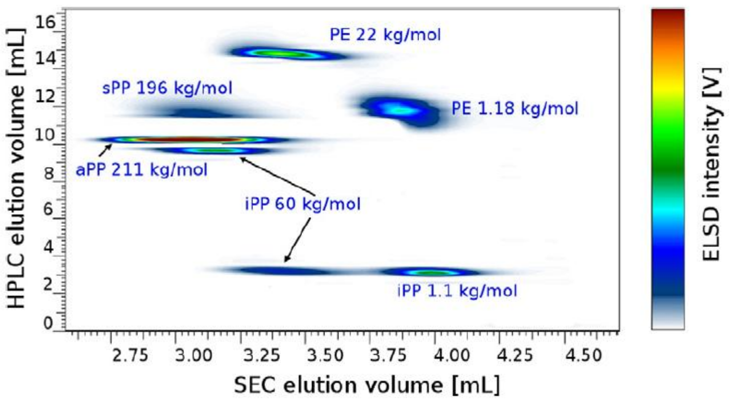

Figure 2.31 Counter plot of a blend of PE and PP with different tacticities by HT-2D-LC.[120]

The HT-2D-LC method has been used to study the effect of catalyst type on the microstructure of poly(ethylene-co-octene). The contour plots for polymers made by Ziegler-Natta, metallocene, and multi-catalyst systems are shown in Figure 2.32.[124] These results indicate that there are differences between these resins in terms of the number of resolved populations, molecular weight, and composition profiles.

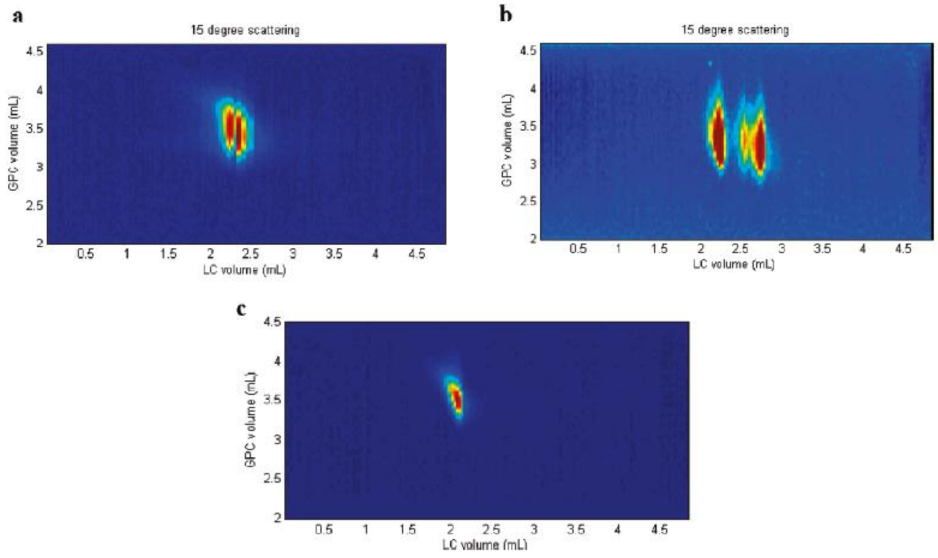

Figure 2.32 Counter plot of a poly(ethylene-co-octene) by HT-2D-LC: (a) ZN resin, (b) multicatalyst resin, (c) metallocene resin with 2.6 mol% octane.[124]

These methods (either one or two dimensional high-temperature adsorption HPLC) need solvent gradient to perform the separation. However, the adsorption of polymer chains on a substrate also depends on temperature. Based on this fact, Lochmüller[125] and Chang[126] were able to separate polyethylene glycol and polystyrene, respectively, using temperature gradient adsorption HPLC. During the 3rd *International Conference on Polyolefin Characterization*, Cong *et al.*[127] showed for the first time that temperature gradient adsorption HPLC can be utilized for polyolefin fractionation. This method opens a new route to characterize crystalline and amorphous polyolefins in fast time. The chromatograms of ethylene/octene copolymers with comonomer content in the range of 0-50 mol% of octene are shown in Figure 2.33.[127] In addition to its simplicity (it does not require the use of a solvent gradient), the use of a single solvent permits the use of quantitative mass detectors such as infrared detectors, eliminating the need to use the non-quantitative evaporative light scattering detector. More details about this technique are provided in the following chapters of this thesis.

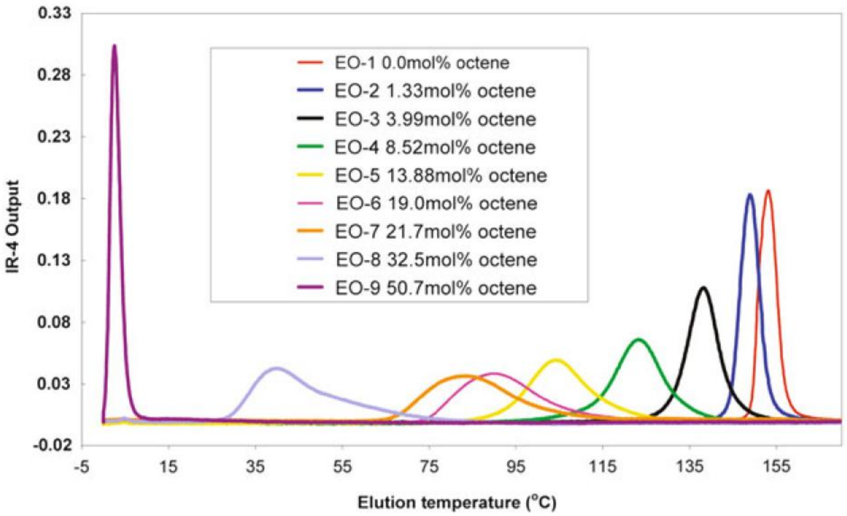

Figure 2.33 Chromatograms of ethylene/octene copolymers by temperature gradient interaction chromatography. Column: Hypercarb, temperature gradient 175°C to 0°C, Solvent: ortho-dichlorobenzen (ODCB).[127]

2.4 MATHEMATICAL MODELING OF MWD AND CCD

Heterogeneous Ziegler-Natta catalysts make polyolefins that have broad MWDs and CCDs that affect the final properties of the product. In order to obtain a more detailed picture of the microstructures of these polyolefins, a mathematical model is required to quantify the information provided by polyolefin analytical techniques such as high-temperature GPC, TREF, and CRYSTAF. Stockmayer[128] derived the instantaneous bivariate distribution of chain length and chemical composition of linear polymer made by single-site-type transition metal catalysts,

$$w_i(r,F) = r\hat{\tau}_i^{\,2}\exp(-r\hat{\tau})\sqrt{\frac{r}{2\pi\beta_i}}\exp\left[-\frac{r(F-\overline{F}_i)^2}{2\beta_i}\right] \tag{2.1}$$

In Equation (2.1), r is the chain length and F is the comonomer mole fraction. The parameters $\hat{\tau}_i$ and β_i are defined as,

$$\hat{\tau}_i = \frac{\text{rate of transfer}}{\text{rate of propagation}} \tag{2.2}$$

$$\beta_i = \overline{F}_i(1-\overline{F}_i)\sqrt{1-4\overline{F}_i(1-\overline{F}_i)(1-r_{1i}r_{2i})} \tag{2.3}$$

where $\overline{F}_i$ is the average mole fraction of comonomer in the copolymer, which can be obtained from the Mayo-Lewis equation, provided that the comonomer reactivity ratios, r_{1i} and r_{2i}, are known. The subscript i indicates site type for the case of multiple-site-type catalysts, as will be explained below.

The instantaneous chain length distribution is given by Flory's most probable distribution which can be obtained by integrating Equation (2.1) over all comonomer compositions,[129 -131]

$$w_i(r) = \int_{-\infty}^{\infty} w_i(r,F)\,d(F-\overline{F}_i) = r\,\hat{\tau}_i^2\,\exp(-r\hat{\tau}_i) \tag{2.4}$$

The number and weight average chain lengths of polymer made by site type i, r_{ni} and r_{wi}, respectively, are related to the parameter $\hat{\tau}_i$ by the following equations

$$r_{ni} = \left[\int_0^\infty \frac{w_i(r)}{r} dr \right]^{-1} = \frac{1}{\hat{\tau}_i} \tag{2.5}$$

$$r_{wi} = \int_0^\infty r\, w_i(r)\, dr = \frac{2}{\hat{\tau}_i} \tag{2.6}$$

Equation (2.4) can be written in terms of molecular weight (MW) of the polymer to describe the experimental MWD measured by GPC using simple mathematical transformations,[75]

$$w_i(\log MW) = 2.3026\, MW^2 \tau_i^2 \exp(-MW\tau_i) \tag{2.7}$$

where τ is the reciprocal of the number average molecular weight, M_n.

Kim *et al.*[132] used the above single-parameter approach to interpret the MWDs of polyethylenes made with two metallocene catalysts supported on silica, as shown in Figure 2.34. The MWD of the whole polymer is well described by the weighted superposition of two Flory's most probable distributions,

$$W(\log MW) = m_1 w_1(\log MW) + (1 - m_1) w_2(\log MW) \tag{2.8}$$

In Equation (2.8) m_1 is the mass fraction of polymer made by metallocene type 1. The same concept can be extended to describe the MWD of polymers made with heterogeneous Ziegler-Natta catalysts, which are assumed to have multiple active site types,

$$W(\log MW) = \sum_{i=1}^{n} m_i w_i(\log MW) = 2.3026 \sum_{i=1}^{n} m_i MW^2 \tau_i^2 \exp(-MW\tau_i^2) \tag{2.9}$$

where n is the number of active site types on the catalyst, m_i is the mass fraction of polymer made by each site type, and τ_i is the ratio of all chain transfer rates to propagation rate on site type i.

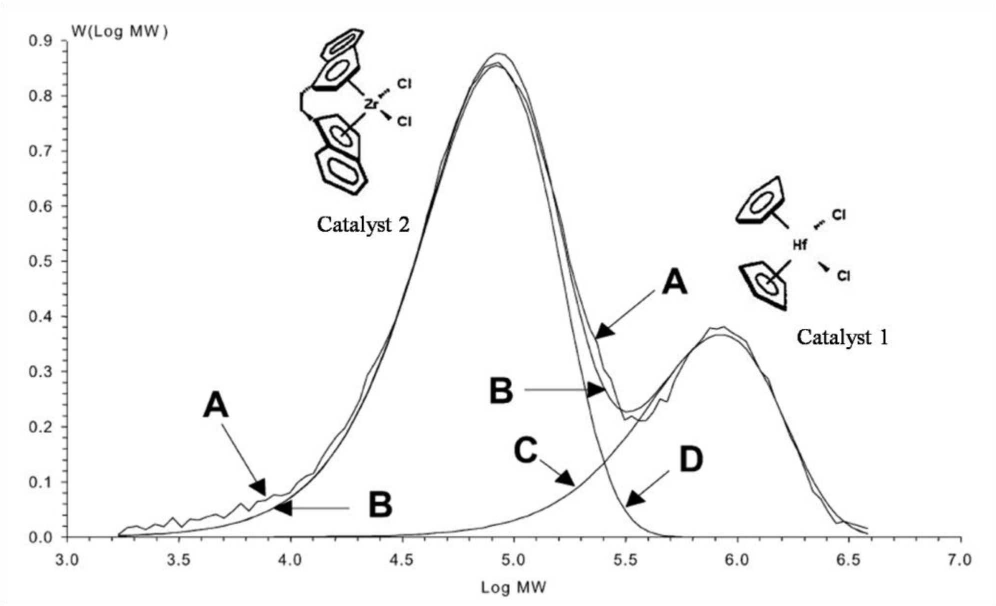

Figure 2.34 MWD of polyethylene made by two metallocene catalysts supported on the same silica support: A: Experimental MWD; B: Superposition of curves C and D; C and D: Flory's most probable distributions for polyethylene produced with catalyst 1 and 2, respectively.[132]

The chemical composition distribution of polymers made with single site type catalysts can be determined by integrating Stockmayer's distribution between the limits of 0 to ∞ for chain length,[128,133,134]

$$w_i(F) = \int_0^\infty w_i(r,F)\,dr = \frac{3}{4\sqrt{2\beta_i\hat{\tau}_i}\left[1+\dfrac{(F-\overline{F}_i)^2}{2\beta_i\hat{\tau}_i}\right]^{5/2}} \tag{2.10}$$

This distribution can be related to the results from TREF fractionation of a LLDPE sample which is synthesized using a single site type catalyst. Thus, the fractionation of the copolymers provides not only structural information, but also information about the ratio of kinetics parameters and mechanism of copolymerization.

The same procedure that has been used to describe the MWD of polymers made with multiple-site-type catalysts can be used to represent the CCD of polymers made with these catalysts,

$$w_i(F) = \sum_{i=1}^{n} m_i w_i(F) \tag{2.11}$$

This model has been used to simulate the CCDs of LLDPE made with a heterogeneous Ziegler-Natta catalyst measured by TREF. For instance, Soares and Hamielec used five active site types to simulate bimodal TREF profiles as depicted in Figure 2.35.[133]

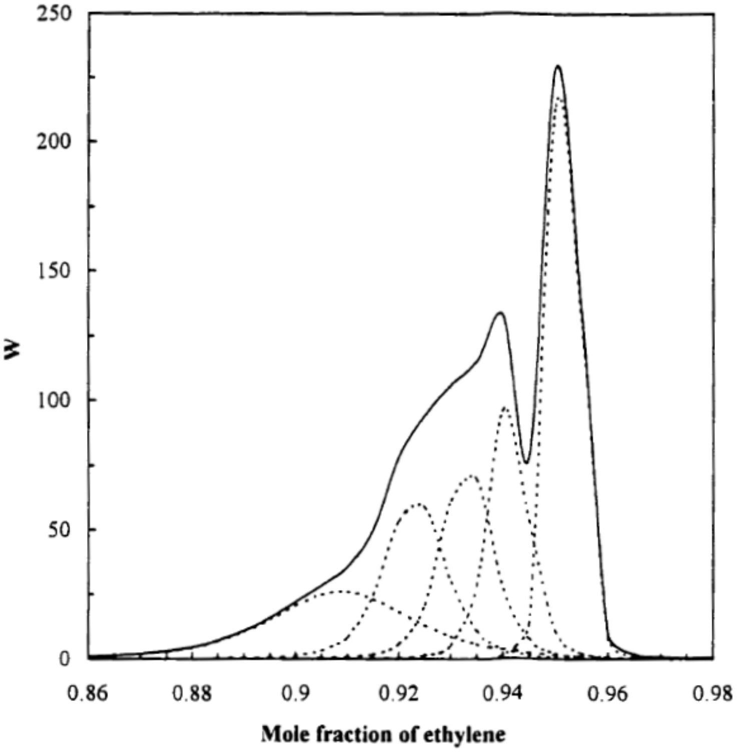

Figure 2.35 Simulation of TREF profiles using five active site types.[133]

da Silva *et al*.[86] used Equation (2.9) to represent the MWD of a typical ethylene/1-butene copolymer made with an industrial heterogeneous Ziegler-Natta catalyst using six different site types (Figure 2.36). They used Gaussian distributions to model TREF and CRYSTAF profiles and found that only five site types were required to deconvolute the CCD of the polymer, as illustrated in Figure 2.37. They assumed that the two active sites that produced the highest MW polymer had similar reactivity ratios towards the incorporation of 1-butene.

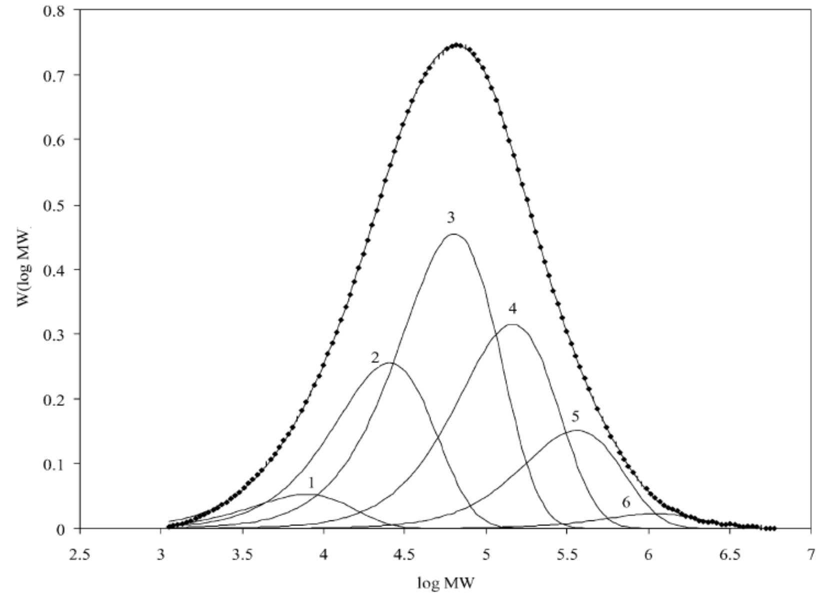

Figure 2.36 MWD deconvolution of a LLDPE made with a heterogeneous Ziegler-Natta catalyst (m_1 = 0.041, M_n = 3,960; m_2 = 0.204, M_n = 12,700; m_3 = 0.364, M_n = 32,000; m_4 = 0.252, M_n = 72,800; m_5 = 0.121, M_n = 181,000; m_6 = 0.018, M_n = 554,000). [86]

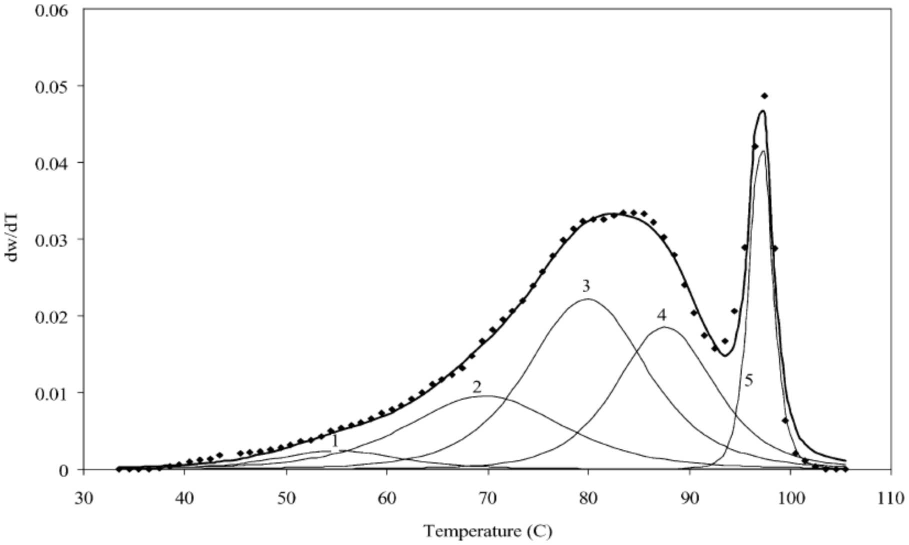

Figure 2.37 TREF Deconvolution of a LLDPE made with a heterogeneous Ziegler-Natta catalyst (m_1 = 0.041, T_1 = 55.2; m_2 = 0.204, T_2 = 69.7; m_3 = 0.364, T_3 = 79.9; m_4 = 0.252, T_4 = 87.6; m_5 = 0.139, T_5 = 97.1). The peak temperatures can be converted to comonomer content using a calibration curve.[86]

Kissin and Fruitwala developed an empirical approach to model the CRYSTAF profiles of ethylene/1-hexene copolymers produced with supported Ti-based Ziegler-Natta catalysts.[135] Their model describes the CCD according to resolution of CRYSTAF peaks using elemental components, where each component represents a fraction of polymer with the same degree of chain imperfections. Eight components were required to represent the CCD of the copolymers while only five Flory's distributions were needed to adequately represent the MWD of the whole polymer. The difference between the number of active sites required to model MWD and CCD may be due to the fact that some CRYSTAF components have significantly different comonomer contents but have close molecular weights that are not separated by GPC.

However, several researchers believe that the 5 to 8 active sites needed to model the MWDs and CCDs of most Ziegler-Natta catalysts may not correspond to chemically distinct sites existing on the catalyst. Soares found that the broad MWDs of polymers made with multiple-site-type catalysts could be well described by two or three MWDs components corresponding to broader versions of Flory's distributions. These fewer distributions were hypothesized to represent chemically distinct site types or to be related to different site-surface interactions.[136] The interactions between catalyst and support may broaden the MWD and CCD of polymer even when only one active site type is present on the catalyst, as in the case of supported metallocene catalysts. Several authors reported that supported metallocene catalysts produces polymer that has MWD broader than Flory's distributions.[137-139] To model this phenomenon, Soares proposed that each chemically distinct active site type had a distribution of $\hat{\tau}$ values. Therefore, Equation (2.4) becomes, [136]

$$w(r) = \int r\hat{\tau}^2 \exp(-r\hat{\tau})\ f(\hat{\tau})d\hat{\tau} \tag{2.12}$$

In Equation (2.12), $f(\hat{\tau})$ is some generic broadening function. For a normal distribution of $\hat{\tau}$ around an average value $\bar{\tau}$, Equation (2.12) is represented as,

$$w(r) = \int r\hat{\tau}^2 \exp(-r\hat{\tau}) \frac{1}{\sqrt{2\pi\sigma^2}} \exp\left[-\frac{(\hat{\tau}-\tau)}{2\sigma^2}\right] d\hat{\tau} \tag{2.13}$$

where σ is the standard deviation of the $f(\hat{\tau})$ distribution. The same concept can be extended to represent CCDs for copolymers. Therefore, modeling MWD and CCD by this approach may provide the minimum number of chemically distinct active site types on supported catalysts. However, several challenges remain to be solved for this modeling methodology, such as the exact form of the broadening function and the possibility of multiple solutions depending on the broadening function form and parameters.

A thermodynamic model based on the Flory-Huggins theory was also proposed to model TREF profiles.[140] This model focuses on the thermodynamic aspects of TREF fractionation by considering the dependence of TREF fractionation on the melting temperature, melting enthalpy, average crystallinity, average crystallizable sequence length, and polymer-solvent interaction parameter. The model helps understand the TREF separation mechanism, but provides little information about copolymerization compared with the model based on Stockmayer's distributions.

Anatawaraskul *et al.*[141] developed a semi-empirical model that could fit the experimental CRYSTAF profiles of polyethylene homopolymers made by a metallocene catalyst. The model takes into account the crystallization kinetics based on the Avrami equation. The model has also been extended to study CRYSTAF profiles of ethylene/α-olefin copolymers.[142] The crystallization kinetics model was used to simulate the effect of operation conditions, MW, and comonomer content on CRYSTAF profiles and calibration curves.[143] The results agreed well with predictions from Stockmayer's distribution. Recently, Siriwongsarn et al. developed a new mathematical model for TREF taking into consideration the kinetics of both crystallization and dissolution steps.[144] TREF profiles of polyethylene, ethylene/1-hexene, and ethylene/1-octene copolymers measured at different operation conditions were used to validate the model profiles. This new TREF model accurately describes the effect of molecular weight, comonomer content and operating conditions (cooling rate, heating rate, and solvent flow rate) of experimental TREF profiles.

2.4.1 MASS AND HEAT TRANSFER RESISTANCES VERSUS MULTIPLICITY OF ACTIVE SITE TYPES

The reason for broad MWDs and CCDs of polyolefins made by heterogeneous Ziegler-Natta catalysts has been given two main explanations. In the first, intraparticle mass and heat transfer resistances during polymerization reactions are used to explain the broad distributions of the product; in the second, multiple active site types have been held responsible for the polymer heterogeneity, as already discussed in the previous section.

At the early stages of polymerization with heterogeneous Ziegler-Natta catalysts, the catalyst particle fragments into a large number of small particles that are encapsulated by the growing polymer chains. The polymer particles grow due to propagation reactions. Due to diffusion resistances, active sites located in catalyst fragments placed along the radius of the polymer particle may be exposed to different concentrations of monomer and hydrogen, producing polymer chains with molecular weight averages that differ spatially inside the polymer particle.[99,145] During copolymerization, spatial compositional heterogeneity may be caused by the different monomer transfer rates and reactivities. Moreover, when heat transfer resistances are significant, temperature gradients and/or hot spots may occur that will change the value of propagation and chain transfer reaction constants. Therefore, polymer with broad MWD and CCD may be produced even if a single-site-type catalyst is employed, simply because of intraparticle heat and mass transfer limitations.

The effects of mass and heat transfer resistances have been modeled by different mathematical models such as the polymer flow model (PFM) and the multigrain model (MGM).[145] The PFM, developed in 1970s, assumes that the catalyst fragments and growing chains form a continuum (the commonly used pseudo-homogeneous hypothesis), in which diffusion and heat transfer occur in the polymeric particle (Figure 2.38). Contrarily, the MGM assumes two levels of mass and heat transfer resistances, as also shown in Figure 2.38. The large polymeric particle (macroparticle) is comprised of many small microparticles, which encapsulate the catalyst fragments. For the monomer to reach the active sites, two diffusion processes are required: macrodiffusion, through the pores of macroparticle, and microdiffusion, within the polymer layer surrounding the active centers in the microparticle.

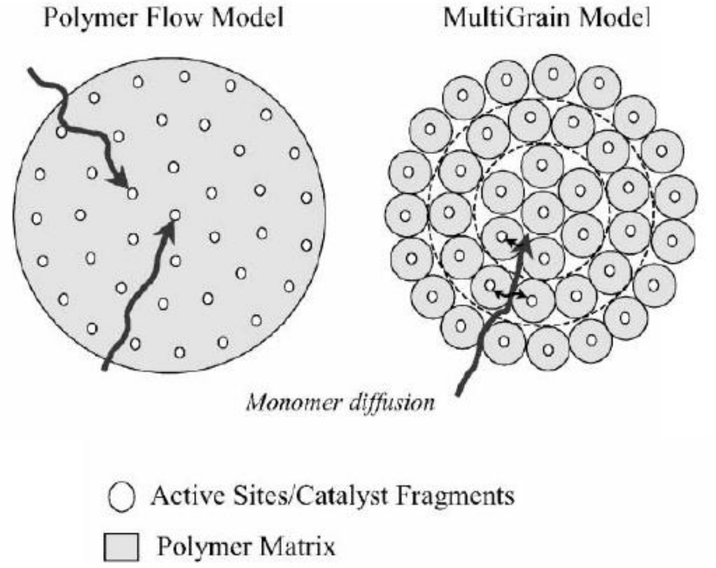

Figure 2.38 Representation of the polymer flow model (PFM) and the multigrain model (MGM).[145]

The application of the MGM, including an extension to include multiple site types, has been reviewed by Floyd *et al*.[146] The authors concluded that mass transfer effects alone could not explain the broad MWD of polymers made by heterogeneous Ziegler-Natta catalysts. They also observed that the intraparticle heat transfer resistances were significant only in gas phase polymerizations using highly active and large catalyst particles. Ray reviewed the MGM applications and concluded that the multiplicity of active site types played the major role in producing polymer with broad distributions.[147] In addition, the bimodal TREF and CRYSTAF profiles shown above cannot be solely attributed to intraparticle mass and heat transfer resistances.

A multiple-site-type model has been developed for olefin copolymerization by de Carvalho *et al*.[148]. The authors concluded that the multiplicity of active site types should be considered to account for the broad MWDs, CCDs, and stereoregularity distributions of polymers made with heterogeneous Ziegler-Natta catalysts. They presented guidelines for the use of TREF, ^{13}C NMR, and GPC in the determination of parameters associated with MWD and CCD.

Soares and Hamielec developed the polymeric multilayer model, a variation of the PFM, in which the catalyst particle was divided into concentric spherical layers as in the multigrain model; however, the microparticles were not considered explicitly.[99] The model used Stockmayer’s bivariate distribution to estimate the complete MWDs and CCDs for each site type, model layer and whole polymeric particle. The authors concluded that mass transfer resistances alone could not be used to explain the broad MWDs and CCDs of polymer made by heterogeneous Ziegler-Natta catalyst, while this behavior was explained very well assuming multiple active site types on the catalyst. Moreover, they showed that the heat transfer resistances can be neglected for polymerizations in slurry reactors.

Chapter 3*

MATHEMATICAL MODELING OF MWD AND CCD

3.1 INTRODUCTION

The molecular weight (MWD) and chemical composition (CCD) distributions of polyolefins have a significant impact on their physical and rheological properties. It is, therefore, very important to develop mathematical models that quantify the information provided by polyolefin analytical techniques such as high-temperature gel permeation chromatography (GPC), crystallization analysis fractionation (CRYSTAF), and temperature rising elution fractionation (TREF). One of the fingerprints of polyolefins made with heterogeneous Ziegler-Natta catalysts is that they have broad MWDs, and broad and very often multimodal CCDs. As discussed in the previous chapter, these broad distributions are attributed to the presence of multiple active site-types on the catalyst.

In theory, the MWD and CCD of the polymer made by each active site type on heterogeneous Ziegler-Natta catalysts can be described with Flory's most probable distribution and the chemical composition component of Stockmayer's distribution, respectively. This MWD deconvolution method was originally suggested by Vickroy *et al.*[149] Soares and Hamielec clearly outlined the methodology that was used to deconvolute the experimental MWDs and CCDs.[131,133] In this chapter, a mathematical model was developed to deconvolute the MWD and CCD of polyolefins simultaneously using Flory's most probable distribution and the cumulative CCD component of Stockmayer's distribution. This is the first time this type of deconvolution procedure has been used for polyolefins.

3.2 SIMULTANEOUS DECONVOLUTION MODEL

As discussed in Chapter 2, Flory's most probable distribution can be used to describe the instantaneous MWD of polymer chains made on each site type of a Ziegler-Natta catalyst.[128-130] Flory's distribution for site type i, $w_i(\log MW)$, is given by

$$w_i(\log MW) = 2.3026\, MW^2 \tau_i^2 \exp(-MW\tau_i) \tag{3.1}$$

where *MW* is the molecular weight of polymer and the parameter τ_i is the ratio of all chain transfer rates to the propagation rate for each site type. The parameter τ_i in Equation (3.1) is given by

$$\tau_i = \frac{\hat{\tau}_i}{mw} = \frac{1}{r_{ni} \cdot mw} = \frac{1}{M_{ni}} \tag{3.2}$$

where *mw* is the molecular weight of the repeating unit, r_{ni} is the number average chain length and M_{ni} is the number average molecular weight of the polymer made on site type *i*.

Similarly, the instantaneous CCD of polymer chains made on each site type can be described using the chemical composition component of Stockmayer's bivariate distribution,[133,134]

$$w_i(F) = \frac{3}{4\sqrt{2mw\,\beta_i\tau_i}\left[1 + \frac{(F - \overline{F}_i)^2}{2mw\,\beta_i\tau_i}\right]^{5/2}} \tag{3.3}$$

where the parameter β_i is defined as,

$$\beta_i = \overline{F}_i(1 - \overline{F}_i)\sqrt{1 - 4\overline{F}_i(1 - \overline{F}_i)(1 - r_{1i}r_{2i})} \tag{3.4}$$

and *F* is the mole fraction of comonomer in a particular polymer chain, $\overline{F}_i$ is the average mole fraction of comonomer in the polymer, and r_{1i} and r_{2i} are reactivity ratios for copolymerization for each site type.

The MWD and CCD of polyolefins produced with multiple-site-type Ziegler-Natta catalysts have been modeled as a weighted sum of Flory's most probable distributions and Stockmayer's distributions, respectively given by Equations (3.5) and (3.6),

$$W(\log MW) = 2.3026 \sum_{i=1}^{n} m_i MW^2 \tau_i^2 \exp(-MW\tau_i^2) \tag{3.5}$$

$$W(F)=\sum_{i=1}^{n} m_i \frac{3}{4\sqrt{2mw\beta_i\tau_i}\left[1+\frac{(F-\overline{F}_i)^2}{2mw\beta_i\tau_i}\right]^{5/2}} \tag{3.6}$$

where m_i is the mass fraction of polymer made on site type i and n is the number of site types on the catalyst.

The CCD of LLDPE resins made with heterogeneous Ziegler-Natta catalysts is normally bimodal with a narrow peak in the low comonomer content region and one or more broad peaks in the high comonomer content region. Figure 3.1 shows a typical CCD of an industrial LLDPE sample measured by TREF. The leftmost peak in Figure 3.1 corresponds to the fraction of polymer that is soluble at room temperature in trichlorobenzene (TCB). Polyethylene production, processing, and applications are strongly affected by this soluble polymer fraction.[150]

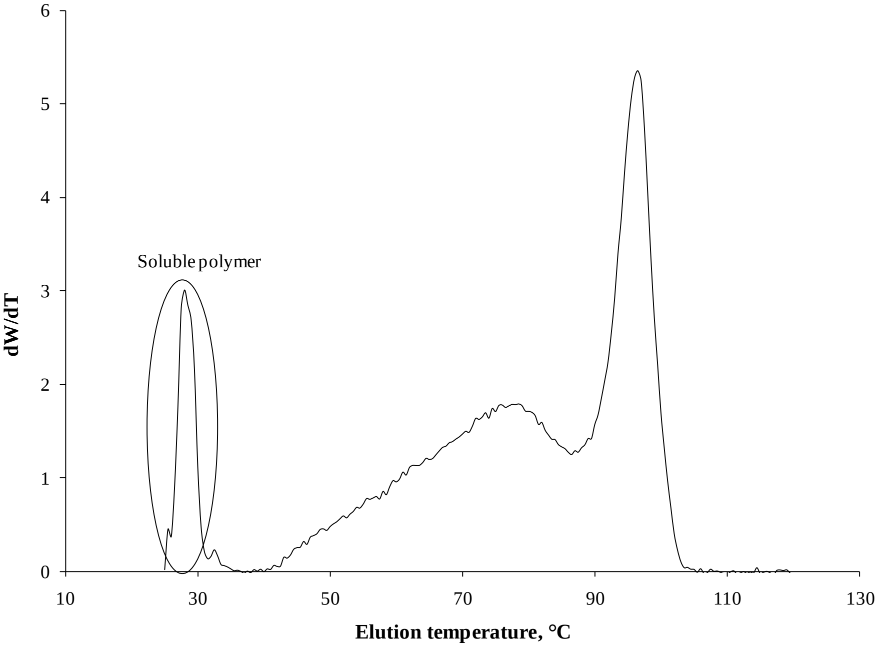

Figure 3.1 CCD distribution of a LLDPE measured by TREF, showing the fraction of polymer soluble at room temperature in trichlorobenzene (TCB).

We face a problem when trying to deconvolute the TREF or CRYSTAF curves of LLDPE resins that contain a significant fraction of soluble polymer using Equation (3.6). The soluble peak that appears in Figure 3.1 is not a chromatographic peak, but simply a purge peak, with an area proportional to the amount of polymer that remains soluble in TCB at room temperature. Consequently, the soluble peak cannot be described with Equation (3.3). It is possible to overcome this problem if we use the cumulative form of Equation (3.3) in the deconvolution procedure as shown below,

$$w_i^c(F) = \int_{-\infty}^{F} w_i(F)\,\mathrm{dF} \tag{3.7}$$

Fortunately, this integral has the following analytical solution,

$$w_i^c(F) = \frac{2[2mw\beta_i\tau_i + (F-\overline{F}_i)^2]^{5/2} + 3(F-\overline{F}_i)(2mw\beta_i\tau_i)^2 + 5(2mw\beta_i\tau_i)(F-\overline{F}_i)^3 + 2(F-\overline{F}_i)^5}{4[2mw\beta_i\tau_i + (F-\overline{F}_i)^2]^{5/2}} \tag{3.8}$$

However, to include the room temperature soluble fraction in the deconvolution procedure, m_i in Equation (3.6) should be redefined as,

$$m_i = m_i^s + m_i^{ns} \tag{3.9}$$

In Equation (3.9), m_i is the total mass fraction of polymer made on site type *i*, and m_i^s and m_i^{ns} are the mass fractions of polymer that are soluble and insoluble at room temperature, respectively. Only the insoluble polymer fraction can be described with Stockmayer's bivariate distribution. Therefore, the cumulative CCD for the whole resin is given by,

$$W^c(F) = \sum_{i=1}^{n} m_i^{ns} w_i^c(F) \quad \text{if } F \geq F_{crit} \tag{3.10.a}$$

$$W^c(F) = \sum_{i=1}^{n} m_i^s \quad \text{if } F < F_{crit} \tag{3.10.b}$$

and

$$m_i^s = \int_{-\infty}^{F_{crit}} w_i(F)\,\mathrm{dF} \tag{3.11}$$

where F_{crit} is the critical ethylene mole fraction below which the polymer chain is soluble at room temperature. The critical ethylene mole fraction depends on solvent type, comonomer type, and analysis conditions; it is easily determined from the calibration curves for TREF or CRYSTAF by extrapolating them to room temperature.

The next step in the deconvolution procedure is to use a non-linear least squares optimization routine to minimize the squares of the differences between the measured and predicted distributions. The objective function for this model, which minimized using Microsoft Excel Solver, is

$$\chi^2 = \min\{[W_{exp}(\log MW) - W_{model}(\log MW)]^2 + [W_{exp}^c(F) - W_{model}^c(F)]^2\} \tag{3.12}$$

where $W_{\mathrm{exp}}(\log MW)$ and $W_{\mathrm{exp}}^c(F)$ are the MWD measured by GPC and the cumulative CCD measured by TREF or CRYSTAF, respectively. In the case of LLDPE resins made with heterogeneous Ziegler-Natta catalysts, the sites that produce polymer with lower average comonomer fractions also have higher number average molecular weights.

From this deconvolution procedure, it is possible to estimate the number of site types necessary to represent the GPC and TREF or CRYSTAF data of a given LLDPE resin. Moreover, it is possible to estimate the mass fraction of soluble polymer made on each site type.

3.3 RESULTS AND DISCUSSION

Several LLDPE samples were analyzed by this new deconvolution procedure. Table 3.1 shows the molecular weight averages and TREF-measured mass fractions of polymer soluble at room temperature in TCB for four industrial LLDPE resins.

All the TREF profiles investigated in this study were converted into their equivalent CCDs using the poly(ethylene-co-1-octene) calibration curve shown in Figure 3.2. The value for F_{crit} adopted in our deconvolutions, $F_{crit} = 0.89$, was obtained by extrapolating the curve in Figure 3.2 to the lowest fractionation temperature of 30 °C.

Table 3.1 Average properties of LLDPE industrial samples

Sample	M_w	M_n	Soluble Fraction (wt%)
1	115,500	29,300	15
2	124,700	33,400	31.2
3	138,200	37,000	11.8
4	158,884	50,120	10

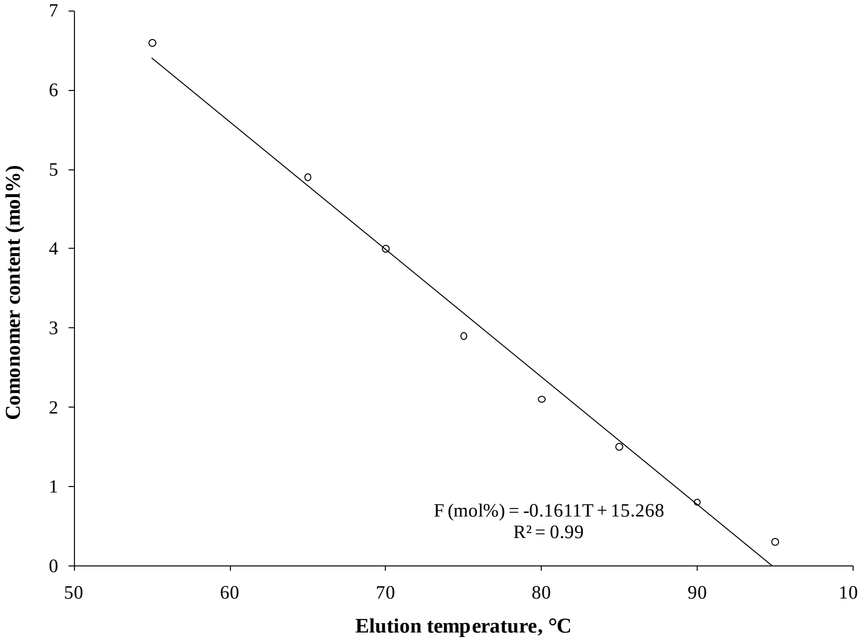

Figure 3.2 TREF Calibration curve for ethylene/1-octene copolymers.[86]

The MWD and CCD of Sample 1 are shown in Figures 3.3 and 3.4, respectively. A typical deconvolution procedure starts by assuming two active sites types and trying to minimize the value of χ^2 defined in Equation (3.12). Figure 3.5 and 3.6 demonstrate that assuming two site types is clearly inadequate to represent both MWD and CCD for this resin. Using three site types improves the model fit, as shown in Figure 3.7 and 3.8 (the value of the objective function, χ^2, drops from 0.334 to 0.033 as n increases from 2 to 3), but still gives inadequate description of the experimental data. We repeated the deconvolution procedure for four, five, and six site types until no more improvement was observed, as illustrated in Figures 3.9 to 3.14. Figure 3.15 shows how the value of χ^2 decreases as the number of site types increases. Notice how the value of χ^2 drops significantly as n varies from two to five (we omitted the value of χ^2 for n = 2, since it is approximately 10 times larger than when n = 3), but remains practically the same when five or six site types are selected. Therefore, within the assumptions of our model, five site types seem to give the best description of the MWD and CCD for Sample 1.

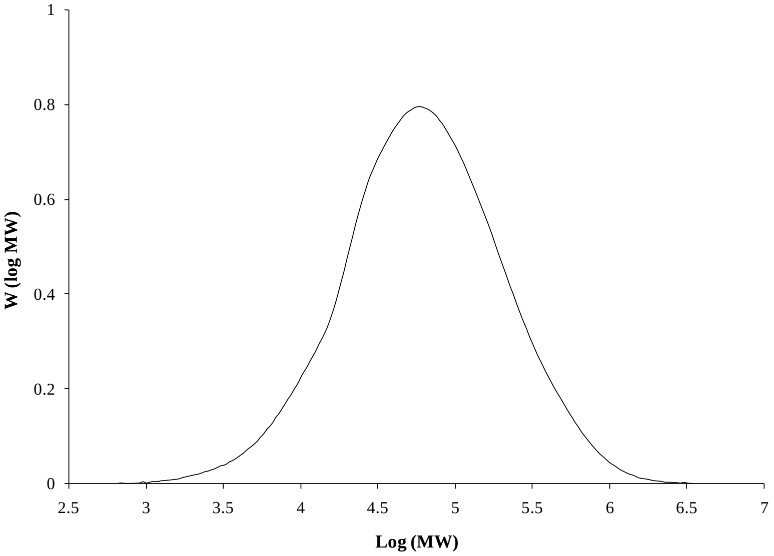

Figure 3.3 MWD of Sample 1.

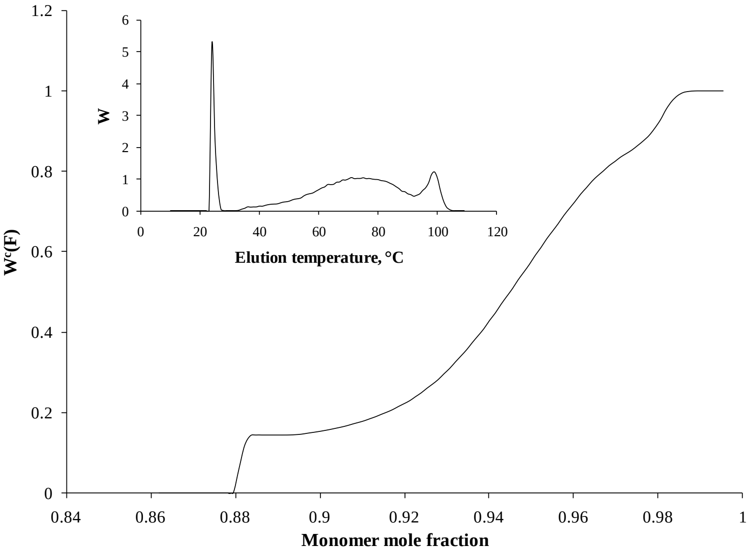

Figure 3.4 Cumulative CCD and TREF curve (insert) of Sample 1.

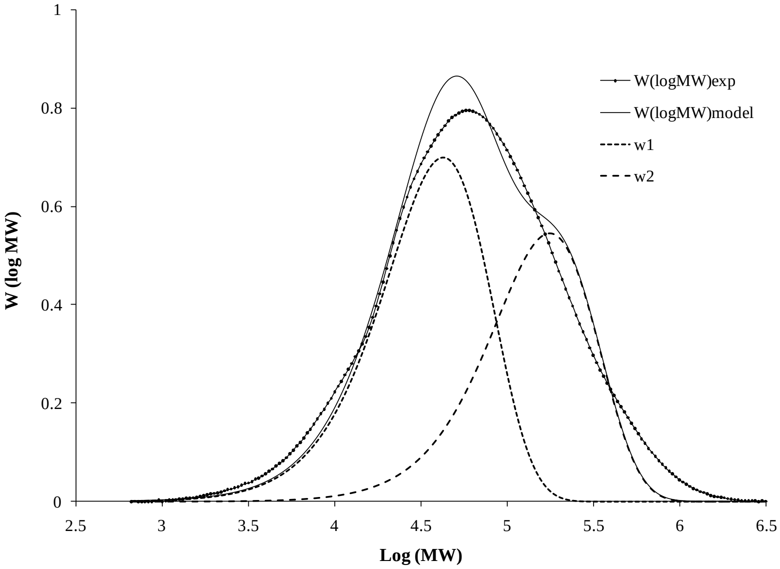

Figure 3.5 MWD deconvolution results of Sample 1 using 2 site types (χ^2 = 0.334).

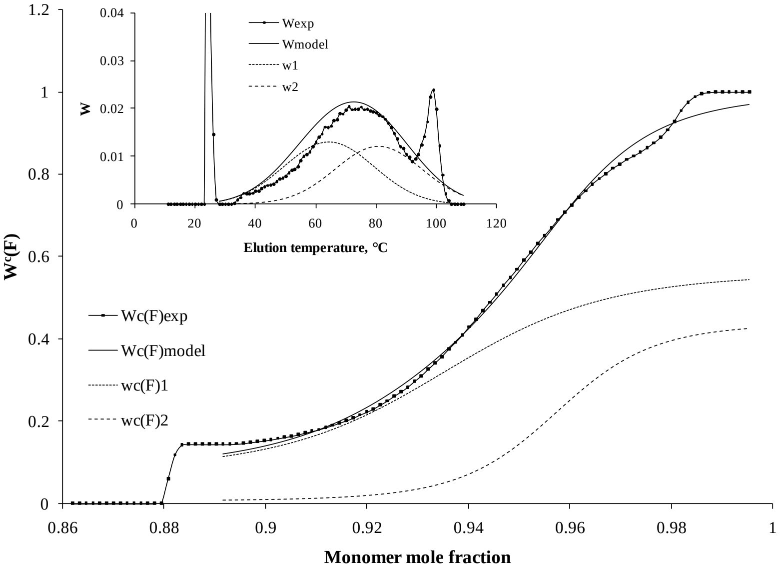

Figure 3.6 Cumulative CCD and TREF curve (insert) deconvolution results of Sample 1 using 2 site types.

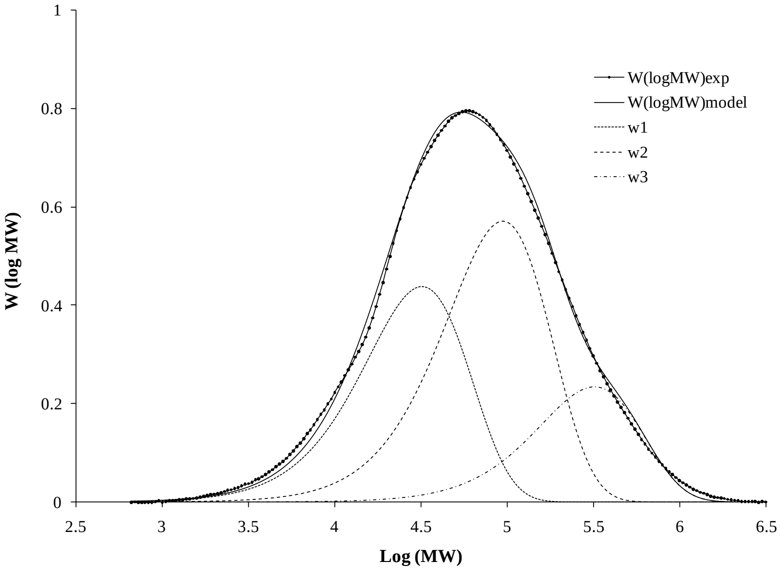

Figure 3.7 MWD deconvolution results of Sample 1 using 3 site types ($\chi^2 = 0.033$).

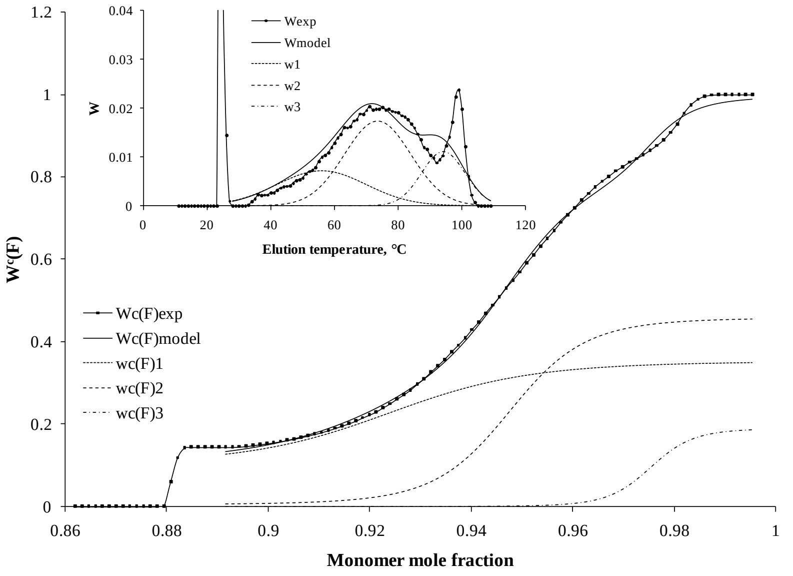

Figure 3.8 Cumulative CCD and TREF curve (insert) deconvolution results of Sample 1 using 3 site types.

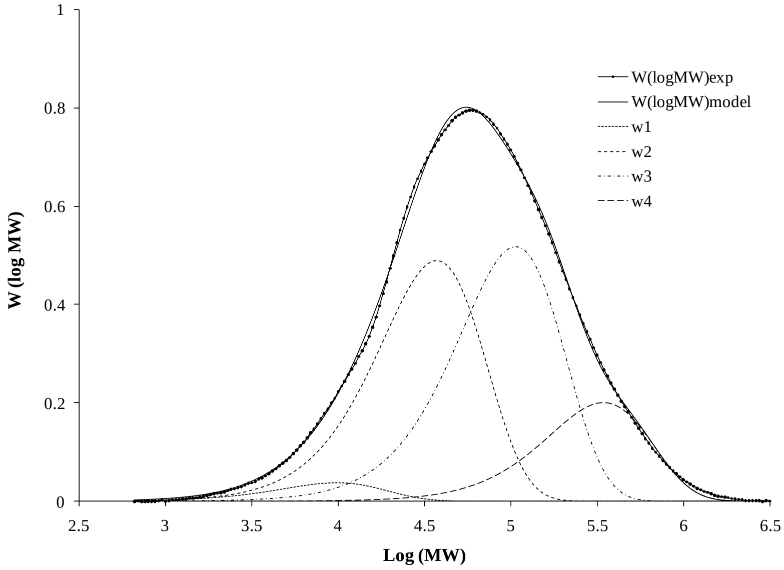

Figure 3.9 MWD deconvolution results of Sample 1 using 4 site types (χ^2 = 0.0175).

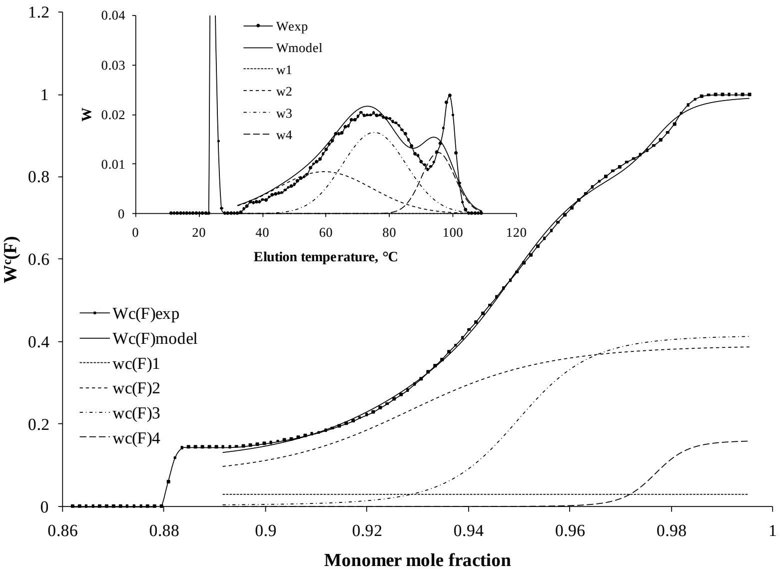

Figure 3.10 Cumulative CCD and TREF curve (insert) deconvolution results of Sample 1 using 4 site types. Site 1 is not shown in TREF curve since it makes polymer that is completely soluble at room temperature in TCB.

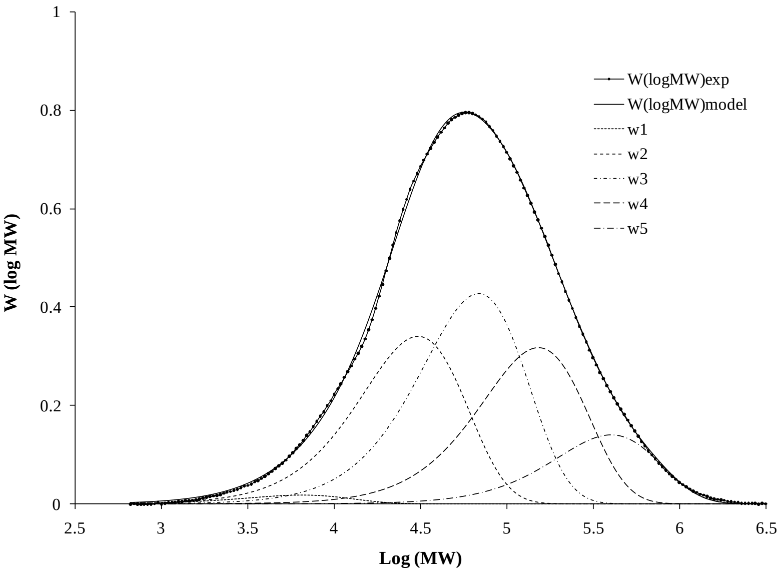

Figure 3.11 MWD deconvolution results of Sample 1 using 5 site types (χ^2 = 0.0068).

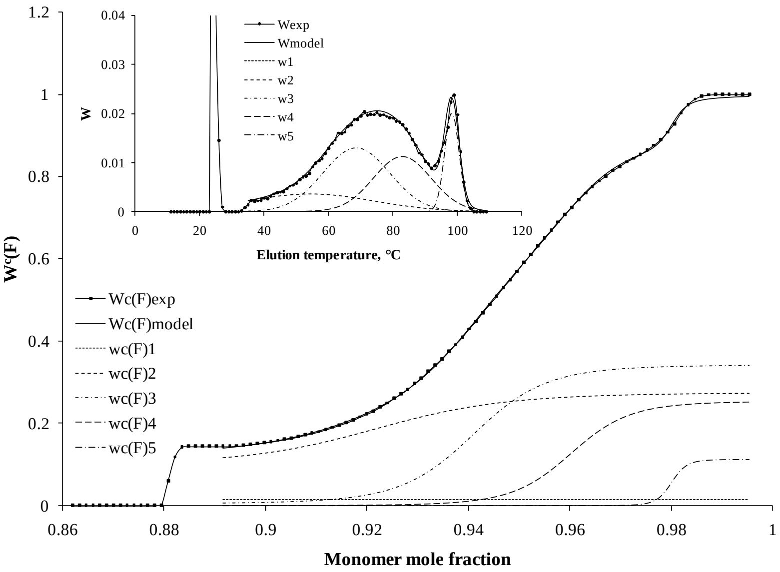

Figure 3.12 Cumulative CCD and TREF curve (insert) deconvolution results of Sample 1 using 5 site types. Site 1 is not shown in TREF curve since it makes polymer that is completely soluble at room temperature in TCB.

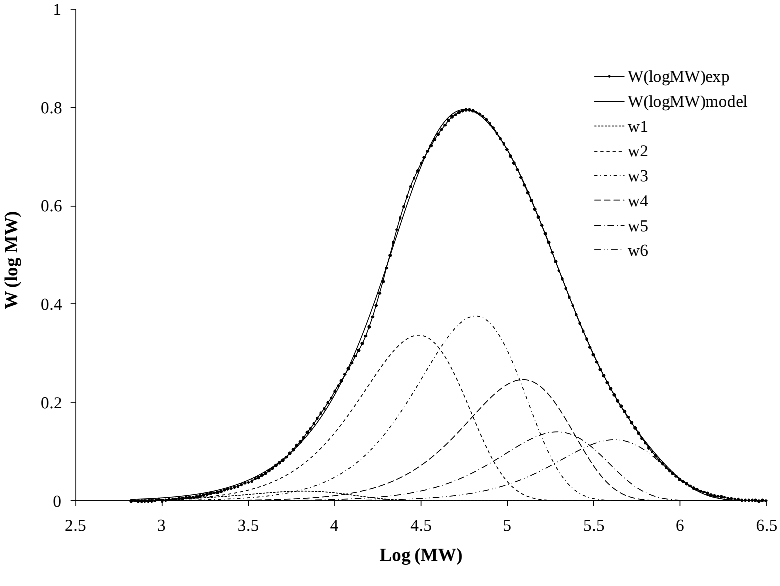

Figure 3.13 MWD deconvolution results of Sample 1 using 6 site types (χ^2 = 0.0065).

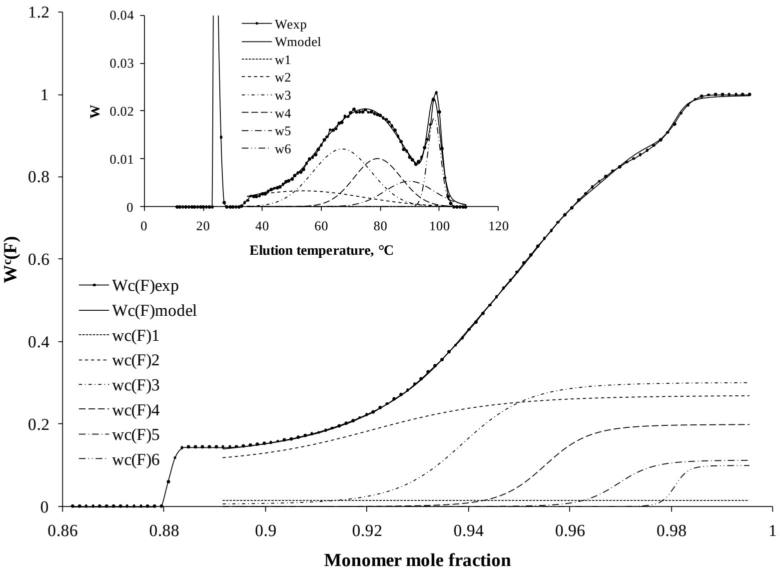

Figure 3.14 Cumulative CCD and TREF curve (insert) deconvolution results of Sample 1 using 6 site types. Site 1 is not shown in TREF curve since it makes polymer that is completely soluble at room temperature in TCB.

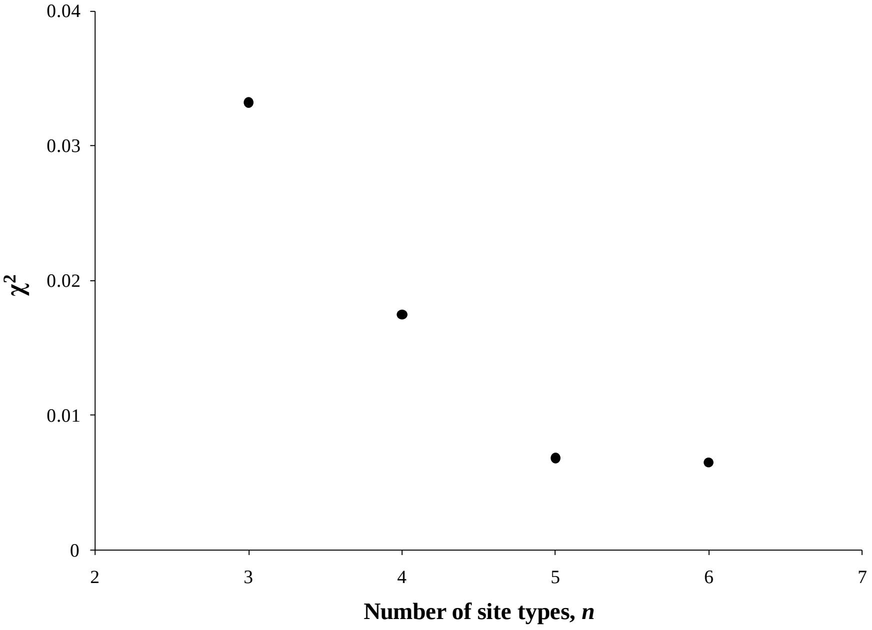

Figure 3.15 Dependency of χ^2 on the number of site types, *n*, for sample 1.

The model parameters calculated using five site types are shown in Table 3.2. Since Site 1 makes polymer that is completely soluble in TCB at room temperature, it is not possible to estimate the parameters $\overline{F_1}$ and β_1 for this site. Notice that the site types that produce polymer with higher comonomer incorporation also make polymer with lower M_n averages, as usually observed in Ziegler-Natta resins. In addition the CCDs of polymer populations with lower M_n averages are broader than those with higher M_n averages, as predicted by Stockmayer distribution. These trends were observed for all resins examined in this study.

Table 3.2 Deconvolution results for Sample 1

n	**1**	**2**	**3**	**4**	**5**
m	0.0166	0.3005	0.3519	0.2185	0.1124
m^{ns}	0	0.2061	0.3459	0.2181	0.1124
m^{s}	0.0166	0.0945	0.0060	0.0005	0
M_n	3,370	15,882	37,513	80,361	198,730
τ	2.97×10^{-4}	6.30×10^{-5}	2.67×10^{-5}	1.24×10^{-5}	5.03×10^{-6}
$1-\overline{F}$		0.9254	0.9417	0.9608	0.9801
β		0.5209	0.3544	0.3541	0.0678

It is important to point out that the catalytic site types identified through this procedure are simply characterized by their different τ and β values. This methodology is useful to obtain the minimum number of site types required to describe the MWD and CCD of a given copolymer sample for mathematical modeling; it is not intended to distinguish between these sites according to their chemical natures.

We applied the same methodology to several other resins to demonstrate its effectiveness, but will only show their final deconvolution results. The deconvolution results for the MWD and CCD of Sample 2 are shown in Figures 3.16 and 3.17, respectively; five site types gave the best data representation for this resin. Table 3 lists the final model parameters. This LLDPE sample has a very large soluble fraction (approximately 30 wt%).

As indicated in Figures 16 and 17, the model describes the MWD and CCD of this resin very well.

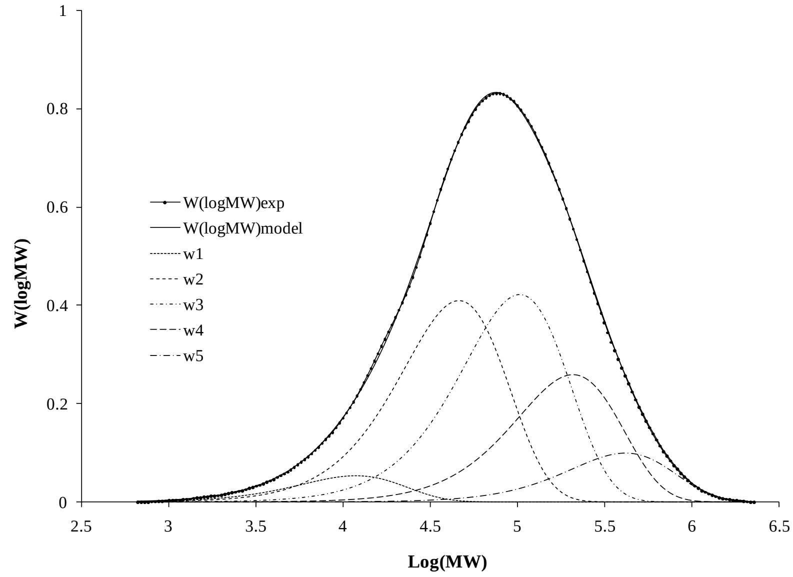

Figure 3.16 MWD deconvolution results of Sample 2 using 5 site types (χ^2 = 0.0035).

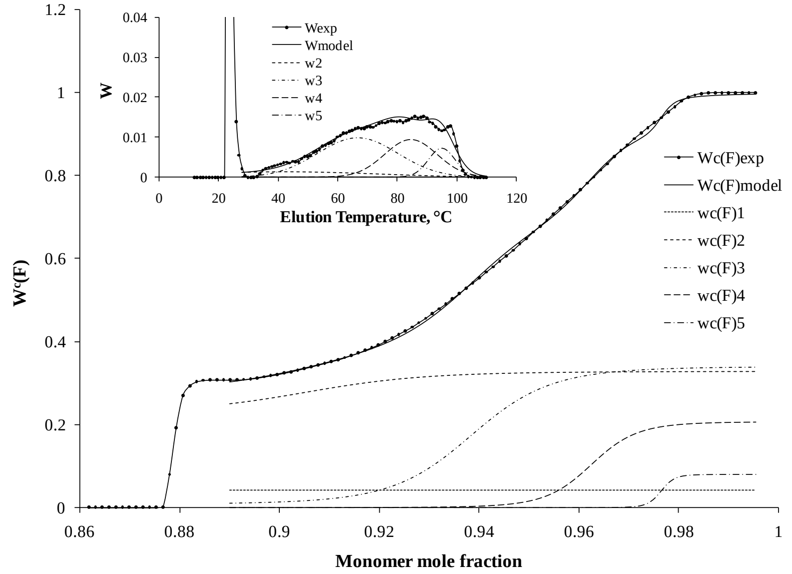

Figure 3.17 Cumulative CCD and TREF curve (insert) deconvolution results of Sample 2 using 5 site types. Site 1 is not shown in TREF curve since it makes polymer that is completely soluble at room temperature in TCB.

Table 3.3 Deconvolution results for Sample 2

n	**1**	**2**	**3**	**4**	**5**
m	0.0429	0.3291	0.3395	0.2082	0.0804
m^{ns}	0	0.1025	0.3312	0.2079	0.0804
m^{s}	0.0429	0.2266	0.0083	0.0003	0
M_n	5,915	23,072	51,507	103,996	208,100
τ	1.69×10^{-4}	4.33×10^{-5}	1.94×10^{-5}	9.62×10^{-6}	4.81×10^{-6}
$1-\overline{F}$		0.9054	0.9385	0.9625	0.9765
β		0.5527	0.5456	0.3685	0.0614

Similarly, Samples 3 and 4, illustrating different LLDPE resin microstructures, were analyzed by the deconvolution model. Five site types were required to represent the MWD and CCD of these samples as well, as illustrated in Figure 3.18 to 3.21. This illustrates how our method can be used to deconvolute the CCD and MWD of LLDPE samples with very different microstructures.

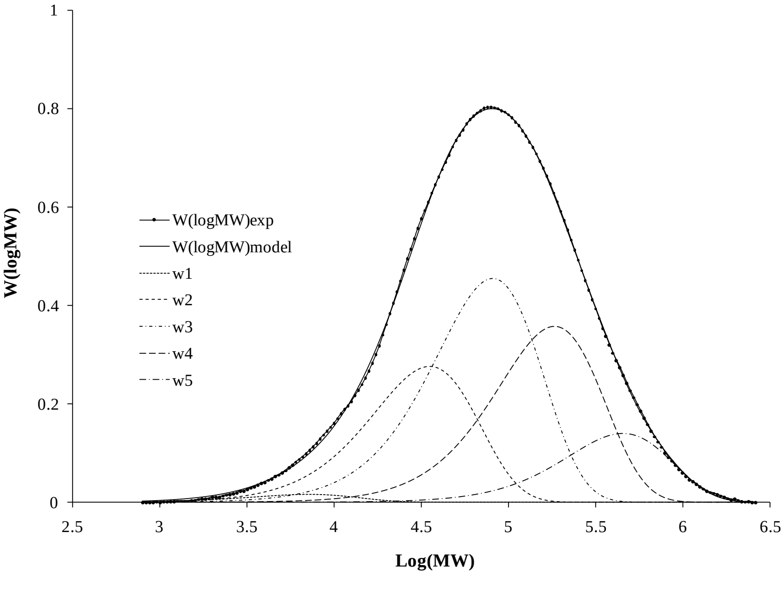

Figure 3.18 MWD deconvolution results of Sample 3 using 5 site types (χ^2 = 0.0045).

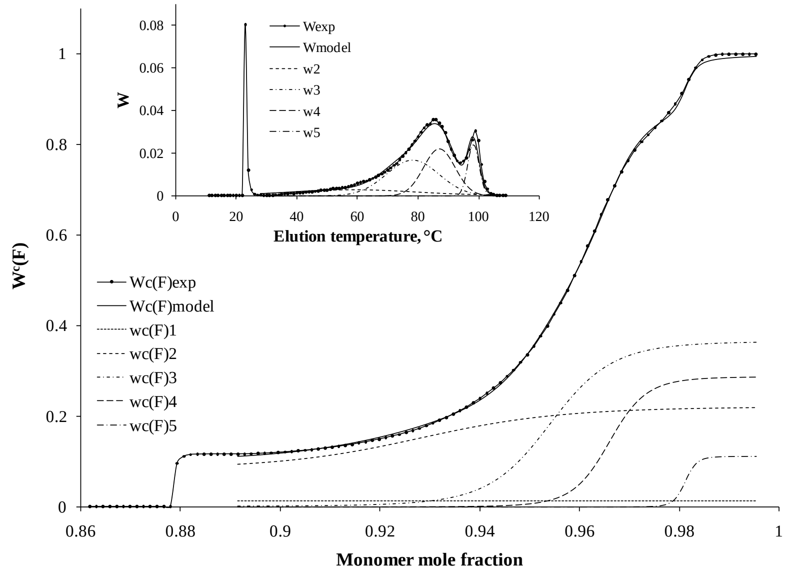

Figure 3.19 Cumulative CCD and TREF curve (insert) deconvolution results of Sample 3 using 5 site types. Site 1 is not shown in TREF curve since it makes polymer that is completely soluble at room temperature in TCB.

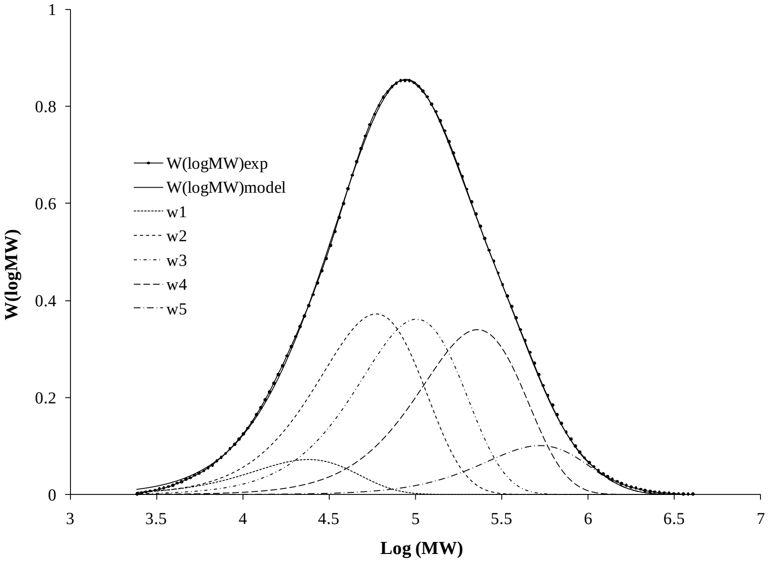

Figure 3.20 MWD deconvolution results of Sample 4 using 5 site types (χ^2 = 0.0038). The GPC and TREF data of this sample are from [151].

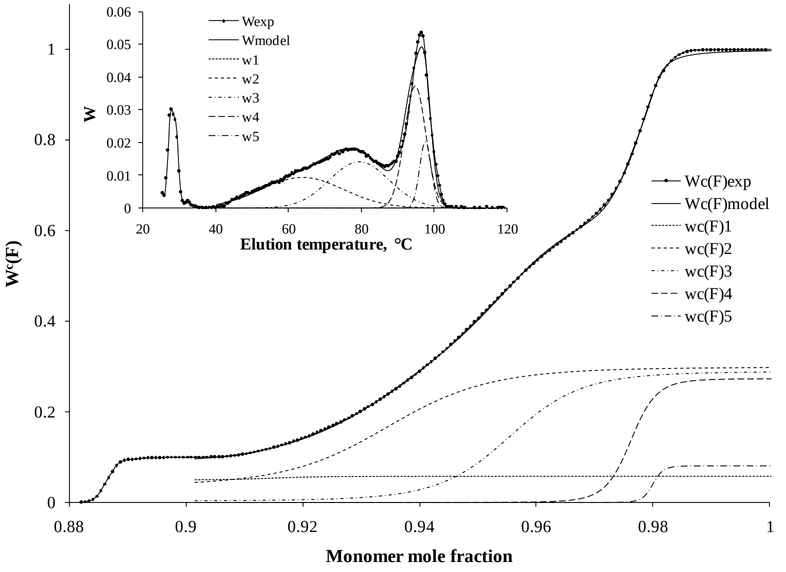

Figure 3.21 Cumulative CCD and TREF curve (insert) deconvolution results of Sample 4 using 5 site types. Site 1 is not shown in TREF curve since it makes polymer that is completely soluble at room temperature in TCB.

Finally, the simultaneous deconvolution procedure was applied to a polymer made with a single-site catalyst as shown in Figures 3.22 and 3.23. One site is able to describe the MWD reasonably well, although the inclusion of an additional site would improve the fit slightly. Assuming that the catalyst used to make this resin is truly behaving as a single-site catalyst, the source of this small deviation may be related to experimental broadening of the GPC curve or, perhaps, to slightly non-uniform polymerization conditions. On the other hand, the CCD is very well described even with only one site type.

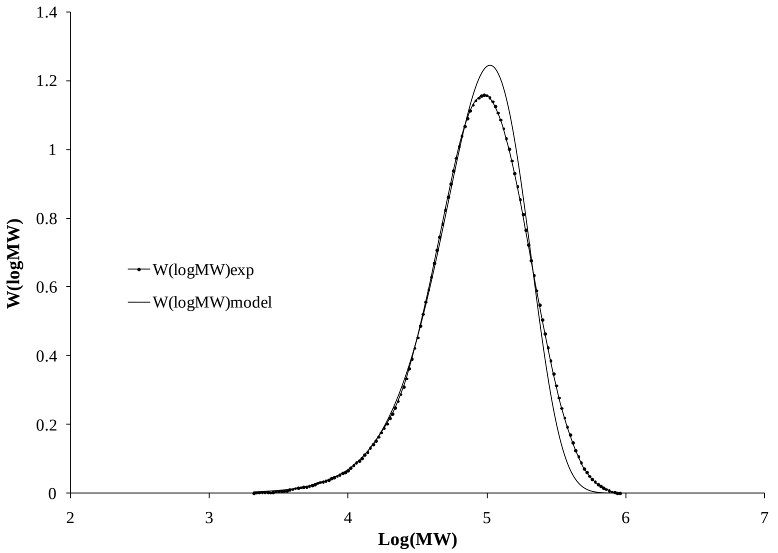

Figure 3.22 MWD deconvolution results of a polymer made with a single site catalyst ($M_{w\ \mathrm{exp}}$ = 111,200, $M_{n\ \mathrm{exp}}$ = 54,400 and χ^2 = 0.32, $M_{n\ \mathrm{model}}$ = 52,840).

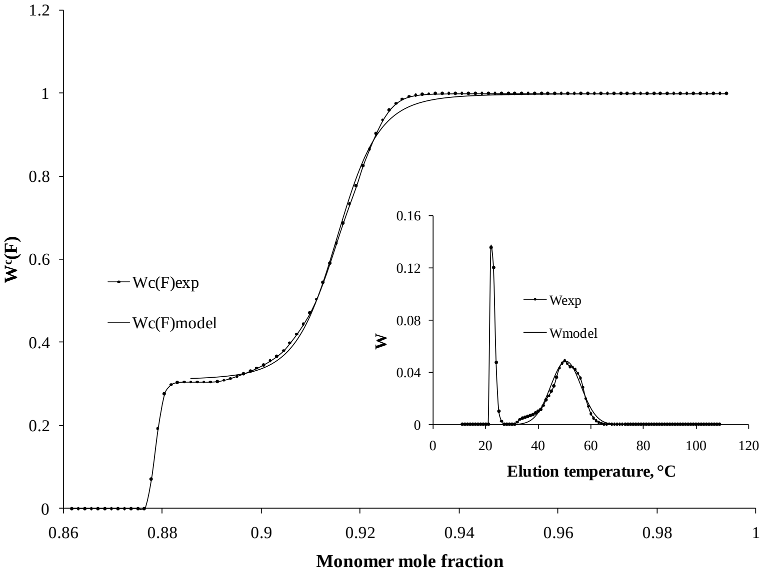

Figure 3.23 Cumulative CCD and TREF curve (insert) deconvolution results of a polymer made with single site catalyst ($1-\overline{F}=0.915$).

3.4 CONCLUSIONS

Polyolefins made with heterogeneous Ziegler-Natta catalysts have broad molecular weight and chemical composition distributions, with MWD polydispersities in the range of 4 to 20 and bi- or multimodal CCDs. These distributions, commonly measured by GPC, TREF and CRYSTAF are very important in determining physical and rheological properties of polyolefins. A mathematical model is needed to link these distributions to the different site types existing on heterogeneous Ziegler-Natta catalysts.

We developed a new mathematical procedure to deconvolute the MWD and cumulative CCD of polyolefins made with heterogeneous Ziegler-Natta catalysts, taking into consideration the room temperature soluble fractions. We applied this novel technique to a series of industrial Ziegler-Natta polyolefins and showed that it could estimate the number of active site types, number average molecular weight, average comonomer mole fraction, and mass fraction of soluble and non soluble polymer made on each site in an accurate and repeatable way.

Chapter 4

POLYOLEFIN CHARACTERIZATION EXPERIMENTS

4.1 POLYMER SAMPLES

One of the main objectives of the experimental part of this research was to study the effect of operating conditions of CEF and HT-TGIC on the CCDs of single-site and multiple-site polyolefins and its blends. Several industrial polyethylene and ethylene/1-octene copolymers made with metallocene and Ziegler-Natta catalyst were used in this research.

A series of ethylene/1-octene copolymers with different 1-octene contents were used to study the effect of comonomer content on CEF and HT-TGIC. These copolymers were made with a single site catalyst in a solution polymerization. Table 4.1 summarizes the properties of these samples. Three samples with low number average molecular weight (M_n) were used to study the effect of molecular weight on CEF and HT-TGIC profiles. The polymer samples were donated by Dow Chemical. The molecular weight averages and the average comonomer contents of these samples were measured at Dow Chemical labs by GPC and ^{13}C NMR, respectively.

TABLE 4.1 Ethylene/1-octene samples

Sample	Octene mol %	M_n
m-1	0	46,600
m-2	0	19,000
m-3	0.16	48,161
m-4	1.16	47,000
m-5	1.14	15,000
m-6	2.2	47,700
m-7	3.51	49,800
m-8	3.59	16,500

4.2 EXPERIMENTAL PROCEDURE

A CEF instrument (Polymer Char, Valencia, Spain) was used to measure the CCDs of the resins in this study. The instrument consists of four main parts: autosampler, main oven, top oven, and isocratic pump. A schematic diagram of this instrument is shown in Figure 4.1.

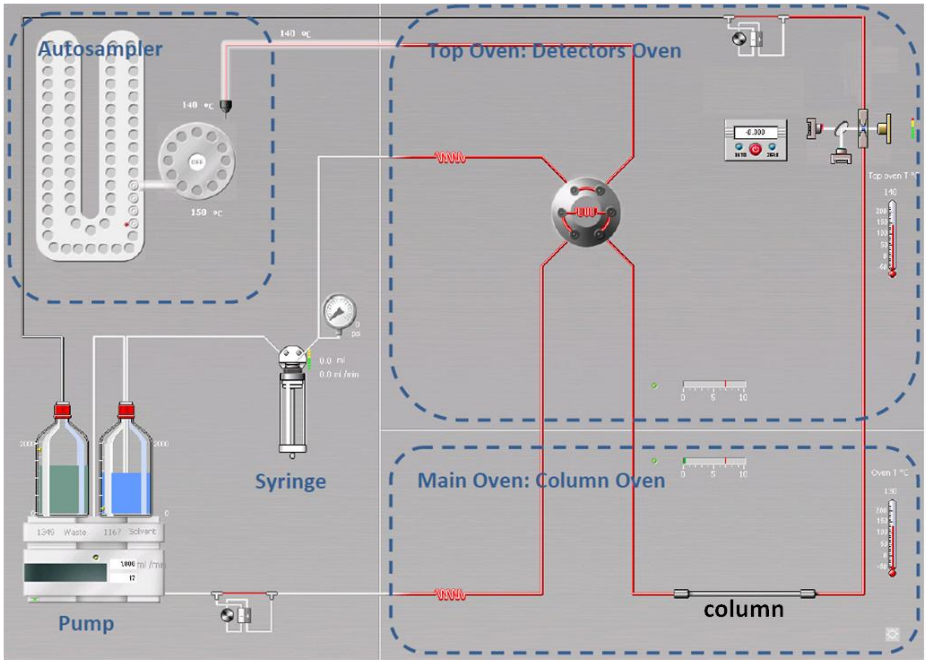

Figure 4.1 Schematic diagram of CEF instrument.

4.2.1 SAMPLE PREPARATION

The samples were first dissolved in 8 ml of solvent inside 10-ml size vials. The dissolution was carried out at the instrument's autosampler at 160 °C. The sample concentrations were 1 mg/ml for the individual resins and 2 mg/ml when two resins were blended. The dissolution time was 1 hour.

4.2.2 INJECTION

At the end of the dissolution period, the samples were transferred from the autosampler to the injection loop using a dispenser. The injection loop is located at the top oven. The content of the loop (0.4 ml) was injected into the column using an isocratic pump. At the column, the polymers were fractionated using two temperature cycles. The analysis method is shown schematically in Figure 4.2. During the cooling cycle, the column temperature is decreased under continuous solvent flow within the limits of the column. This solvent flow rate is calculated from the column volume, cooling rate, and the difference between the first and the last temperatures in the cooling cycle.[82] At the end of the cooling cycle, the temperature is kept constant for few minutes and the solvent flow rate is increased to the elution flow rate value to allow the soluble polymer to leave the column and reach the detector. The deposited fractions are then dissolved as the temperature increases during the elution cycle using a continuous solvent flow that allows the fractions to move from the column to the detector in order to measure their concentrations. The infrared detector (IR4, Polymer Char, Valencia, Spain) is located at the instrument's top oven and is kept at constant temperature. At the end of elution cycle, the column is cleaned with fresh solvent at high flow rate (1.2 mL/min for 10 min) in order to be ready for the injection of the next sample.

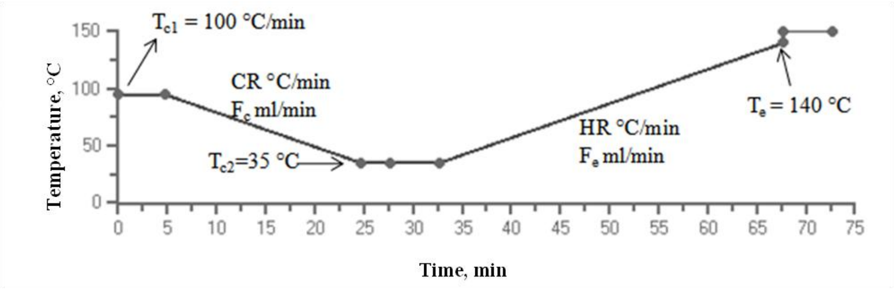

Figure 4.2 CEF analysis method: T_{c1} and T_{c2} are the first and last temperatures in the crystallization cycle, *CR* is the cooling rate, F_c is the solvent flow rate during the cooling cycle, *HR* is the heating rate, F_e is the solvent flow rate during the heating cycle, and T_e is the last temperature in the heating cycle.

4.2.3 Columns

The column is located inside the instrument's main oven. When a CEF column is installed, the instrument can be used to measure the CCDs based on the polymers crystallinity. The HT-TGIC profiles can be measured when a hypercarb® column is used. The columns are shown in Figure 4.3. Two CEF columns were used: Column-1 (2.1 mm i.d. × 2 m length); Column-2 (3.7 mm i.d. × 1 m length) both filled with stainless steel shots. The hypercarb® column is packed with porous graphitic carbon with the following parameters: column size 100 × 4.6 mm i.d., average particle size of 5 µm, surface area of 120 m^2/g and pore size of 250 Å (Thermo Scientific).

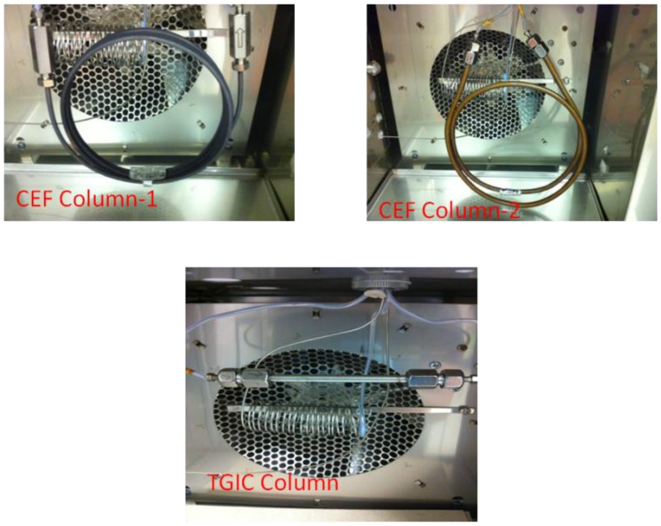

Figure 4.3 Columns used for CEF and HT-TGIC experiments.

4.2.4 Solvents

1,2,4-trichlorobenzene (TCB) was used as a solvent for all the CEF experiments. To study the effect of solvent on HT-TGIC adsorption/ desorption processes three different solvents were used: o-dichlorobenzene (ODCB), 1,2,4-trichlorobenzene (TCB), and chloronaphthalene (CN). Antioxidant (Irganox 1010) was added to the solvents at a concentration of 0.25 g/L to prevent the sample from thermal degradation during the analysis.

4.3 GPC EXPERIMENTS

High-temperature gel permeation chromatography (GPC) (Polymer Char, Valencia, Spain) was used to measure the MWD of polymer samples. The samples were dissolved in TCB in a 10 mL vial for 1 hour at 160 °C. The sample concentration was 2 mg/ml. The GPC analysis was carried out at 145 ^{o}C using a TCB flow rate of 1 mL/min. The instrument was equipped with linear SEC column (Polymer Labs) and three detectors in series: infra-red (IR4 from Polymer Char, Valencia, Spain), light scattering, and differential viscometer. Narrow polystyrene standards were used to calibrate the GPC.

Chapter 5

EFFECT OF OPERATING CONDITIONS ON HT-TGIC

5.1 INTRODUCTION

The use of polyethylene and its copolymers is rapidly growing in part because their properties can be tuned by changing their crystallinity via comonomer incorporation. Therefore, the characterization of comonomer fraction distribution in olefin copolymers is of great importance for industrial and academic applications. Basically, these commodity polymers can be separated based on their ability to crystallize from dilute solutions. As discussed in Chapter 2, TREF and CRYSTAF were used routinely for characterization of polyolefins. CEF has been invented by the research group at Polymer Char (Valencia, Spain) to enhance the separation resolution of TREF and CRYSTAF and to shorten the analysis time. However, these techniques cannot be used to fractionate the amorphous polyolefins since they do not crystallize. High-temperature HPLC, on the other hand, extends the range of CCDs that can be measured by crystallization based techniques.

Although polyolefins have been produced industrially for more than 70 years, the characterization of polyolefins based on their chemical composition by HPLC was unknown until recent years. The majority of the HPLC applications published in the open literature were performed at low temperatures (< 60°C).[152-154] However, dissolution and characterization of polyolefins in solvents such as TCB and ODCB need temperatures of up to 140-160 °C. The pioneering work of Macko and Pasch[112-114] opened the route to characterize polyolefins using high-temperature HPLC based on adsorption-desorption mechanism. The use of Hypercarb® porous graphitic carbon (PGC) was the key for their successful characterizations of polyolefins. They reported that polyethylene, ethylene/1-alkene copolymers, atactic polypropylene (a-PP), and syndiotactic polypropylene (s-PP) were fully adsorbed on PGC columns at 160 °C. The retained polymers were desorbed and eluted from the column using a solvent gradient (from 100% 1-decanol to 100% TCB).[112-115]

Very recently, high-temperature thermal gradient interaction chromatography (HT-TGIC) was used to fractionate polyolefins based on adsorption-desorption mechanism using single solvent.[127] In this system, the polymers were dissolved in good solvent, o-dichlorobenzene (ODCB), and injected into a Hypercarb column at high temperature. HT-TGIC is similar to temperature rising elution fractionation (TREF) and crystallization elution fractionation (CEF) in that it needs two temperature cycles: cooling to adsorb the polymer chains on PGC and heating to desorb and elute the retained fractions from the column using constant solvent flow rate. Cong *et al.* have used HT-TGIC to fractionate a series of ethylene/1-octene copolymers. They found that the peak temperatures of HT-TGIC chromatograms depended linearly on the 1-octene content.[127] Monrabal *et al.*[155] claimed that the dependence of HT-TGIC elution peaks on the molar mass of polymer is insignificant for samples with molar mass above 25 kg/mol. Moreover, they combined the TGIC and CEF on the same analytical run to enhance peak separation.

In this chapter, a systematic study of HT-TGIC of ethylene/1-octene copolymers and their blends was conducted to provide better understanding of the separation mechanism in this new technique. The effect of operating conditions such as cooling rate, heating rate, adsorption/desorption temperature range, and sample size were studied carefully to find out the best set of conditions that enhances the resolution of HT-TGIC.

5.2 EXPERIMENTAL

All the HT-TGIC experiments were performed using the crystallization elution fractionation (CEF) instrument (Polymer Char, Valencia, Spain). The detailed experimental procedure was described in Section 4.2. In summary, HT-TGIC analysis was conducted in three main steps:

1. The samples were dissolved in ODCB at 160 °C. Then, they were loaded to the column at a temperature of 155 °C. The sample was kept at the front of the column for 5 minutes to stabilize its temperature. Increasing the stabilization time to 30 minutes did not affect the obtained chromatograms. Therefore, 5 minutes stabilization time was used for all the experiments.

2. After the stabilization, the column temperature was reduced gradually to allow the polymer chains to adsorb on the PGC column. At the end of the cooling cycle, the temperature of the column was kept constant at the final cooling temperature for 3 minutes. Then, the pump flow rate was increased to elution flow rate to remove the entire soluble fraction that was not adsorbed at the final cooling temperature.
3. The temperature was then increased at a certain heating rate to desorb and elute the retained polymers. All the experiments in this study were performed using ODCB as a solvent.

The average properties of the polyethylene and ethylene/1-octene copolymers were listed in Table 4.1. In addition, three blends were used in this study to test the separation resolution by HT-TGIC. The components of these blends are listed in Table 5.1. It is very important to point out that the HT-TGIC profiles measured using different operating conditions will be compared in this work and the term “resolution” will be used to represent the quality of peak separation obtained at different condition. This resolution term in this work does not have the same meaning used to describe the chromatography results of small molecules at ambient temperature.

Table 5.1 Blend components, mol% of 1-octene

Sample	Component 1	Component 2
Blend-1	2.2%	1.16%
Blend-2	3.51%	1.16%
Blend-3	3.51%	0.16%

5.3 RESULTS AND DISCUSSION

Table 5.2 lists the main parameters studied in this chapter. The reproducibility of the HT-TGIC chromatograms was excellent, as illustrated in Figure 5.1 for the individual resins and Figure 5.2 for the blends. The analysis of two individual resins (1.16 mol % and 2.2 mol % 1-octene) and their 50/50 wt-% blend (Blend-1) was repeated twice using a cooling rate of 5 °C/min, a heating rate of 1 °C/min and elution flow rate of 0.5 mL/min. The three chromatograms overlay very well.

Table 5.2 Main operating conditions

Parameter	Symbol	values
Cooling rate (°C/min)	CR	5 and 1
Cooling cycle (°C)	--	(155 - 35) and (155 - 90)
Cooling Flow rate (mL/min)	Fc	0, 0.01, 0.02
Heating rate (°C/min)	HR	3 and 1
Elution Flow rate (mL/min)	Fe	0.5
Sample size (μL)	SZ	400, 100, and 50

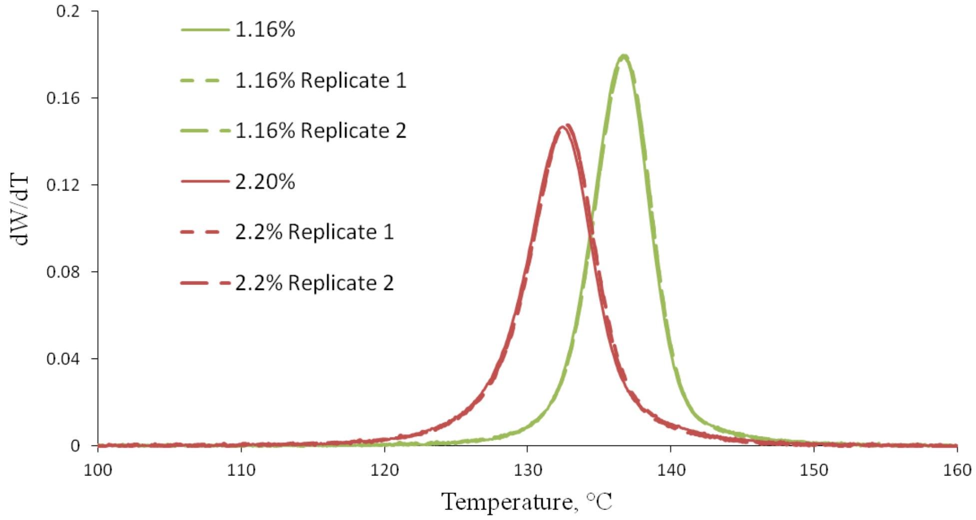

Figure 5.1 Repeatability of HT-TGIC profiles for individual resins. Experimental conditions: SZ = 400 µL, CR = 5 °C/min (155 - 90 °C), Fc = 0.02 mL/min, HR = 1 °C/min [90 - 160 °C], Fe = 0.5mL/min.

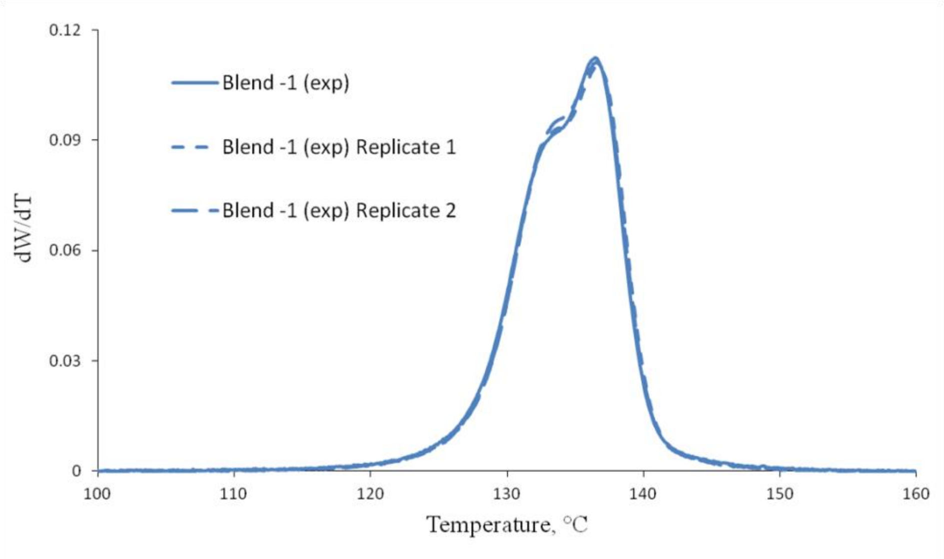

Figure 5.2 Repeatability of HT-TGIC profiles for Blend-1. Experimental conditions: SZ = 400 µL, CR = 5 °C/min (155 - 90 °C), Fc = 0.02 mL/min, HR = 1 °C/min [90 - 160 °C], Fe = 0.5mL/min.

5.3.1 EFFECT OF ADSORPTION/DESORPTION TEMPERATURE RANGE

HT-TGIC analyses need two temperature cycles: cooling and heating. In the cooling cycle, the adsorption of the polymer chains on the PGC material takes place while the column temperature is decreasing. The fraction with the lowest comonomer content is adsorbed first at the highest temperature, while the other fractions remain in the solvent phase until their adsorption temperatures are reached. In the next fractionation cycle, the retained polymer chains are eluted with the solvent at increasing temperatures. The solvent first removes the fractions with higher comonomer content followed by those with lower comonomer content.

In this study, two adsorption/desorption temperature ranges were studied for the individual resins and their blend. In both sets of experiments, the polymer samples were injected in the column at 155 °C. Then, the column temperature was decreased either to 35 °C in the first set of experiments, or to 90 °C in the second one. During the heating cycle, the column temperature was increased to 160 °C. The HT-TGIC profiles using these two temperature ranges are shown in Figure 5.3 and Figure 5.4 for three individual resins and Blend-1, respectively. The obtained results at [155 °C – 35 °C – 160 °C] and [155 °C – 90 °C – 160 °C] overlay almost completely, indicating that these resins were fully adsorbed at a temperature above 90 °C. Therefore, the HT-TGIC analysis of such resins can be done in shorter time without affecting the quality of the obtained profile. These resins are also totally soluble in ODCB at 90 °C. Thus, the HT-TGIC analyses using an adsorption/desorption temperature range of [155 °C – 90 °C – 160 °C] were performed without formation of polymer crystals during the cooling cycle. Consequently, the fractionation can be considered to be free of co-crystallization effects that usually reduce the resolution of crystallinity-based techniques such as TREF and CEF.

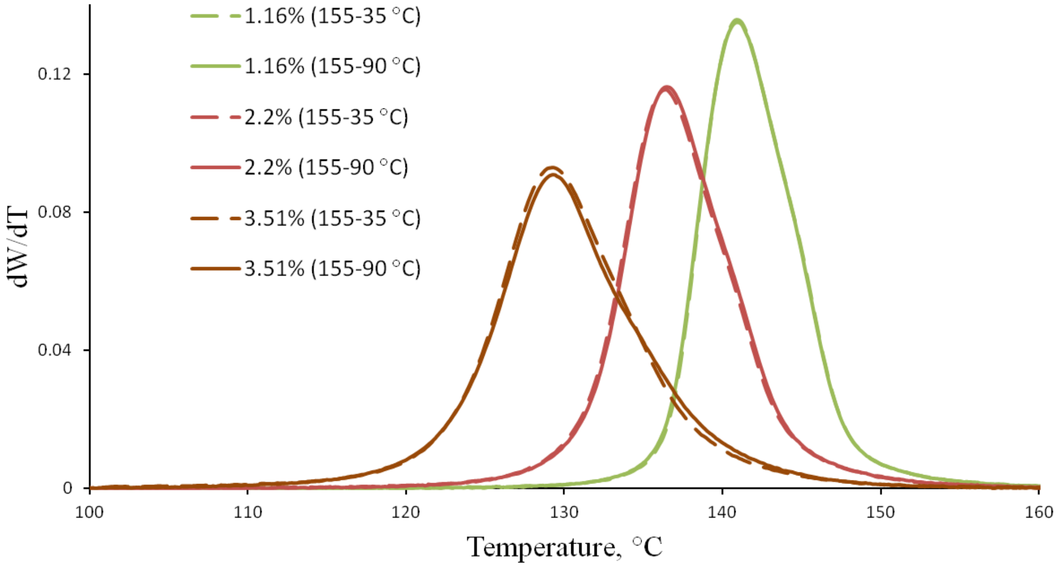

Figure 5.3 Effect of adsorption/desorption temperature range on HT-TGIC profiles for individual resins. Experimental conditions: SZ = 400 µL, CR = 5 °C/min, Fc = 0.02 mL/min for [155 – 90 °C] and Fc = 0.01 mL/min for [155 – 35 °C], HR = 3°C/min, Fe = 0.5mL/min.

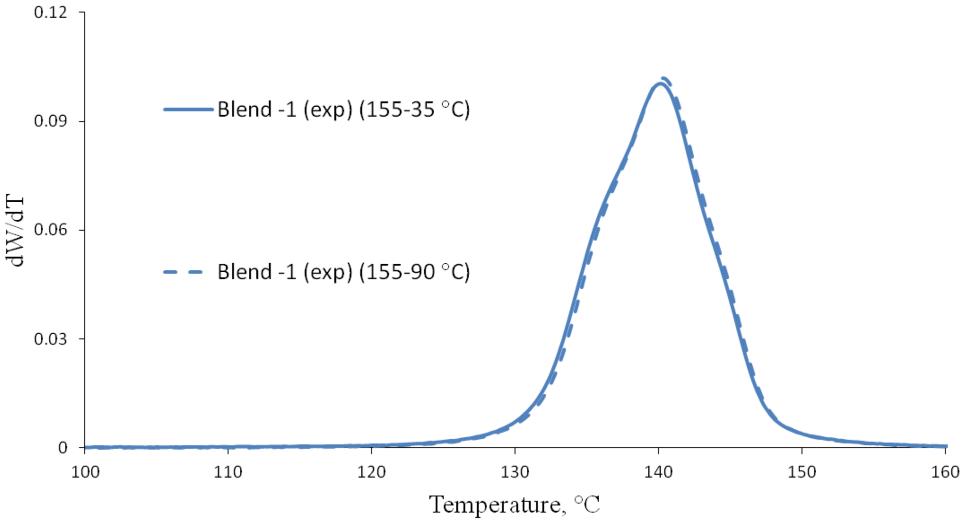

Figure 5.4 Effect of adsorption/desorption temperature range on HT-TGIC profiles for Blend-1. Experimental parameters: SZ = 400 µL, CR = 5 °C/min, Fc = 0.02 mL/min for [155 – 90 °C] and Fc = 0.01 mL/min for [155 – 35 °C], HR = 3 °C/min, Fe = 0.5mL/min.

5.3.2 CR AND HR EFFECTS ON HT-TGIC OF INDIVIDUAL RESINS

HT-TGIC separates polymer chains based on adsorption/desorption mechanism in a temperature gradient. To study the effect of cooling rate on the adsorption process, two cooling rates were used, 5 °C/min and 1 °C/min. Figure 5.5 shows the chromatograms of three individual resins (3.51 %, 2.2 % and 1.16 mol % 1-octene) measured using these cooling rates. The results indicate that the cooling rate has insignificant effect on the HT-TGIC profiles.

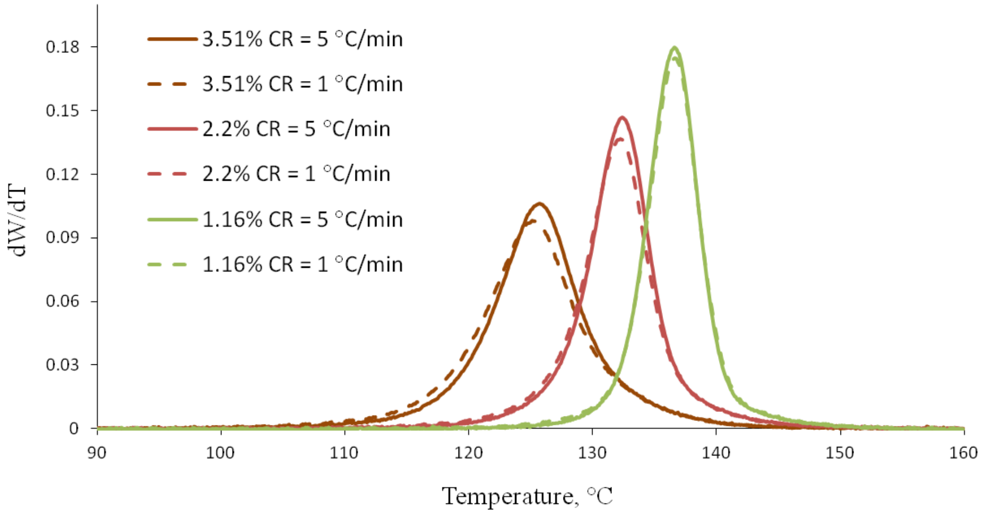

Figure 5.5 Effect of cooling rate on HT-TGIC profiles of individual resins. Experimental conditions: SZ = 400 µL, Fc = 0.02 mL/min for CR = 5 °C/min and Fc = 0.01 mL/min for CR = 1 °C/min, HR = 3 °C/min, Fe = 0.5mL/min.

The polymer desorption occurs during the heating cycle. Figure 5.6 and Figure 5.7 show the chromatograms of individual resins using a heating rate of 3 °C/min and 1 °C/min, respectively. It is very important to point out that ethylene homopolymer elutes from the column at higher temperature and has narrower distribution when compared with the ethylene/1-octene copolymers. The CCDs of ethylene/1-octene copolymers tend to broaden HT-TGIC profiles and shift them to lower temperature as the comonomer content increases. The same behavior was observed by Macko *et al.*[115] for ethylene/1-hexene copolymers studied by HT-HPLC using solvent gradient method. In their system, the retention volume decreased as the comonomer content increased. This behavior can be attributed to a stronger adsorption of polyethylene chains without short chain branches (SCB) on the PGC columns, compared with that of ethylene/1-alkene copolymers. It has been suggested that PE chains without SCBs form closely packed monomolecular layers parallel to the PGC surface, as illustrated in Figure 5.8. The incorporation of α-olefin SCBs in the chains may sterically hinder and disrupt the formation of these closely packed layers. Therefore, the presence of SCBs hinders chain adsorption and reduces their elution temperature. The analysis is very sensitive to comonomer content. The difference between an ethylene homopolymer and a copolymer with only 0.16 mol % of 1-octene was easily observed.

The relationship between the elution peak temperature and comonomer content is linear and can be used to calibrate the profiles of HT-TGIC. From the resins studied in this work, the parallel calibration curves were obtained using a heating rate of 3 and 1 °C/min, as shown in Figure 5.9.

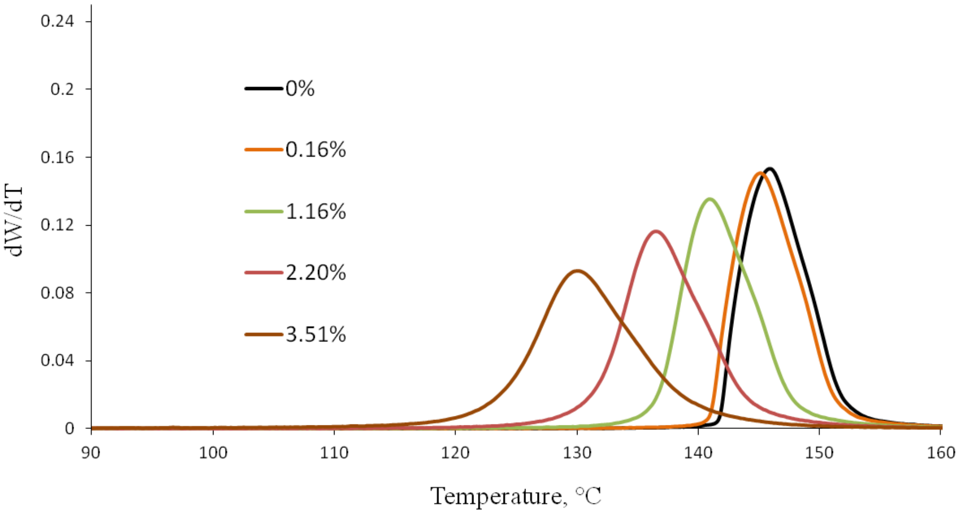

Figure 5.6 HT-TGIC profiles of individual resins. Experimental conditions: SZ = 400 µL, CR = 5 °C/min [155 – 90 °C], Fc = 0.02 mL/min, HR = 3 °C/min, Fe = 0.5mL/min.

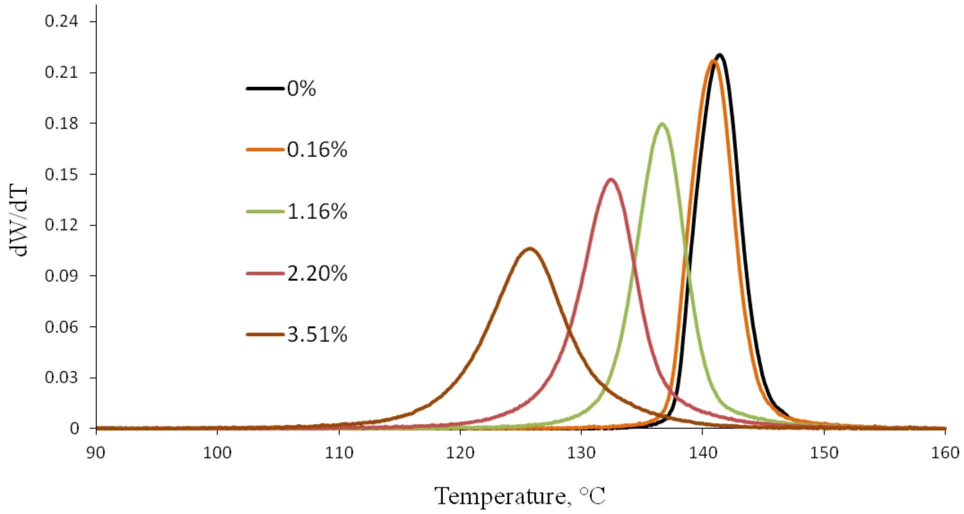

Figure 5.7 HT-TGIC profiles of individual resins. Experimental conditions: SZ = 400 µL, CR = 5 °C/min [155 – 90 °C], Fc = 0.02 mL/min, HR = 1 °C/min, Fe = 0.5mL/min.

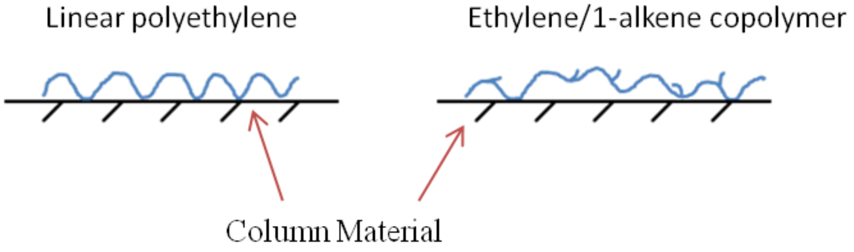

Figure 5.8 The presence of short chain branches hinder polymer chain adsorption on the graphite surface.

All the individual resins show broader chromatograms at a heating rate of 3 °C/min than at 1 °C/min, as clearly shown in Figure 5.10. This broadness may be attributed to a more significant co-desorption of the chains at the faster heating rate. It may be argued that the adsorbed polymer chains may not have enough time to desorb and elute from the column at its own desorption temperature when the column is heated at 3 °C/min.

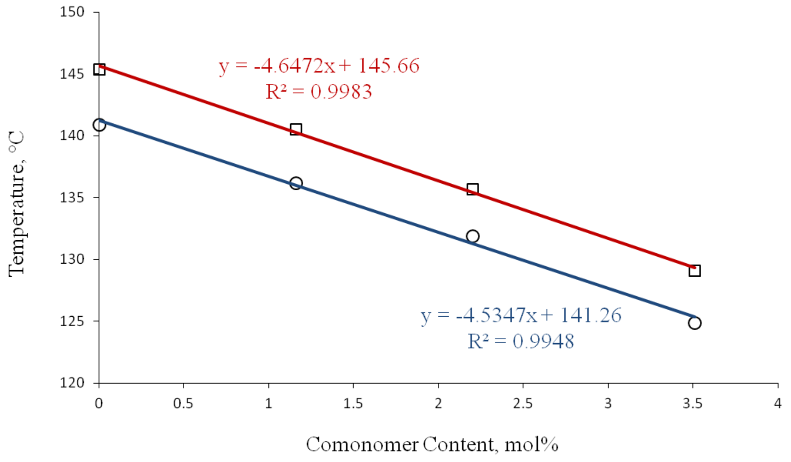

Figure 5.9 Calibration curves for HT-TGIC using a heating rate of 3 °C/min (red line) and 1 °C/min (blue line). Experimental conditions: SZ = 400 μL, CR = 5 °C/min [155 – 90 °C], Fc = 0.02 mL/min, Fe = 0.5mL/min.

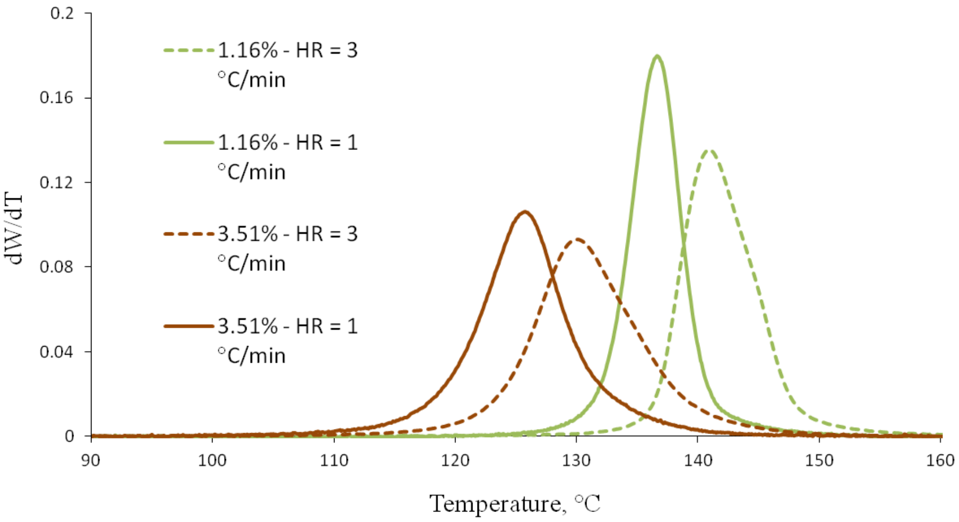

Figure 5.10 Effect of heating rate on HT-TGIC of individual resins. Experimental conditions: SZ = 400 μL, CR = 5 °C/min [155 – 90 °C], Fc = 0.02 mL/min, Fe = 0.5mL/min.

5.3.3 HT-TGIC OF BLENDS

The resolution of the HT-TGIC profiles were tested using the blends listed in Table 5.1. The experimental profile of Blend-1 as compared with the chromatograms of the individual component resins is shown in Figure 5.11. The dotted line in Figure 5.11

represents the profile of the blend calculated from the weighted sum of the experimental profile of each component obtained using the same run conditions. The components of Blend-1, 2.2 % and 1.16 mol % of 1-octene, have similar crystallizabilities. Adequate peak resolution between these components by crystallization-based techniques is difficult to achieve due to significant co-crystallization effects. On the other hand, the experimental HT-TGIC profile using a cooling rate of 5 °C/min and a heating rate of 3 °C/min, matches the calculated one, as shown in Figure 5.11. However, the blend of these two components shows only one peak. Peak separation was improved by reducing the heating rate to 1 °C/min and keeping the cooling at 5 °C/min, as seen on Figure 5.12, the experimental profile starting to show a shoulder at a temperature of 134 °C. The results of Blend-1 using a cooling and a heating rate of 1 °C/min, Figure 5.13, showed the best peak separation between the two blend components and excellent agreement between the calculated and experimental profiles of the blend.

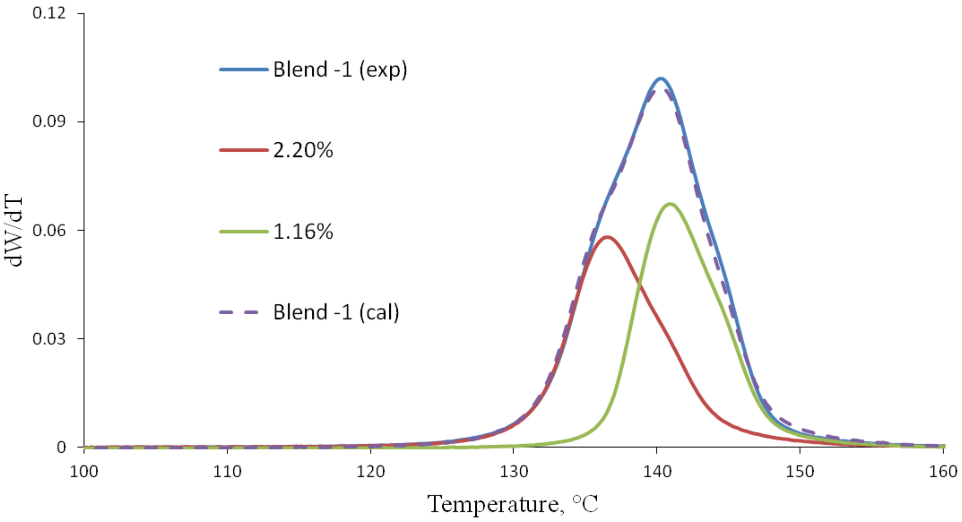

Figure 5.11 HT-TGIC profile of Blend-1 and its components. Experimental conditions: SZ = 400 µL, CR = 5 °C/min [155 – 90 °C], Fc = 0.02 mL/min, HR = 3 °C/min, Fe = 0.5mL/min.

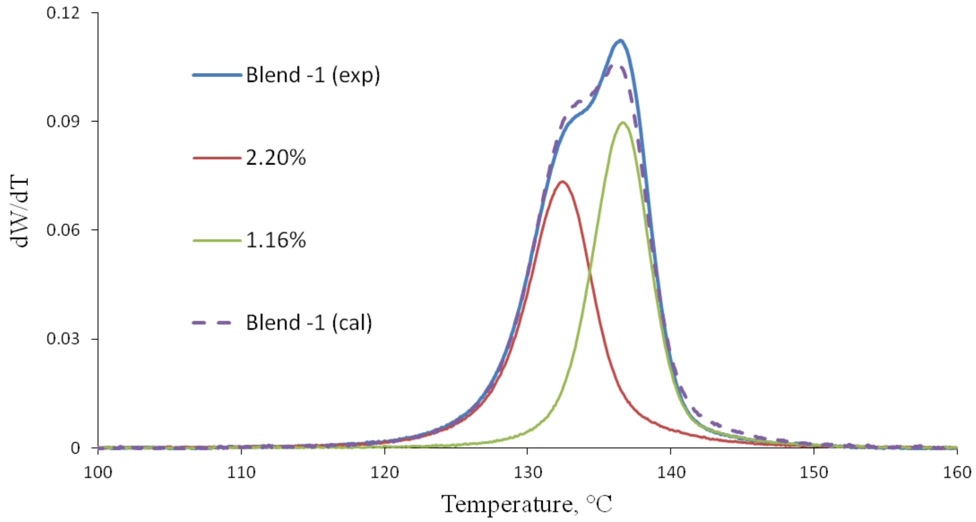

Figure 5.12 HT-TGIC profile of Blend-1 and its components. Experimental conditions: SZ = 400 µL, CR = 5 °C/min [155 – 90 °C], Fc = 0.02 mL/min, HR = 1 °C/min, Fe = 0.5mL/min.

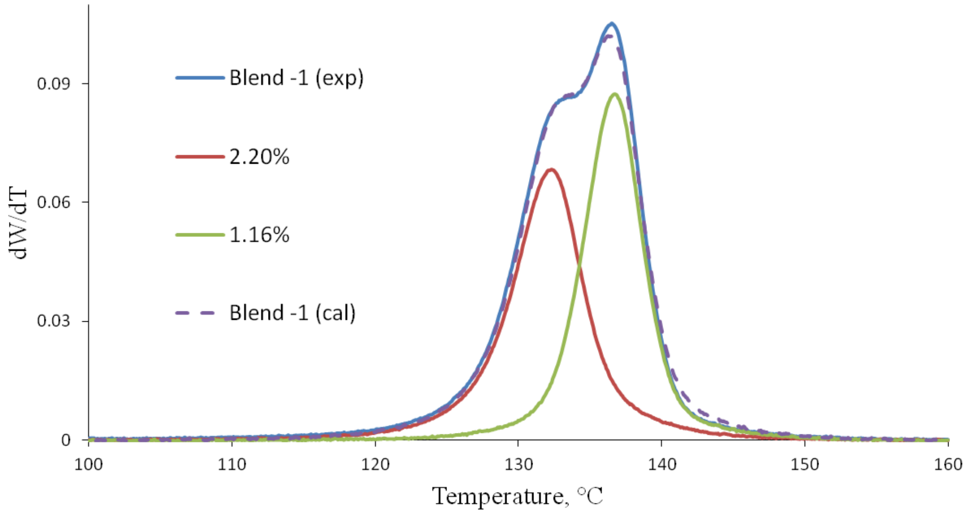

Figure 5.13 HT-TGIC profile of Blend-1 and its components. Experimental conditions: SZ = 400 µL, CR = 1 °C/min [155 – 90 °C], Fc = 0.02 mL/min, HR = 1 °C/min, Fe = 0.5mL/min.

Blend-2 (3.51 % and 1.16 mol % of 1-octene) was analyzed by HT-TGIC using heating rates of 3 °C/min and 1 °C/min. The results are shown in Figure 5.14 and 5.15, respectively. For both heating rates, the experimental profile of the blend did not match the calculated one. A slight improvement was observed by reducing the heating rate to 1° C/min, as shown in Figure 5.16. However, there was still a clear distortion in the experimental blend profile (as compared to the predicted profile), especially in the high comonomer content region. The same distortion was observed for Blend-3 (3.51 % and 0.16 mol % of 1-octene) in Figure 5.17. During the adsorption process of Blend-3, the component with 0.16 mol % 1-octene adsorbs at high temperature before the second component, since it has the lower comonomer content. It may be argued that the presence of these adsorbed chains on the surface of the PGC affect the adsorption of the second component. Therefore, during the heating cycle, the component with high comonomer content on the blend leaves the column at temperatures higher than the elution temperatures of this component when analyzed individually. A similar argument may be proposed for Blend-2. Blend-1 is apparently not much affected by this effect because its two components have very similar comonomer contents. The results shown for Blend-2 and Blend-3 indicate that the peak separation for the blend components is affected by co-adsorption and co-desorption of polymer chains on the PGC column.

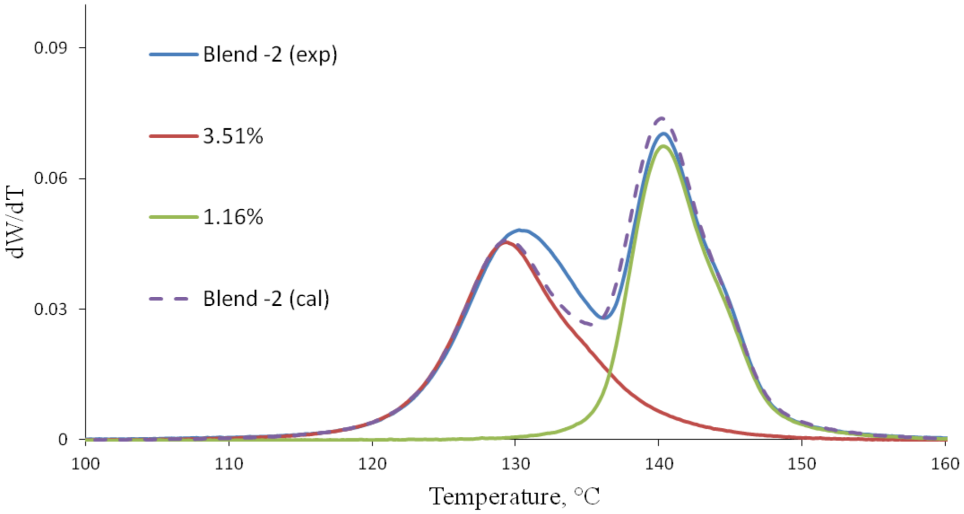

Figure 5.14 HT-TGIC profiles of Blend-2 and its components. Experimental conditions: SZ = 400 µL, CR = 5 °C/min [155 – 90 °C], Fc = 0.02 mL/min, HR = 3 °C/min, Fe = 0.5mL/min.

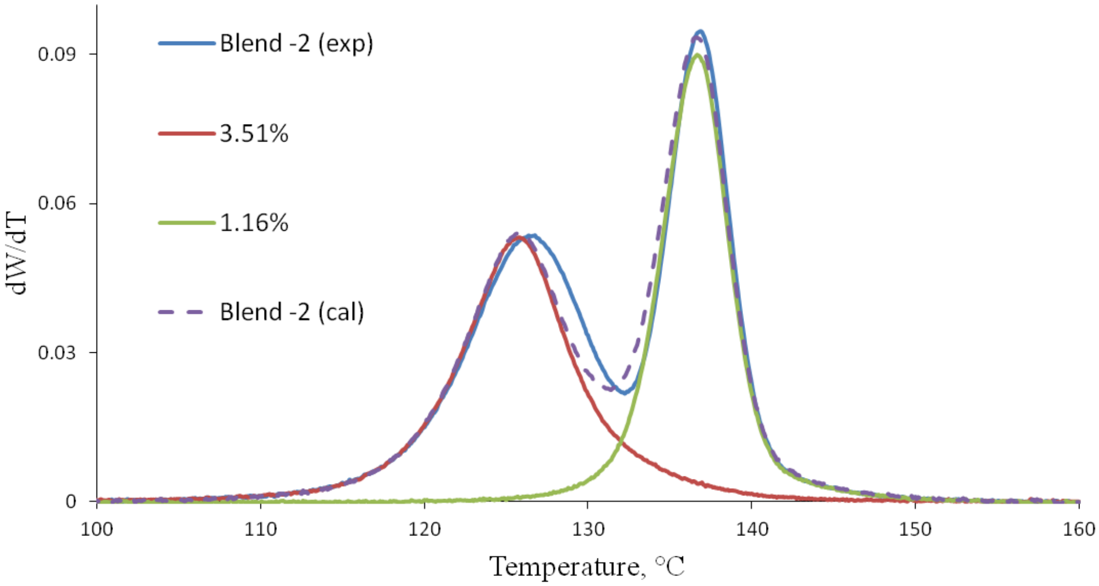

Figure 5.15 HT-TGIC profiles of Blend-2 and its components. Experimental conditions: SZ = 400 μL, CR = 5 °C/min [155 – 90 °C], Fc = 0.02 mL/min, HR = 1 °C/min, Fe = 0.5mL/min.

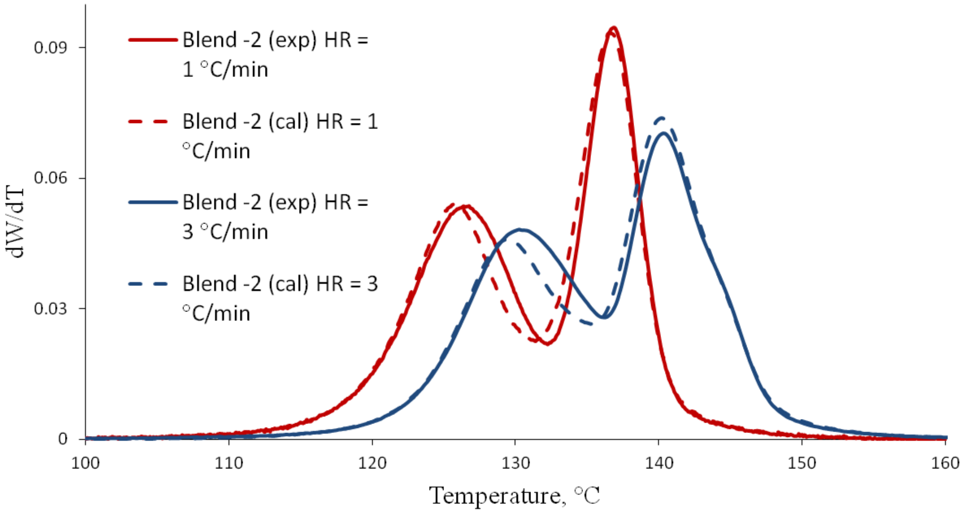

Figure 5.16 Comparison between experimental and calculated profiles of Blend-2 using heating rates of 3 °C/min and 1 °C/min. Experimental conditions: SZ = 400 μL, CR = 5°C/min [155 – 90 °C], Fc = 0.02 mL/min, Fe = 0.5mL/min.

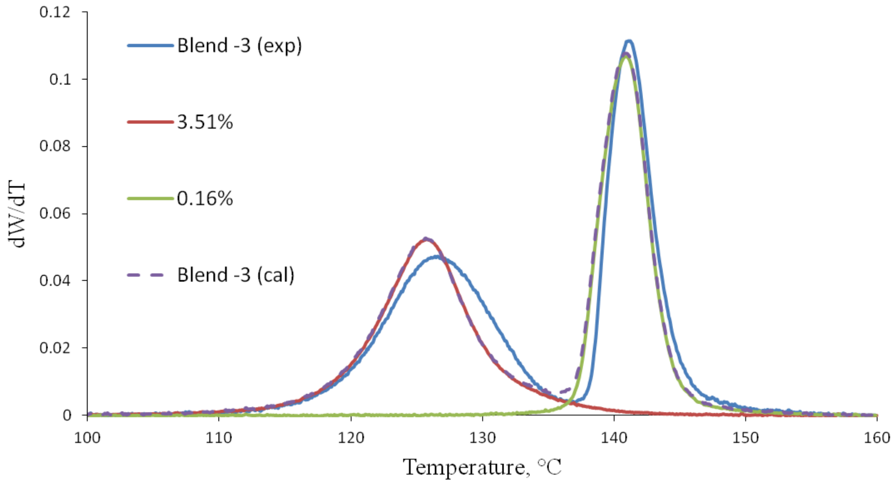

Figure 5.17 HT-TGIC profiles of Blend-3 and its components. Experimental conditions: SZ = 400 µL, CR = 5 °C/min [155 – 90 °C], Fc = 0.02 mL/min, HR = 1 °C/min, Fe = 0.5mL/min.

Trying to further investigate this phenomenon, the sample concentration of Blend-3 was reduced by 50 % (from 2 mg/mL to 1 mg/mL). However, no significant change was observed in the HT-TGIC curve, as illustrated in Figure 5.18, indicating that the observed distortion on the blend profile is not related to the sample concentration.

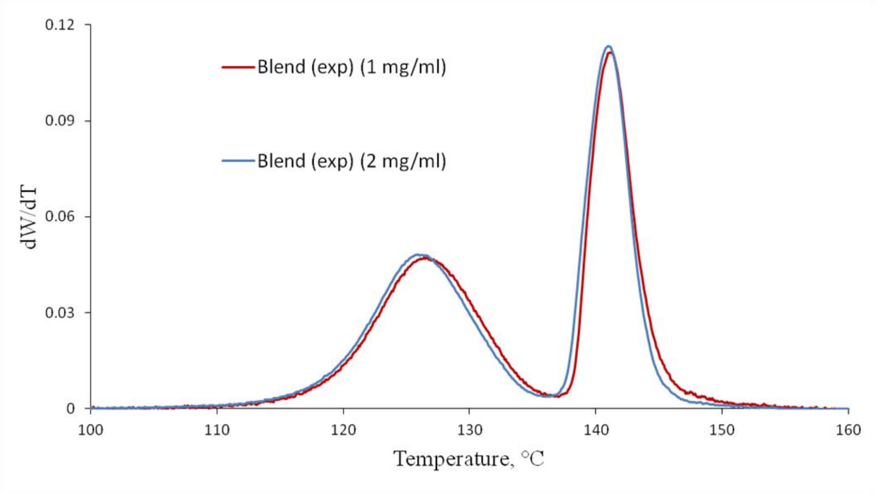

Figure 5.18 Effect of sample concentration on HT-TGIC profiles of Blend-3. Experimental conditions: SZ = 400 µL, CR = 5 °C/min [155 – 90 °C], Fc = 0.02 mL/min, HR = 1 °C/min, Fe = 0.5 mL/min.

Interestingly, reducing the volume of the sample injected into the column from 400 µL to 100 µL, had a great influence on the results. The profile of Blend-3 using a sample volume of 100 µL is shown in Figure 5.19. At these conditions, excellent agreement between experimental and calculated profiles was observed. Figure 5.20 and 5.21 compare the experimental and calculated profiles for Blend-3 using sample volume of 100 and 400 µL, respectively. Similarly, the experimental profile for Blend-2, depicted in Figure 5.22, has been improved by reducing the sample volume to 100 µL. Figure 5.23 compares the profiles for Blend-2 measured using injection volumes of 400, 100, and 50 µL. While a significant improvement is noticed when the sample volume decreases from 400 to 100 µL, little change results when it is further decreased to 50 µL. These results indicate that sample volume plays a major role in co-adsorption and co-desorption effects. It may be proposed that small sample volumes reduce the competition among the blend components adsorbing on the graphitic surface.

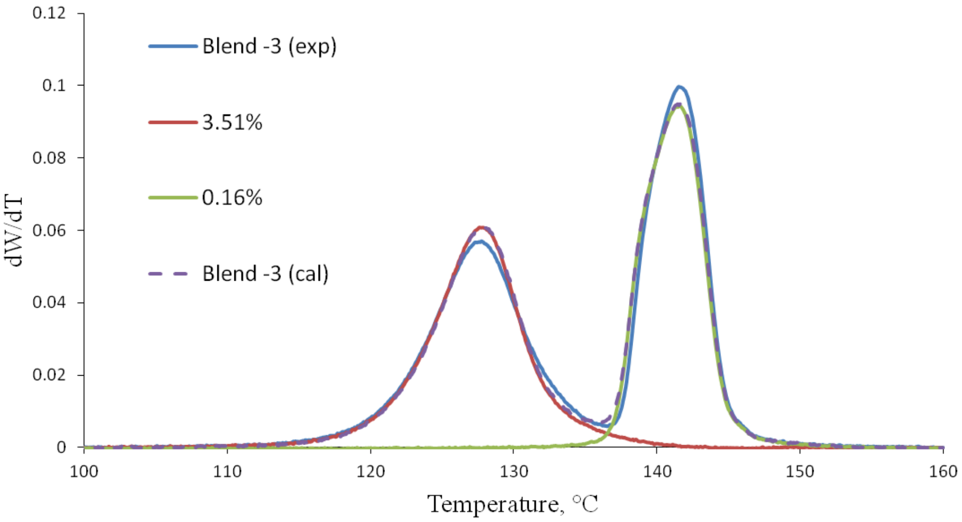

Figure 5.19 HT-TGIC profiles of Blend-3 and its components. Experimental conditions: SZ = 100 µL, CR = 5 °C/min [155 – 90 °C], Fc = 0.02 mL/min, HR = 1 °C/min, Fe = 0.5mL/min.

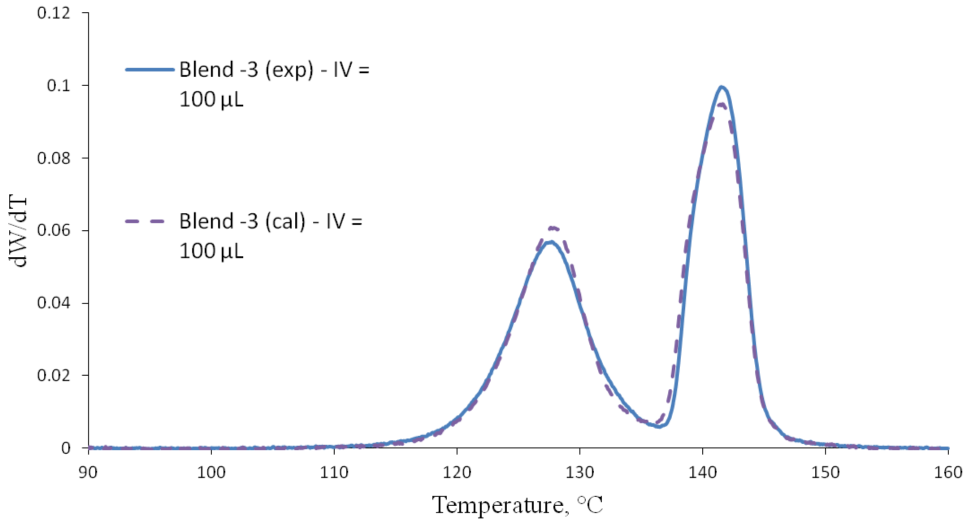

Figure 5.20 Comparison between experimental and calculated profiles for Blend-3 using a sample volume of 100 µL. Experimental conditions: CR = 5 °C/min [155 – 90 °C], Fc = 0.02 mL/min, HR = 1 °C/min, Fe = 0.5 mL/min.

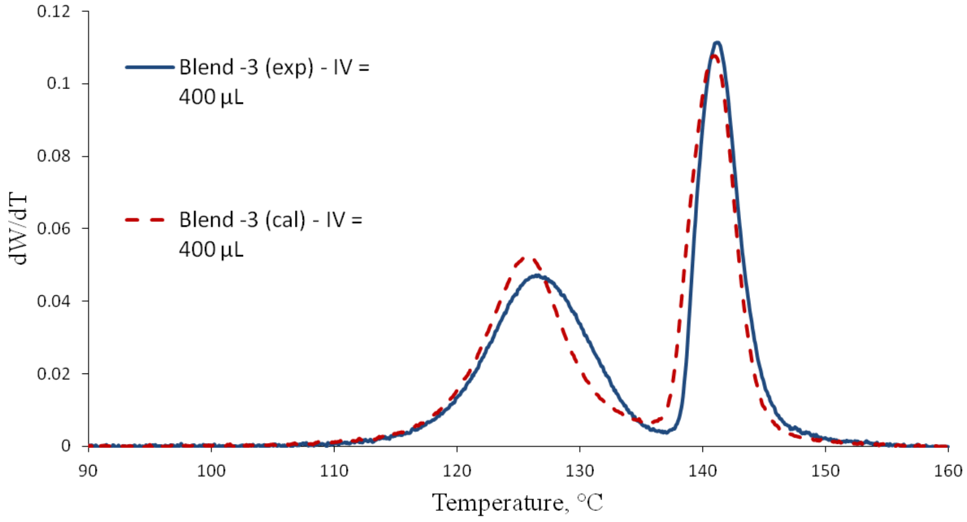

Figure 5.21 Comparison between experimental and calculated profiles for Blend-3 using a sample volume of 400 µL. Experimental conditions: CR = 5 °C/min [155 – 90 °C], Fc = 0.02 mL/min, HR = 1 °C/min, Fe = 0.5mL/min.

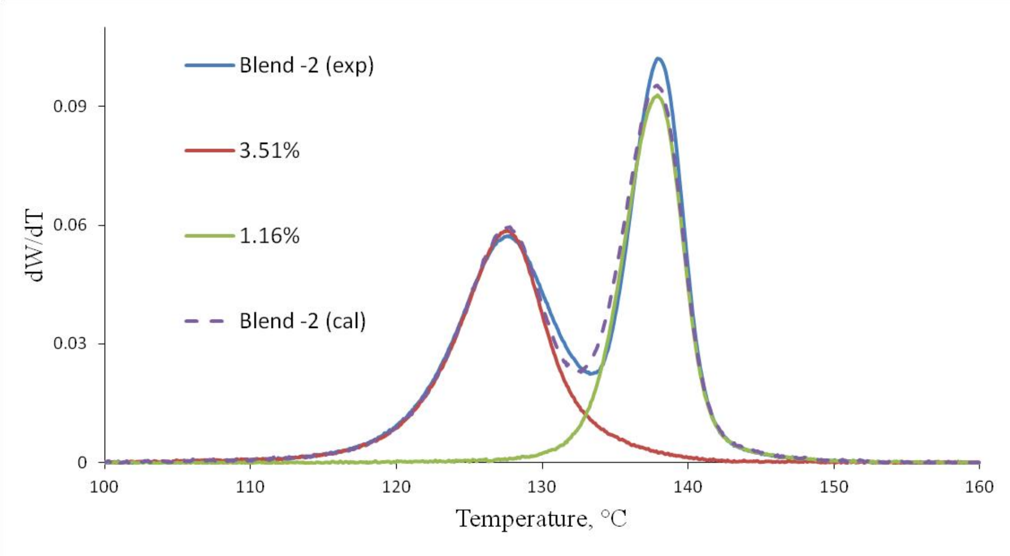

Figure 5.22 HT-TGIC profiles of Blend-2 and its components. Experimental conditions: SZ = 100 μL, CR = 5 °C/min [155 – 90 °C], Fc = 0.02 mL/min, HR = 1 °C/min, Fe = 0.5mL/min.

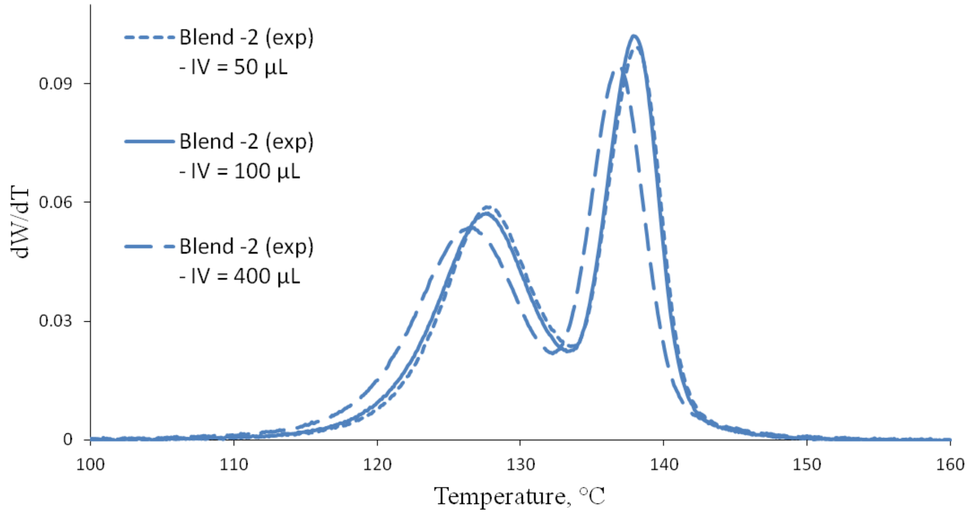

Figure 5.23 Effect of sample volume (50, 100, 400 μL) on HT-TGIC profiles for Blend-2. Experimental parameters: CR = 5 °C/min [155 – 90 °C], Fc = 0.02 mL/min, HR = 1 °C/min, Fe = 0.5mL/min.

All the above mentioned experiments were performed in CEF mode. A small amount of solvent was pumped through the column during the cooling cycle. To discuss the effect of the flow rate (Fc) on the resolution of the obtained profiles, Blend-2 and its components were analyzed using different solvent flow rates during the cooling step.

Interestingly, when the sample size was 100 µL using a heating rate of 1 °C/min, no effect for the solvent flow rate during cooling step was observed. Figure 5.24 and Figure 5.25 compare profiles measured with Fc = 0.02 mL/min and 0 mL/min (TREF mode) for individual resins and Blend-2, respectively. However, using a heating rate of 3 °C/min, a clear flow rate effect was observed for Blend-2 and its components when 400 µL of each sample was injected to the column as illustrated in Figure 5.26 for the individual resins and Figure 5.27 for Blend-2.

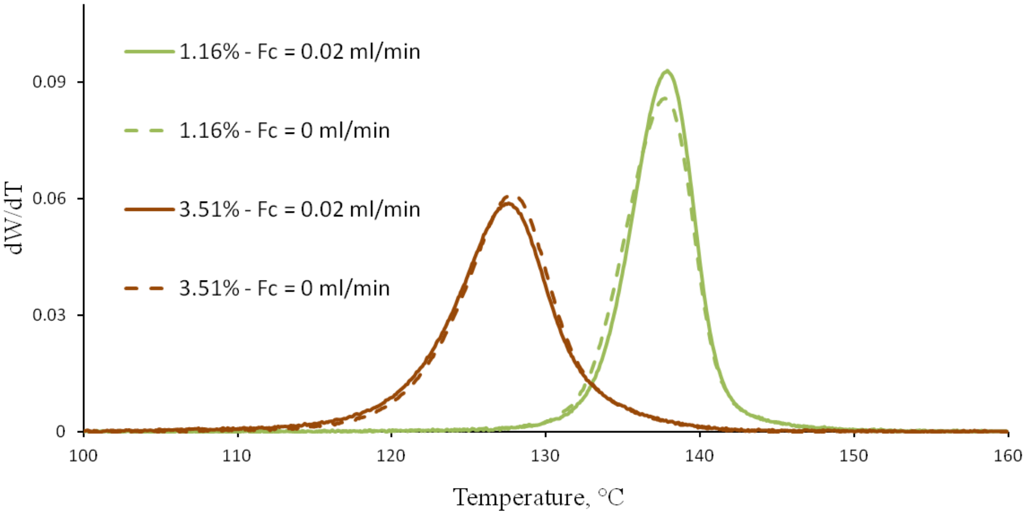

Figure 5.24 Effect of cooling cycle solvent flow rate (0 and 0.02 mL/min) on HT-TGIC profiles of individual resins. Experimental conditions: SZ = 100µL, CR = 5 °C/min, HR = 1 °C/min, Fe = 0.5mL/min.

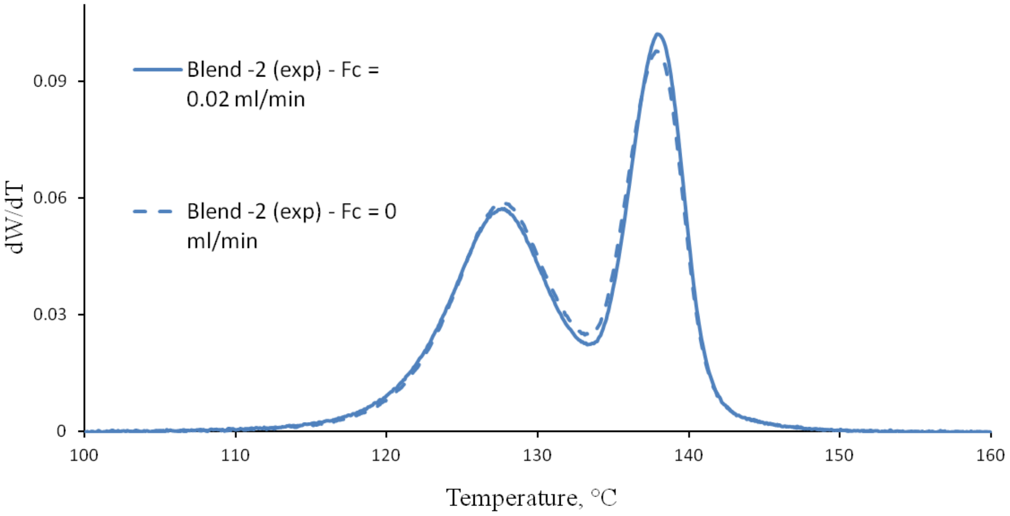

Figure 5.25 Effect of cooling cycle solvent flow rate (0 and 0.02 mL/min) on HT-TGIC profiles of Blend-2. Experimental conditions: SZ = 100μL, CR = 5 °C/min [155 – 90 °C], HR = 1 °C/min, Fe = 0.5mL/min.

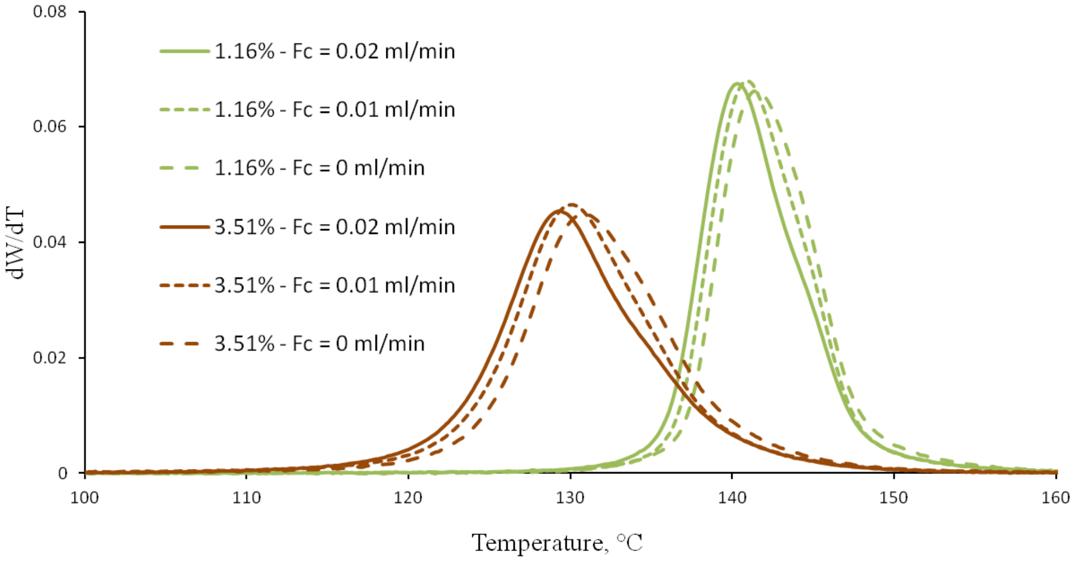

Figure 5.26 Effect of cooling cycle solvent flow rate (0, 0.01and 0.02 mL/min) on HT-TGIC profiles of individual resins. Experimental conditions: SZ = 400 μL CR = 5 °C/min [155 – 90 °C], HR = 3 °C/min, Fe = 0.5mL/min.

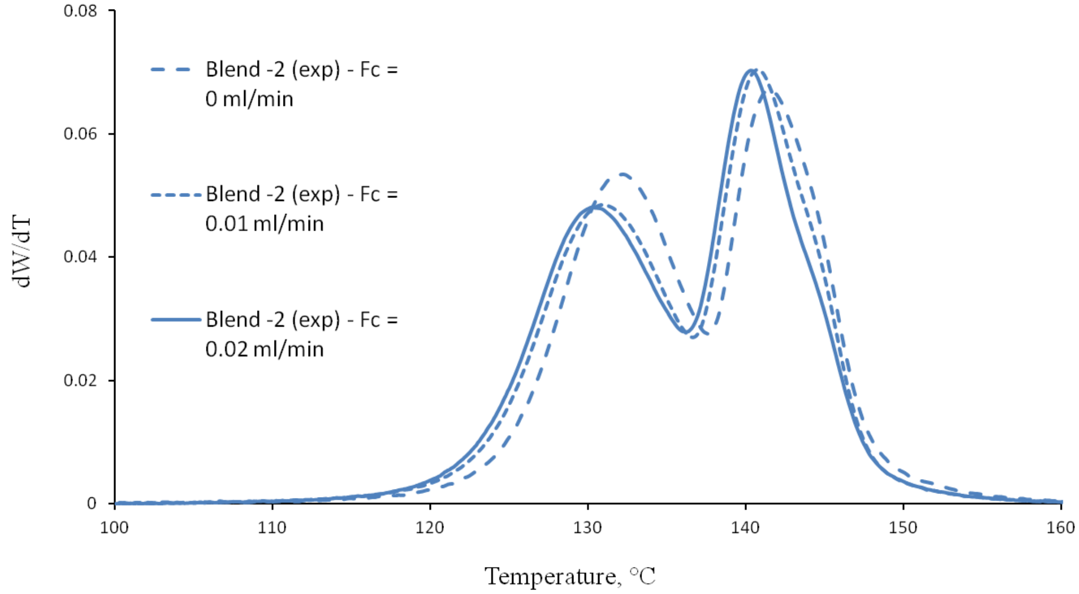

Figure 5.27 Effect of cooling cycle solvent flow rate (0, 0.01and 0.02 mL/min) on HT-TGIC profiles of Blend-2. Experimental conditions: SZ = 400 μL CR = 5 °C/min [155 – 90 °C], HR = 3 °C/min, Fe = 0.5mL/min.

5.4 CONCLUSIONS

The effects of operating conditions on HT-TGIC analysis have been studied using polyethylene and ethylene/1-octene copolymers made with a metallocene catalyst. HT-TGIC fractionates polymer chains based on their interaction with porous graphitic carbon. The adsorption process takes place during the cooling cycle. The results indicate that this process is independent of the cooling rate within the range investigated in this study. Thus, to minimize analysis time, the HT-TGIC runs can be performed using the fastest cooling rate and a narrow cooling cycle. The resins could also be analyzed at temperatures higher than their crystallization temperatures, thus avoiding any co-crystallization effects.

The HT-TGIC elution peak temperatures depend linearly on the comonomer content. The obtained calibration curves at different heating rates are parallel and shifted to high temperature as the heating rate increases.

On the other hand, the heating rate during desorption has a major effect on HT-TGIC profiles. Slower heating rates are required to enhance the resolution of individual resins and their blends. The chromatograms obtained with fast heating rate are broad and have low resolution, supposedly due to co-desorption effects.

Sample volume is a very important parameter affecting the chromatograms of polyolefin blends. Experimental profiles for blends show excellent agreement with calculated ones when small sample volumes (equal to or less than 100 μL) are employed. This behavior may be attributed to the stronger effects of co-adsorption and co-desorption phenomena when large sample volume is injected to the column.

This systematic study shows that the HT-TGIC can be used to obtain CCDs of individual resins and their blends with excellent peak separation if the operating conditions are carefully optimized.

Chapter 6

EFFECT OF SOLVENT TYPE ON HT-TGIC FRACTIONATION

6.1 INTRODUCTION

The effects of the operating conditions on HT-TGIC profiles were investigated in Chapter 5. All the HT-TGIC experiments studied in Chapter 5 were performed using (ODCB) as the mobile phase. In this chapter, the effects of solvent type on HT-TGIC analysis were investigated using polyethylene, ethylene/1-octene copolymers, and their blends. The solvents used in this study were o-dichlorobenzene (ODCB), 1,2,4-trichlorobenzene (TCB), and chloronaphthalene (CN). To the best of our knowledge, this is the first work that studies the importance of solvent selection on HT-TGIC profiles of polyolefins.

It has been shown in Chapter 5 that the heating rate and the sample size were the most important parameters affecting HT-TGIC profiles of individual resins and their blends. It was proposed that using a sample size of 100 μL and a heating rate of 1 °C/min reduced co-adsorption and co-desorption effects. Therefore, most of the experiments in this chapter were performed using these conditions.

This chapter also investigates the effect of molecular weight on HT-TGIC profiles of polyethylene and ethylene/1-octene copolymers. Finally, the last section of this chapter compares HT-TGIC and CEF profiles.

6.2 RESULTS AND DISCUSSION

6.2.1 EFFECT OF SOLVENT TYPE ON HT-TGIC OF INDIVIDUAL RESINS

Individual resins were analyzed by HT-TGIC using ODCB, CN, and TCB. The results for polyethylene, ethylene/1-octene copolymers (1.16 and 3.51 mol % 1-octene) are shown in Figure 6.1, 6.2, and 6.3, respectively. Small differences in elution peak temperatures (< 2 °C) were observed between the profiles measured using TCB and CN. However, elution peak temperatures using ODCB are significantly higher than those measured with TCB and CN. During the HT-TGIC heating cycle, the retained polymer chains desorb from the PGC column more easily when TCB and CN are used, exiting the column at lower temperatures. The calibration curves (Figure 6.4) with TCB and ODCB are almost parallel, with the better solvent having lower elution peak temperatures for the same comonomer content.

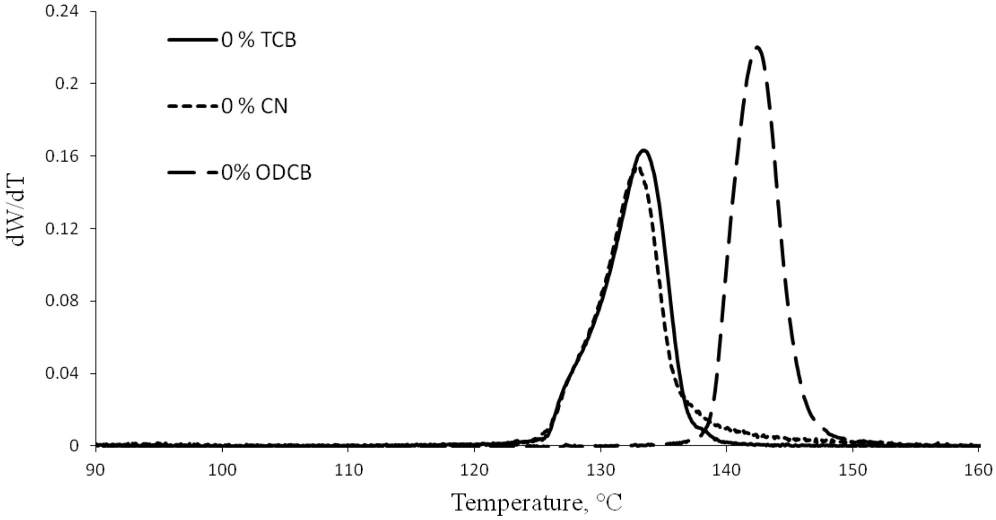

Figure 6.1 Effect of solvent type on HT-TGIC profiles of polyethylene. Experimental conditions: SZ = 100 μL, CR = 5 °C/min, Fc = 0.02 mL/min for [155 – 90 °C], HR = 1 °C/min, Fe = 0.5 mL/min.

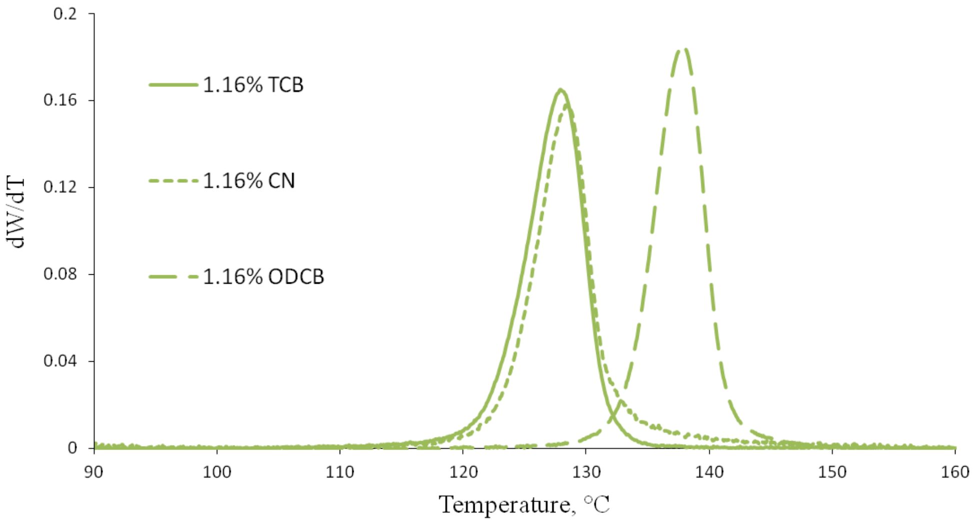

Figure 6.2 Effect of solvent type on HT-TGIC profiles of an ethylene/1-octene copolymer (1.16 mol % 1-octene). Experimental conditions: SZ = 100 µL, CR = 5 °C/min, Fc = 0.02 mL/min for [155 – 90 °C], HR = 1 °C/min, Fe = 0.5 mL/min.

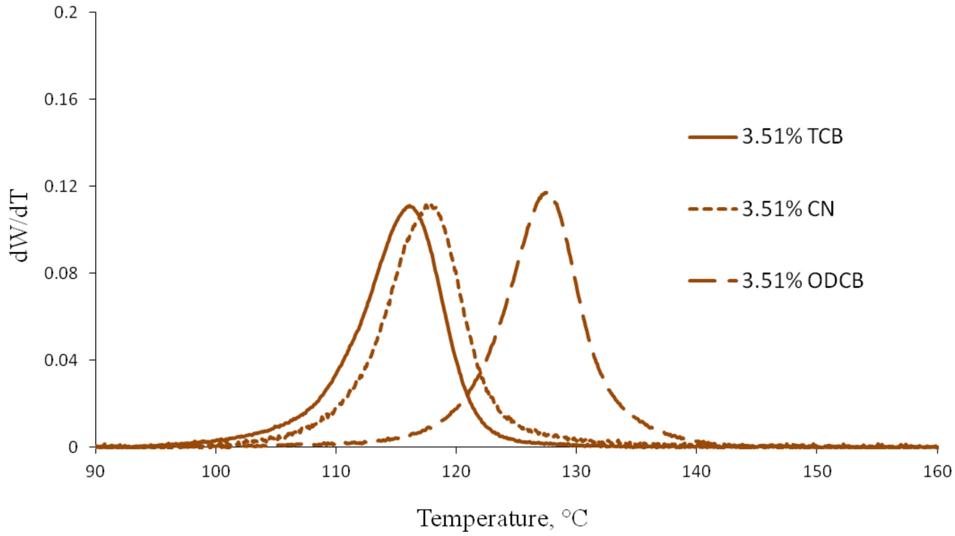

Figure 6.3 Effect of solvent type on HT-TGIC profiles of an ethylene/1-octene copolymer (3.51 mol % 1-octene). Experimental conditions: SZ = 100 µL, CR = 5 °C/min, Fc = 0.02 mL/min for [155 – 90 °C], HR = 1 °C/min, Fe = 0.5 mL/min.

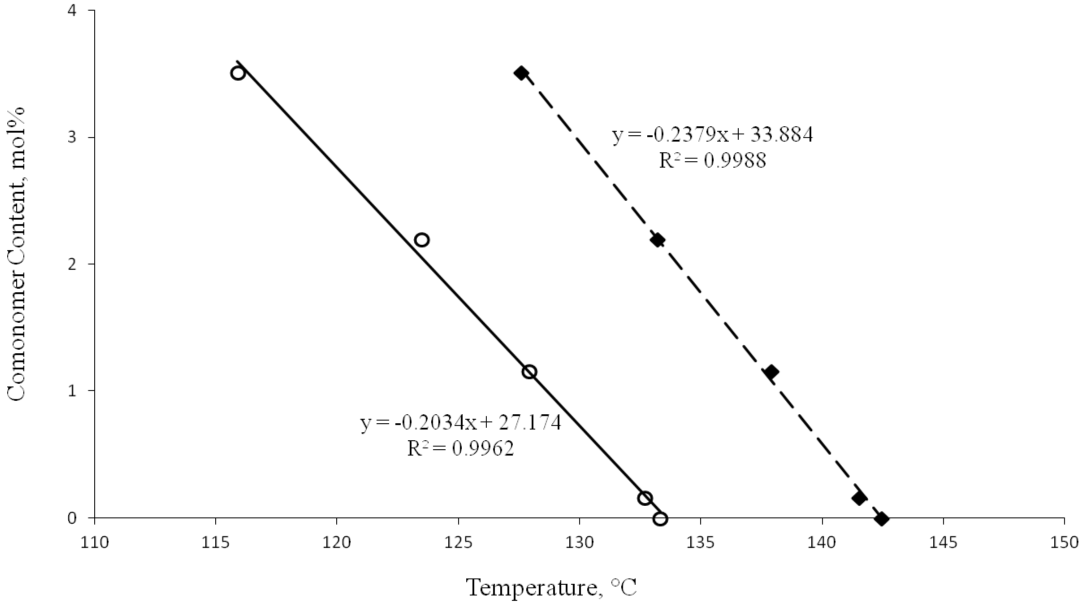

Figure 6.4 Calibration curves for HT-TGIC using TCB (continuous line) and ODCB (dotted line). Experimental conditions: SZ = 100 μL, CR = 5 °C/min [155 – 90 °C], Fc = 0.02 mL/min, HR = 1 °C/min Fe = 0.5 mL/min.

In Figure 6.5, the profiles measured with TCB were shifted to higher temperatures to match the elution peaks measured with ODCB. The chromatograms of copolymers measured using TCB and ODCB have similar shapes, but it may be argued that the peaks are slightly narrower when ODCB is used as a solvent. Contrarily, the elution peak for polyethylene (0 mol % 1-octene) is broad and non-symmetric when the analysis was performed with TCB solvent. This behavior will be further explored in Section 6.2.3.

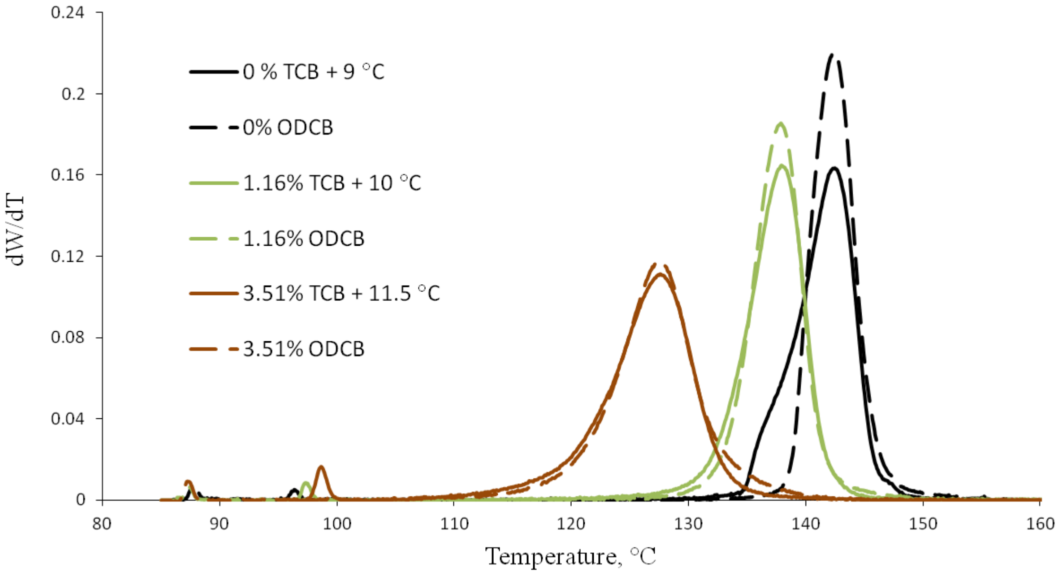

Figure 6.5 Comparison between profiles measured with TCB and ODCB. TCB profiles were shifted to higher temperatures to match the peak temperatures of those measure using ODCB. Experimental conditions: SZ = 100 µL, CR = 5 °C/min [155 – 90 °C], Fc = 0.02 mL/min, HR = 1 °C/min, Fe = 0.5 mL/min.

6.2.2 EFFECT OF SOLVENT TYPE ON THE BLENDS

Figure 6.6 and 6.7 show the experimental profiles of Blend-2 (1.16 and 3.51 mol% 1-octene) as compared with the chromatograms of its components using TCB and CN. Clear differences between the experimental and the calculated profiles of Blend-2 were observed with both solvents. On the other hand, better peak separation was seen when the HT-TGIC analysis was performed with ODCB. The results of Blend-2 with ODCB were already discussed in Chapter 5 (Figure 5.22).

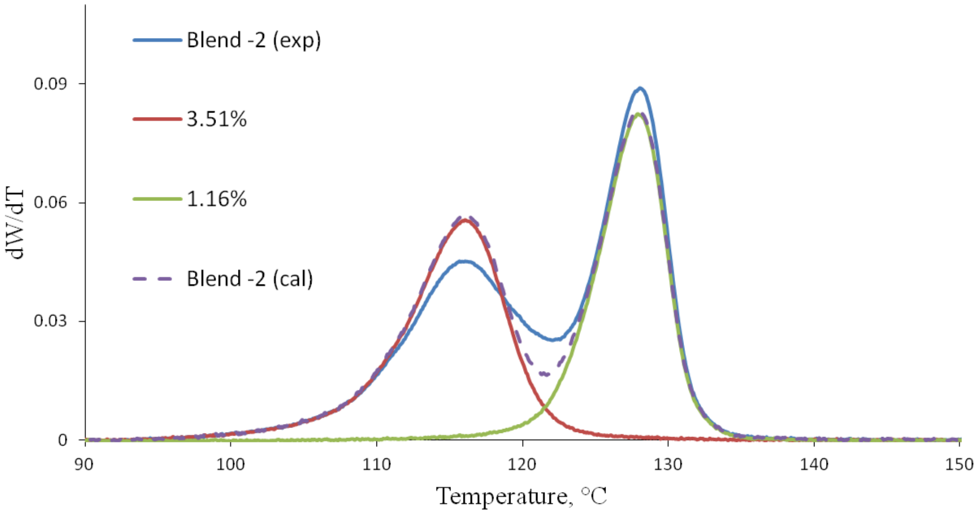

Figure 6.6 HT-TGIC profiles of Blend-2 and its components measured using TCB. Experimental conditions: SZ = 100 µL, CR = 5 °C/min [155 – 90 °C], Fc = 0.02 mL/min, HR = 1 °C/min, Fe = 0.5 mL/min.

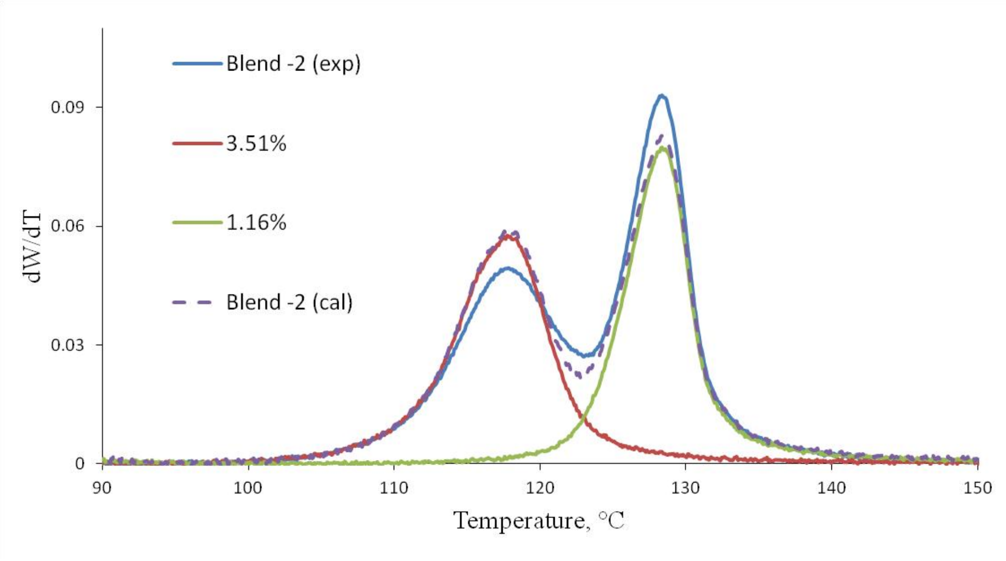

Figure 6.7 HT-TGIC profiles of Blend-2 and its components measured with CN. Experimental conditions: SZ = 100 µL, CR = 5 °C/min [155 – 90 °C], Fc = 0.02 mL/min, HR = 1 °C/min, Fe = 0.5 mL/min.

Trying to further investigate this phenomenon, a mixture of 60% TCB and 40% ODCB (by volume) was used as solvent during the HT-TGIC experiments for Blend-2 and its components. The results are shown in Figure 6.8. The behavior of Blend-2 using the mixed solvent is similar to the behavior observed when the analysis was performed with TCB alone. However, the results are shifted to higher temperatures due to the presence of ODCB in the mixture. Figure 6.9 compares experimental and calculated profiles for Blend-2 measured with TCB, ODCB, and the TCB-ODCB mixture. The differences in the elution peak temperatures between Blend-2 components (1.16 and 3.51 mol% of 1-octene) are 10.3 °C and 12 °C when the analysis is performed with ODCB and TCB, respectively. Although the peaks for the components are closer when ODCB is employed, they are separated from each other in the blend better than when the analysis is performed with TCB. The "distortion" in the HT-TGIC profiles of Blend-2 measured with TCB and CN seems to be due mainly to co-adsorption and co-desorption effects.

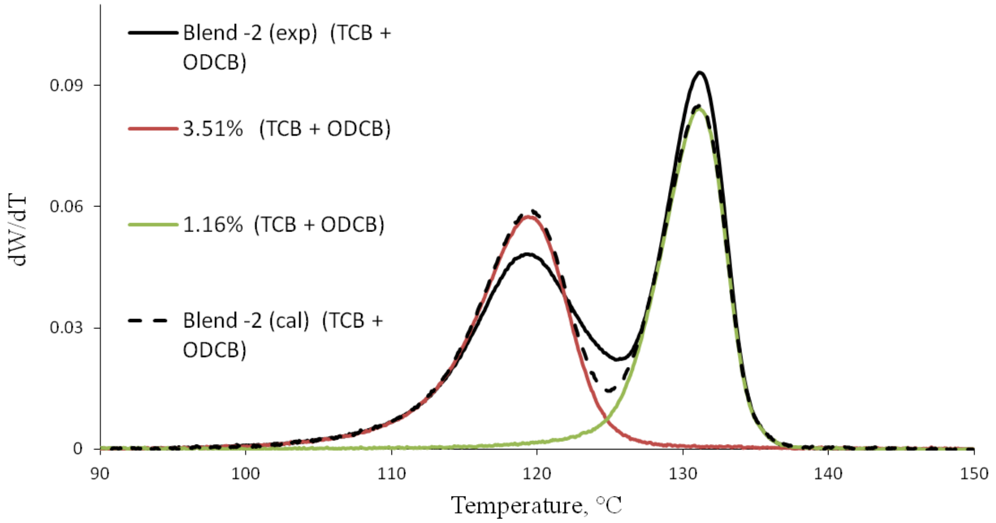

Figure 6.8 HT-TGIC profiles of Blend-2 and its components measured with a mixture of TCB and ODCB. Experimental conditions: SZ = 100 µL, CR = 5 °C/min [155 – 90 °C], Fc = 0.02 mL/min, HR = 1 °C/min, Fe = 0.5 mL/min.

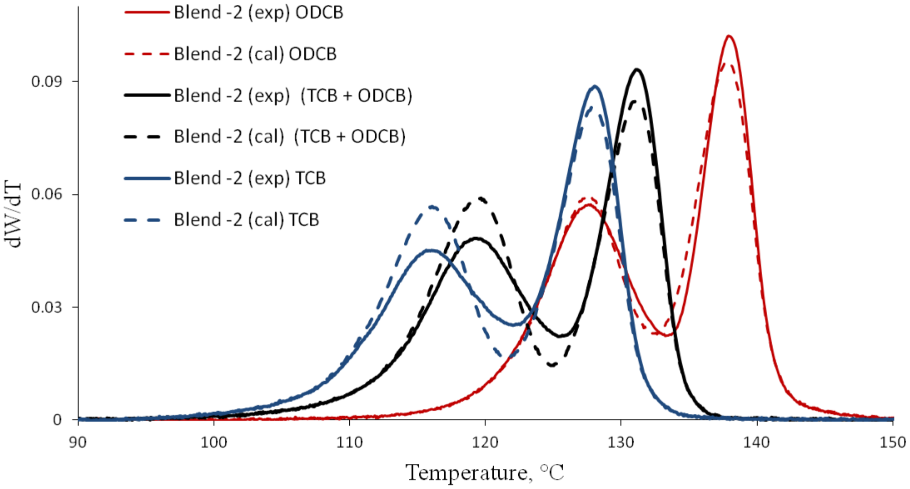

Figure 6.9 Comparison between experimental and calculated profiles (dotted lines) for Blend-2 using TCB, ODCB, and the TCB-ODCB mixture. Experimental conditions: SZ = 100 µL, CR = 5 °C/min [155 – 90 °C], Fc = 0.02 mL/min, HR = 1 °C/min, Fe = 0.5 mL/min.

Figure 6.10 shows the HT-TGIC results of Blend-3 and its components measured with TCB solvent. Similarly to Blend-2, using TCB as a mobile phase during the analysis gives inadequate peak separation of the blend components. The profiles measured with TCB and ODCB of this blend are compared in Figure 6.11.

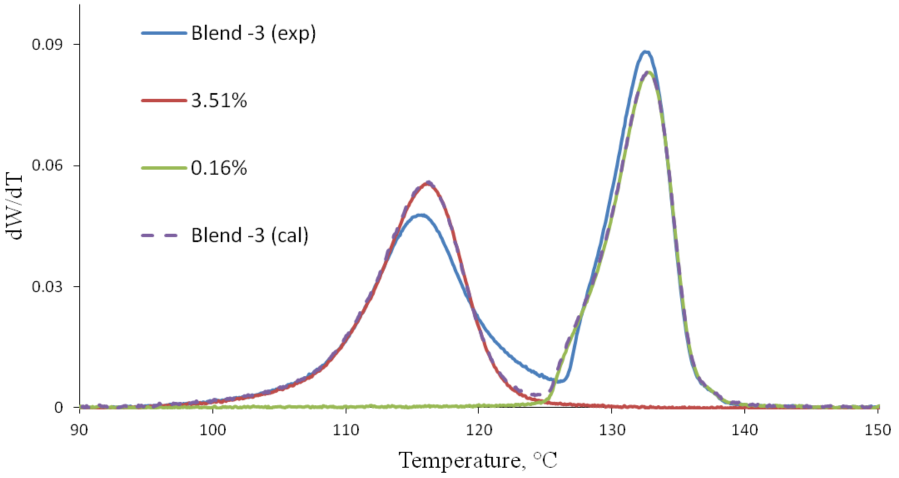

Figure 6.10 HT-TGIC profiles of Blend-3 and its components measured with TCB. Experimental conditions: SZ = 100 µL, CR = 5 °C/min [155 – 90 °C], Fc = 0.02 mL/min, HR = 1 °C/min, Fe = 0.5 mL/min.

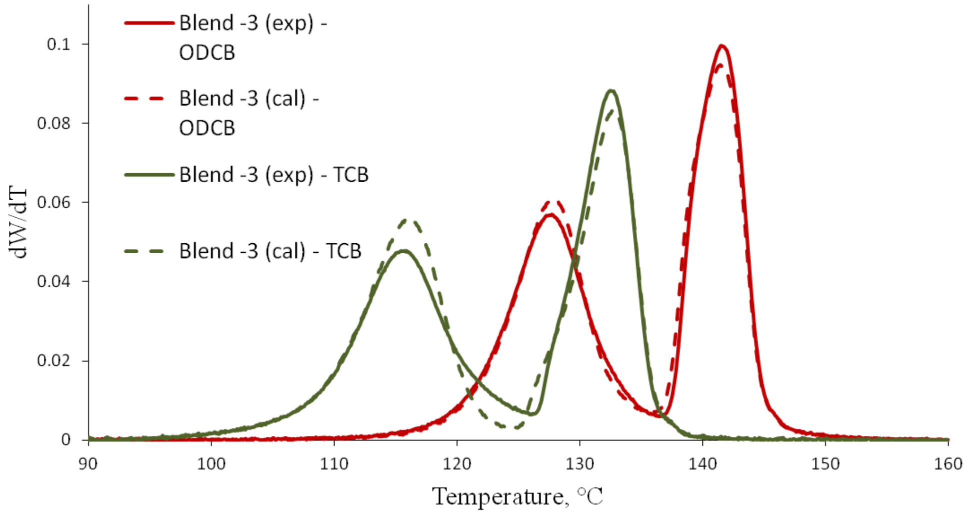

Figure 6.11 Comparison between experimental and calculated profiles (dotted lines) for Blend-3 using TCB and ODCB. Experimental conditions: SZ = 100 μL, CR = 5 °C/min [155 – 90 °C], Fc = 0.02 mL/min, HR = 1 °C/min, Fe = 0.5 mL/min.

Blend-4 (8.5 and 1.16 mol % 1-octene) was studied to further investigate this unexpected behavior for blends analyzed by HT-TGIC using TCB. The difference between the elution peak temperatures of Blend-4 components is 31 °C. Figure 6.12, 6.13, and 6.14 show the chromatograms of Blend-4 and for three compositions, 30/70, 50/50, and 70/30 wt-%, respectively. The profile for Blend-4 is affected by co-adsorption and co-desorption in a similar way that has been observed with Blend-2 and Blend-3. The chromatogram of the (8.5 mol% 1-octene) component in Blend-4 can be divided in approximately two fractions. The first represents polymer chains that desorb and leave the column in the temperature range [40 °C - 94 °C]. The results for this temperature range show excellent agreement with the profile of the same component when analyzed individually. However, likely due to co-adsorption and co-desorption effects, the second fraction of this component in the blend [94 °C - 115 °C] is broader and shifted to higher elution temperatures as compared with the profile of the component when measured individually.

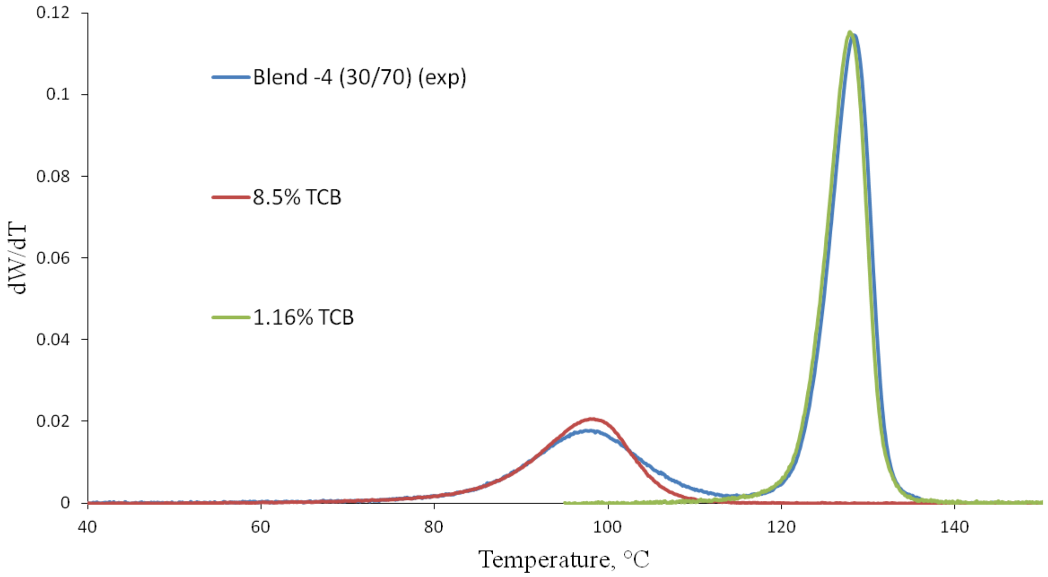

Figure 6.12 HT-TGIC profiles of Blend-4 (30/70 wt-%) and its components measured with TCB. Experimental conditions: SZ = 100 μL, CR = 5 °C/min [155 – 35 °C], Fc = 0.01 mL/min, HR = 1 °C/min, Fe = 0.5 mL/min.

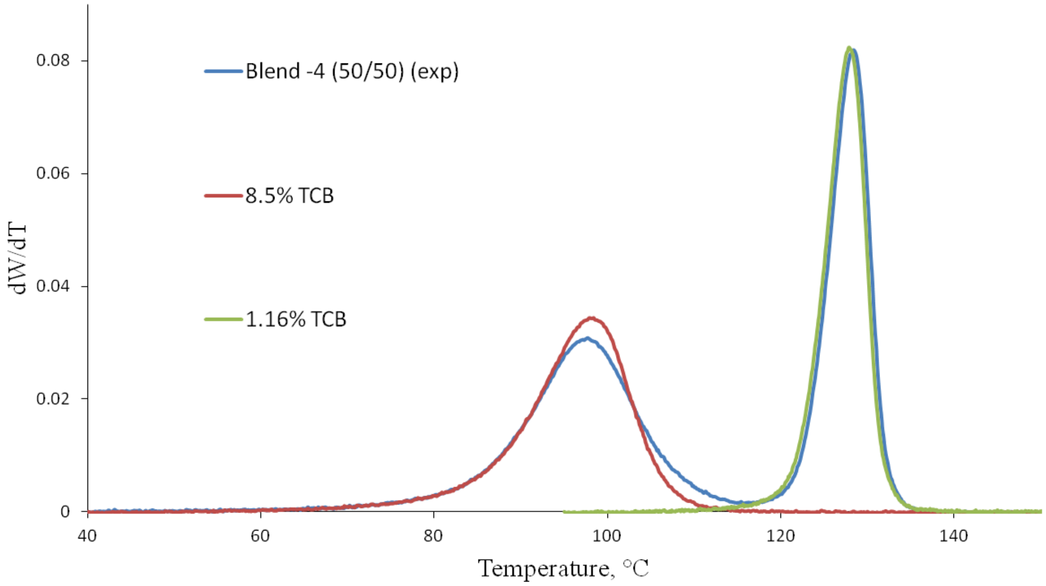

Figure 6.13 HT-TGIC profiles of Blend-4 (50/50 wt-%) and its components measured with TCB. Experimental conditions: SZ = 100 μL, CR = 5 °C/min [155 – 35 °C], Fc = 0.01 mL/min, HR = 1 °C/min, Fe = 0.5 mL/min.

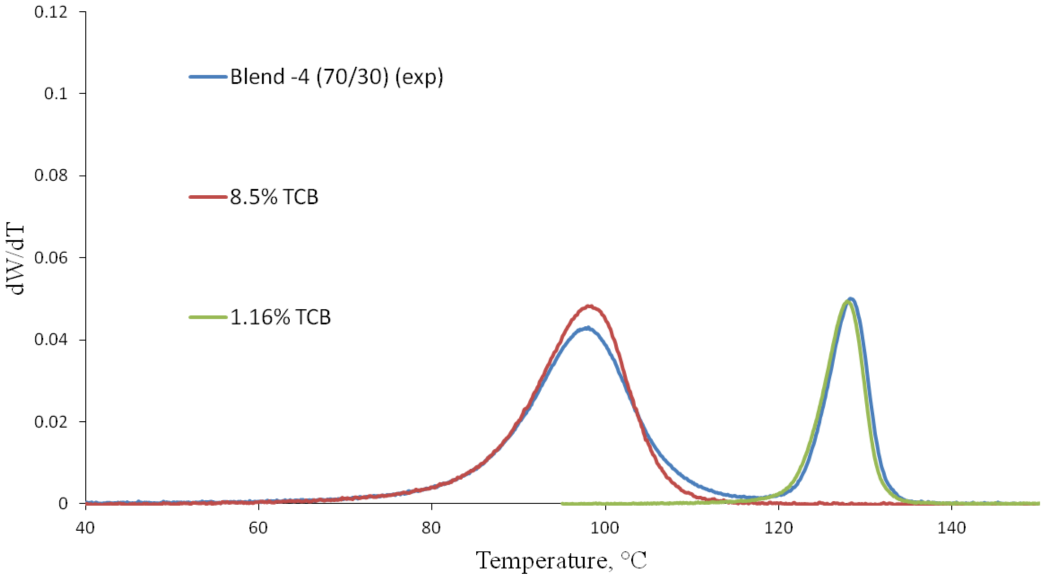

Figure 6.14 HT-TGIC profiles of Blend-4 (70/30 wt-%) and its components measured with TCB. Experimental conditions: SZ = 100 μL, CR = 5 °C/min [155 – 35 °C], Fc = 0.01 mL/min, HR = 1 °C/min, Fe = 0.5 mL/min.

To study the effect of the 8.5 mol % 1-octene component mass fraction in the blend (30, 50, and 70 wt-%), the profiles for this component in the range [40 °C – 115 °C] were normalized and superimposed in Figure 6.15. These results indicate that the profile gets broader as the amount of this component decreases in the blend. Therefore, the extent of co-adsorption and co-desorption depends on the mass fractions of the blend components.

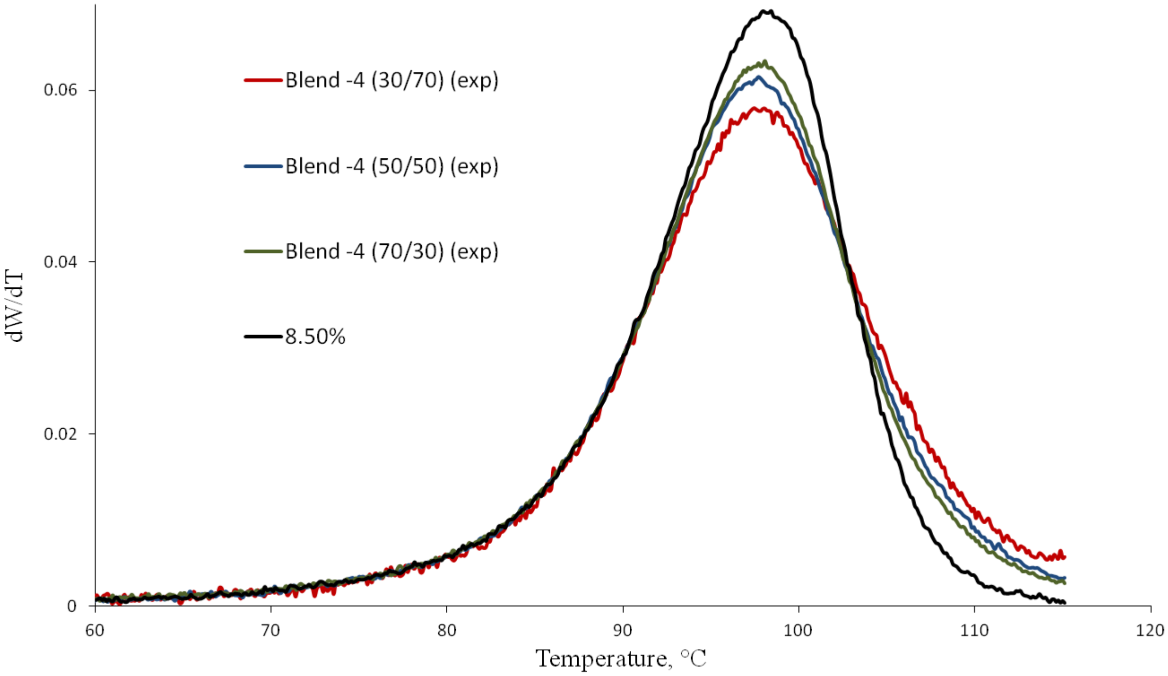

Figure 6.15 HT-TGIC profiles of (8.5 mol% 1-octene) component in Blend-4 (30/70, 50/50, 70/30 wt-%) as compared with the component profile measured individually. Experimental conditions: SZ = 100 μL, CR = 5 °C/min [155 – 35 °C], Fc = 0.01 mL/min, HR = 1 °C/min, Fe = 0.5 mL/min.

Figure 6.16 and 6.17 show the chromatograms of Blend-4 with two replicates using 30/70 and 70/30 wt-% ratios. Excellent repeatability was observed. Replicates for the 8.5 mol% 1-octene component in Blend-4 [40 °C – 115 °C] as compared with the profile of the same component measured individually are shown in Figure 6.18.

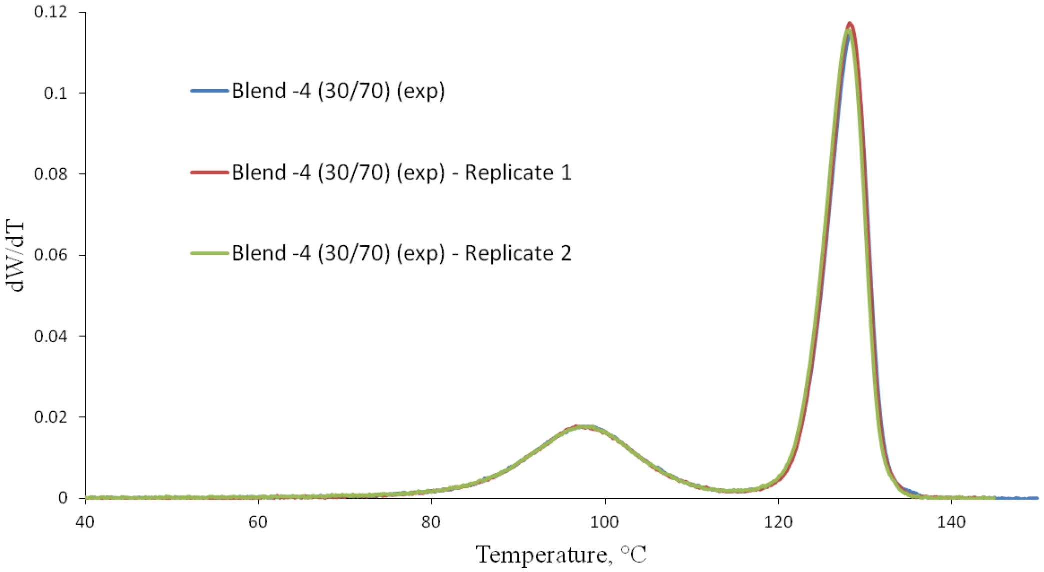

Figure 6.16 Repeatability of HT-TGIC profiles for Blend-4 (30/70 wt-%). Experimental conditions: SZ = 100 µL, CR = 5 °C/min [155 - 35 °C], Fc = 0.01 mL/min, HR = 1 °C/min, Fe = 0.5 mL/min.

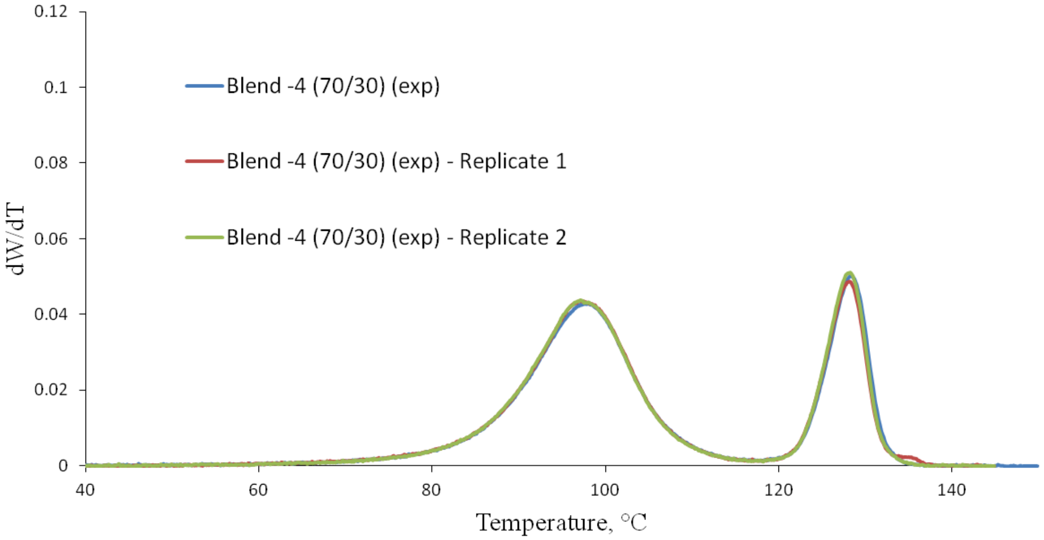

Figure 6.17 Repeatability of HT-TGIC profiles for Blend-4 (70/30 wt-%). Experimental conditions: SZ = 100 µL, CR = 5 °C/min [155 - 35 °C], Fc = 0.01 mL/min, HR = 1 °C/min, Fe = 0.5 mL/min.

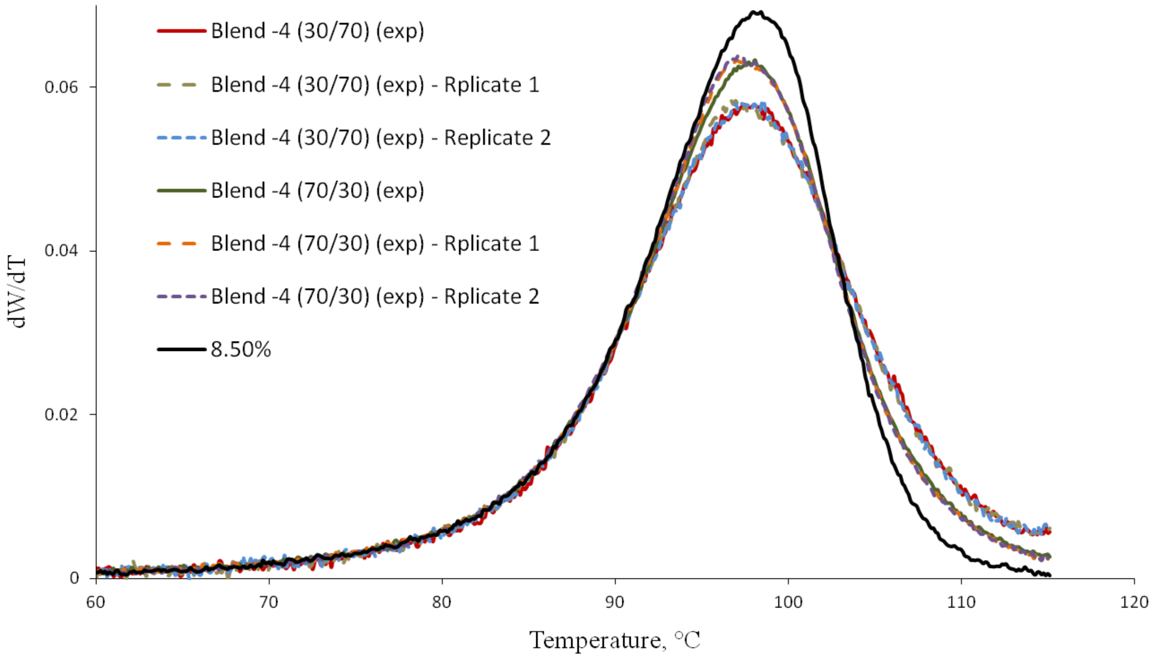

Figure 6.18 HT-TGIC profiles of the 8.5 mol% 1-octene component in Blend-4 (30/70 and 70/30 wt-%) as compared with the component profile measured individually. Two replicates of each blend are shown. Experimental conditions: SZ = 100 μL, CR = 5 °C/min [155 – 35 °C], Fc = 0.01 mL/min, HR = 1 °C/min, Fe = 0.5 mL/min.

Blend-4 was studied using HT-TGIC with TCB in three adsorption/desorption temperature ranges [155 °C – 35 °C – 160 °C], [155 °C – 70 °C – 160 °C], and [155 °C – 90 °C – 160 °C], as illustrated in Figure 6.19. No significant difference was observed between the profiles measured using [155 °C – 35 °C – 160 °C] and [155 °C – 70 °C – 160 °C] adsorption/desorption temperature ranges. This is very important information since it can be used to shorten the analysis time and reduce the consumption of the solvent without affecting the resolution of the separation. When the cooling cycle was stopped at 90 °C, 30 % of the component with 8.5 mol% 1-octene eluted from the column without adsorption.

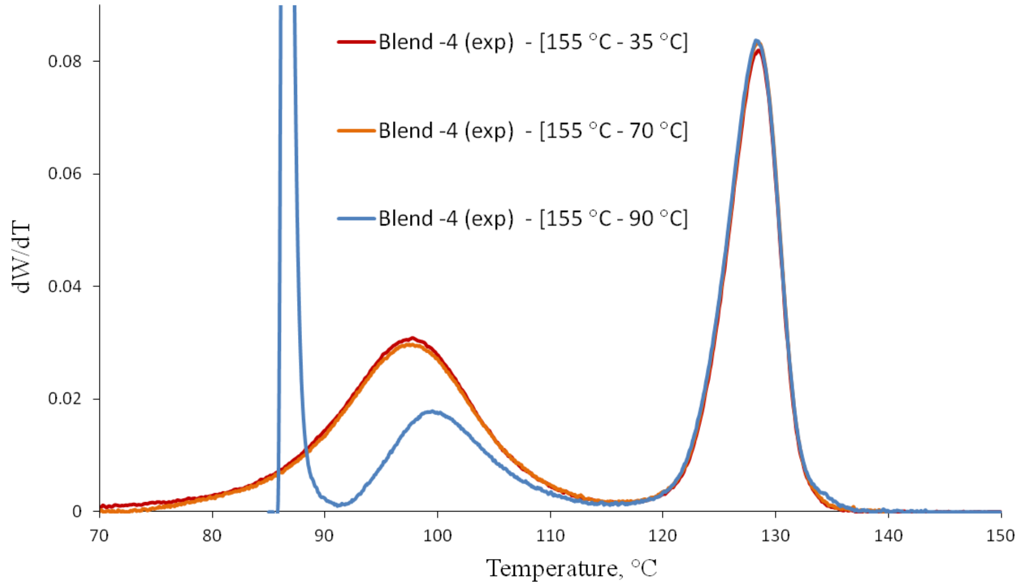

Figure 6.19 Effect of adsorption/desorption temperature range on HT-TGIC profiles for Blend-4. Experimental conditions: SZ = 100 µL, CR = 5 °C/min, HR = 1 °C/min, Fe = 0.5 mL/min.

6.2.3 EFFECT OF MOLECULAR WEIGHT

To study the effect of molecular weight on HT-TGIC profiles, individual resins with similar comonomer content but different molecular weight averages were analyzed. The results measured with TCB and ODCB for polyethylene resins with different molecular weight averages are shown in Figure 6.20. The high and low molecular weight resins (M_n = 46,000 and M_n = 19,000) had the same elution peak temperature when ODCB was used as solvent. However, the low molecular weight sample has a broader distribution and shows a significant low temperature tail due to the presence of polymer chains with lower molecular weights. Using TCB, the chromatograms for these polymers have different elution peak temperatures. The low molecular weight sample (M_n = 19,000) is shifted to a lower elution peak temperature and has a broader distribution than that for the high molecular weight (M_n = 46,600) sample.

A polyethylene standard with narrow MWD (M_n = 28,900 and PDI = 1.1) was also analyzed by HT-TGIC using TCB. As shown in Figure 6.19, the elution peak temperature of the polyethylene standard is similar to the peak temperature of ethylene homopolymer with

M_n = 19,000 and PDI = 2, but it has a narrower distribution, demonstrating that molecular weight does play a role on HT-TGIC fractionation.

Similarly, the effect of molecular weight on the HT-TGIC of ethylene/1-octene copolymers was studied using copolymers with similar comonomer contents but different molecular weights. The chromatograms measured using TCB are shown in Figure 6.21. The elution peak temperatures of the low and high molecular weight copolymers (1.14 mol %, M_n = 15,000 and 1.16 mol %, M_n = 47,000; 3.59 mol % 1-octene, M_n = 16,500 and 3.51 mol % 1-octene, M_n = 49,800) are the same. However, the samples with low molecular weight (1.14 mol %, M_n = 15,000; 3.59 mol % 1-octene, M_n = 16,500) have a broader distribution and a significant lower temperature tail.

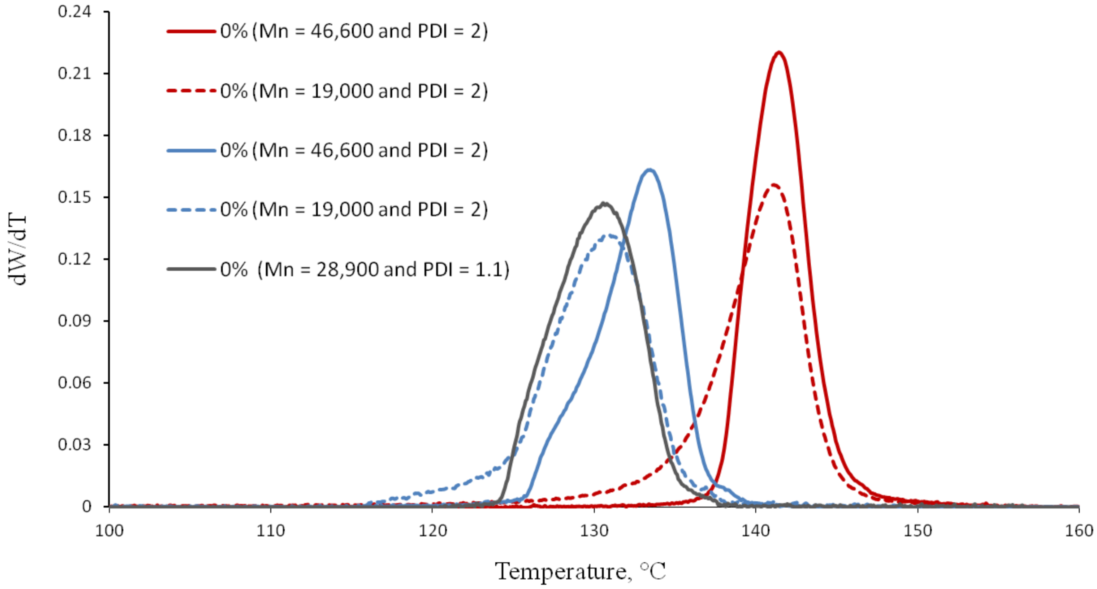

Figure 6.20 Effect of molecular weight on HT-TGIC profiles of polyethylene resins using TCB (blue lines) and ODCB (red lines). Experimental conditions: SZ = 100 µL, CR = 5 °C/min [155 – 90 °C], Fc = 0.02 mL/min HR = 1 °C/min, Fe = 0.5 mL/min.

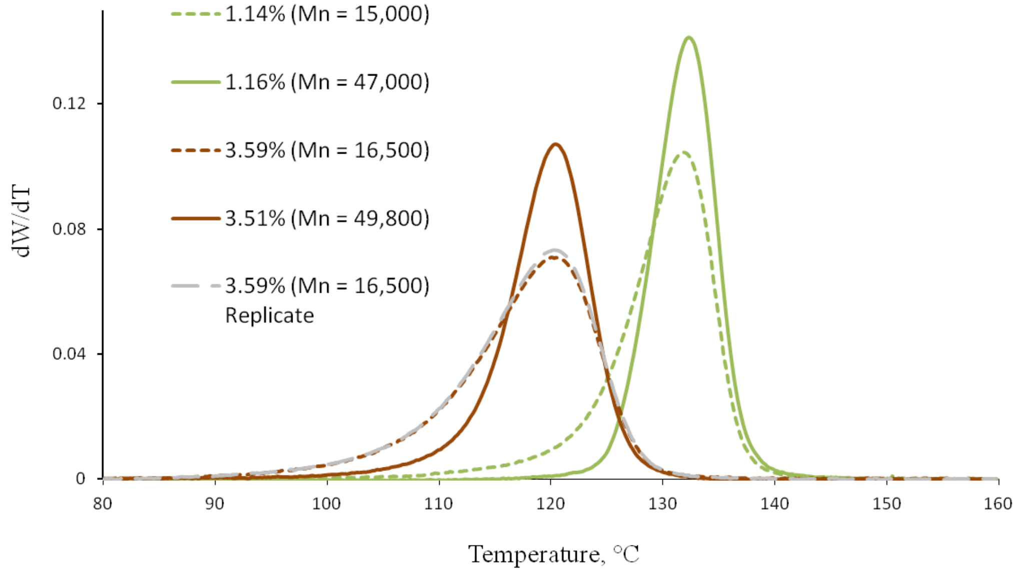

Figure 6.21 Effect of molecular weight on HT-TGIC profiles of ethylene/1-octene copolymers. Experimental conditions: SZ = 100 μL, CR = 5 °C/min [155 – 90 °C], Fc = 0.02 mL/min HR = 1 °C/min, Fe = 0.5 mL/min.

It is very important to point out that the HT-TGIC profile of polyethylene homopolymer is greatly affected by solvent type. For instance, the polyethylene sample with M_n = 46,600 had a broader HT-TGIC distribution when the analysis was performed with TCB than when measured using ODCB. Moreover, the profile measured using TCB was not symmetric, showing a significant low temperature tail in the range [122 °C – 130 °C]. A similar behavior was observed for the sample containing only 0.16 mol% 1-octene. Figure 6.22 compares the profiles for this sample measured with ODCB, TCB, and TCB – ODCB mixture. The best resolution was obtained when ODCB was used as the mobile phase, but the shape of the profile improved when a mixture of TCB and ODCB was employed.

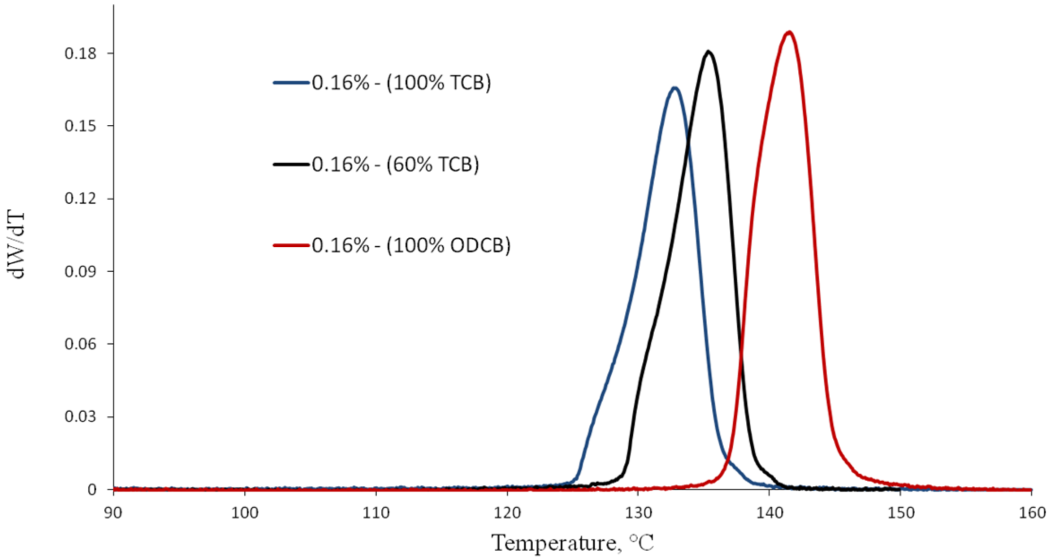

Figure 6.22 Effect of solvent type on HT-TGIC profiles a polyethylene sample having 0.16 mol% 1-octene using ODCB (red lines), TCB (blue lines), and a mixture of TCB and ODCB (black line). Experimental conditions: SZ = 100 μL, CR = 5 °C/min [155 – 90 °C], Fc = 0.02 mL/min HR = 1 °C/min, Fe = 0.5 mL/min.

The low 1-octene content sample was also studied using the following adsorption/desorption temperature ranges: [155 °C – 90 °C – 160 °C], [155 °C – 110 °C – 160 °C], [155 °C – 115 °C – 160 °C]. The results using these conditions are shown in Figure 6.23. Interestingly, narrowing the adsorption/desorption temperature range had a large effect on the profiles obtained for this resin. The profiles become narrower as the final cooling temperature increases from 90 °C to 115 °C. These findings indicate that polymer crystallization effects are responsible for the peak distortion observed for resins with low comonomer content. When the cooling cycle was stopped at 90 °C, chains with high molecular weight and high crystallinity may crystallize on the PGC surface, which may affect the adsorption of chains with lower crystallinity (higher comonomer content). These chains adsorb more weakly, being responsible for the lower temperature shoulder in the HT-TGIC peak. Therefore, increasing the final temperature during the cooling cycle to 110 °C and 115 °C reduced the chances of polymer crystallization taking place and caused the HT-TGIC profile to become more symmetric.

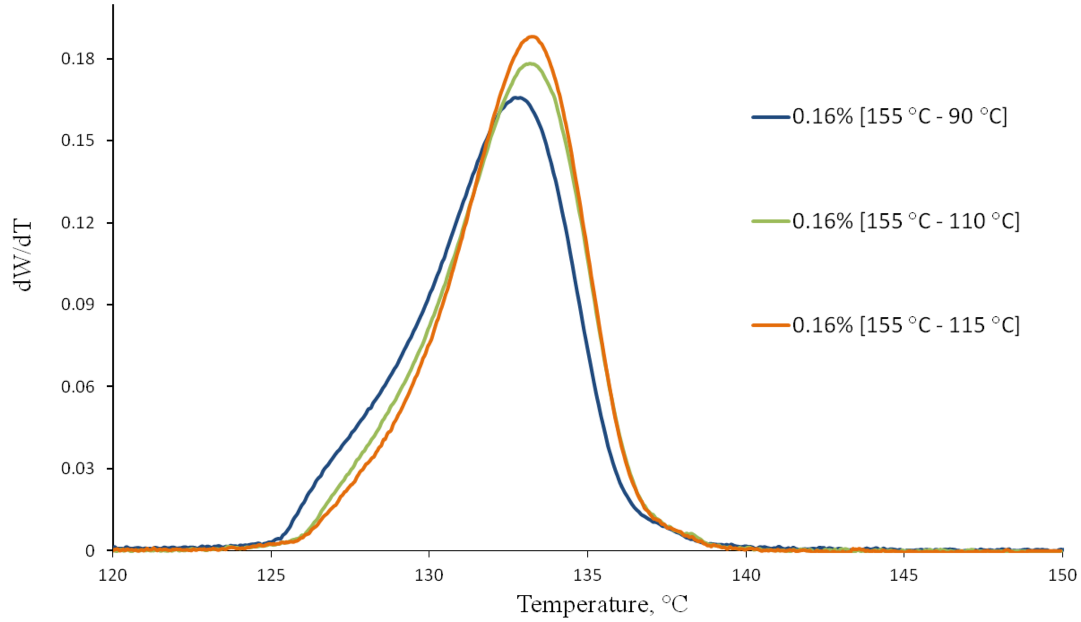

Figure 6.23 Effect of adsorption/desorption temperature range on HT-TGIC profiles for the low 1-octene content resin (0.16 mol% 1-octene) using TCB. Experimental conditions: SZ = 100 µL, CR = 5 °C/min, HR = 1 °C/min, Fe = 0.5 mL/min.

Using the adsorption/desorption temperature range of [155 °C – 115 °C – 160 °C], the analysis of this HDPE resin was repeated using small sample concentration of 0.3 mg/mL instead of 1 mg/mL. The results, as shown in Figure 6.24, indicate that the effect of sample concentration on the profile shape is limited. The sample was also analyzed by HT-TGIC using slow cooling rate (1 °C/min) and slow heating rate (0.5 °C/min), as illustrated in Figure 6.25. The results overlay very well on the profile measured using a cooling rate of 5 °C/min and heating rate of 1 °C/min.

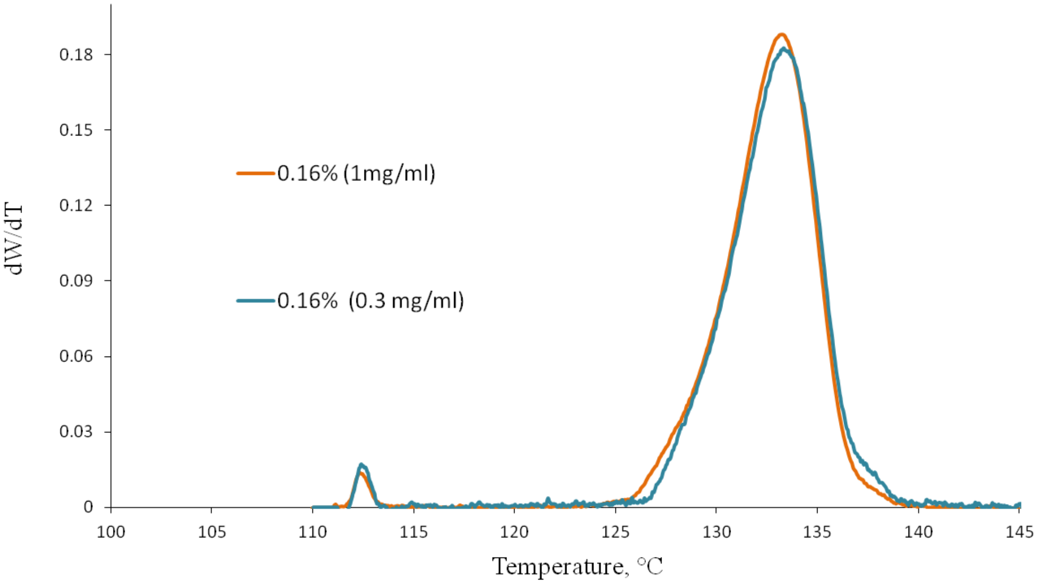

Figure 6.24 Effect of sample concentration on HT-TGIC profiles for the HDPE resin (0.16 mol% 1-octene) using TCB. Experimental conditions: SZ = 100 μL, CR = 5 °C/min [155 – 115 °C], HR = 1 °C/min, Fe = 0.5 mL/min.

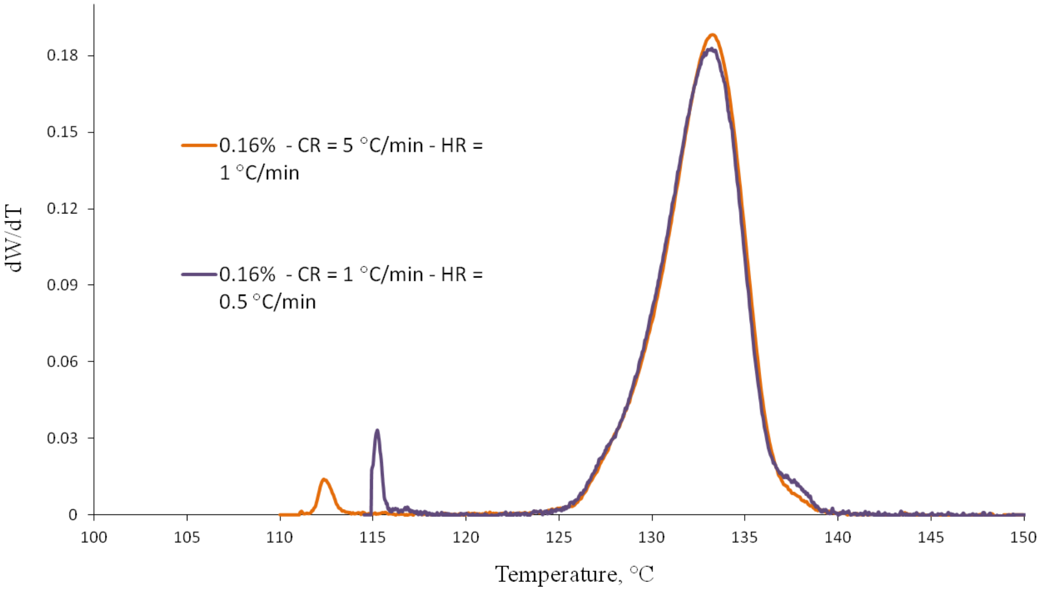

Figure 6.25 Comparison between the HT-TGIC profiles for HDPE resin (0.16 mol% 1-octene) using (CR = 1 °C/min and HR = 0.5 °C/min) and (CR = 5 °C/min and HR = 1 °C/min).

Similarly, the polyethylene homopolymer sample with M_n = 46,600 and PDI = 2 was analyzed using the adsorption/desorption temperature range of [155 °C – 115 °C – 160 °C]. The results, illustrated in Figure 6.26, clearly indicate that increasing the final temperature during the cooling cycle to 115 °C generates a narrower profile. Although, the result is improved by narrowing the adsorption temperature range, the result is still broader than the profile obtained with ODCB.

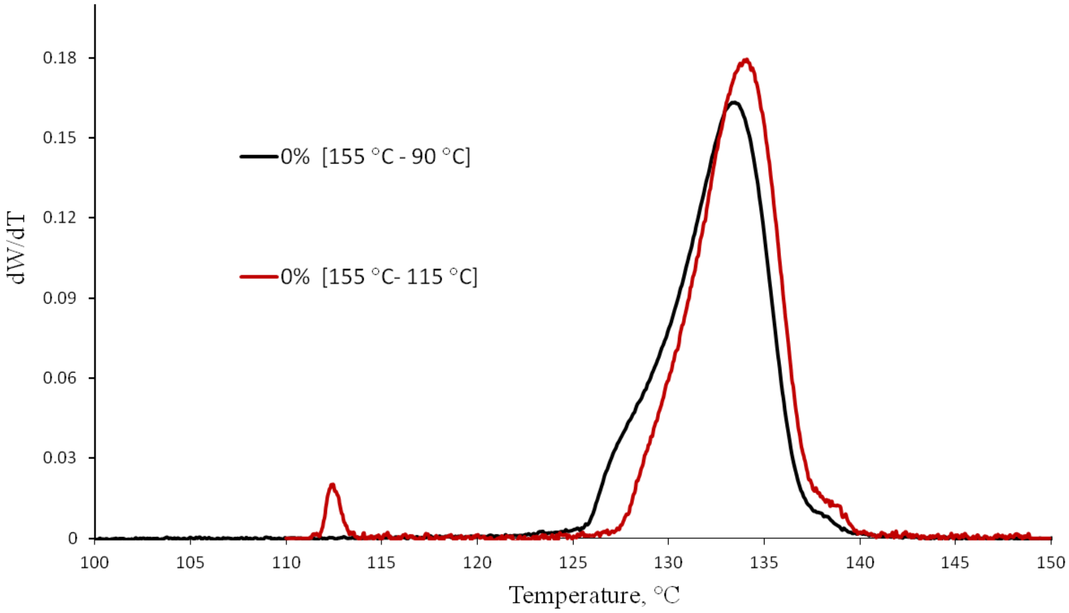

Figure 6.26 Effect of adsorption/desorption temperature range on HT-TGIC profiles for linear polyethylene (0 mol% 1-octene) using TCB. Experimental conditions: SZ = 100 µL, CR = 5 °C/min, HR = 1 °C/min, Fe = 0.5 mL/min.

6.2.4 COMPARISON BETWEEN HT-TGIC AND CEF

CEF experiments of the individual resins and their blends were performed using the CEF instrument from Polymer Char (Valencia, Spain). CEF experimental procedure was described in Chapter 4. In this section, HT-TGIC profiles for individual resins were compared with their respective CEF profiles.

CEF fractionates polyolefins according to their crystallizability, while HT-TGIC fractionates samples based on their interaction with the packing material of the Hypercarb® column. CEF profiles, as will be further discussed in Chapter 7, are strongly affected by the cooling rate. On the other hand, the effect of cooling rate on HT-TGIC profiles is limited. Figure 6.27 compares the HT-TGIC and CEF profiles of a polyethylene homopolymer. Both experiments were performed using TCB as solvent. The heating rate and the elution solvent flow rate were 1 °C/min and 0.5 mL/min, respectively. The HT-TGIC profile is much broader than the equivalent CEF curve.

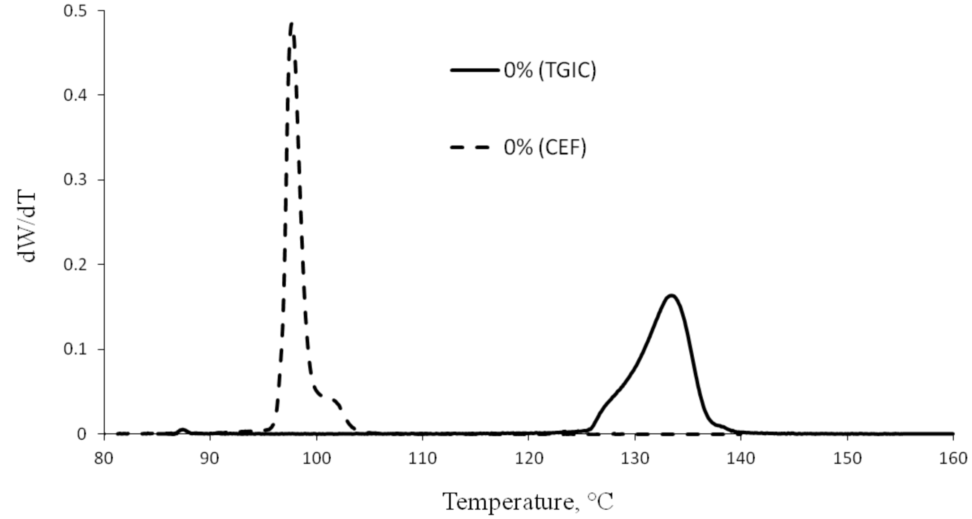

Figure 6.27 Comparison of HT-TGIC and CEF profiles of a polyethylene sample (0 mol% 1-octene). CEF: CR = 0.5 °C/min [120 °C – 35 °C] and Fc = 0.005 mL/min, HR = 1 °C/min and Fe = 0.5 mL/min. HT-TGIC: CR = 5 °C/min [155 °C – 90 °C] and Fc = 0.02 mL/min, HR = 1 °C/min and Fe = 0.5 mL/min.

Ethylene/1-octene copolymers (3.51% and 2.2 mol% of 1-octene) were also analyzed by HT-TGIC and CEF using the same conditions. The results are shown in Figure 6.28. As the comonomer content increases, both HT-TGIC and CEF profiles become broader and shifted to lower temperatures, as expected. Interestingly, differences between the HT-TGIC and CEF profiles decrease as the comonomer content increases.

CEF profiles were shifted to higher temperatures to match the HT-TGIC peak temperatures as illustrated in Figure 6.29. The CEF profile of the copolymer containing 3.51 mol% of 1-octene is only slightly narrower than the HT-TGIC profile. The same behavior was observed when the analysis of both CEF and HT-TGIC were performed using a heating rate of 3 °C/min, as shown in Figure 6.30.

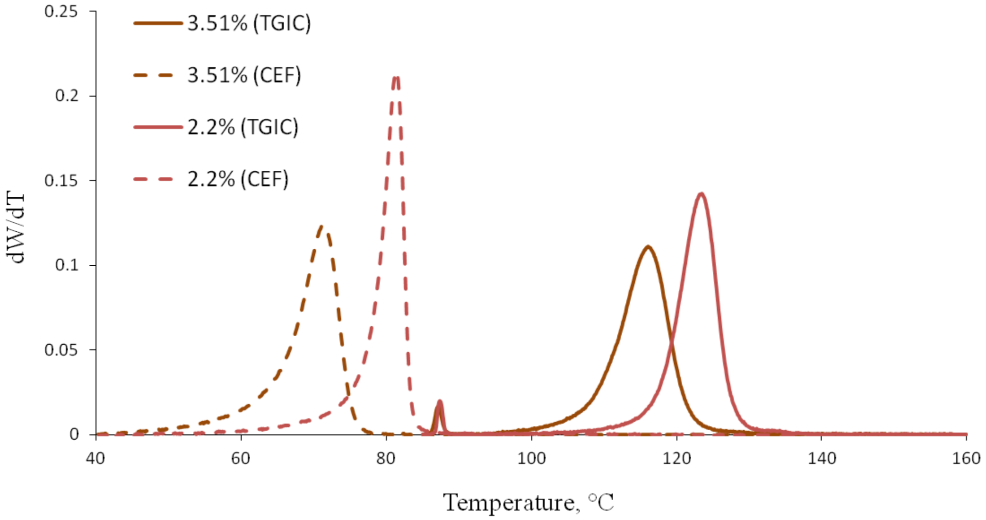

Figure 6.28 Comparison between HT-TGIC and CEF profiles of ethylene/1-octene copolymers (3.51% and 2.2 mol% 1-octene). CEF: CR = 0.5 °C/min [120 °C – 35 °C] and Fc = 0.005 mL/min, HR = 1 °C/min and Fe = 0.5 mL/min. HT-TGIC: CR = 5 °C/min [155 °C – 90 °C] and Fc = 0.02 mL/min, HR = 1 °C/min and Fe = 0.5 mL/min.

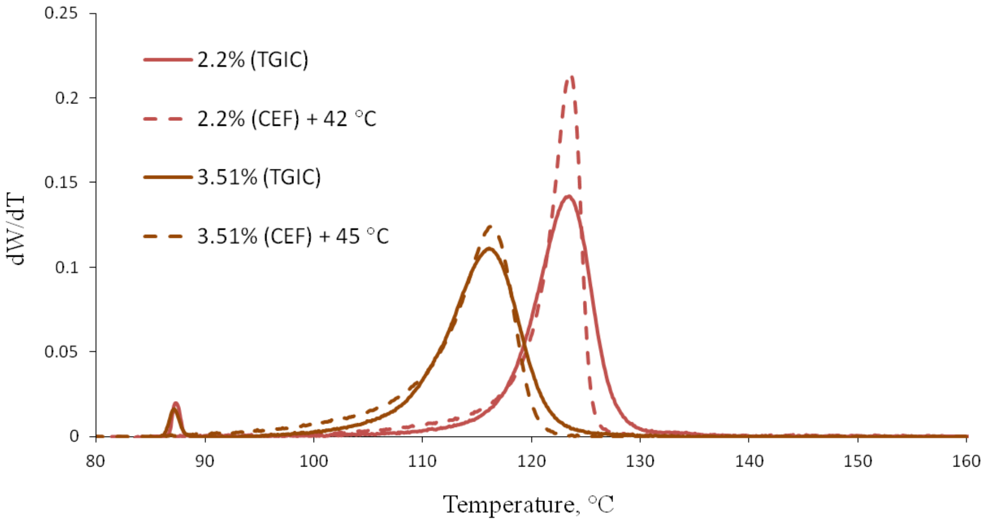

Figure 6.29 Comparison between HT-TGIC and CEF profiles of ethylene/1-octene copolymers (3.51% and 2.2 mol% 1-octene). The CEF profiles were shifted to higher temperature to match the HT-TGIC profiles. Experimental conditions are similar to those in Figure 6.27.

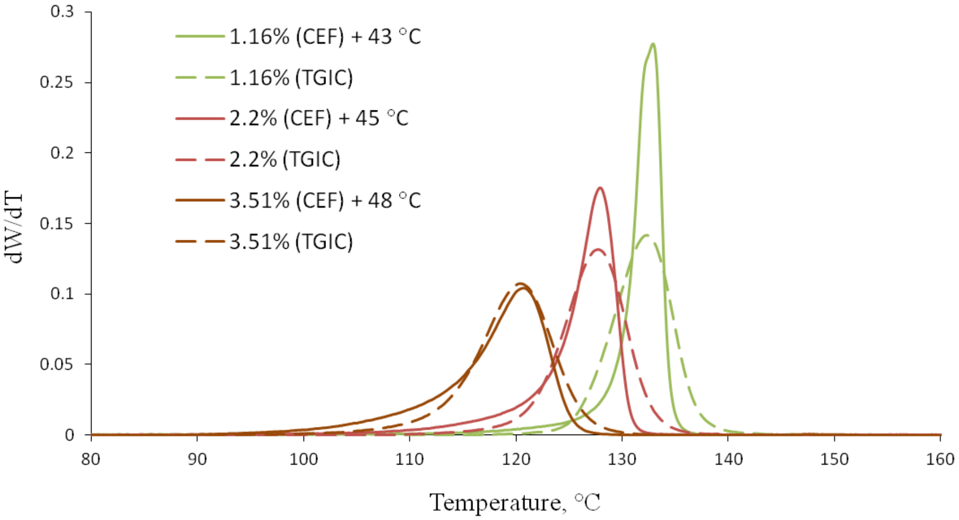

Figure 6.30 Comparison between HT-TGIC and CEF profiles of ethylene/1-octene copolymers (3.51% 2.2%, and 1.16 mol% 1-octene) using a heating rate of 3 °C/min. CEF profiles were shifted to higher temperatures to match the HT-TGIC profiles.

6.3 CONCLUSIONS

The effect of the solvent type on HT-TGIC has been studied using polyethylene homopolymers, ethylene/1-octene copolymers, and their blends. Co-adsorption and co-desorption phenomena depend strongly on the type of solvent used during the analysis. It has been shown that using ODCB minimizes co-adsorption and co-desorption effects and gives the best peak separation for the blend components. Although TCB is a good solvent for polyethylene, poor peak separation of the blend components has been observed when TCB was used as the mobile phase. The analysis of Blend-4 (8.5 and 1.16 mol % 1-octene) by HT-TGIC using TCB was performed for three blend compositions (30/70, 50/50, and 70/30 wt-%). The results indicate that the degree of co-adsorption and co-desorption increases as the amount of the 8.5 mol % component decreases in the blend.

Calibration curves using TCB and ODCB are almost parallel, with the better solvent (TCB) having lower elution peak temperatures for the same comonomer content. The profiles measured with TCB and CN were similar and both were more affected by co-adsorption and co-desorption than when ODCB was used.

The effect of the molecular weight on HT-TGIC profiles was studied using samples with the same comonomer content and different molecular weights. Samples with low molecular weight have broader distributions and significant lower temperature tails. Polyethylene (0 mol % 1-octene) profiles measured with TCB were broader than those measured with ODCB. This behavior may be attributed to the weak adsorption of the fractions with low molecular weight when a better solvent like TCB is used for the analysis.

The HT-TGIC profiles of polyethylene samples (0 mol % 1-octene) were broader than the equivalent CEF profiles, indicating that molecular weight effects on HT-TGIC analysis are stronger than in CEF analysis. However, the differences between the profiles measured by these techniques decrease as the comonomer content increases.

Chapter 7

CHARACTERIZATION OF POLYETHYLENE AND ETHYLENE/1-OCTENE COPOLYMERS BY CEF

7.1 INTRODUCTION

As described in Chapter 2, TREF and CRYSTAF have been widely used to measure the CCD of polyolefins based on their crystallizabilities from dilute solution. TREF fractionation requires two temperature cycles: cooling and heating. During the cooling cycle, the crystallized polymers are deposited onto the surface of the column packing material (ideally) in layers of different crystallinities. During the heating cycle, the precipitated polymers are eluted with the solvent at increasing temperatures. The solvent first removes the least crystalline fractions, followed by the more crystalline fractions. The fractionation in CRYSTAF, as a fast alternative to TREF, needs only one temperature cycle. In this technique, the concentration of the polymer solution is continuously monitored during the crystallization. Then, the first derivative of the obtained cumulative curve of the polymer solution concentration gives the CRYSTAF CCD as a function of crystallization temperature.

Co-crystallization reduces the resolution of TREF and CRYSTAF profiles. It has been investigated by many researchers.[84, 90, 94] It has been found that using a slow cooling rate was necessary to minimize, but was not always capable of overcoming this limitation. Therefore, the analysis time may be very long to obtain CCDs with high resolution by TREF and CRYSTAF. CEF was invented recently at Polymer Char (Valencia, Spain) to provide high resolution results in shorter period of time as compared with TREF and CRYSTAF. The main difference between CEF and TREF is that the crystallization cycle in CEF is performed dynamically under solvent flow in a long column. Therefore, CEF minimizes co-crystallization effects by segregating crystallites of different crystallizabilites within the column. Consequently, the analysis time is dramatically decreased without compromising CEF resolution.

In this chapter, several ethylene/1-octene copolymers made with metallocene catalysts were analyzed by CEF to generate a calibration curve and to study the effect of main operating conditions on CEF profiles. A new methodology was also developed to quantify the degree of co-crystallization on CEF profiles using blends of ethylene/1-octene copolymers. These individual resins and their blends were used to study the effect of column void volume on the obtained results. Polyethylene resins of similar comonomer content and different molecular weight averages were used to study the effect of the polymer molecular weight on the CEF profiles.

Moreover, a detailed study on the effect of the CEF operating conditions on CCD resolution was conducted using industrial LLDPE resins that have broad MWDs and CCDs. This chapter also compares CEF and HT-TGIC profiles of these resins.

7.2 RESULTS AND DISCUSSION

All CEF experiments were performed using Polymer Char (Valencia, Spain) instrument. The detailed experimental procedure was described in Chapter 4, Section 4.2. The average properties of polyethylene and ethylene/1-octene copolymers used in the present investigation were also presented in Chapter 4, Table 4.1.

7.2.1 EFFECTS OF CEF OPERATING CONDITIONS ON THE PROFILES OF INDIVIDUAL RESINS

Several ethylene/1-octene copolymers with similar molecular weight averages and different comonomer contents (0.16, 1.16, 2.2, and 3.51 mol% 1-octene) were analyzed by CEF. Figure 7.1 shows the CEF profiles of these copolymers. As expected, the measured profiles became narrower as the comonomer content decreased and the elution peak temperature depended linearly on the comonomer content. These results were used to generate a calibration curve for CEF. The cooling rate was one of the main factors changing the elution peak temperatures of these resins. Figure 7.2 compares the CEF profiles of individual resins (1.16, 2.2, and 3.51 mol% 1-octene) using cooling rates of 3 °C/min and 0.25 °C/min. The profiles became broader as the cooling rate decreased. The calibration curves are almost parallel at these two cooling rates (Figure 7.3) with the faster cooling rate having lower elution peak temperatures.

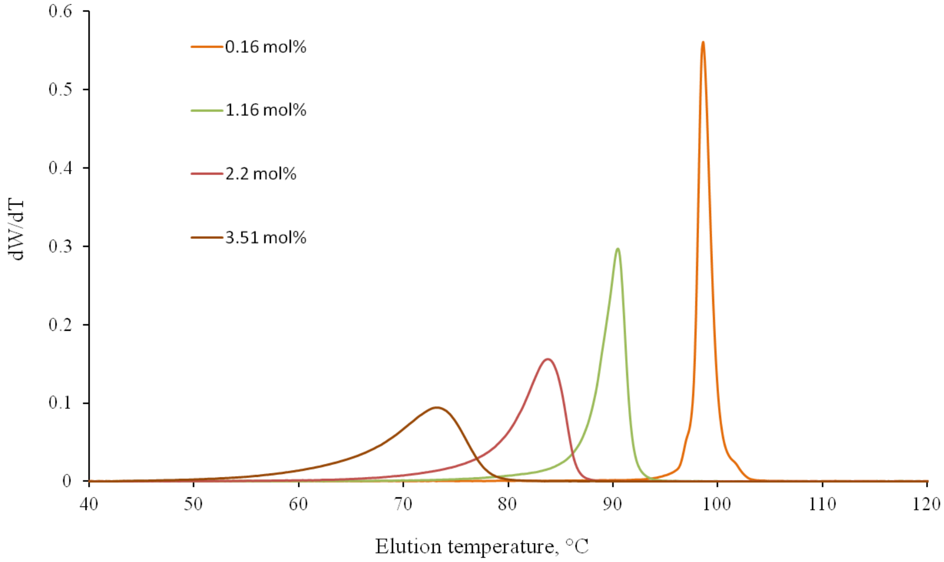

Figure 7.1 CEF profiles of ethylene/1-octene resins. Experimental conditions: CR = 0.25 °C/min, Fc = 0.002 mL/min [120 – 35 °C], HR = 3 °C/min, Fe = 1 mL/min.

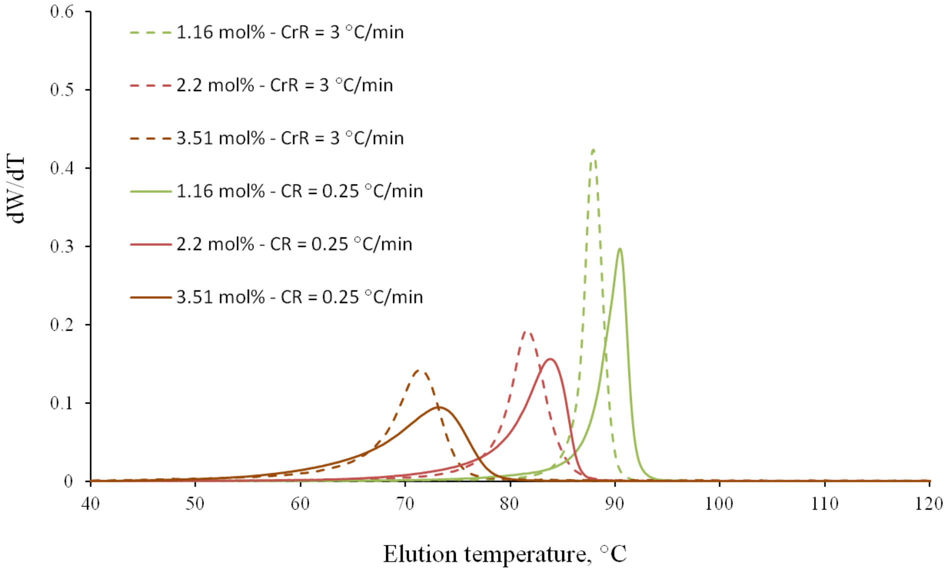

Figure 7.2 Effect of cooling rate on CEF profiles of ethylene/1-octene resins. Experimental conditions: (CR = 0.25 °C/min, Fc = 0.002 mL/min), (CR = 3 °C/min, Fc = 0.04 mL/min), HR = 3 °C/min, Fe = 1 mL/min.

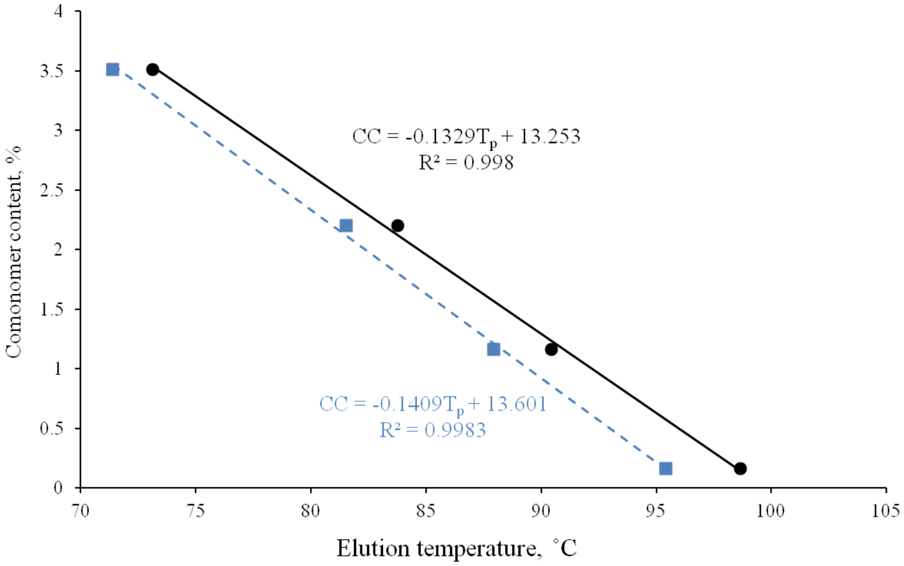

Figure 7.3 CEF calibration curves using cooling rates of 0.25 °C/min (black line) and 3 °C/min (blue line). Experimental conditions: (CR = 0.25 °C/min, Fc = 0.002 mL/min), (CR = 3 °C/min, Fc = 0.04 mL/min), HR = 3 °C/min, Fe = 1 mL/min.

Although the faster cooling rate gives narrower CEF profiles, the peak separation of blend components is inadequate, as described in the following section. Figure 7.4 shows CEF profiles of individual resins (1.16 and 3.51 mol% 1-octene) using different heating rate and elution solvent rate (3 °C/min + 1 mL/min and 1 °C/min + 0.5 mL/min). CEF profiles became narrower when the slower heating rate was used. Calibration curves at different heating rates are compared in Figure 7.5.

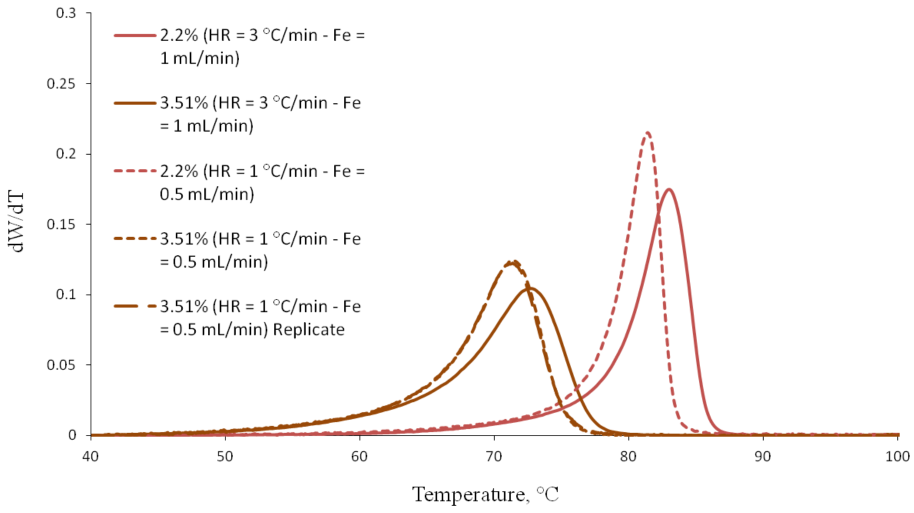

Figure 7.4 Effect of heating rate on CEF profiles of ethylene/1-octene resins. Experimental conditions: CR = 0.5 °C/min, Fc = 0.005 mL/min.

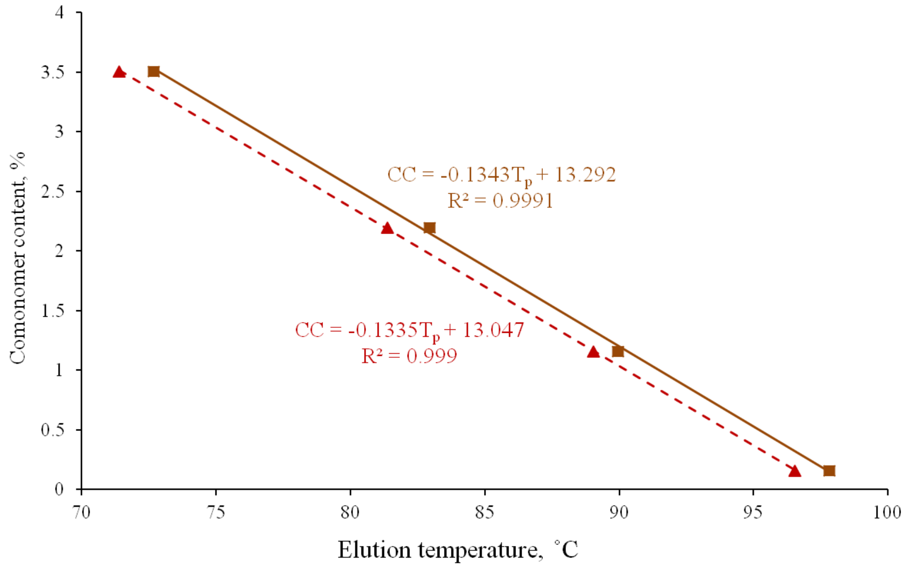

Figure 7.5 CEF calibration curves using heating rate of 3 °C/min (Fe = 1 mL/min) (brown line) and 1 °C/min (Fe = 0.5 mL/min) (red line). Experimental conditions: CR = 0.5 °C/min, Fc = 0.005 mL/min.

It is important to point out that CEF elution peak temperatures may be affected by other operating conditions, such as the solvent flow rate during cooling, injection point in the column, and starting and ending temperatures of the cooling cycle. For instance, Figure 7.6 compares the CEF profiles of individual resins (1.16 and 2.2 mol% 1-octene) using two different cooling cycles: [120 – 35 °C] and [120 – 50 °C]. During the crystallization cycle, the column temperature was decreased under continuous TCB flow within the limits of the column. This solvent flow rate is calculated based on the column volume, cooling rate, and difference between starting and ending temperatures in the cooling cycle. Therefore, by narrowing the cooling cycle, the solvent flow rate during this step can be increased to obtain better chain separation in the column. As a result, the elution peak temperatures are shifted to lower temperatures, as shown in Figure 7.6.

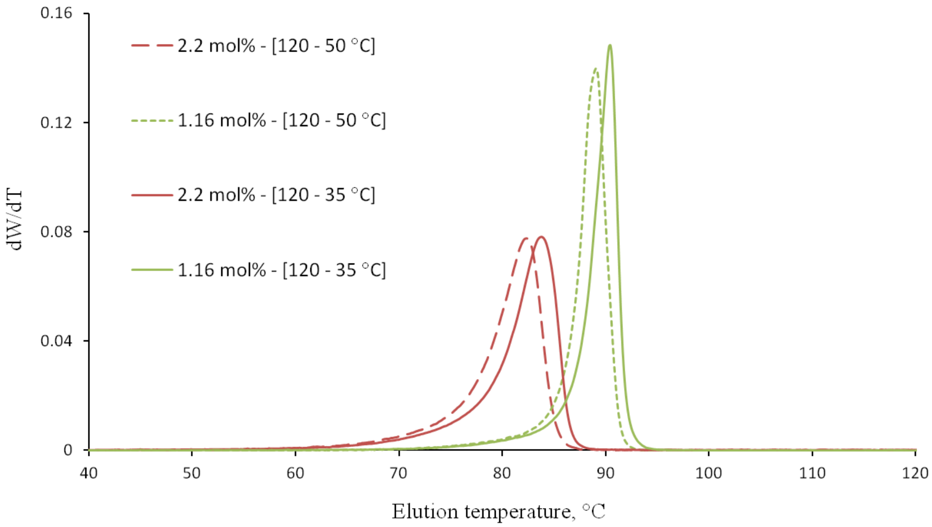

Figure 7.6 Effect of cooling cycle on CEF profiles of ethylene/1-octene resins. Experimental conditions: CR = 0.25 °C/min, Fc = 0.002 mL/min [120 – 35 °C] and Fc = 0.004 mL/min [120 – 50 °C], HR = 3 °C/min, Fe = 1 mL/min.

7.2.2 MOLECULAR WEIGHT EFFECT

To study the effect of molecular weight on CEF profiles, polyethylene resins with similar comonomer content but different molecular weight averages were analyzed. The results are shown in Figure 7.7. The peak temperature of the sample with 1.16 mol% 1-octene and M_n = 47,000 is almost the same for that with 1.14 mol% 1-octene and M_n = 15,000. However, the sample with lower molecular weight had broader CCD with a significant low temperature tail. The same behavior was observed for the samples with 3.51 mol% 1-octene and M_n = 49,800 and with 3.59 mol% 1-octene and M_n = 16,500. The broader CEF profile measured for the lower molecular weight samples may be attributed to the presence of polymer chains with lower molecular weights, but it is also a result of the fact that chains with lower molecular weight will have a broader CCD than those of higher molecular weight averages and similar comonomer content due to purely statistical reasons. However, most of the samples of commercial interest will not be significantly influenced by molecular weight effects since they usually have high molecular weight averages.

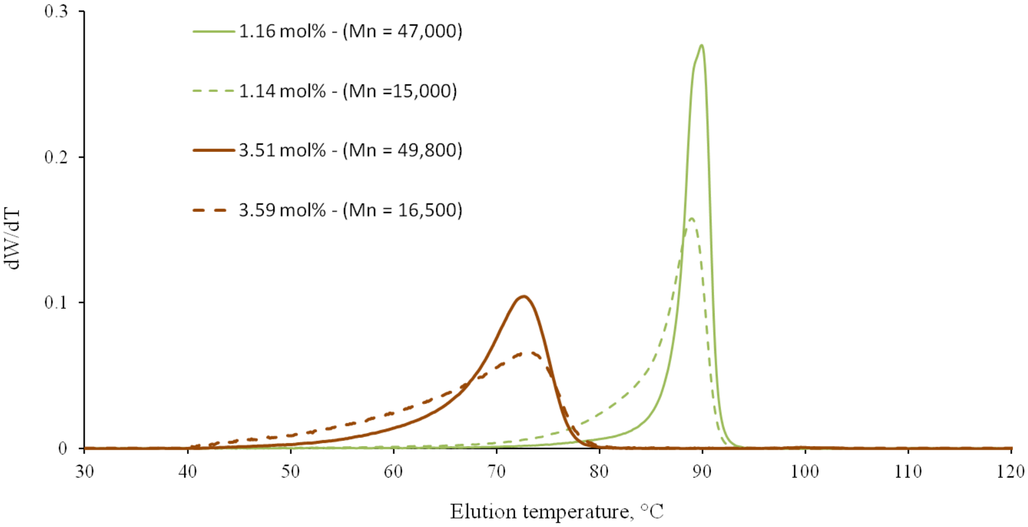

Figure 7.7 Molecular weight effect on CEF profiles of individual resins. Experimental conditions: CR = 0.5 °C/min, Fc = 0.005 mL/min [120 – 35 °C], HR = 3 °C/min, Fe = 1 mL/min.

Trying to further investigate the effect of molecular weight on CEF profiles, three ethylene homopolymers were analyzed by CEF: M_n = 46,000 (PDI = 2), M_n = 19,000 (PDI = 2), and M_n = 28,900 (PDI = 1.1). The results are shown in Figure 7.8. The polymer with the highest molecular weight had the highest elution peak temperature. The other samples had similar elution peak temperatures. However, the profiles of the polyethylene narrow MWD standard sample (PDI = 1.1) was narrower than the other two, indicating that the broadness and the low temperature tail observed in the sample with M_n = 19,000 was due to polymer chains with lower molecular weights.

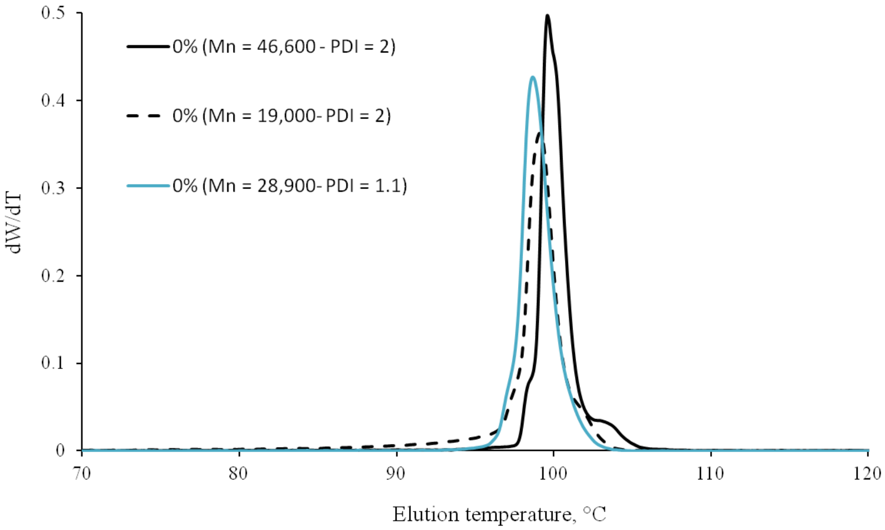

Figure 7.8 Molecular weight effect on CEF profiles using ethylene homopolymers. Experimental conditions: CR = 0.5 °C/min, Fc = 0.005 mL/min [120 – 35 °C], HR = 3 °C/min, Fe = 1 mL/min.

The CEF profile for the sample with M_n = 46,600 illustrated in Figure 7.8 had a small peak or shoulder at a higher temperature (103 °C) due to the presence of polymer chains with higher crystallizabilities (and high molecular weight). The analysis of this sample was repeated using slow heating rate (1 °C/min) and elution flow rate of 0.5 mL/min, as shown in Figure 7.9. The profile was shifted to lower temperatures under these new experimental conditions. However, the high temperature shoulder was still observed. We have made numerous attempts to find operating conditions that eliminated this small peak by increasing the dissolution time from 1 hour to 2 hours before the injection, and by increasing the starting temperature of the cooling cycle to 140 °C and 160 °C, but without significant improvements.

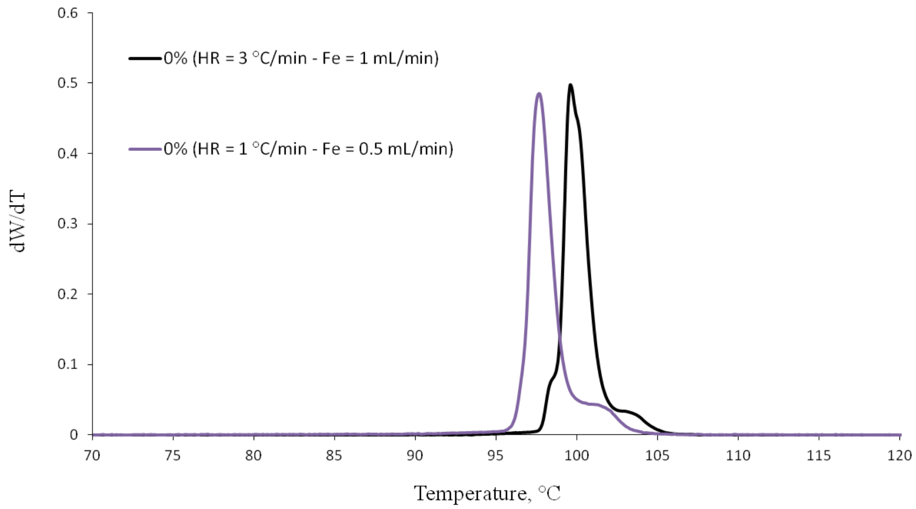

Figure 7.9 Effect of heating rate on CEF profiles of polyethylene (0% 1-octene, M_n = 46, 600). Experimental conditions: CR = 0.5 °C/min, Fc = 0.005 mL/min.

7.2.3 CO-CRYSTALLIZATION EFFECT

Co-crystallization phenomenon is by far the most important factor reducing the resolution of CCDs measured by crystallization-based techniques. In this section, the effect of co-crystallization on CEF profiles was studied using two blends of ethylene/1-octene copolymers: Blend-1 (2.2 and 1.16 mol% 1-octene) and Blend-2 (3.51 and 1.16 mol% 1-octene). Figures 7.10 and 7.11 show the CEF profiles of these blends superimposed on the profiles of the individual resins using a cooling rate of 3 °C/min, a heating rate of 3 °C/min, and an elution solvent flow rate of 1 mL/min. The dotted lines in Figures 7.10 and 7.11 represent the profiles of the blends calculated from the weighted sum of the experimental profiles of each component under the same operation conditions. Significant co-crystallization is observed for Blend-1, since the individual resins (2.2 and 1.16 mol% 1-octene) have similar crystallizabilities. However, the degree of co-crystallization of Blend-2 (3.51 and 1.16 mol% 1-octene) was lower than for Blend-1. The analysis of Blend-2 and its components was repeated using a cooling rate of 0.5 °C/min, as illustrated in Figure 7.12. These results showed an excellent agreement between the experimental and calculated profiles of Blend-2, indicating that the analysis was practically free of co-crystallization effects under these conditions.

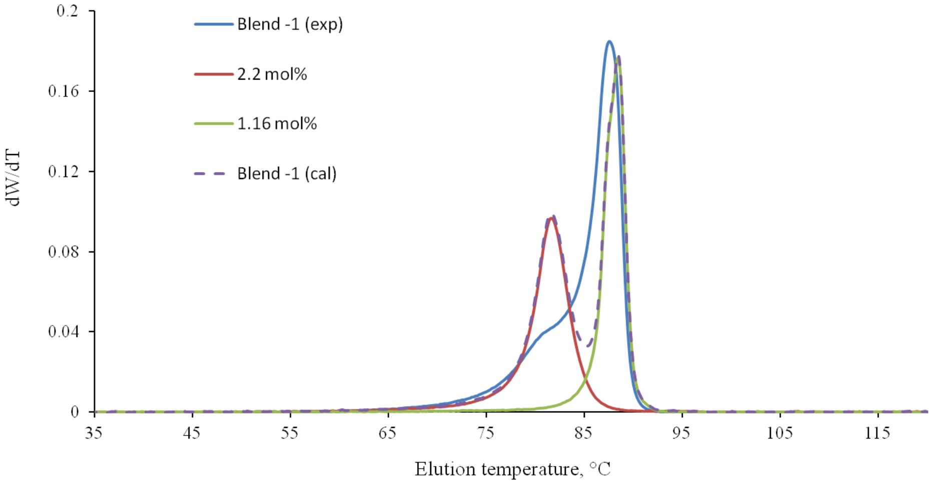

Figure 7.10 CEF profile of Blend-1 and its components. Experimental conditions: CR = 3 °C/min , Fc = 0.04 mL/min, HR = 3 °C/min, Fe = 1 mL/min.

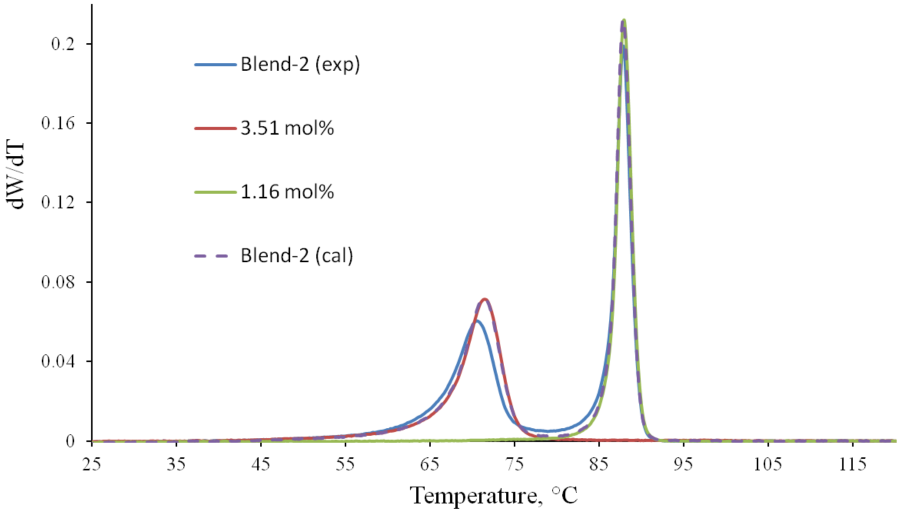

Figure 7.11 CEF profile of Blend-2 and its components. Experimental conditions: CR = 3 °C/min , Fc = 0.04 mL/min, HR = 3 °C/min, Fe = 1 mL/min.

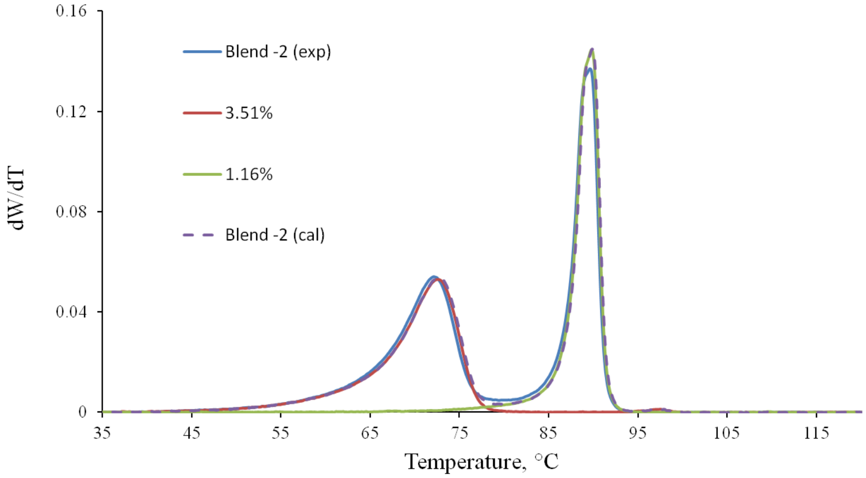

Figure 7.12 CEF profile of Blend-2 and its components. Experimental conditions: CR = 0.5 °C/min , Fc = 0.005 mL/min, HR = 3 °C/min, Fe = 1 mL/min.

Blend-1 and its components were analyzed by the CEF using a cooling rate of 0.25 °C/min (Figure 7.13). Co-crystallization effects were substantially reduced as the cooling rate decreased from 3 to 0.25 °C/min. Figure 7.14 compares the experimental and calculated profiles of Blend-1 using these cooling rates.

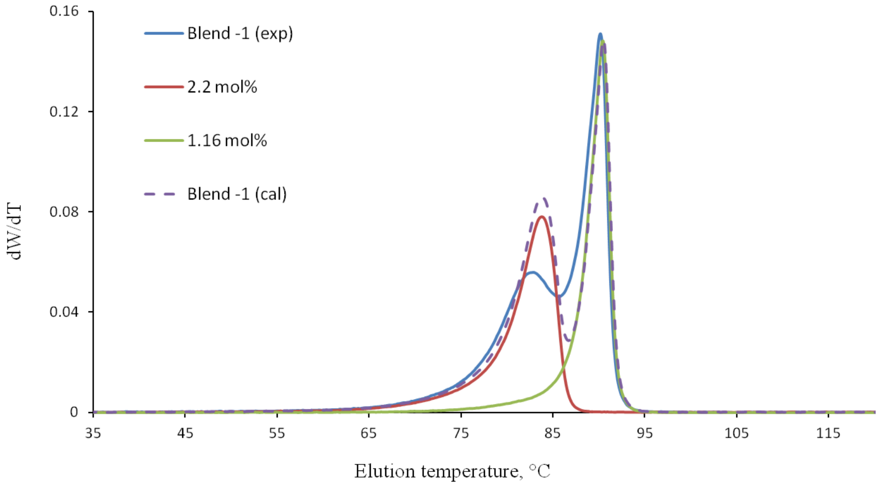

Figure 7.13 CEF profile of Blend-1 and its components. Experimental conditions: CR = 0.25 °C/min , Fc = 0.002 mL/min, HR = 3 °C/min, Fe = 1 mL/min.

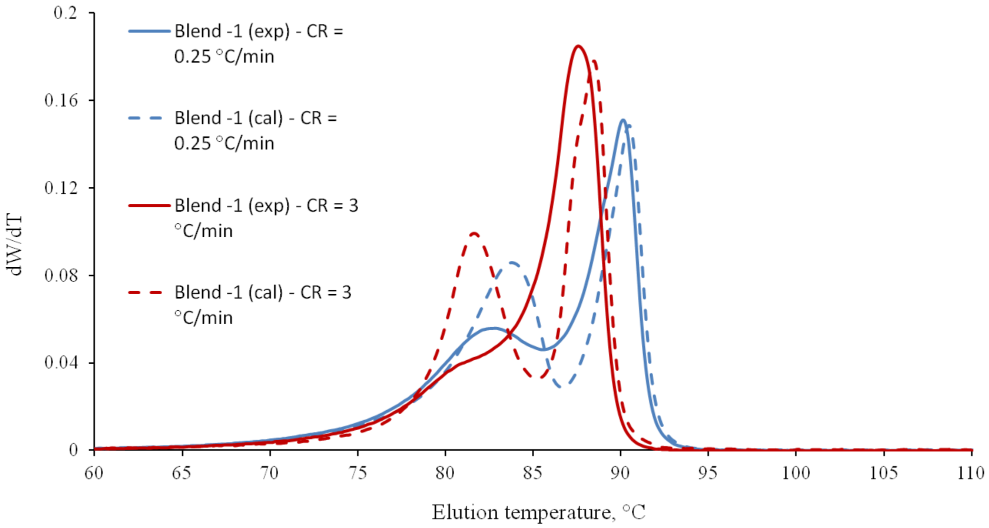

Figure 7.14 Comparison between experimental and calculated profiles for Blend-1 using cooling rates of 3 °C/min and 1 °C/min.

To determine the degree of co-crystallization on the blend profiles quantitatively, a co-crystallization index from each experiment was defined and calculated using the following equation:

$$\Delta = \sum_{i=1}^{n} \left| y_{i(\exp)} - y_{i(cal)} \right| \tag{7.1}$$

where Δ is the co-crystallization index, $y_{i(exp)}$ and $y_{i(cal)}$ are the height of experimental and calculated CEF profiles at each data point *i*, and *n* is the number of data points in the elution temperature range [35 – 120 °C]. Equation (7.1) calculates a co-crystallization index as the sum of the differences between experimental and calculated CEF profiles of the blend for all the elution temperatures. For instance, the co-crystallization index for Blend-1 using cooling rates of 3 and 0.25 °C/min were 3.82 and 2.16, respectively.

To study the effect of operating conditions on the degree of co-crystallization using Blend-1, a 2^3 experimental factorial design was performed. The three factors studied were starting cooling temperature, cooling rate, and heating rate. The ratio between the heating rate and the elution solvent flow rate was kept constant for this study. The upper and lower values of the factors used in this study are shown in Table 7.1. The 8 experiments in this design were performed in a random order, as illustrated in Table 7.2. The output from each experiment (degree of co-crystallization) is shown in Table 7.2. With this factorial design and the defined output values, the main effects and the interactions were computed according to Montgomery.[156] The results of the analysis of variance (ANOVA) using 95 % confidence interval are illustrated in Table 7.3. The error term was calculated from five replicate experiments performed at the central conditions.

Table 7.1 Defined levels of the factors

Factor	Upper level	Lower level	Coded value Upper level	Coded value Lower level
A (T_{c1}), °C	120	100	+1	-1
B (CR), °C/min	0.5	0.25	+1	-1
C (HR), °C/min	3	0.25	+1	-1

Table 7.2 The output from each experiment in the 2^3factorial design

Run	Factor (A)	Factor (B)	Factor (C)	Co-crystallization Index
1	-1	-1	-1	1.97
2	-1	-1	+1	1.72
3	-1	+1	-1	2.32
4	-1	+1	+1	2.88
5	+1	-1	-1	1.92
6	+1	-1	+1	2.16
7	+1	+1	-1	3.07
8	+1	+1	+1	2.90

The F test results showed that the effects of factor A and factor B were significant. However, the effect of heating rate (factor C) was not significant. The interaction between these factors had a significant effect; however, the major effect on the degree of co-crystallization was from the cooling rate. Therefore, Blend-1 and its components were analyzed by CEF using a slow cooling rate of 0.09 °C/min, as shown in Figure 7.15. The calculated degree of co-crystallization using this cooling rate was 1.24. Although a very slow cooling rate was used, the profile of Blend-1 was still affected by co-crystallization since the components of this blend have very close elution peak temperatures.

Monrabal *et al.*[157] proposed a new method to minimize the degree of co-crystallization by using multiple crystallization and elution cycles. Their results indicated that the CEF resolution can be improved by increasing the number of cycles, but this approach was not attempted in this investigation.

Table 7.3 ANOVA table for the experiments presented in Table 7.2

Source of variation	Effect	Sum of squares	Degree of freedom	Mean squares	F
A	0.286	0.164	1	0.164	41.5
B	0.848	0.144	1	0.144	364
C	0.095	0.018	1	0.018	4.6
AB	0.098	0.019	1	0.019	4.8
AC	-0.063	0.0078	1	0.0078	2
BC	0.097	0.019	1	0.019	4.8
ABC	-0.306	0.187	1	0.187	47.3
Error			4	0.0039	

F(1,4,0.05) = 7.71

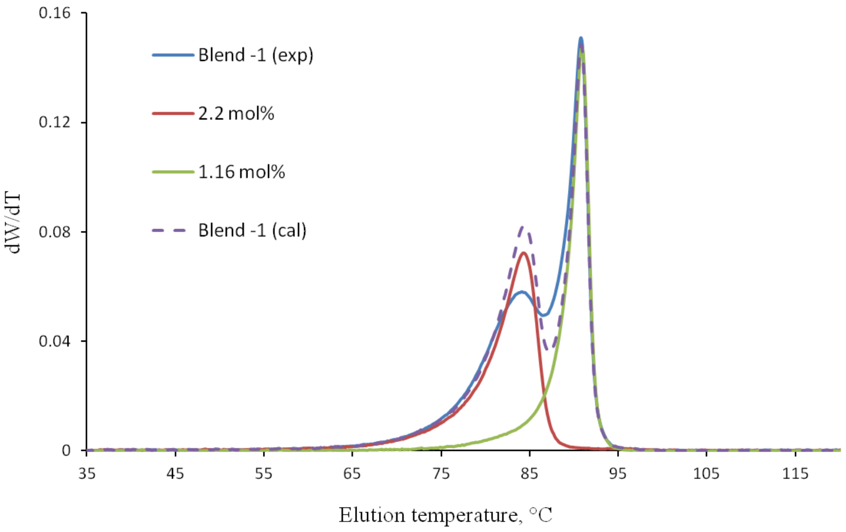

Figure 7.15 CEF profile of Blend-1 and its components. Experimental conditions: CR = 0.09 °C/min , Fc = 0.001 mL/min, HR = 3 °C/min, Fe = 1 mL/min.

7.2.4 EFFECT OF COLUMN VOID VOLUME

The most important part of the CEF instrument is the column. TREF uses a short column usually (10-15 cm long) while CEF needs a long column to obtain the physical separation of polymer chains in the packing according to their crystallizabilities. Two CEF columns were used to study the effect of column volume on the degree of co-crystallization. Column-1 (2.1mm × 2 m) has 1.62 mL void volume, while Column-2 (3.7 mm × 1 m) has 6.7 mL void volume. Both were filled with stainless steel shots. The columns were shown in Chapter 4, Figure 4.3.

Figures 7.16 and 7.17 compare the results using Column-1 and Column-2 for Blend-1 and individual resins, respectively. These results indicate that the profiles obtained using Column-2 (larger void volume) were broader and shifted to higher temperatures as compared with profiles measured using Column-1. Using a cooling rate of 0.25 °C/min, the CEF profiles of Blend-1 were compared in Figure 7.18 for Column-1 and Column-2.

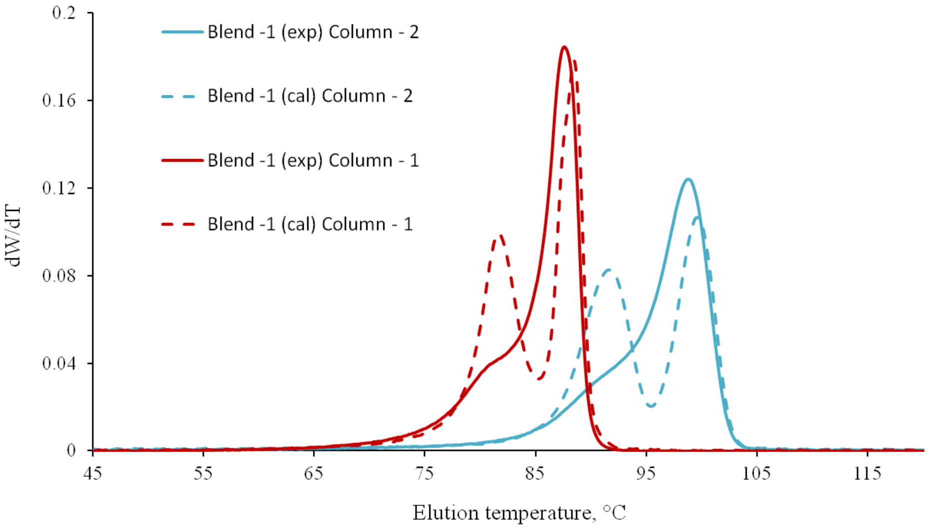

Figure 7.16 Comparison between experimental and calculated profiles of Blend-1 using Column-1 (lower void volume) and Column-2 (higher void volume). Experimental conditions: CR = 3 °C/min, (Fc = 0.04 mL/min – Column-1), (Fc = 0.22 mL/min – Column-2), HR = 3 °C/min, and Fe = 1 mL/min.

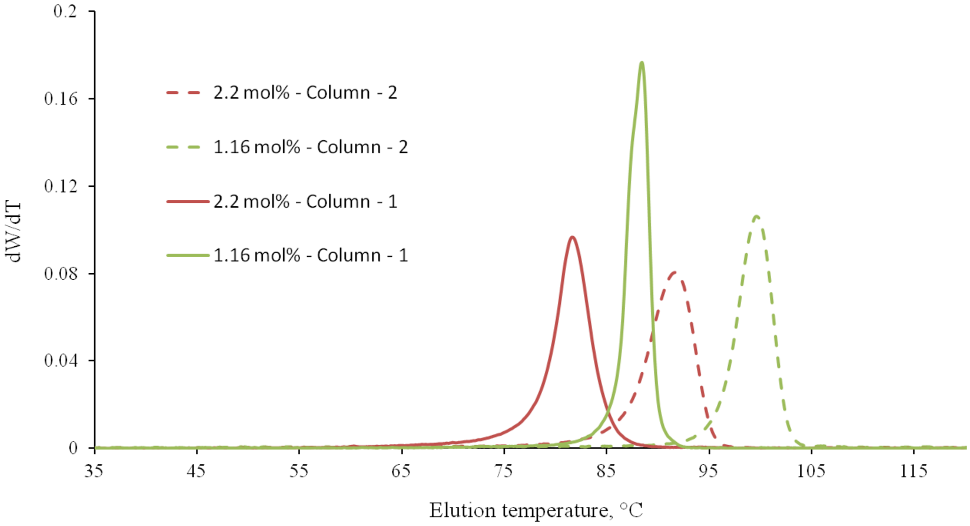

Figure 7.17 CEF profiles of individual resins (1.16 and 2.2 mol% 1-octene) using Column-1 (lower void volume) and Column-2 (higher void volume). Experimental conditions: CR = 3 °C/min, (Fc = 0.04 mL/min – Column-1), (Fc = 0.22 mL/min – Column-2), HR = 3 °C/min, and Fe = 1 mL/min.

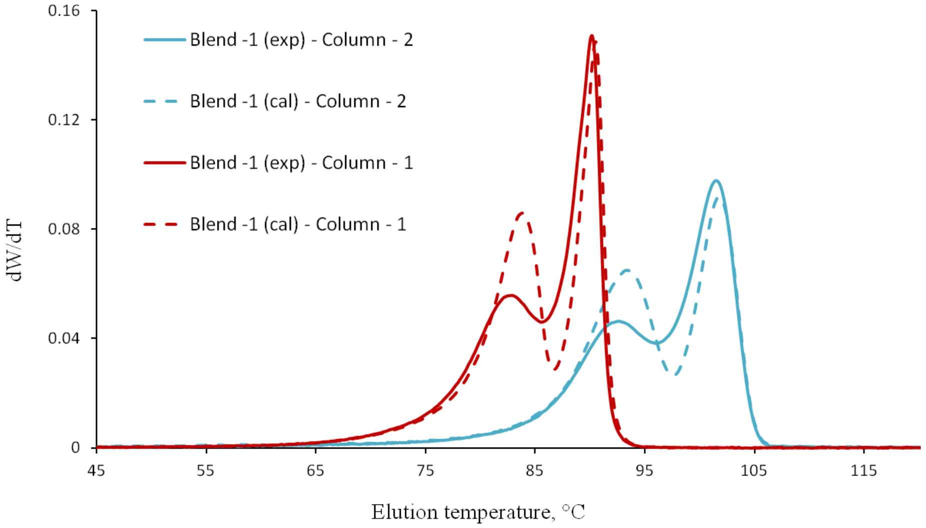

Figure 7.18 Comparison between experimental and calculated profiles of Blend-1 using Column-1 (lower void volume) and Column-2 (higher void volume). Experimental conditions: CR = 0.25 °C/min, (Fc = 0.002 mL/min – Column-1), (Fc = 0.02 mL/min – Column-2), HR = 3 °C/min, and Fe = 1 mL/min.

Table 7.4 compares the degree of co-crystallization using Column-1 and Column-2 at different conditions. The degree of co-crystallization decreased slightly by increasing the column void volume. However, at the same analysis conditions, Column-2 gives broader CCDs. This unexpected behavior may be due to the differences in the dimensions of the columns.

Interestingly, identical profiles were obtained for the two columns when their heating cycles were performed with same ratio calculated from Equation (7.2).

$$R = \frac{Fe/A}{HR} \tag{7.2}$$

where R is the ratio in (m/°C) and A is the cross sectional area of the column. The value of R for column-1 using a heating rate of 3 °C/min and a solvent flow rate of 1 mL/min was 0.093 m/°C. Similar value of R (0.096 m/°C) was obtained for Column-2 using heating rate of 0.5 C/min and solvent flow rate of 0.5 mL/min. Therefore, at these conditions the two columns provide identical profiles as shown in Figure 7.19 for the blends and Figure 7.20 for the individual resins.

Table 7.4 Co-crystallization index (Δ) for profiles measuredusing Column-1 and Column-2

	Column-1		**Column-1**	
CR (°C/min)	0.5	0.25	0.5	0.25
Fc (mL/min)	0.005	0.002	0.04	0.02
HR (°C/min)	3	3	3	3
Fe (mL/min)	1	1	1	1
Δ	2.88	1.73	2.15	1.60

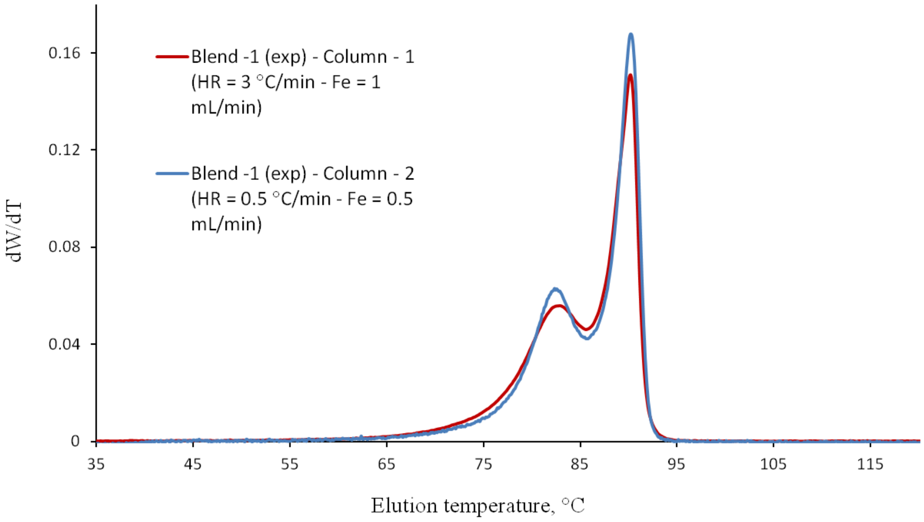

Figure 7.19 Comparison between experimental profiles for Blend-1 using Column-1 and Column-2. Experimental conditions: CR = 0.25 °C/min, (Fc = 0.002 mL/min – Column-1), (Fc = 0.02 mL/min – Column-2).

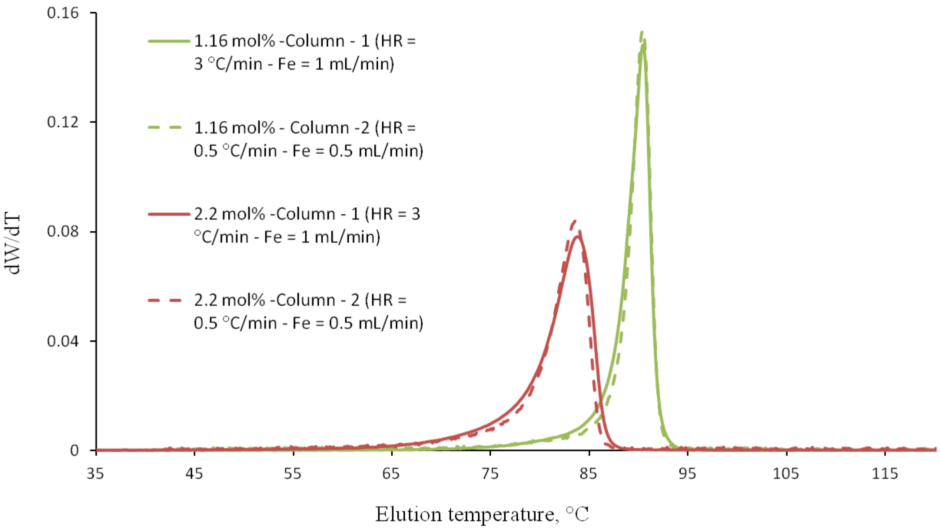

Figure 7.20 Comparison between experimental profiles of individual resins (1.16 and 2.2 mol% 1-octene) using Column-1 and Column-2. Experimental conditions: CR = 0.25 °C/min, (Fc = 0.002 mL/min – Column-1), (Fc = 0.02 mL/min – Column-2).

7.3 CEF RESULTS OF INDUSTRIAL LLDPE RESINS

CEF was also used to analyze four industrial LLDPE resins donated by Dow Chemical. The MWDs for these resins were measured by GPC (Figure 7.21). Samples C and D were made with a Ziegler-Natta catalyst, while samples E and F were made with a mixture of Ziegler-Natta and metallocene catalysts. These resins have similar MWDs; however, they have different CCDs. Figures 7.22 to 7.25 show the CEF profiles of these resins using a cooling rate of 1.5 °C/min, a heating rate of 3 °C/min and an elution solvent flow rate of 1 mL/min. The obtained profiles of Samples C and D show the typical bimodal and broad CCD of Ziegler-Natta resins. Samples E and F have three peaks: the two peaks at high temperature represent the polymer made by Ziegler-Natta catalyst while the third peak represents the polymer made by the metallocene catalyst. However, the amounts of the polymer made by each catalyst are different in these resins that make the shape of their CCDs different. Excellent reproducibility of the CEF profiles were observed, as illustrated in Figure 7.25.

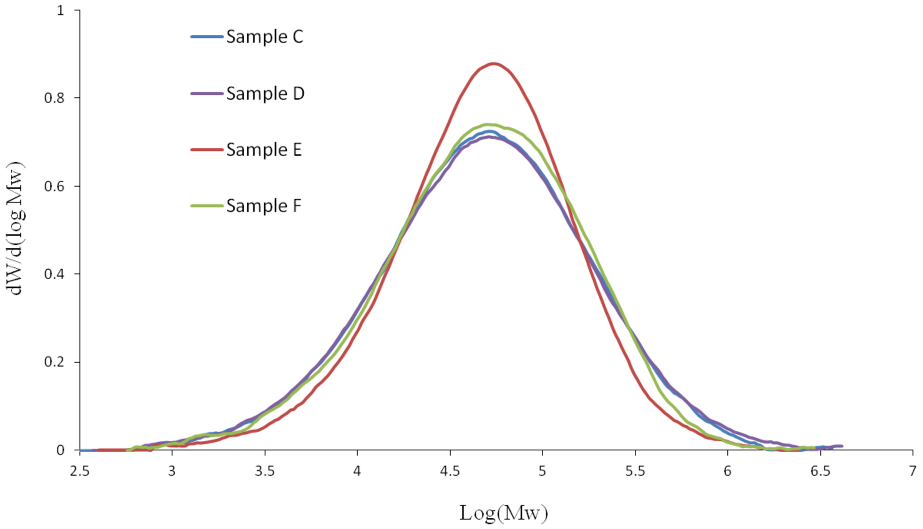

Figure 7.21 MWDs of industrial LLDPE resins.

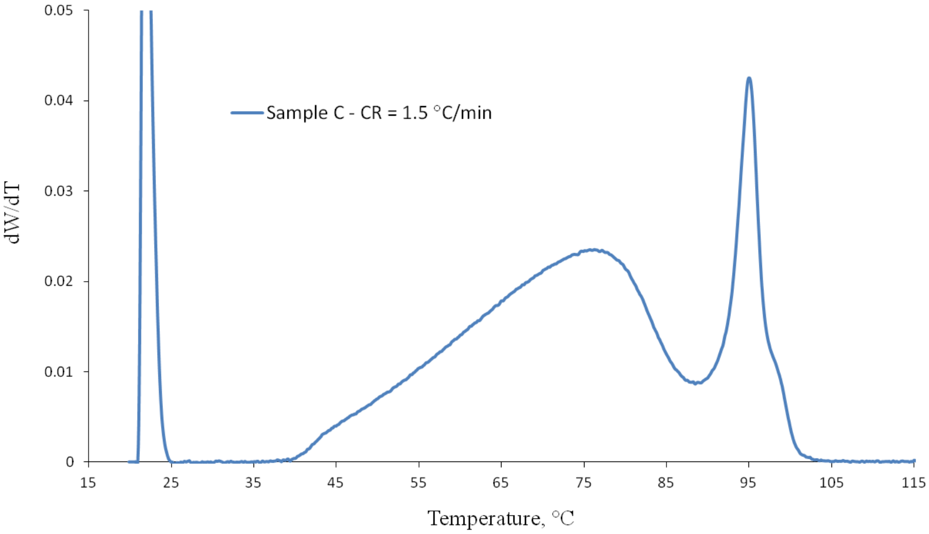

Figure 7.22 CEF profile of Sample C. Experimental conditions: CR = 1.5 °C/min , Fc = 0.015 mL/min, HR = 3 °C/min, Fe = 1 mL/min.

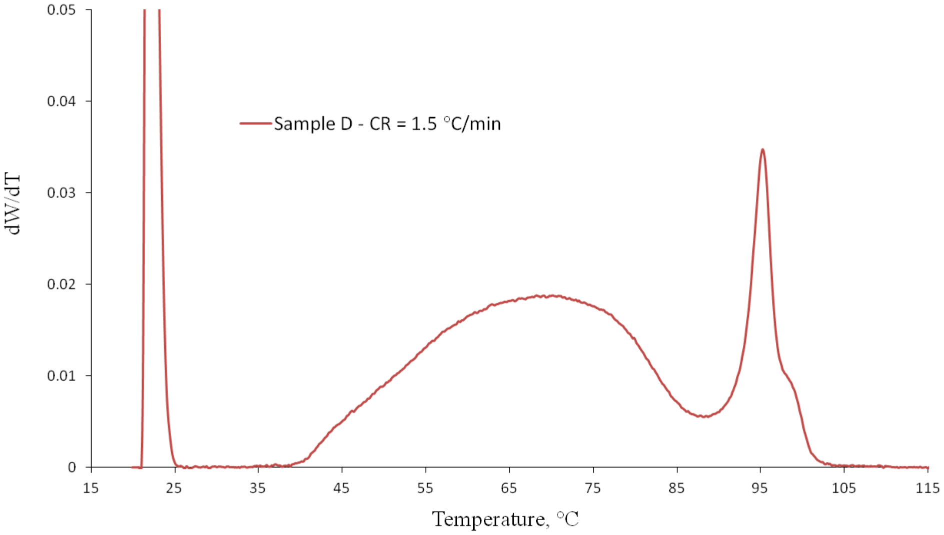

Figure 7.23 CEF profile of Sample D. Experimental conditions: CR = 1.5 °C/min , Fc = 0.015 mL/min, HR = 3 °C/min, Fe = 1 mL/min.

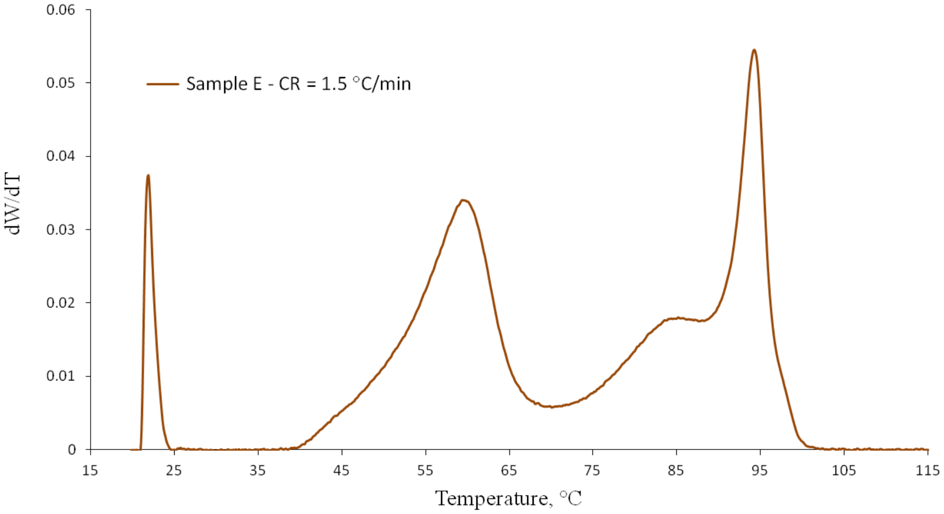

Figure 7.24 CEF profile of Sample E. Experimental conditions: CR = 1.5 °C/min , Fc = 0.015 mL/min, HR = 3 °C/min, Fe = 1 mL/min.

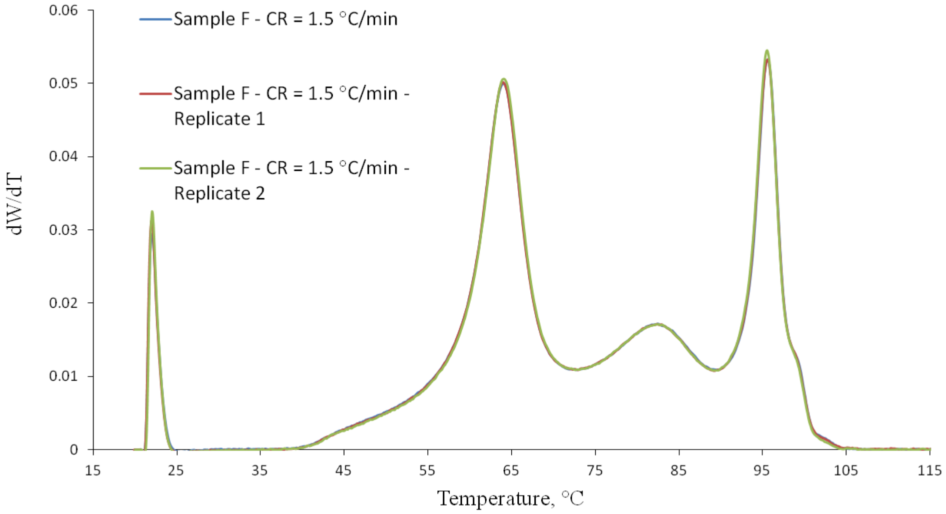

Figure 7.25 CEF profile of Sample F. Experimental conditions: CR = 1.5 °C/min , Fc = 0.015 mL/min, HR = 3 °C/min, Fe = 1 mL/min.

7.3.1 EFFECT OF STARTING TEMPERATURE OF THE COOLING CYCLE

Figure 7.26 compares the CEF profiles of Sample C using cooling rate of 3 °C/min starting from 95 °C or 120 °C. The obtained profiles have similar shapes. However, the profile measured starting from 120 °C was shifted to slightly lower temperatures. Interestingly, when the analysis of this sample was performed at a cooling rate of 1.5 °C/min starting from 95 °C, a small peak at high temperature (105 °C) was observed, as shown in Figure 7.27. However, when the cooling cycle started from 120 °C, this additional peak disappeared. The formation of this small peak may be attributed to the presence of a fraction of very high crystallizability (high molecular weight) that did not crystallize properly when the cooling cycle started from 95 °C. Therefore, during the heating step, this fraction was separated from the others and left the column at higher temperatures.

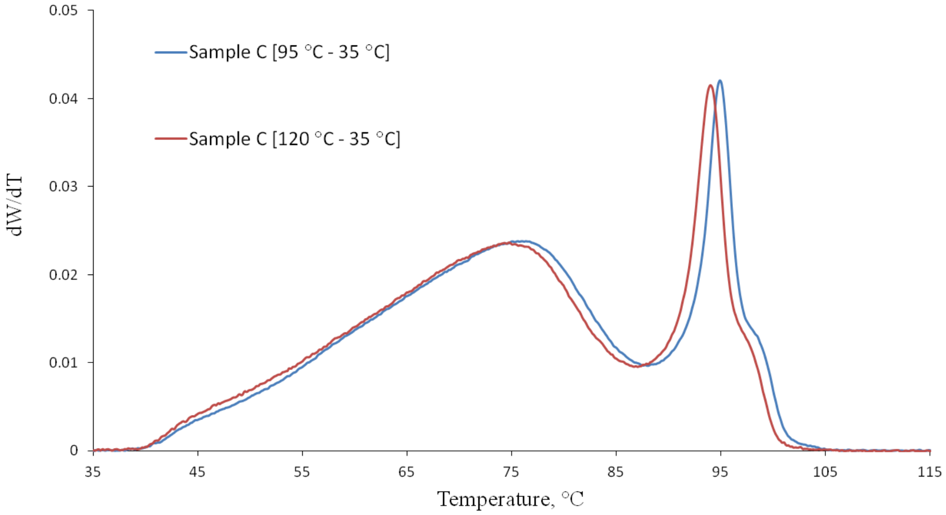

Figure 7.26 CEF profiles of Sample C using different cooling cycles. Experimental conditions: CR = 3 °C/min , HR = 3 °C/min, Fe = 1 mL/min.

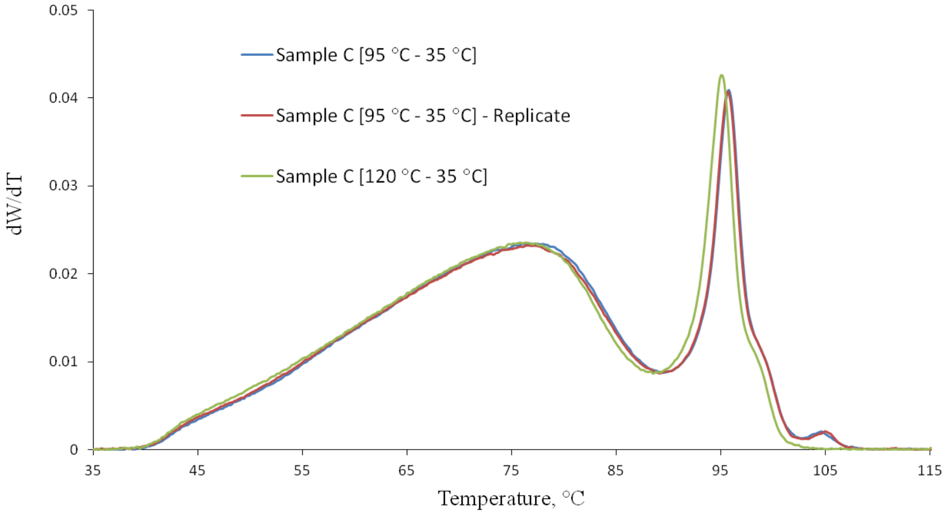

Figure 7.27 CEF profiles of Sample C using different cooling cycles. Experimental conditions: CR = 1.5 °C/min , HR = 3 °C/min, Fe = 1 mL/min.

The starting temperature of the cooling cycle also affects the CEF profiles measured using slow cooling rates. Figure 7.28 compares the CEF profiles of Sample C using a cooling rate of 0.5 °C/min, staring at 95, 120, and 140 °C. Similarly, the profiles obtained at this cooling rate starting at 95 °C had a high temperature peak at 105 °C. Small differences were observed between profiles measured when the cooling cycle started at 120 or 140 °C. The same behavior was observed for Sample D using the same cooling rate of 0.5 °C/min, as illustrated in Figure 7.29.

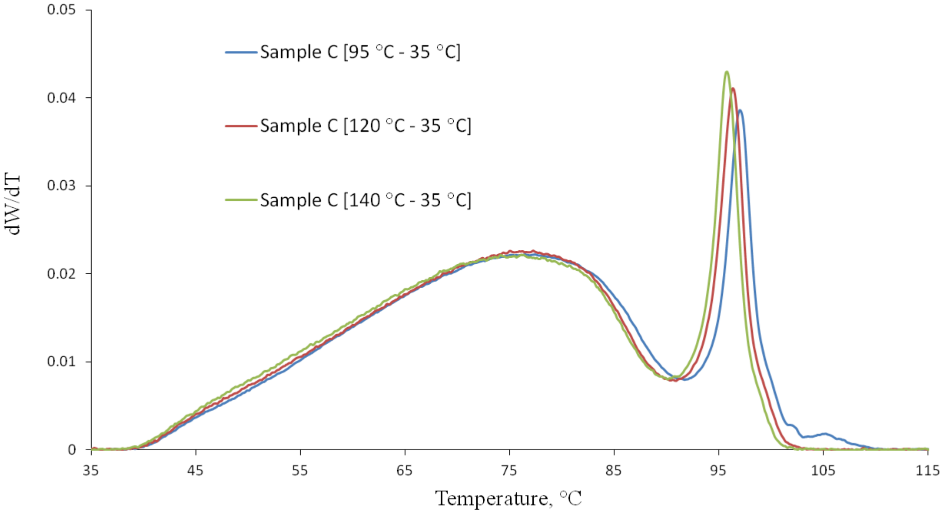

Figure 7.28 CEF profiles of Sample C using different cooling cycles. Experimental conditions: CR = 0.5 °C/min , HR = 3 °C/min, Fe = 1 mL/min.

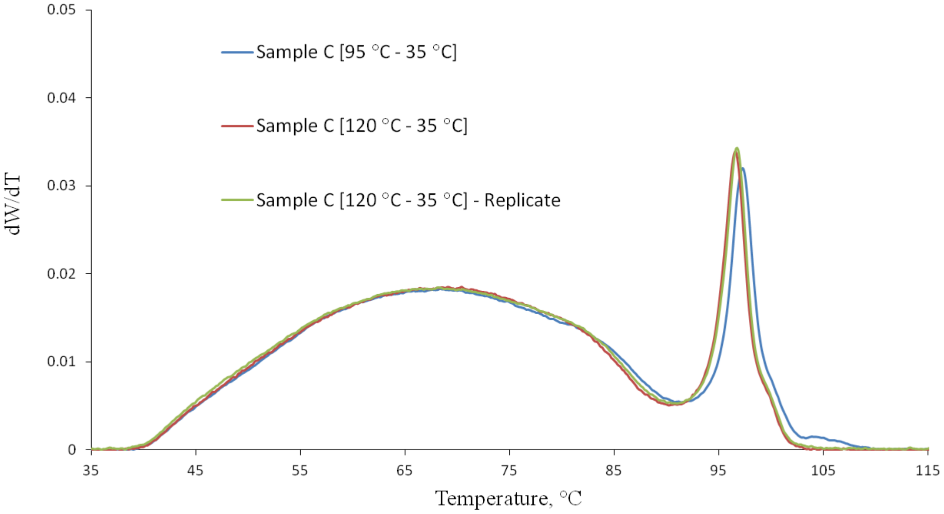

Figure 7.29 CEF profiles of Sample D using different cooling cycles. Experimental conditions: CR = 0.5 °C/min , HR = 3 °C/min, Fe = 1 mL/min.

7.3.2 COOLING RATE EFFECT

As shown in the previous section, the cooling rate plays a major role in reducing co-crystallization effects. Figure 7.30 and 7.31 illustrate the cooling rate effect on the CEF profiles of Samples C and D, respectively. All these experiments were performed using the maximum solvent flow rate during the cooling cycle to have the polymer chains fractionated and distributed over the whole length of the column. No effect was observed for polymer chains eluting from 35 to 65 °C. However, a significant cooling rate effect was detected for polymer chains eluting from 65 to 120 °C.

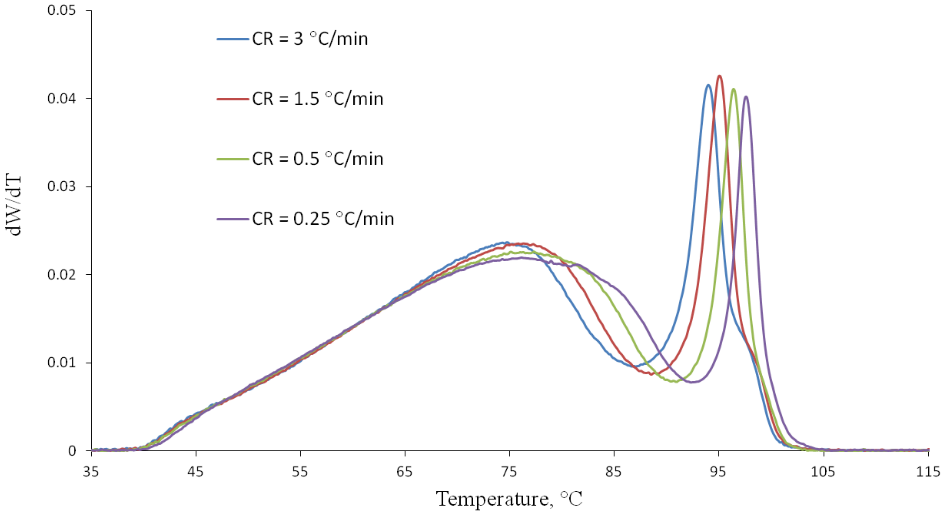

Figure 7.30 Effect of cooling rate on CEF profiles of Sample C. Experimental conditions: HR = 3 °C/min, Fe = 1 mL/min.

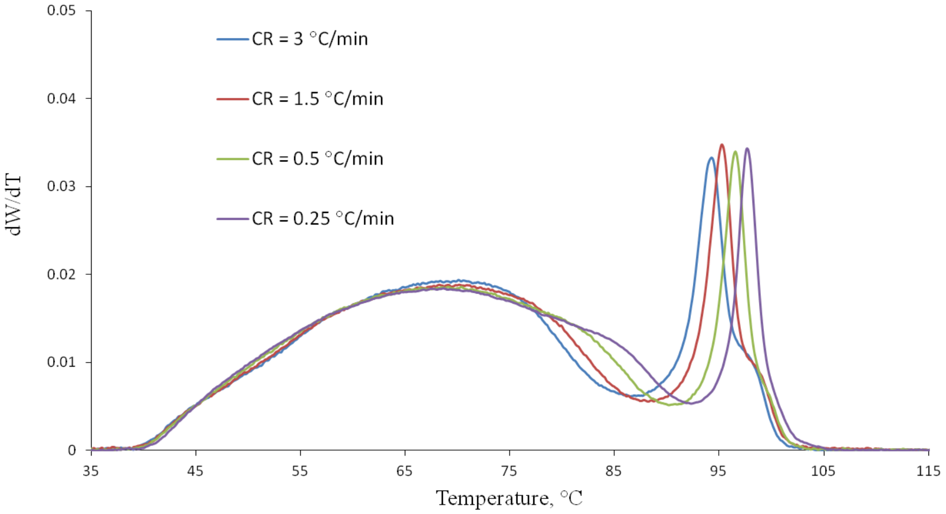

Figure 7.31 Effect of cooling rate on CEF profiles of Sample D. Experimental conditions: HR = 3 °C/min, Fe = 1 mL/min.

Using a fast cooling rate of 3 °C/min, the mass fraction of polymer eluted from 88 to 120 ^{o}C was about 24%. This fraction decreased to only 15% by reducing the cooling rate to 0.25 °C/min. The amount of polymer eluting under the narrow higher-temperature peak using different cooling rates was plotted in Figure 7.32. These results indicate that using slow cooling rates minimizes the degree of co-crystallization. Therefore, the fraction of polymer eluting under the high crystallinity peak decreases as the cooling rate decreases. Similarly, cooling rate effects on the CEF profiles for Sample E is shown in Figure 7.33. Better peak separation was observed using slower cooling rates.

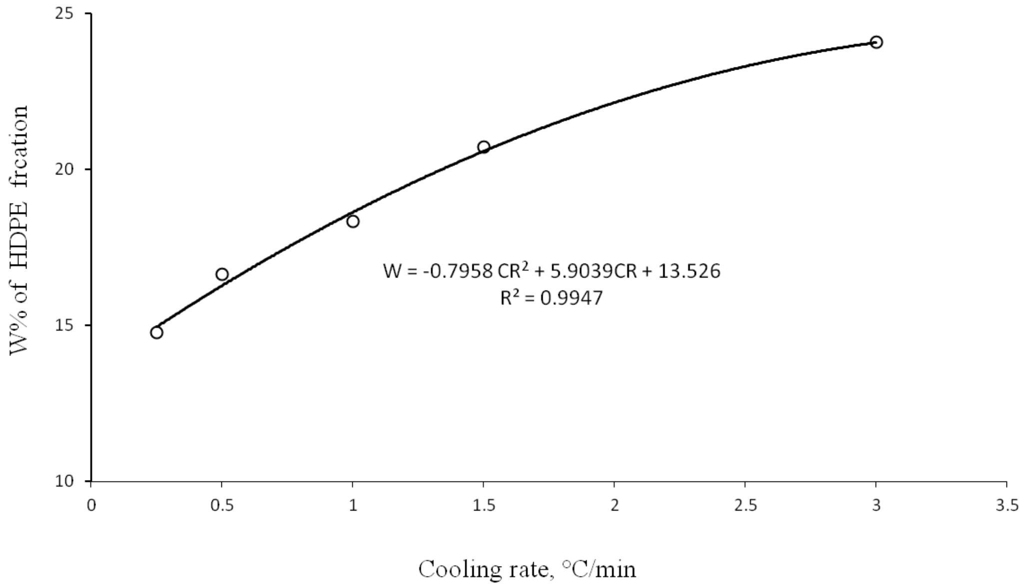

Figure 7.32 Relation between cooling rate and polymer fraction under the narrow high-temperature peak of Sample C.

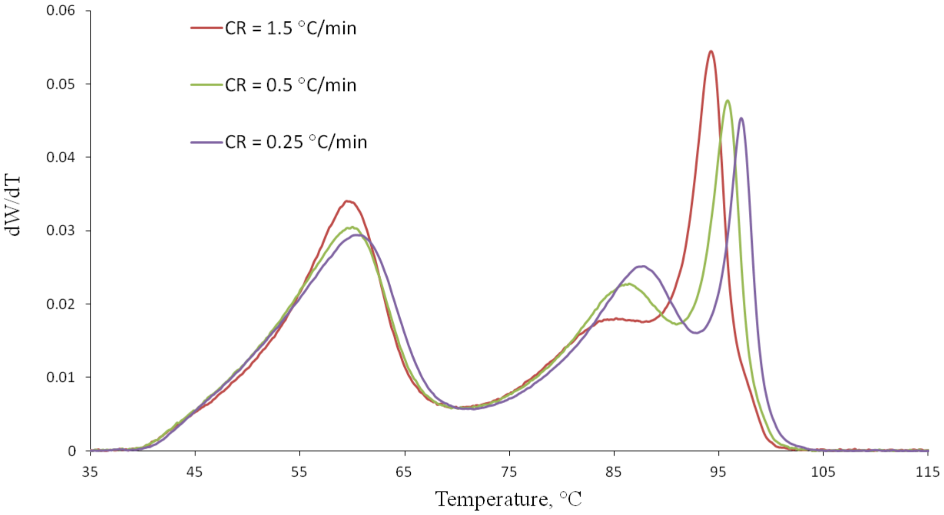

Figure 7.33 Effect of cooling rate on CEF profiles of Sample E. Experimental conditions: HR = 3 °C/min, Fe = 1 mL/min.

7.3.3 EFFECT OF SOLVENT FLOW RATE DURING THE COOLING CYCLE

The effect of solvent flow rate during the cooling cycle was studied in details for Sample C. Figure 7.34 shows the CEF profiles of this sample measured using a cooling rate of 1.5 °C/min with different solvent flow rates (0.015, 0.01, 0.005, and 0.002 mL/min). The fraction of polymer eluting under the narrow high-temperature peak (88 – 120 °C range) was used to determine the degree of co-crystallization using different solvent flow rates. This amount was about 20.8% using a solvent flow rate of 0.015 mL/min; however, it increased to 26.8% when the solvent flow rate decreased to 0.002 mL/min due to significant co-crystallization effects.

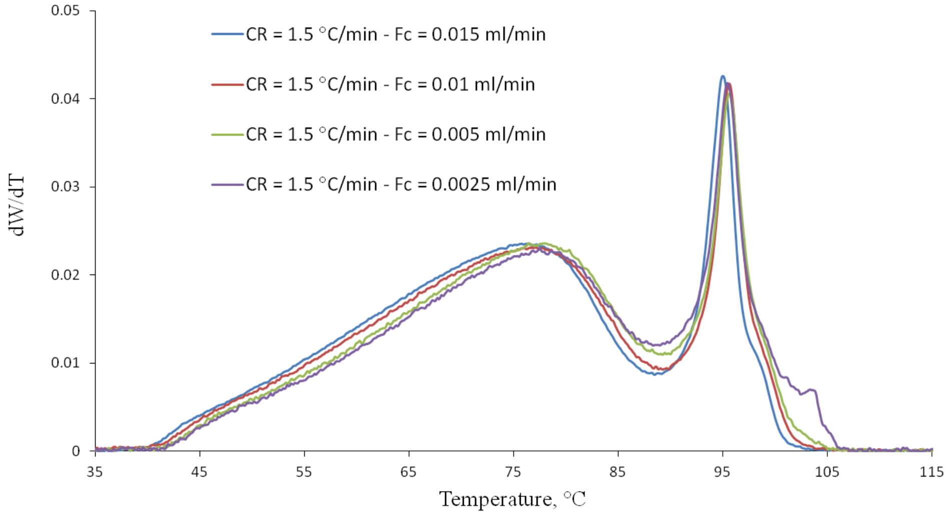

Figure 7.34 Effect of solvent flow rate during the cooling cycle on CEF profiles of Sample C. Experimental conditions: HR = 3 °C/min, Fe = 1 mL/min.

Figure 7.35 compares the CEF profiles of Sample C using cooling rate of 0.5 °C/min and solvent flow rates of 0.005, 0.002, and 0 mL/min (TREF mode). It is clear that the solvent flow rate during cooling plays an important role in reducing co-crystallization effects in CEF.

Table 7.5 lists the mass fractions of the high density fraction of Sample C that elutes in the narrow high-temperature peak using three solvent flow rates (0.002, 0.005, and 0.01 mL/min) and different cooling rates. Interestingly, when these values are plotted (as shown in Figure 7.36), linear relations are observed between the high-density fraction of Sample C and cooling rate for each solvent flow rate. All the three lines can be extrapolated to the same value around 13.5% when a very small cooling rate is used, which can then be considered the limiting value for this high-density fraction. A similar limiting value is obtained by extrapolating to zero cooling rate in Figure 7.32 (at maximum solvent flow rate).

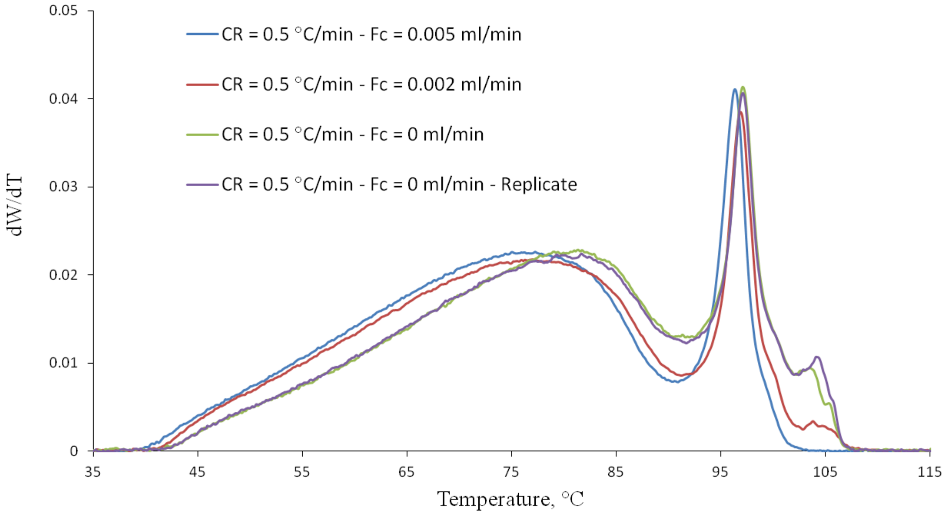

Figure 7.35 Solvent flow rate effect during CEF cooling cycle for Sample C. Experimental conditions: CR = 0.5 °C/min, HR = 3 °C/min, Fe = 1 mL/min.

Table 7.5 Effect of Solvent flow rate on the mass fraction of high-density polymer for Sample C

CR (°C/min)	**Fc = 0.002**	**Fc = 0.005**	**Fc = 0.01**
0.5	17.59	16.65	---
0.7	20.56	17.62	---
1	22.56	20.34	18.33
1.25	25.65	21.32	19.63
1.5	26.8	22.71	20.78

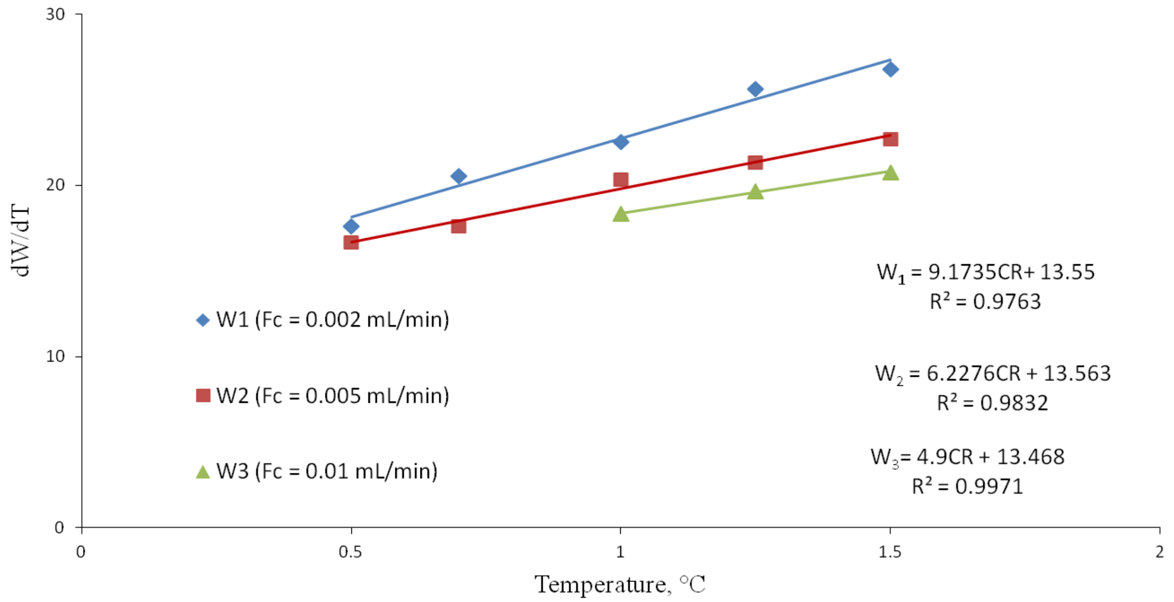

Figure 7.36 Solvent flow rate effect on the calculated mass fraction of polymer eluting under the high-temperature peak for Sample C.

7.3.4 HEATING RATE EFFECT

Figures 7.37 and 7.38 show the heating rate (3 and 1.5 °C/min) effect on CEF profiles of Samples C and D, respectively. A small peak at 96 °C was observed when the slower heating rate (1.5 °C/min) was used for both samples.

Sample D was analyzed using a cooling rate of 0.5 °C/min and two different heating rates of 1.5 and 1 °C/min. The elution solvent flow rate was 0.5 mL/min for both experiments. Figure 7.39 shows that heating rate effects were limited under these conditions. The profile was slightly shifted to lower temperatures by reducing the heating rate; however, the shapes of these profiles were almost the same indicating that the heating rate effect was insignificant in this case.

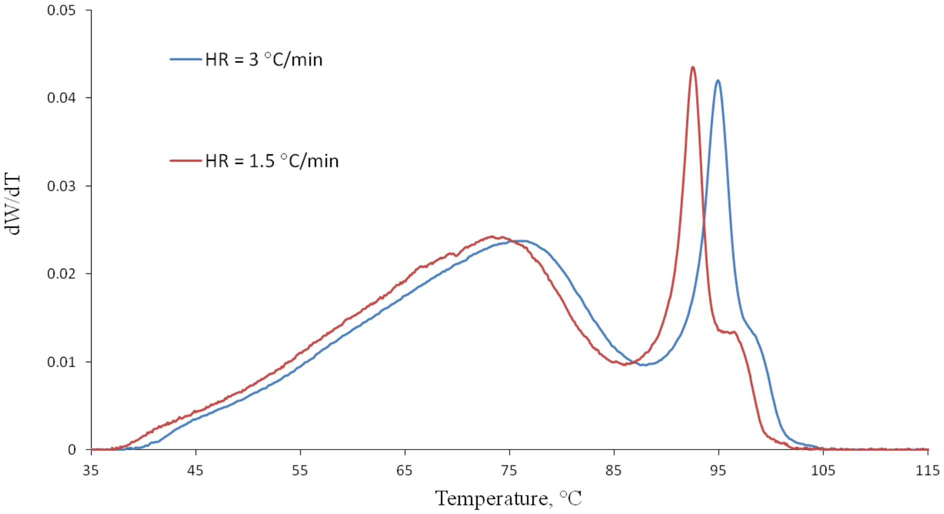

Figure 7.37 Heating rate effect on CEF profiles of Sample C. Experimental conditions: CR = 3 °C/min, Fc = 0.04 mL/min, and Fe = 1 mL/min

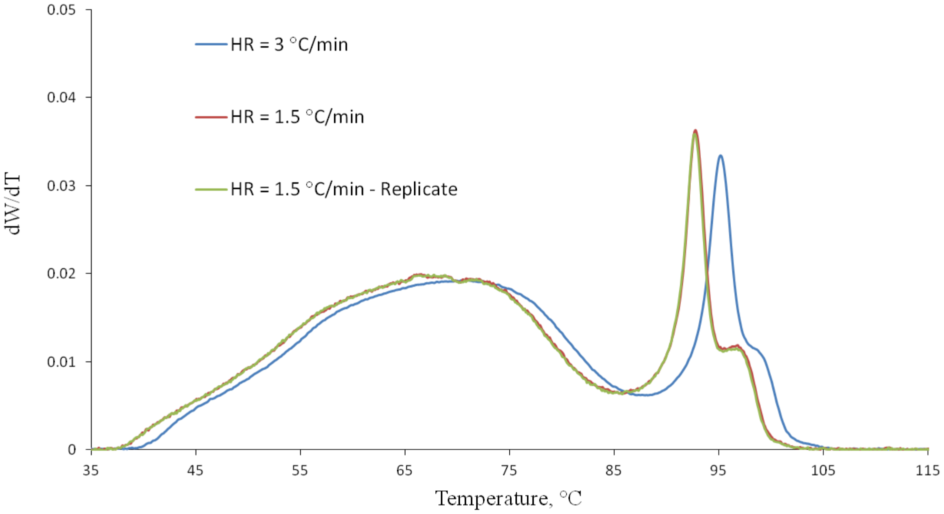

Figure 7.38 Heating rate effect on CEF profiles of Sample D. Experimental conditions: CR = 3 °C/min, Fc = 0.04 mL/min, and Fe = 1 mL/min

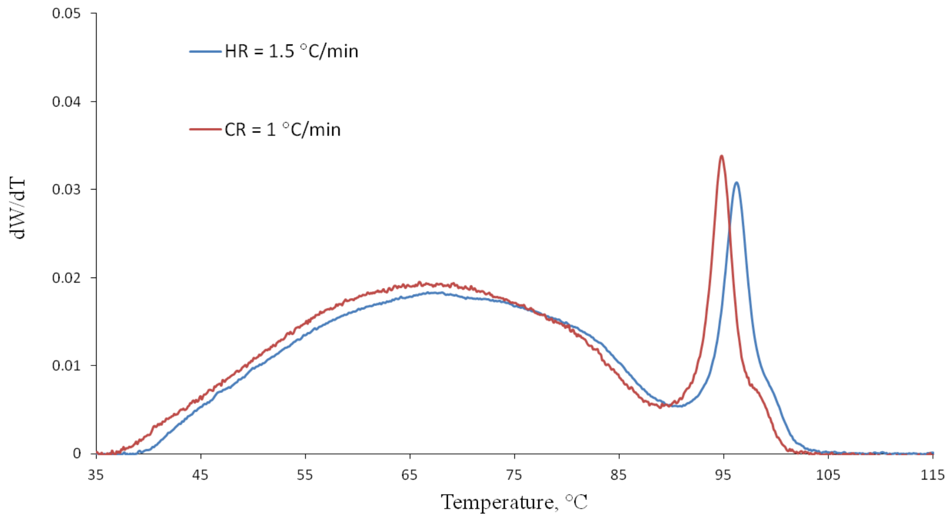

Figure 7.39 Heating rate effect on CEF profiles of Sample D. Experimental conditions: CR = 0.5 °C/min, Fc = 0.005 mL/min, and Fe = 0.5 mL/min

7.3.5 COMPARISON BETWEEN CEF AND HT-TGIC PROFILES

Figures 7.40 and 7.41 compare CEF and HT-TGIC profiles of Sample D and Sample F. The CEF results were performed at a slow cooling rate of 0.5 °C/min to minimize co-crystallization effects. However, cooling rate does not affect the resolution of HT-TGIC profiles, as described in Chapter 5 and 6. Therefore, the HT-TGIC profiles of Sample D and F were performed using a faster cooling rate of 5 °C/min. On the other hand, the resolution of the HT-TGIC analysis depends more significantly on the heating rate. The resins were analyzed using a heating rate of 1 °C/min and solvent flow rate of 0.5 mL/min for both CEF and HT-TGIC. The x-axis of Figure 7.40 and Figure 7.41 can be converted to comonomer composition using the liner calibration curves for the CEF and HT-TGIC (Figure 7.5 for CEF and Figure 6.4 for HT-TGIC). The comparison between CEF and HT-TGIC profiles of Sample F using the calculated comonomer content as the x-axis is illustrated in Figure 7.42. The CEF profiles give more details about the microstructure of these resins as compared with HT-TGIC. For instance, Sample F was fractionated by the CEF into three different peaks in the temperature ranges [35 – 70 °C], [70 – 90°C], and [90 – 110°C]. However, the last two peaks emerge together in the HT-TGIC profile in the range [116 – 140 °C]. The amount of the polymer eluted in this range was about 52.2% of the whole polymer. Interestingly, the corresponding CEF fraction is in the range [70 – 100 °C]. The calculated amount of this fraction from the CEF profile was 51.2%, which is very close to the amount calculated from HT-TGIC. Similarly, the calculated amount of the high crystallinity polymer eluting in the range [88 – 102 °C] was 13.5% by CEF and 14.3% [128 – 142 °C] by the HT-TGIC. This indicates that the quantitative information generated by both techniques is similar, albeit their graphical representation may differ significantly. CEF clearly leads to a better separation of the peaks of these more complex resins.

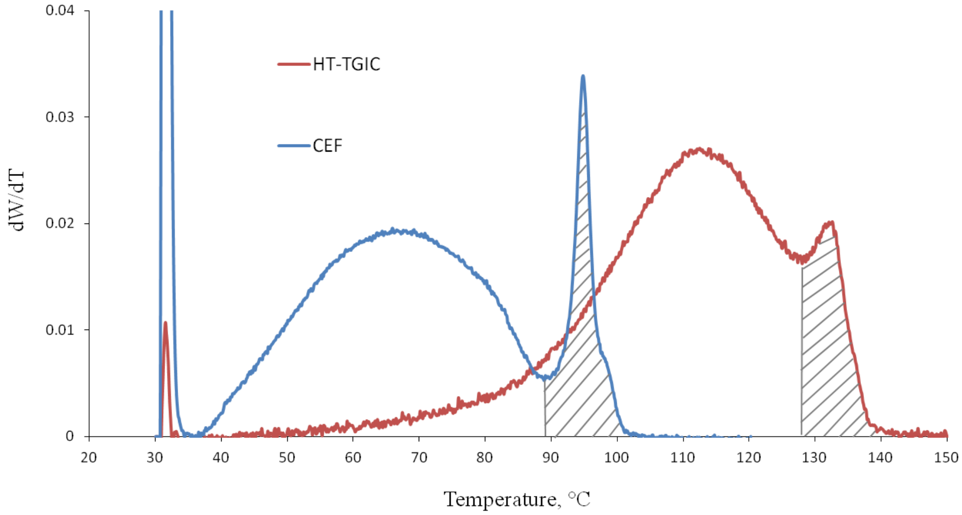

Figure 7.40 Comparison between experimental profiles of Sample D using CEF and HT-TGIC.

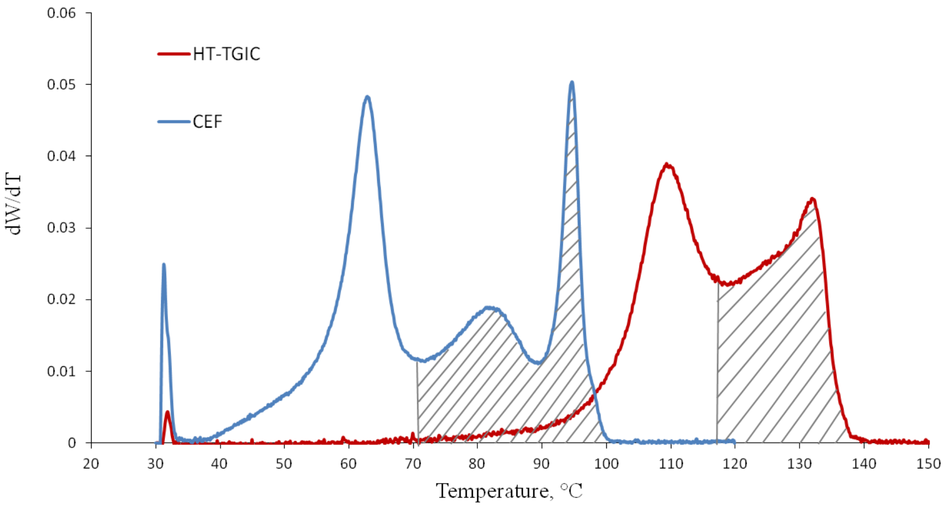

Figure 7.41 Comparison between experimental profiles of Sample F using CEF and HT-TGIC.

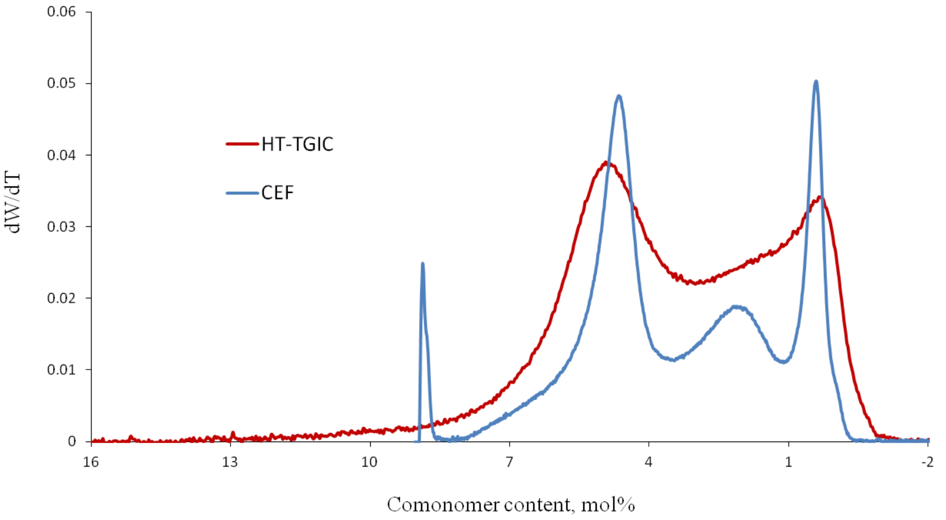

Figure 7.42 Comparison between experimental profiles of Sample F using CEF and HT-TGIC, the x-axis is calculated from the CEF and HT-TGIC calibration curves.

7.4 CONCLUSIONS

Several ethylene/1-octene copolymers with similar molecular weight averages and different commoner contents were analyzed by CEF. These results were used to generate CEF calibration curves at different cooling and heating rates.

The effect of molecular weight on CEF profiles of individual resins were studied using polyethylene samples with the same comonomer content but different molecular weight averages. CEF profiles of low molecular weight average resins had broader distribution, with low temperature tails, likely due to the presences of low molecular weight chains.

A new methodology was developed to quantify the degree of co-crystallization on the profiles of the polyolefin blends. This method was used to determine the most important factors that could be used to minimize co-crystallization effects. The results indicate these effects can be minimized using slow cooling rates. However, using columns with large void volumes slightly improved the separation resolution.

Industrial LLDPE resins were studied by CEF at different operating conditions. Cooling rate and the solvent flow rate during the cooling cycle significantly affect the degree of co-crystallization of CEF profiles. Moreover, peak separation increases as the starting temperature in the cooling cycle increases. However, varying the heating rate does not have a marked impact on these separations.

Finally, CEF profiles were compared with HT-TGIC profiles using the same solvent and the heating rate. The results clearly show that CEF separates the peaks more effectively and provides more details on the microstructure of the industrial resins investigated herein.

Chapter 8

CONCLUSIONS

A new mathematical model was developed to simultaneously deconvolute the MWD and CCD of polyolefins made with heterogeneous Ziegler-Natta catalysts, considering the room temperature soluble fraction. This novel procedure can be used to predict the minimum number of site types required to describe the MWD and CCD of a polyolefin sample for mathematical modeling applications. The model was applied to a series of industrial Ziegler-Natta LLDPE resins. The results showed that the proposed methodology could be used to estimate the number average molecular weight, average comonomer mole fraction, and mass fraction of soluble and non-soluble polymer made on each site type.

The use of polyethylene and its copolymers is rapidly growing in part because their properties can be tuned by changing their crystallinity via comonomer incorporation. TREF and CRYSTAF have been used routinely for the characterization of comonomer fraction distribution in polyolefins. CEF has been invented by the research group at Polymer Char (Valencia, Spain) to enhance the separation resolution of TREF and CRYSTAF and to shorten the analysis time. However, these techniques cannot be used to fractionate the amorphous polyolefins since they do not crystallize. High-temperature HPLC, on the other hand, extends the range of CCDs that can be measured by crystallization based techniques.

The effects of HT-TGIC operating conditions were studied using polyethylene and ethylene/1-octene copolymers. The resolution of HT-TGIC profiles was found out to be independent of cooling rate within the range investigated in this study. It was shown that ethylene/1-octene copolymers could be analyzed at temperatures higher than their crystallization temperatures, thus avoiding any co-crystallization effects.

It has also been found that the heating rate during HT-TGIC desorption cycle had a major effect on the obtained profiles. Slower heating rates were required to obtain profiles with higher resolution. The chromatograms of the individual resins and their blends measured at faster heating rates were broader and had lower resolution, supposedly due to the co-desorption effects. The obtained calibration curves at different heating rates were parallel and shifted to high temperature as the heating rate increased.

The analysis of polyolefin blends by HT-TGIC using ODCB showed that the volume of the injected sample was a very important parameter affecting the chromatograms. Excellent agreement between the experimental and calculated profiles of the blends was obtained when small sample volumes (equal or less than 100 μL) were used. This behavior may be due to co-adsorption and/or co-desorption effects when large sample volumes are injected into the column.

The effect of solvent type on HT-TGIC analysis was investigated using polyethylene, ethylene/1-octene copolymers, and their blends. The solvents used in this study were o-dichlorobenzene (ODCB), 1,2,4-trichlorobenzene (TCB), and chloronaphthalene (CN). Co-adsorption and co-desorption phenomena depend strongly on the type of solvent used during the analysis. Poor peak separation was observed when TCB was employed. The HT-TGIC calibration curves using TCB and ODCB where almost parallel, with the better solvent having lower elution peak temperatures for the same comonomer content. The chromatograms measured with TCB and CN were similar and both were more affected by co-adsorption and co-desorption than when ODCB was used.

Several samples with similar comonomer contents and different molecular weight averages were used to study the effect of the molecular weight on HT-TGIC. Samples with low molecular weight have broader distributions and significant lower temperature tails. The profiles of ethylene homopolymers (0 mol % 1-octene) measured using TCB were broader than those measured with ODCB. This behavior may be attributed to the weak adsorption of the fractions with low molecular weight when a better solvent like TCB is used for the analysis.

HT-TGIC profiles of polyethylene and ethylene/1-octene copolymers were compared with the equivalent CEF profiles. HT-TGIC chromatograms for polyethylene were broader than the CEF profiles, indicating that molecular weight effects on HT-TGIC analysis are stronger than in CEF analysis. On the other hand, as the comonomer content increased the difference between the two techniques decreased.

CEF operating condition effects have been studied using several ethylene/1-octene copolymers made with metallocene catalysts. The CEF calibration curves were generated from the elution peak temperatures of these ethylene/1-octene copolymers at different operating conditions such as cooling and heating rates. The calibration curves were parallel and shifted to lower temperature as the cooling rate increased.

A new method was developed to quantify degree of co-crystallization on the CEF profiles of polyolefin blends. This method was used to study the effects of the main CEF operating conditions. The results showed that the cooling rate plays a major role on the degree co-crystallization. In addition, co-crystallization effects were slightly less important when columns with larger void volume were used.

A systematic study of CEF operating conditions was conducted using several industrial LLDPE resins made with Ziegler-Natta catalysts. The results showed that the cooling rate, the starting temperature of cooling cycle, and the solvent flow rate during the cooling cycle were the most important factors affecting CEF resolution. Heating rate was not significant for the range of conditions investigated in this thesis.

Finally, CEF profiles of the industrial LLDPE resins were compared with HT-TGIC profiles using the same solvent and the same heating rate. Although the CEF needs longer analysis time, it separates the peaks much more effectively than the HT-TGIC. From the systematic studies of the CEF and HT-TGIC operating conditions provided in this thesis, it is suggested to operate the CEF using a slow cooling rate of 0.5 or 0.25 °C/min to enhance the peak separation. For HT-TGIC, using ODCB as a mobile phase during the analysis with slow heating rate of 1 °C/min and a sample size of 100 μL is highly recommended to minimize the degree of co-adsorption amd co-desorption effects.

REFERENCES

1. P. S. Chum, K.W. Swogger, *J. Prog. Polym. Sci.* **2008**, 33, 797.
2. A. J. Peacock, Handbook of Polyethylene: Structure, Properties and Applications, Marcel Dekker, New York, 2000.
3. A. J. Peacock, A. Calhoun, Polymer Chemistry: Properties and Applications, Carl Hanser Verlag, Munich, 2006.
4. K. Ziegler, *Angew. Chem.* **1964**, 76, 545.
5. Y. V. Kissin, Alkene Polymerization Reactions with Transition Metal Catalysts, Elsevier, London, 2008.
6. K. Ziegler, H. G. Gellert, Polymerization of Ethylene, US Patent 2,699,457; 1953.
7. K. Ziegler, E. Holzkamp, H. Breil, H. Martin, *Angew. Chem.* **1955**, 67, 426.
8. N. Kashiwa, H. Fujimura, Y. Tokuzumi, JP Patent 1,031,698; 1968.
9. N. Kashiwa, *J. Polym. Sci., Part A: Polym. Chem.* **2006**, 42, 1.
10. W. Kaminsky, M. Miri, H. Sinn, R. Woldt, *Makromol. Rapid. Commun.* **1983**, 4, 417.
11. W. Kaminsky, R. Steiger, *Polyhedron* **1988**, 7, 2375.
12. W. Kaminsky, *Macromol. Symp.* **1995**, 97, 79.
13. M. H. Prosenc, *Organometallics* **1992**, 11, 4037.
14. J. C. W. Chien, B. P. Wang, *J. Polym. Sci., Part A: Polym. Chem.* **1990**, 28, 15.
15. W. Kaminsky, K. Kulper, S. Niedoba, *Makromol. Chem., Makromol. Symp.* **1986**, 3, 377.
16. T. Piel, T. Saarinen, B. Lofgren, E. Kokko, J. Maaranen, P. Pitkanen, *Macromol. Chem. Phys.* **2007**, 208, 851.
17. H. G. AH, A. Köppl, *Chem. Rev.* **2000**, 100, 1205.
18. J. Tian, B. Huang, *Macromol. Rapid. Commun.* **1994**, 15, 923.
19. P. C. Möhring, N. J. Coville, Coord. *Chem. Rev.* **2006**, 250, 18.
20. B. Wang, *Coord. Chem. Rev.* **2006**, 250, 242.
21. L. rescni, L. Cavallo, A. Fait, F. Piemontesi, *Chem. Rev.* **2000**, 100, 1253.
22. J. L. Eilertsen, J. A. Stvneng, M. Ystenes, E. Rytter, *Inorg. Chem.* **2005**, 44, 4843.
23. S. S. Reddy, S. Sivaram, *Prog. Polym. Sci.* **1995**, 20, 309.
24. J. Huang, G. L. Rempel, *Prog. Polym. Sci.* **1995**, 20, 459.
25. A. E. Hamielec, J. B. P. Soares, *Prog. Polym. Sci.* **1996**, 21, 651.

26. Y. V. Kissin, *J. Polym. Sci., Part A: Polym. Chem.* **2003**, 41, 1745.
27. Y. V. Kissin, F. M. Mirabella, C. C. Meverden, *J. Polym. Sci., Part A: Polym. Chem.* **2005**, 43, 4351.
28. W. Kaminsky, M. Schlobohm, *Macromol. Chem. Macromol. Symp.* **1986**, 4, 103.
29. S. Y. Lai, J. R. Wilson, G. W. Knight, J. C. Stevens, US Patent 5,278,272; 1994.
30. J. B. P. Soares, *Chem. Eng. Sci.* **2001**, 56, 4131.
31. J. B. P. Soares, T. Mckenna, C. P. Cheng, Polymer Reaction Engineering, J. M. Asua, Ed., Blackwell, Oxford, UK, **2007**, p. 28-117.
32. P. J. Cossee, *J. Catal.* **1964**, 3, 80.
33. E. J. Arlman, *J. Catal.* **1964**, 3, 89
34. E. J. Arlman, P. J. Cosee, *J. Catal.* **1964**, 3, 99
35. P. Corradini, G. Guerra, *Prog. Polym. Sci.* **1991**, 16, 239.
36. J. C. W. Lohrenz, T. K. Woo, L. Fan, T. Ziegler, *J. Organomet. Chem.* **1995**, 497, 91.
37. M. Ystenes, *J. Catal.* **1991**, 129, 383.
38. M. Ystenes, *Makromol. Chem. Macromol. Symp.* **1993**, 66, 71.
39. S. Juengling, R. Mulhaupt, U. Stehling, H. H. Brintzinger, D. Fischer, F. Langhauser, *J. Polym. Sci., Part A: Polym. Chem.* **1995**, 33, 1305.
40. J. C. W. Chien, Z. Yu, M. Marques, J. C. Flores, M. D. Rausch, *J. Polym. Sci., Part A: Polym. Chem.* **1998**, 36, 319.
41. L. L. Bohm, *Polymer* **1978**, 19, 562.
42. L. L. Bohm, *Angew. Chem. Int. Ed.* **2003**, 42, 5010
43. P. L. Watson, G. W. Parshall, *Acc. Chem. Res.* **1985**, 18, 51.
44. T. K. Han, H. K. Choi, D. W. Jeung, Y. S. Ko, S. I. Woo, *Macromol. Chem. Phys.* **1995**, 196, 2637.
45. W. kaminsky, *Macromol. Chem. Phys.* **1996**, 197, 3907.
46. L. D’Agnillo, J. B. P. Soares, A. Penlidis, *Macromol. Chem. Phys.* **1998**, 199, 955.
47. K. Thorshaug, E. Rytter, M. Ystenes, *Macromol. Rapid Commun.* **1997**, 18, 715.
48. M. Smit, X. Zheng, R. Brull J. Loos, J. C. Chadwick, *J Polym. Sci., Part A: Polym. Chem.* **2006**, 44, 2883.
49. C. Piel, P. Starck, J. V. Seppala, W. Kaminsky, *J. Polym. Sci., Part A: Polym. Chem.* **2006**, 44, 1600.

50. W. Kaminsky, C. Piel, K. Scharlach, *Macromol. Symp.* **2005**, 226, 25.

51. G. Scheier, H. H. Brintznger, *Marcromol. Symp.* **2001**, 173, 89.

52. J. S. Yoon, D. H. Lee, W. S. Park, I. M. Lee, D. K. Park, S. O. Jung, *Polymer* **2000**, 41, 4523.

53. L. Sun, C. C. Hsu, D. W. bacon, *J. Polym. Sci., Part A: Polym. Chem.* **1994**, 32, 2135.

54. Y. V. Kissin, R. I. Mink, T. E. Nowlin, *J. Polym. Sci., Part A: Polym. Chem.* **1999**, 37, 4255.

55. Y. V. Kissin, *J. Polym. Sci., Part A: Polym. Chem.* **2001**, 39, 1681.

56. T. T. Tsui, N. Kashiwa, *Polym. Commun.* **1988**, 29, 180.

57. P. J. T. Tait, I. G. Berry, Catalyst design for tailor-made polyolefins, K. Soga, M. Terano, Ed., Elsevier-Kodansha, Tokyo, **1994**, p. 55-72.

58. Y. V. Kissin, A. J. Brandolini, *J. Polym. Sci., Part A: Polym. Chem.* **1999**, 37, 4273.

59. Y. V. Kissin, R. I. Mink, A. J. Brandolini, *J. Polym. Sci., Part A: Polym. Chem.* **1999**, 37, 7281.

60. Z. Xu, L. Feng, D. Wang, S. Yang, *Makromol. Chem.* **1999**, 192, 1835.

61. H. Yanagihara, D. H. Lee, Transition Metal Catalyzed Polymerization, R. D. Quirk, Ed., Cambridge University Press, New York, **1988**, p. 995.

62. I. Kim, M. C. Chung, H. K. Choi, J. H. Kim, S. I. Woo, Catalytic Olefin Polymerization, T. Keii, K. Soga, Ed., Elsevier, New York, **1990**, p. 323-343.

63. Y. P. Chen, Z. Fan, *Eur. Polym. J.* **2006**, 42, 2441.

64. R. Spitz, L. Duranel, P. Masson, M. F. Darricades, A. Guyot, Transition Metal Catalyzed Polymerization, R. D. Quirk, Ed., Cambridge University Press, New York, **1988**, p. 719-728.

65. P. J. T. Tait, Transition Metal Catalyzed Polymerization, R. D. Quirk, Ed., Cambridge University Press, New York, **1988**, p. 834-860.

66. J. C. W. Chien, T. Nozaki, *J. Polym. Sci., Part A: Polym. Chem.* **1993**, 31, 227.

67. J. A M. Awudza, P. J. T. Tait, *J. Polym. Sci., Part A: Polym. Chem.* **2008**, 46, 267.

68. T. Usami, Y. Gotah, S. Takayama, *Macromolecules* **1986**, 19, 2722.

69. L. Wild, T. R. Ryle, D. C. Knobeloch, *Am. Chem. Soc. Div. Polym. Chem. Polym. Prepr.* **1986**, 23, 133.

70. F. M. Mirabella Jr., E. A. Ford, *J. Polym. Sci. Polym. Phys. Ed.* **1987**, 25, 777.

71. R. Lew, P. Cheung, S. T. Balke, T. H. Mourey, *J. Appl. Polym. Sci.* **1993**, 47, 1685.
72. C. Y. Kuo, T. Provder, M. E. Koehler, *J. Liq. Chromatogr.* **1990**, 13, 3177.
73. L. Jeng, S. T. Balke, T. H. Mourey, L. Wheeler, P. Romeo, *J. Appl. Polym. Sci.* **1993**, 49, 1359.
74. T. H. Mourey, H. Coll, *J. Appl. Polym. Sci.* **1995**, 56, 65.
75. J. B. P. Soares, *Macromol. Symp.* **2007**, 257, 1.
76. Y. Youlu, P. J. DesLauriers, D. C. Rohlfing, *Polymer* **2005**, 46, 5165.
77. P. J. Flory, *J. Chem. Phys.* **1949**, 17, 223.
78. F. M. Mirabella Jr., Proceeding of International GPC Symposium 87, Itasca, IL, 1987, p. 180.
79. J. B. P. Soares, A. E. Hamielec, *Polymer* **1995**, 36, 1639.
80. B. Monrabal, US Patent 5,222,390; 1991.
81. B. Monrabal, *J. Appl. Polym. Sci.* **1994**, 52, 491.
82. B. Monrabal, J. Sancho-Tello, N. Mayo, L. Romero, *Macroml. Symp.* **2007**, 257, 71.
83. A. J. Pennings, *J. Polym. Sci.* **1967**, 16, 1799.
84. L. Wild, T. R. Ryle, D. C. Knobeloch, I. R. Peat, *J. Polym. Sci. Polym. Phys.* **1982**, 20, 441.
85. J. Nieto, T. Oswald, F. Blanco, J. B. P. Soares, B. Monrabal, *J. Polym. Sci., Part B: Polym. Phys.* **2001**, 39, 1616.
86. A.A. da Silva Filho, J. B. P. Soares, G. B. deCalland, *Macromol. Chem. Phys.* **2000**, 201, 1226.
87. M. H. Kim, P. J. Phillips, *J. Appl. Polym. Sci.* **1998**, 70, 1893.
88. D. M. Sarzotti, J. B. P. Soares, A. Penlidis, *J. Polym. Sci., Part B: Polym. Phys.* **2002**, 40, 2595.
89. N. Luruli, L. C. Heinz, V. Grumel, R. Brull, H. Pasch, H. G. Raubenheimer, *Polymer* **2006**, 47, 56.
90. S. Anantawaraskul, J. B. P. Soares, P. M. Wood-Adams, *J. Polym. Sci., Part B: Polym. Phys.* **2003**, 41, 1762.
91. N. Aust, M. Gahleitner, K. Reichelt, B. Raninger, *Polymer Testing* **2006**, 25, 896.
92. E. C. Kelusky, C. T. Elston, R. E. Murray, *Polym. Eng. Sci.* **1987**, 27, 1562.

93. S. Anantawaraskul, J. B. P. Soares, P. M. Wood-Adams, *Macromol. Chem. Phys.* **2004**, 205, 771.
94. W. W. Yau, *Macromol. Symp.* **2007**, 257, 29.
95. A. Ortin, B. Monrabal, J. Sancho-Tello, *Macromol. Symp.* **2007**, 257, 13.
96. A. Ortin, B. Monrabal, J. Montesinos, P. del Hierro, *Macromol. Symp.* **2009**, 282, 65.
97. G. Balbontin, I. Camurati, T. Dall'Occo, R. C. Zeigler, *J. Molecular Cat. A: Chem.* **1995**, 98, 123.
98. H. N. Cheng, M. Kakugo, *Macromolecules* **1991**, 24, 1724.
99. J. B. P. Soares, A. E. Hamielec, *Polym. React. Eng.* **1995**, 3, 261.
100. I. Mingozzi, S. Nascetti, *Int. J. Polym. Anal. Character.* **1996**, 3, 59.
101. D. Berek, *Prog. Polym. Sci.* **2000**, 25, 873.
102. T. Chang, *Adv. Polym. Sci*. **2003**, 163, 1.
103. T. Macko, H. Pasch, Y. V. Kazakevich, A. Y. Fadeev, *J. Chromatogr. A* **2003**, 988, 69.
104. T. Macko, H. Pasch, J. F. Denayer, *J. Chromatogr. A* **2003**, 1002, 55.
105. A. Y. Fadeev, Y. V. Kazakevich, *Langmuir* **2002**, 18, 2665.
106. Y. V. Kazakevich, A. Y. Fadeev, *Langmuir* **2002**, 18, 3117.
107. A. Lehtinen, R. Paukkeri, *Macromol. Chem. Phys.* **1994**, 195, 1539.
108. L.-C. Heinz, H. Pasch, *Polymer* **2005**, 46, 12040.
109. A. Albrecht, L.-C. Heinz, D. Lilge H. Pasch, *Macromol. Symp.* **2007**, 257, 46.
110. V. Dolle, A. Albrecht, R. Brüll, T. Macko, *Macromol. Chem. Phys.* **2011**, 212, 959.
111. T. Macko, H. Pasch, J. F. Denayer, *J. Sep. Sci.* **2005**, 28, 59.
112. T. Macko, H. Pasch, Y. Wang, *Macromol. Symp.* **2009**, 282, 93.
113. T. Macko, R. Brüll, H. Pasch, *Chromatographia* **2003**, 57, 39.
114. T. Macko, H. Pasch, *Macromolecules* **2009**, 42, 6063.
115. T. Macko, R. Brüll, R. G. Alamo, Y. Thomann, V. Grumel, *Polymer* **2009**, 50, 5443.
116. T. Macko, R. Brüll, Y. Wang, Y. Thomann, *Column* **2009**, 4, 15.
117. R. Chitta, T. Macko, R. Brüll, G. van Doremaele, L.-C. Heinz, *J. Polym. Sci. Part A: Polym. Chem.* **2011**, 49, 1840.
118. T. Macko, R. Brüll, Y. Wang, B. Coto, I. Suarez, *J. App. Polym. Sci.* **2011**, 122, 3211.

119. T. Macko, R. Brüll, R. G. Alamo, F. J. Stadler, S. Losio, *Anal. Bioanal. Chem.* **2011**, 399, 1547.

120. A. Ginzburg, T. Macko, V. Dolle, R. Brüll, *Eur. Polym. J.* **2011**, 47, 319.

121. M.D. Miller, A. W. deGroot, J. W. Lyons, F. A. Van Damme, W. L. Winniford, J. *Appl. Polym. Sci.* **2011**, 123, 1238.

122. R. Chitta, T. Macko, R. Brüll, G. Kalies, *J. Chromatogr. A* **2010**, 1217, 7717.

123. A. Ginzburg, T. Macko, V. Dolle, R. Brüll, *J. Chromatogr. A* **2010**, 1217, 6867.

124. A. Roy, M.D. MillerD. M. Meunier, A. W. deGroot, W. L. Winniford, F. A. Van Damme, R. J. Pell, J. W. Lyons, *Macromolecules* **2010**, 43, 3710.

125. C. H. Lochmüller, M. A. Moebus, Q.C. Liu, C. Jung, M. Elomaa, *J. Chromatogr. Sci.* **1996**, 34, 69.

126. H. C. Lee, T. Chang, *Polymer* **1996**, 37, 5747.

127. R. Cong, A. W. deGroot, A. Parrott, W. Yau, L. Hazlitt, R. Brown, M. Miller, Z. Zhou, *Macromolecules* **2011**, 44, 3062.

128. W. H. Stockmayer, *J. Chem. Phys.* **1945**, 13, 199.

129. Y. V. Kissin, *Makromol. Chem., Macromol. Symp.* **1993**, 66, 83.

130. Y. V. Kissin, *J. Molecular Cat. A: Chem.* **1995**, 33, 227.

131. J. B. P. Soares, A. E. Hamielec, *Polymer* **1995**, 36, 2257.

132. J. D. Kim, J. B. P. Soares, G. L. Rempel, *J. Polym. Sci., Part A: Polym. Chem.* **1999**, 37, 331.

133. J. B. P. Soares, A. E. Hamielec, *Macromol. Theory Simul.* **1995**, 4, 305.

134. J. B. P. Soares, R. F. Abbott, J. N. Willis, X. Liu, *Macromol. Chem. Phys.* **1996**, 197, 3383.

135. Y. V. Kissin, H. A. Fruitwala, *J. Appl. Polym. Sci.* **2007**, 106, 3872.

136. J. B. P. Soares, *Polym. React. Eng.* **1998**, 6, 225.

137. J. D Kim, J. B. Soares, *Macromol. Rapid Commun.* **1999**, 20, 347.

138. K. J. Chu, C. L. P. Shan, J. B. P Soares, A. Penlidis, *Macromol. Chem. Phys.* **1999**, 200, 2372.

139. M. Smit, X. Zheng, R. Brull, J. Loos, J. C. Chadwick, C. E. Koning, *J. Polym. Sci., Part A: Polym. Chem.* **2006**, 44, 2883.

140. J. Borrajo, C. Cordon, J. M. Carella, S. Toso, G. Goizueta, *J. Polym. Sci., Part B: Polym. Phys.* **1995**, 33, 1627.

141. S. Anantawaraskul, J. B. P. Soares, P. Jirachaithorn, J. Limtrakul, *J. Polym. Sci., Part B: Polym. Phys.* **2006**, 44, 2749.

142. S. Anantawaraskul, P. Jirachaithorn, J. B. P. Soares, J. Limtrakul, *J. Polym. Sci., Part B: Polym. Phys.* **2007**, 45, 1010.

143. S. Anantawaraskul, P. Somnukguandee, J. B. P. Soares, J. Limtrakul, *J. Polym. Sci., Part B: Polym. Phys.* **2009**, 47, 866.

144. E. Siriwongsarn, S. Anantawaraskul, N. Chokputtanawuttilerd, A. A. Alghyamah, J. B. P. Soares, Macromol. Chem. And Phys. 2012, DOI:10.1002/macp.201200238.

145. T. F. McKenna, J. B. P. Soares, *Chem. Reac. Eng. Sci.* **2001**, 56, 3931.

146. S. Floyd, T. Heiskanen, T. W. Taylor, G. E. Mann, W. H. Ray, *J. Appl. Polym. Sci.* **1987**, 33, 1021.

147. W. H. Ray, Transition Metal Catalyzed Polymerization, R. D. Quirk, Ed., Harwood, New York, p. 563-590.

148. A. B. deCarvalho, P. E. Gloor, A. E. Hamielec, *Polymer* **1989**, 30, 280.

149. V. V. Vickroy, H. Schneider, R. F. Abbott, *J. Appl. Polym. Sci.* **1993**, 50, 551.

150. Y. L. Yu., C. C. Tso, P. J. DesLauriers, *J. Appl. Polym. Sci.* **2006**, 100, 4992.

151. C. C. Tso, P. J. DesLauriers, *Polymer* 2004, 45, 2657.

152. H. Pasch, B. Trathnigg, HPLC for Polymers, Berlin: Springer, 1997.

153. D. Berek, *Prog. Polym. Sci.* **2000**, 25, 873.

154. T. Chang, *Adv. Polym. Sci.* **2003**, 163, 1.

155. B. Monrabal, N. Mayo, R. Cong, *Macromol. Symp.* **2012**, 312, 115.

156. D. C. Montgomery, Design and Analysis of Experiments, Hoboken, John Wiley and Sons, New York, Chichester, Toronto 1991.

157. B. Monrabal, L. Oomero, N. Mayo, J. Sanch-Tello, *Macromol. Symp.* **2009**, 282, 14.